



Evolution expérimentale et spécialisation dans le paysage adaptatif d'un gradient environnemental

Noémie Harmand

► To cite this version:

Noémie Harmand. Evolution expérimentale et spécialisation dans le paysage adaptatif d'un gradient environnemental. Evolution [q-bio.PE]. Université Montpellier, 2017. Français. NNT : 2017MONTT062 . tel-01704551

HAL Id: tel-01704551

<https://theses.hal.science/tel-01704551>

Submitted on 8 Feb 2018

HAL is a multi-disciplinary open access archive for the deposit and dissemination of scientific research documents, whether they are published or not. The documents may come from teaching and research institutions in France or abroad, or from public or private research centers.

L'archive ouverte pluridisciplinaire **HAL**, est destinée au dépôt et à la diffusion de documents scientifiques de niveau recherche, publiés ou non, émanant des établissements d'enseignement et de recherche français ou étrangers, des laboratoires publics ou privés.

THÈSE

Pour obtenir le grade de Docteur

Délivré par **l'Université de Montpellier**

Préparée au sein de l'école doctorale **Gaia**
Et de l'unité de recherche **Centre d'Ecologie
Fonctionnelle et Evolutive**

Spécialité : **Evolution, Ecologie, Ressources
génétiques, Paléobiologie**

Présentée par **Noémie HARMAND**

**Evolution expérimentale et spécialisation
dans le paysage adaptatif d'un gradient
environnemental**

Soutenue le 21 juin 2017 devant le jury composé de

M. Thomas BATAILLON, Ass.Prof, Aarhus University	Rapporteur
Mme Isabel GORDO, DR, Instituto Gulbenkian de Ciênciam	Rapporteur
M. Guillaume ACHAZ, MC, Université Pierre-et-Marie-Curie	Examinateur
Mme Delphine SICARD, DR, INRA Montpellier	Examinateur

M. Thomas LENORMAND, DR, CNRS Montpellier	Directeur de thèse
M. Guillaume MARTIN, CR, CNRS Montpellier	Coencadrant de thèse



Experimental evolution and specialization in the adaptive landscape of an environmental gradient

Noémie Harmand

Thèse supervisée par Thomas Lenormand et Guillaume Martin
pour obtenir le grade de docteur, délivrée par l'Université de Montpellier.
Préparée au sein de l'école doctorale SIBAGHE et de l'unité de recherche

CEFE-CNRS

Remerciements

Je tiens à remercier, en premier lieu, Thomas et Guillaume de m'avoir entraînée dans cette grande aventure. Vous avez été des excellents guides pour traverser les pics et les vallées de cette thèse. Merci pour tout ce que vous m'avez appris, votre considération et votre soutien. J'ai beaucoup apprécié nos séances de science artistique à base de croix, ronds, ellipses et triangles. A quand la prochaine forme ?

Un grand merci à Romain et Jean-Nicolas, mes mentors de la microbiologie. Un remerciement particulier à Romain, avec qui l'aventure a commencé, et qui m'a énormément encouragée et soutenue dans les manips comme dans le quotidien. Merci également à Roula et à Marie-Pierre pour leurs aides et précieux conseils au laboratoire et surtout pour leur humanité. Pour moi, vous êtes des piliers de ce laboratoire. Merci Roula d'avoir été présente et rassurante au cours de toute cette thèse.

Je remercie toutes les personnes des équipes GEE du CEFE et Métapopulations de l'ISEM avec qui j'ai pu interagir au cours de ma thèse. Les échanges, pauses café, repas, bières en votre compagnie ont rendu mon quotidien très agréable. Une mention spéciale à tous mes supers co-bureaux! Merci également aux habitants du troisième et à tous ceux avec qui j'ai organisé les séminaires. Merci à Valentine et Sara, qui ont contribué aux travaux de cette thèse. Merci à Fabien pour tes nombreuses aides au début de cette thèse et pour le projet IloGen, qui, faute de temps et à mon grand regret, ne fait pas partie de la thèse. Un énorme merci à Eva, ma sœur de thèse, d'avoir traversé avec moi ces dernières années.

Je tiens à remercier les membres de mon jury, Isabel Gordo, Thomas Bataillon, Delphine Sicard et Guillaume Achaz, d'avoir accepté de lire et discuter mon travail de thèse. Je remercie également les membres de mes comités de thèse d'avoir contribué aux réflexions sur l'ensemble des projets: Nicolas Bierne, Stéphanie Bedhomme, Thomas Hindré, Pierrick Labbé et Pilar Francino.

Merci aux amis de Montpel, les colocs, les copains de Nancy et de Paris. Merci particulièrement à Nina, Sophia, Carole, Cécilia d'avoir été présentes dans les bons et les mauvais moments de cette thèse. Merci à ma grande famille, mon frère et mes sœurs, mes parents pour leur présence, leurs encouragements et leur soutien inconditionnel. Merci enfin à ADM de m'avoir supportée et d'avoir vécu cette thèse avec moi, elle n'aurait pas été la même sans toi.

Sommaire

Introduction	1
Contexte	1
- <i>Pourquoi veut-on prédire l'évolution?</i>	1
- <i>Est-il possible de prédire l'évolution?</i>	1
- <i>Observer, reproduire et tester les trajectoires évolutives</i>	3
Trajectoires et paysages adaptatifs	4
- <i>Quel modèle d'adaptation?</i>	4
- <i>Quelle forme de paysage adaptatif?</i>	5
- <i>Extensions et applications de la notion de paysage adaptatif</i>	9
- <i>Au-delà des paysages adaptatifs</i>	12
Etudes réalisées dans la thèse	13
Décrire la variabilité génétique disponible au cours de l'adaptation	13
- <i>Avec quoi s'adapte-t-on?</i>	13
- <i>Décrire les dynamiques mutationnelles entre génotypes et environnements</i>	14
- <i>Approches expérimentales</i>	17
Décrire et comparer les contraintes sélectives entre environnements	18
- <i>Variations de l'environnement abiotique</i>	18
- <i>Compromis adaptatifs entre environnements</i>	19
- <i>Environnement biotique au sein des lignées évolutives</i>	22
- <i>Interactions de fréquence-dépendance et maintien de la diversité</i>	22
Plan de la thèse	24
Chapitre 1: Fisher's geometrical model and the mutational patterns of antibiotic resistance	25
Chapitre 2: Fitness trade-offs in the evolution of bacterial antibiotic resistance at different concentrations along a gradient	53
Chapitre 3: Mapping the topography of adaptive fitness landscapes across environments: An experimental landscape for bacterial adaptation across an antibiotic dose gradient	85

Chapitre 4: Fast evolution of frequency-dependent selection between coexisting species of bacteria.....	125
Discussion et perspectives.....	157
La variabilité génétique à travers plusieurs environnements.....	158
Que révèle l'approche multi-environnementale sur les variations d'effets sélectifs entre environnements.....	158
Comment les interactions avec les autres espèces s'intègrent dans la dynamique évolutive	159
Retour sur les multiples effets des modules mutationnels.....	159
Caractériser et comparer des environnements	162
Vers une intégration du contexte écologique.....	163
Conclusion.....	166
Bibliographie	167
Annexe 1 : The genetic architecture of local adaptation in a continuous space.....	177

Introduction

Contexte

- Pourquoi veut-on prédire l'évolution?

La première réponse à cette question repose sur un argument purement fondamental. On cherche avant tout à comprendre rétrospectivement d'où vient la diversité du vivant telle qu'on la connaît aujourd'hui et comment elle est maintenue. La question cruciale qui en découle est: est-ce que comprendre le passé peut nous conduire à prévoir l'avenir ? Avant d'aborder cette vaste polémique, il est important de préciser que vouloir prédire l'évolution relève également de motivations concrètes. De nos jours plus que jamais, il est nécessaire d'anticiper et de comprendre les réponses évolutives des organismes vivants, face à des habitats instables et hétérogènes. Depuis plusieurs dizaines d'années, les activités humaines modifient intensément le régime naturel de variation de l'environnement en imposant des modifications brusques, fréquentes, directionnelles et globales. Ces changements s'avèrent intenses par rapport au rythme d'adaptation des populations (Parmesan 2006; Hendry et al. 2008; Gonzalez et al. 2012; Lawson et al. 2015). Les conséquences sont directement observables sur le terrain: l'extinction de populations, la fuite vers de nouveaux habitats ou des changements phénotypiques majeurs dans les populations locales. Pour illustrer ce dernier point, il suffit de constater à quel point le nombre de phénotypes résistants a explosé en réponse à l'utilisation massive de molécules pesticides, insecticides et antibiotiques au cours des 60 dernières années (Levy and Marshall 2004; Davies and Davies 2010). Le bilan est inquiétant aujourd'hui et pour les décennies à venir en terme d'impact sur les écosystèmes, la biodiversité et la santé humaine. Il motive donc à mobiliser les connaissances de la biologie évolutive pour prévoir les conséquences des modifications d'habitats et proposer des scénarios alternatifs.

- Est-il possible de prédire l'évolution?

La réponse à cette question n'est certainement pas blanche ou noire et a déjà été souvent discutée (par exemple dans Lobkovsky and Koonin 2012; Achaz et al. 2013; Orgogozo 2015; Blount 2016; Lenormand et al. 2016). Les fondements théoriques de la biologie évolutive introduits par Fisher, Wright et Haldane, en particulier, ont largement contribué à décrire comment la sélection naturelle, la mutation, la dérive et les autres facteurs évolutifs définissent les changements de fréquence des gènes dans les populations. Du point de vue de la synthèse moderne de l'évolution, les trajectoires évolutives répondent à plusieurs « lois » déterministes

ainsi qu'à un ensemble de processus stochastiques qui rendraient l'évolution imprévisible. C'est par exemple le point de vue adopté par Francois Jacob (1977) qui compare la sélection naturelle à un « bricoleur » qui crée avec ce qui lui passe sous la main. C'est également la vision de Gould (1989) quand il pose la fameuse question : si on rembobinait la cassette du vivant, est-ce que le résultat que l'on observerait serait similaire au monde d'aujourd'hui ? Le « non » tranché est discutable. Les expériences de sélection artificielle ont déjà montré depuis longtemps que l'on peut « contrôler » l'évolution de caractères phénotypiques, en général 'au champs' et sur des organismes pluricellulaires sexués (développé dans Bell 2008). Dans les expériences d'évolution plus récentes, au laboratoire et principalement sur des microbes asexués, les trajectoires adaptatives répétées dans les mêmes conditions peuvent aussi montrer des patrons très répétables, pour des caractères phénotypiques complexes comme la taille des cellules ou la valeur sélective (Lenski and Travisano 1994; Ramiro et al. 2016; Lässig et al. 2017) et même parfois, à l'échelle des séquences génétiques (Stern 2013). Il est donc important de se demander ce qui est prévisible ou ne l'est pas dans une trajectoire évolutive.

Il existe plusieurs sources de stochasticité qui se cumulent à différentes échelles d'observations dans les processus évolutifs (Lenormand et al. 2009). Les mutations, ou plus largement la variabilité génétique, arrivent aléatoirement à l'échelle du génome. Les individus sont confrontés à des événements démographiques aléatoires au cours de leur vie. Enfin les environnements dans lesquels évoluent les populations fluctuent avec des tendances plus ou moins prévisibles. Je reviendrai plus précisément sur la stochasticité au niveau génétique dans la suite de l'introduction, mais il est important d'insister sur le fait que ces processus aléatoires répondent à un certain nombre de contraintes, communes à tous les individus et les répliques. Il en résulte que si l'on étudie un grand nombre de cas pris en même temps, on peut révéler des comportements globaux qui peuvent être décrits par des lois statistiques. De ce fait, plusieurs aspects des processus évolutifs ont été comparés et transposés à la thermodynamique statistique (par exemple Iwasa 1988; Sella and Hirsh 2005; Barton and Coe 2009): la trajectoire d'une molécule ne peut pas être décrite individuellement, mais le mouvement global d'un grand ensemble le peut. Il découle de cela qu'on pourrait comprendre bien plus que les conséquences des processus évolutifs à l'œuvre mais également les « lois » sources quantitatives qui permettent de reproduire la totalité du déroulé d'un processus évolutif. Par exemple, il n'est pas possible de prédire l'effet sélectif que va avoir une mutation aléatoire particulière dans un contexte donné, mais on peut proposer des prédictions pour la distribution des effets de l'ensemble des mutations aléatoires (Kimura 1965; Martin and Lenormand 2006a).

Ce dernier point ne permet certainement pas de clore le débat sur la prédictibilité ou non de l'adaptation, mais il permet de faire avancer les réflexions à la fois théoriques et empiriques sur

le sujet. Il amène aussi à se poser les questions au cœur des recherches actuelles en biologie évolutive et sous-jacentes à cette thèse. L'évolution telle qu'elle est décrite aujourd'hui fait état de nombreux processus évolutifs simultanés qui, sont de mieux en mieux décrits, analysés et modélisés. Reste à savoir quelle part de chacun de ces processus détermine les trajectoires évolutives de différentes populations, lorsqu'ils agissent conjointement. Quelle est la résultante des assemblages de processus ? En particulier est-ce que, dans certain cas, il existe un nombre limité de « voies » pour s'adapter, conduisant à une certaine répétabilité et prédictibilité évolutive ? Ou est-ce que au contraire l'assemblage de ces processus crée une forte contingence historique, compréhensible (jusqu'à un certain point) mais peu prévisible ?

- Observer, reproduire et tester les trajectoires évolutives

L'évolution expérimentale offre depuis quelques dizaines d'années une occasion incroyable d'étudier l'évolution en action. Elle a permis notamment de bâtir un pont entre des modèles évolutifs purement théoriques reposant sur des hypothèses souvent éloignées d'un contexte naturel et des données de terrain issues d'un contexte évolutif complexe et largement inconnu (quelques exceptions existent, comme par exemple le suivi en nature de l'évolution de la résistance aux insecticides Labbé et al. 2007, 2009). Couplée aux avancées technologiques en biologie moléculaire et en robotisation/miniaturation, l'évolution expérimentale a contribué à redécouvrir ce large corpus théorique et à tester plusieurs hypothèses non accessibles jusque-là par des données empiriques. Différents organismes modèles ont été utilisés pour coller plus particulièrement à un cadre spécifique et à une question scientifique sous-jacente (Kassen 2002; Bell 2008; Garland and Rose 2009). Plus généralement, les microorganismes représentent un modèle hors-pair pour étudier l'évolution à long-terme (Elena and Lenski 2003). De nombreuses questions ont ainsi été abordées, en particulier à travers l'évolution expérimentale réalisée par l'équipe de Richard Lenski depuis 1988 (année de ma naissance!) : entre autres les dynamiques de l'adaptation (Lenski and Travisano 1994; Ostrowski et al. 2005; Wiser et al. 2013), et ses bases génétiques (Elena and Lenski 2003; Barrick and Lenski 2013), les effets de l'interférence clonale (Gerrish and Lenski 1998; Maddamsetti et al. 2015), le maintien du polymorphisme à long terme (Rozen and Lenski 2000; Le Gac and Doebeli 2010; Plucain et al. 2014), l'origine d'innovations évolutives (Blount et al. 2012a).

Le fait que cette expérience se limite à des conditions extrêmement simplifiées d'adaptation mettant en jeu un nombre réduit de processus évolutifs (environnement constant, espèce asexuée, population non-structurée) montre bien le potentiel énorme que garde l'évolution expérimentale pour apporter des éclairages dans différents contextes. Notamment, cette étude ne prend pas en compte comment différents facteurs environnementaux influencent la

trajectoire adaptative. Comprendre comment l'environnement modèle les populations et la diversité représente encore un défi pour la biologie évolutive (Angilletta and Sears 2011). Il est clair que différents environnements font varier les valeurs sélectives de différents génotypes et vont sélectionner des traits phénotypiques plutôt que d'autres (Kassen 2002). Par contre, on ne sait pas encore clairement mesurer à quel point deux environnements sont différents et quels défis évolutifs ils représentent pour une population. Dans un monde où l'environnement fluctue constamment en plus de changer rapidement et directionnellement, il paraît donc indispensable de comprendre quelles sont les contraintes imposées aux populations dans leurs environnements naturels et à quel point elles peuvent expliquer l'évolution du vivant tel qu'on l'observe aujourd'hui.

Trajectoires et paysages adaptatifs

- Quel modèle d'adaptation?

Historiquement, plusieurs approches existent pour décrire les processus d'adaptation, notamment les approches de génétique quantitative (Lynch and Walsh 1998) et les approches de dynamique de l'adaptation (Orr 2005). Il est intéressant de voir que, malgré des cadres de travail différents, ces deux approches se retrouvent complémentaires dans la vision globale des processus d'adaptation. Très caricaturalement, ces deux approches se justifient par deux grandes différences d'échelles : la temporalité et les bases génétiques de l'adaptation. Les approches de génétique quantitative s'appliquent à l'évolution à court terme, chez des sexués, sous sélection faible ou augmentant graduellement (ce qui n'est pas toujours le cas même pour les variations environnementales « naturelles »). Ce type d'approche a été beaucoup utilisé pour comprendre comment la sélection agit sur les moyennes phénotypiques dans les populations polymorphes soumises à sélection artificielle ou naturelle. Les changements étudiés sont des changements de fréquences d'allèles préexistants (matrice G). Ces méthodes ont été communément appliquées à des mesures répétées de dynamique à court terme de traits phénotypiques dans des populations naturelles.

Les trajectoires adaptatives à plus long terme, chez des asexués comme c'est souvent le cas de celles issues d'évolutions expérimentales, sont plus couramment illustrées par des modèles de « dynamique adaptative» (au sens large). A cette échelle, on considère que les trajectoires adaptatives émergent d'innovations génétiques avantageuses (la variation génétique préexistante dans la population est supposée négligeable en comparaison), qui se substituent, plus ou moins successivement, dans la population (modèles d' « origine-fixation », McCandlish

and Stoltzfus 2014). Ces modèles prennent particulièrement sens lorsque la mutation est faible et la sélection forte, de telle sorte que la variance génétique reste faible à tout temps. Cette simplification, comme la précédente, est un cas extrême le long d'un continuum. Par exemple, dans le cas de populations microbiennes clonales assez grandes, les évènements de mutations sont assez fréquents et génèrent de la variabilité. Cependant, l'absence de reproduction sexuée empêche la combinaison de mutations avantageuses apparues dans des lignées différentes, ce qui entraîne la fixation récurrente de lignées avantageuses (pouvant porter une ou plusieurs mutations) qui 'balayent' la diversité.

Les modèles de paysage adaptatif considérés dans cette thèse puisent leur inspiration de ces deux approches. Les principes fondamentaux de la génétique quantitative sont repris à travers la représentation de traits phénotypiques, qui sont optimaux en un certain point déterminé par les conditions environnementales. Ces traits s'organisent dans un espace phénotypique continu, de sorte qu'un nombre infini de combinaisons (=phénotypes) sont possibles. Dans notre système, nous considérons des lignées bactériennes clonales. Elles sont représentées par un point unique dans cet espace. Les dynamiques des lignées résultent de la fixation successive de mutations qui déplacent le point dans le paysage. Ainsi chaque mutation peut potentiellement affecter l'ensemble des traits phénotypiques à la fois (pléiotropie totale). Dans sa version la plus basique, le modèle que j'ai utilisé dans ma thèse correspond à celui appelé « modèle géométrique » et décrit originellement par Fisher (Fisher 1930; Orr 2005).

- Quelle forme de paysage adaptatif?

Le concept de paysage adaptatif a énormément marqué les théories de l'adaptation, en premier lieu parce qu'il permet de se faire une représentation imagée des forces évolutives à la base de l'adaptation et ainsi de proposer une théorie très visuelle et accessible. C'est d'ailleurs dans cet objectif que le concept a été introduit par Sewall Wright en 1932. Le paysage adaptatif n'est ni plus ni moins qu'une carte topographique, pour un environnement donné, des valeurs sélectives associées à des coordonnées qui représentent les phénotypes ou les génotypes d'individus ou de populations (on relie alors phénotypes ou génotypes moyens et valeur sélective moyenne). La métaphore a été largement reprise jusqu'à aujourd'hui comme outil visuel mais aussi comme outil standard de modélisation mathématique par exemple pour étudier l'adaptation (résumé dans Orr 2005), la spéciation (Barton 2001; Chevin et al. 2014; Fraïsse et al. 2016), l'évolution parallèle (Chevin et al. 2010b; Lenormand et al. 2016), les effets de la sélection (Lande and Arnold 1983) ou les distributions d'effets des mutations (résumé dans Tenaillon 2014). Depuis cette époque, cependant, il subsiste des polémiques quant à la forme que doivent prendre ces paysages.

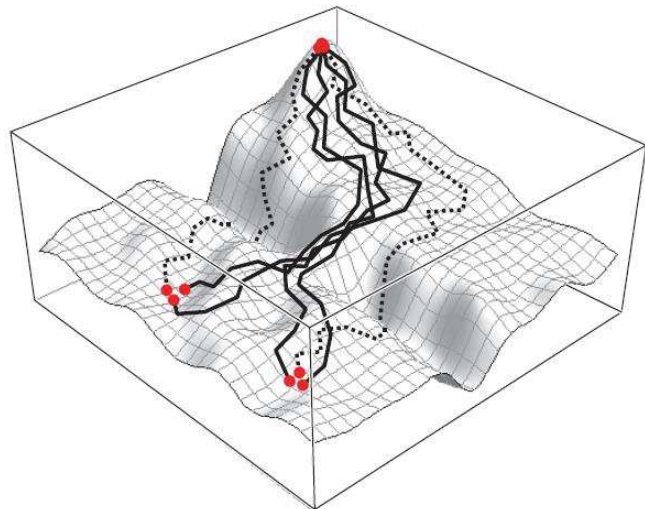
Ces polémiques résultent initialement (historiquement entre Wright et Fisher) d'un désaccord sur la contribution des processus évolutifs dominants pour décrire l'évolution. De mon point de vue, toutes les formes de paysage peuvent prendre sens dans un contexte précis dès lors qu'elles justifient du caractère essentiel de chaque élément utilisé pour illustrer le contexte étudié. Une des différences entre les visions de Fisher et Wright (au niveau des paysages) porte sur l'échelle de rugosité relativement à l'échelle d'effet des mutations disponibles (Gavrilets 2010). Du point de vue de Wright, il existe des vallées adaptatives qui ne peuvent pas être traversées par l'effet seul de la sélection : les mutations disponibles pour progresser dans cette direction sont toutes délétères (elles entraînent la population dans la vallée) et ne sont donc pas sélectionnées (épistasie « de signe » Weinreich et al. 2005) Une conséquence directe de cela est que les populations peuvent rester bloquées sur des pics adaptatifs intermédiaires. Une des solutions proposées par Wright pour que les populations traversent ces vallées (la « shifting balance theory »,) requiert l'effet temporaire de la dérive, qui réduit les contraintes sélectives et permet à la population d'atteindre un autre pic adaptatif (scénario détaillé par exemple dans l'introduction de Whitlock and Phillips 2000). Ce scénario en particulier a été très largement critiqué (voir Coyne et al. 1997) mais les concepts théoriques du paysage de Wright ont joué et jouent encore un rôle prépondérant dans les théories de spéciation et de divergences évolutives (résumé dans Gavrilets 2004). Cette version de paysage est également massivement employée pour illustrer tous types de «blocages» évolutifs (taux d'adaptation variables, épistasie, combinaison de mutations létales, etc.), interprétés comme résultant de l'attraction vers des pics adaptatifs locaux, par le jeu de la mutation et la sélection (Whitlock et al. 1995; Elena and Lenski 2003; Weinreich et al. 2005).

Au contraire, dans le modèle géométrique proposé par Fisher, de tels blocages sont a priori inexistants : après suffisamment de temps, une population peut accéder à n'importe quel pic adaptatif sans recours à d'autres processus que la mutation et la sélection (la dérive étant plutôt un frein au processus). En effet, le fait que la sélection agisse cette fois dans un espace phénotypique continu a pour conséquences que les rugosités du paysage ne sont pas perçues comme des « obstacles » absolus à l'adaptation. Il existe toujours, dans le continuum des possibles, des mutations capables de 'sauter' d'un pic à l'autre. Il a parfois été proposé que cette moindre contingence apparait également dans le modèle de paysage « génétique » de Wright lorsqu'un nombre suffisant de dimensions (loci pouvant muter) est considéré, par un effet similaire de grande dimensionnalité des possibles (Gavrilets 2004). Il a en effet été récemment montré (Hwang et al. in prep.) que le modèle de Fisher à un pic adaptatif (sur l'espace des phénotypes) génère, une fois transposé sur un espace génotypique (comme dans le paysage de Wright) un très grand nombre de pics locaux (épistasie de signe), Pourtant, malgré cette

« rugosité », les modèles de dynamique de l'adaptation dans ce paysage de Fisher à un pic (Martin and Roques 2016) n'identifient pas de contrainte particulière empêchant les populations d'atteindre le pic adaptatif le plus haut (l'optimum phénotypique unique), à partir de n'importe quelle condition initiale.

Sans rentrer plus en détails dans les aspects historiques, je voudrais seulement faire ressortir ici le lien qu'ils partagent avec les polémiques actuelles sur les paysages adaptatifs et la question de la contingence en évolution. La version de paysage de Wright est représentée avec plusieurs pics adaptatifs séparés par des vallées alors que le modèle de Fisher considère un seul pic, correspondant à une combinaison de traits optimale. Cette question du nombre de pics adaptatifs est au cœur de la problématique que j'ai présentée plus haut sur la répétabilité de l'évolution: existe-t-il un grand nombre de solutions équivalentes pour s'adapter à un environnement (plusieurs pics à proximité, figure 1B) ou bien à l'extrême n'y a-t-il qu'une seule solution optimale (un seul pic à proximité, figure 1A)? Cette question devrait se poser très largement plutôt que d'être vue comme allant de pair avec un modèle en particulier. Les critères de sélection d'un modèle à plusieurs pics sur le motif d'un « blocage » sélectif sont critiquables. L'existence d'une vallée adaptative n'est pas l'unique façon de générer des situations d'épistasie complexe ou des phénotypes létaux. Nous venons de voir plus haut que le paysage décrit par Fisher intègre bien par exemple les motifs d'épistasie entre mutations (Martin et al. 2007; Phillips 2008) et de « rugosité » du paysage à l'échelle génétique (Hwang et al. in prep.). Les mutations létales, s'expliquent dans des versions de paysage à « trous » tel que proposé par Gavrilets (Gavrilets 1997; Manna et al. 2011). Cette thèse propose également une alternative pour expliquer des taux d'adaptation très ralenti dans un paysage de type Fisher. Toutefois, il reste une question ouverte mais déterminante dans l'utilisation des connaissances en biologie évolutive : celle du nombre de pics adaptatifs dans le voisinage d'une population qui s'adapte, c'est-à-dire du degré de convergence évolutive qui est attendu sur des temps évolutivement longs.

A



B

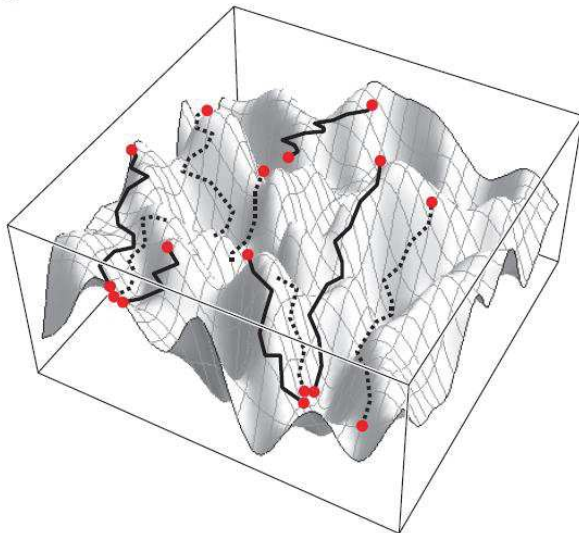


Figure 1 : Trajectoires évolutives dans des paysages adaptatifs plus (A) ou moins (B) déterministes. Dans Koonin 2012.

(A) : "The rugged fitness landscape and accessible evolutionary trajectories. Quasideterministic evolution: canalization of the accessible trajectories. Solid lines show monotonic ascending trajectories that are accessible to evolution driven solely by selection. Broken lines show nonmonotonic trajectories that are accessible only with the involvement of genetic drift."

(B) : "The rugged fitness landscape and accessible evolutionary trajectories. Stochastic evolution: random scattering of accessible trajectories. Solid lines show monotonic ascending trajectories that are accessible to evolution driven solely by selection. Broken lines show nonmonotonic trajectories that are accessible only with the involvement of genetic drift."

- Extensions et applications de la notion de paysage adaptatif

Un autre mécanisme proposé par Wright pour qu'une population franchisse des vallées adaptatives est une modification temporaire de la topographie générée par une variation des conditions environnementales. Une variation de l'environnement correspond à une modification du paysage adaptatif. Mais laquelle? Et comment l'ensemble des processus évolutifs s'en retrouve-t-il impacté? Les paysages adaptatifs ont été largement pensés dans un environnement unique et fixé (mais il existe des propositions de paysages dynamiques par exemple dans Simpson 1944; Arnold et al. 2001; Matuszewski et al. 2014) pour se concentrer sur les processus adaptatifs qui permettent d'atteindre un optimum phénotypique donné.

Alternativement, toute une branche de l'écologie évolutive, s'est intéressée à l'évolution de traits quantitatifs dans un habitat hétérogène ou variable. Dans ces modèles, différents environnements sont assimilés à différents optimums le long d'un axe phénotypique unique. Ils ont été notamment utilisés pour étudier la plasticité phénotypique (Via and Lande 1985; Chevin et al. 2010a), ou les niches écologiques le long d'un gradient (*e.g.* Levins 1966; Lynch and Lande 1993; Kirkpatrick and Barton 1997). Cependant l'approche mathématique utilisée dans ces modèles repose sur le modèle infinitésimal (valide *a priori* à court terme et dans des populations sexuées polymorphes), où les covariances phénotypiques (G matrix) sont supposées constantes. Par conséquent, les patrons mutationnels dans un contexte inter-environnemental (voir Martin and Lenormand 2006b, 2015 discuté plus tard) restent encore assez peu étudiés. L'intégration d'une composante multi-environnementale dans les paysages adaptatifs (théoriques et empiriques) ouvre de nombreuses opportunités dans ce sens. Cette question se pose aussi bien au-delà des modèles de paysages adaptatifs. On sait encore très peu quel est l'impact de différents environnements sur l'ensemble des processus évolutifs et particulièrement sur l'effet des mutations. S'il s'avérait que les paysages adaptatifs, sous leur forme la plus communément utilisée dans nos modèles, ne sont pas un bon outil pour atteindre cette vision multi-environnementale, il sera nécessaire de proposer d'autres modèles plus réalistes.

Les approches empiriques, sur cette question, ont permis de dégager beaucoup de « petits bouts » de paysages empiriques (sur un nombre réduit de traits phénotypiques) mais on ignore à quel point ils sont représentatifs de la globalité de la forme du paysage. Plus récemment, des morceaux de paysages empiriques ont également été révélés par des approches génotypiques : en considérant l'effet sur la fitness de multiples combinaisons possibles d'un lot de mutations (Weinreich et al. 2013; Bank et al. 2015). Ces approches ont largement permis de mettre en avant l'importance des interactions épistatiques pour décrire l'effet des mutations sur la fitness (Phillips 2008; Hartl 2014). Par contre elles ne semblent pas non plus permettre d'accéder à la

forme globale du paysage adaptatif, ni de décrire de multiples environnements (Blanquart and Bataillon 2016).

En parallèle, la question de l'adaptation inter-environnements s'est aussi développée théoriquement (Martin and Lenormand 2006b, 2015). Sans rentrer tout de suite dans les détails, un point très important est que ce corpus théorique développé sur la base du modèle géométrique de Fisher a permis de dégager un certain nombre de prédictions empiriques en lien avec la topographie du paysage (et donc les caractéristiques des processus évolutifs dont la mutation). Une autre approche empirique des paysages adaptatifs consiste ainsi à générer des données expérimentales qui permettent spécifiquement de tester et discuter ces prédictions. Plusieurs travaux empiriques ont déjà contribué à progresser dans cette voie (par exemple Martin and Lenormand 2006b; MacLean and Buckling 2009; Sousa et al. 2012; Trindade et al. 2012; Perfeito et al. 2014), avec notamment des propositions pour estimer des « distances » entre environnements dans un paysage adaptatif (Hietpas et al. 2011). Les travaux proposés dans cette thèse se placent directement dans le prolongement de cette approche.

- Au-delà des paysages adaptatifs

A ce point de la réflexion, il me semble important de prendre du recul et de renouer avec les questions présentées plus tôt dans cette introduction. Quels sont les processus déterminants pour comprendre les trajectoires évolutives des populations? Les paysages adaptatifs sont des outils puissants dans ce sens mais ils ne prennent pas en compte tous ces processus. Ils reflètent assez bien l'évolution d'une population isolée dans un environnement constant, comme c'est le cas pour les lignées évolutives en laboratoire. Par contre ils prennent peu en compte le contexte écologique des populations naturelles.

Par exemple, ils négligent les interactions entre espèces, populations, individus et leurs effets sur les trajectoires adaptatives. Elles constituent pourtant une contrainte omniprésente dans les populations naturelles. La limite des paysages mise en avant sur ce point est qu'une population ne va pas chercher nécessairement à optimiser ses traits par rapport aux conditions environnementales, mais aussi par rapport aux autres organismes. En fait les composantes biotiques peuvent très bien être considérées comme partie intégrante de l'environnement dans la topographie du paysage (par exemple Mangel 1991). Cependant, la forme statique du paysage peut s'avérer inappropriée. C'est le cas par exemple lorsque la sélection de la population est rendue fréquence-dépendante par ses interactions (Lewontin 1958; Haldane and Jayakar 1963; Ayala and Campbell 1974; Bell 2008). Ces relations de fréquence-dépendance jouent un rôle particulièrement important dans l'évolution des populations à long-terme, car on considère

qu'elles maintiennent la coexistence de polymorphismes (au niveau des espèces, populations, individus, gènes). L'évolution expérimentale se révèle encore une fois pertinente pour étudier de manière isolée, la contribution de ces interactions sur les trajectoires évolutives à longs-termes. Je détaillerai cette thématique par la suite, en lien avec un des chapitres de la thèse.

Etudes réalisées dans la thèse

Au cours de cette thèse, nous avons cherché à décrire les différents processus évolutifs à l'œuvre au cours d'évolutions expérimentales de lignées bactériennes en laboratoire. Les conditions d'évolution incluent différentes concentrations d'un antibiotique (l'acide nalidixique ou Nal) qui jouent le rôle d'une variation de l'environnement le long d'un gradient. Dans ce contexte très simplifié, les lignées bactériennes s'adaptent par accumulation de nouvelles mutations en répondant aux contraintes sélectives imposées par l'environnement. Ces dynamiques peuvent donc être décomposées très caricaturalement en deux étapes : 1) la production de variabilité génétique par événements de mutations et 2) la fixation d'un phénotype adaptatif. Pour chacune de ces étapes on se demande : quelles « lois » peuvent décrire les processus évolutifs impliqués ? Quelles sont leurs variations entre les différents environnements ? Quel rôle joue la contingence historique? Quel est le paysage adaptatif associé? Dans la suite de cette introduction, j'exposerai plus précisément des éléments de réflexions théoriques et expérimentaux sur ces points 1) et 2) sur lesquels s'appuient les travaux de la thèse.

La dernière partie de la thèse est consacrée au rôle des interactions biotiques dans les dynamiques évolutives. Cette étude repose sur une expérience de coévolution à long terme de deux souches bactériennes maintenues par sélection fréquence-dépendante. On se demande comment l'interaction entre l'adaptation à l'environnement et à un compétiteur biotique influence l'évolution des lignées. Quelles sont les conditions de maintien de ces lignées au cours du temps? Quel rôle joue la sélection environnementale dans ces interactions?

Décrire la variabilité génétique disponible au cours de l'adaptation

- Avec quoi s'adapte-t-on?

La variabilité génétique est l'élément source des processus d'adaptation: elle définit l'univers des possibles en termes d'innovations adaptatives. En se plaçant à la base des processus évolutifs, elle est déterminante dans l'issue de la quasi-totalité des modèles d'évolution existants. Il existe donc un intérêt énorme à formuler des hypothèses les plus réalistes et

précises possibles pour décrire cette variabilité. Il existe une grande diversité de bases génétiques impliquées dans l'adaptation des populations naturelles : mutations ponctuelles, duplications, inversions, insertions d'éléments transposables, transferts horizontaux de gènes et de plasmides pour en citer quelques-unes. Sans aller beaucoup plus loin pour chaque cas, il est important de noter que ces bases peuvent générer une large gamme d'effets phénotypiques et plusieurs alternatives qui permettent de contourner des situations que l'on conçoit *a priori* comme des « obstacles » adaptatifs. Par exemple, hors du laboratoire, l'évolution de la résistance aux antibiotiques chez les bactéries peut être résolue rapidement par l'acquisition d'un plasmide de résistance plutôt que par la fixation d'une mutation. L'ensemble de ces possibilités joue un rôle crucial dans les processus d'adaptation et dans l'émergence et le maintien de la diversité.

Dans notre système expérimental, la variabilité génétique émerge des événements de mutations. Les mutations arrivent aléatoirement dans le génome et indépendamment de leurs effets sélectifs dans l'environnement considéré. Elles représentent donc une source d'aléas dans le processus adaptatif. Leurs propriétés peuvent en revanche être décrites, en théorie, par des paramètres statistiques qui permettent de quantifier le processus mutationnel. Par exemple, on peut caractériser la distribution des effets sélectifs associés à un grand nombre de mutations échantillonées aléatoirement dans cet ensemble. Ces effets sélectifs dépendent à la fois de l'environnement considéré et du fond génétique dans lequel les mutations s'expriment (effets d'épiplatie). Ainsi seulement une infime partie de ce que représente l'ensemble des possibles contenus dans la variabilité génétique est révélée à travers les effets sélectifs d'un assemblage génétique dans un environnement. Etendre ces connaissances passe par décrire les variations générées par différents environnements et différents assemblages génétiques.

- Décrire les dynamiques mutationnelles entre génotypes et environnements

Le modèle géométrique de Fisher prend en compte à la fois l'effet du fond génétique par la position du phénotype dans le paysage et de l'environnement au travers de la fonction de fitness associée aux phénotypes dans un environnement. Il permet également d'intégrer la multiplicité des effets phénotypiques des mutations à travers la multi-dimensionnalité de l'espace phénotypique (les mutations agissent sur un grand nombre de traits à la fois). Ce type de paysage adaptatif peut donc être un bon modèle pour servir de base théorique aux « lois » de la mutation, en maintenant une certaine généralité (aucun mécanisme biologique particulier n'est requis) tout étant accessible à l'analyse mathématique et donc statistique.

C'est d'ailleurs historiquement dans cet objectif que Fisher utilisa son modèle géométrique d'adaptation. Il cherchait à déterminer quelle gamme d'effets phénotypiques avait la plus grande probabilité d'avoir un effet sélectif avantageux au cours des processus d'adaptation (Fisher 1930; Orr 2005). Il démontra que cette probabilité diminue exponentiellement avec l'effet phénotypique des mutations. En tirant la conclusion, à partir de ce résultat, que les mutations de très petits effets jouent un rôle prépondérant dans l'adaptation, il négligea toutefois plusieurs aspects du processus d'adaptation. D'abord, un point mis en avant par Kimura (1983) est que la dérive joue un rôle important dans la fixation de ces mutations initialement en très faible fréquence dans la population (portée par un seul individu au moment où elle apparaît): quand la taille de population est grande cet effet est approximé par une probabilité de fixation linéairement reliée à l'effet des mutations ($p \sim 2s$). Ainsi les mutations de petits effets ont plus de chance d'être initialement perdues que celles de grands effets. Le deuxième point négligé par Fisher est l'aspect dynamique de la trajectoire adaptative. Il est bien illustré dans un paysage adaptatif (figure 2). Intuitivement, on peut se rendre compte que, plus la population progresse vers l'optimum, moins des mutations de forts effets vont lui permettre de l'atteindre (Orr 1998). Cette vision dynamique est largement validée par les trajectoires adaptatives obtenues expérimentalement en laboratoire. Ce motif d'évolution ralentie avec la progression de l'adaptation est qualifié de rendement décroissant («*diminishing return*», par exemple dans MacLean et al. 2010; Gordo and Campos 2013; Wiser et al. 2013).

Par la suite, plusieurs études théoriques basées sur le modèle de Fisher, ont formulé des hypothèses pour caractériser les processus mutationnels et leurs dynamiques (par exemple Orr 2003, 2006; Martin and Lenormand, 2006a, 2008; Martin and Roques 2016). Ces dynamiques ont été notamment intégrées sous la forme d'une expression analytique décrivant la distribution des effets des mutations en fonction de la distance du phénotype focal à l'optimum considéré, de l'intensité de la sélection dans l'environnement considéré et de la dimensionnalité «équivalente» de l'espace phénotypique sous sélection (Martin and Lenormand 2006a, 2008). Plus récemment, une extension de cette théorie a été proposée pour décrire la distribution bivariée de l'effet des mutations entre deux environnements intégrant, en plus des paramètres cités précédemment, l'angle entre les directions vers les optima des deux environnements du point de vue du phénotype focal (Martin and Lenormand 2015). Ces prédictions (reprises dans les chapitres) présentent plusieurs gros avantages : d'abord elles proposent un modèle de base pour une comparaison directe avec des données expérimentales. Ensuite, elles permettent de caractériser le paysage adaptatif sous-jacent et donc potentiellement de formuler des prédictions sur les trajectoires évolutives à plus long-terme. Les comparaisons empiriques réalisées jusqu'ici sont très encourageantes vis-à-vis de ces prédictions: au travers de plusieurs

études elles montrent une bonne appréciation de la forme de la distribution (MacLean and Buckling 2009; Bataillon et al. 2011; Sousa et al. 2012b; Trindade et al. 2012), des variations associées à différents fonds génétiques (Martin et al. 2007; Manna et al. 2011), des variations associées à différentes contraintes environnementales (Martin and Lenormand 2006b; Trindade et al. 2012), du niveau d'adaptation dans un environnement donné (Sousa et al. 2012b; Perfeito et al. 2014)

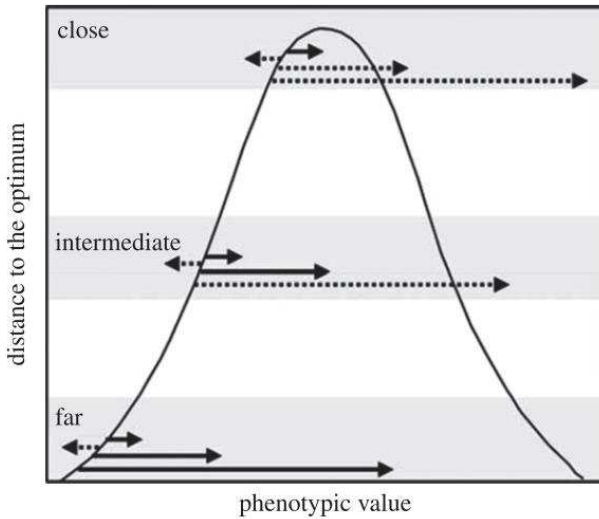


Figure 2 : Dynamique des effets des mutations dans la trajectoire adaptative, dans Dittmar et al. 2016:

« *The relationship between distance to the optimum and the possible effect sizes of mutations fixed during a bout of adaptation following Orr (1998). A Gaussian fitness function is depicted for natural selection on a single trait with a fixed optimum. The adaptive value of mutations of different sizes is given for three different stages of adaptation, reflected as the distance to the optimum (far, intermediate, close). The length of the arrow gives the effect size, solid arrows signify adaptive mutations and dashed arrows signify maladaptive mutations.*

Cependant, ces prédictions reposent sur plusieurs hypothèses fortes liées au modèle, qui peuvent créer des décalages importants avec les observations empiriques. Par exemple, une des forces du modèle, sa capacité à prendre en compte les effets pléiotropes des mutations, peut aussi s'avérer en partie une faiblesse. Notamment, dans sa version la plus basique, le modèle considère une forme extrême de pléiotropie dans laquelle les mutations peuvent affecter tous les traits et avec un effet moyen constant. Les effets pléiotropes de mutations ont été démontrés empiriquement mais cela n'implique pas qu'ils soient « universellement » pléiotropes. S'ajoute surtout à cela l'observation qu'un même caractère adaptatif mobilise plus souvent que prévu dans le cas de pléiotropie totale, les mêmes éléments du génome. Cette évolution parallèle est

répandue dans le monde vivant (Stern 2013; Bailey et al. 2016) mais absente des trajectoires évolutives prédites par le modèle de Fisher (Chevin et al. 2010b; Lenormand et al. 2016). C'est d'ailleurs une critique qui a été formulée très tôt à l'encontre du modèle d'adaptation de Fisher (Shull 1935). Alternativement, il a été proposé dans plusieurs études qu'il existe des modules mutationnels, c'est-à-dire des parties du génome (par exemple un gène mais pas nécessairement) pour lesquelles les mutations n'affectent qu'un groupe de traits. Intégrés au modèle de Fisher, ces modules permettent à la fois de prendre en compte un certain niveau de pléiotropie mais aussi de reproduire des cas d'évolution parallèle (Chevin et al. 2010b; Lenormand et al. 2016). En contrepartie, ils constituent un nouvel aspect « inconnu » au modèle et aux prédictions car on a peu d'idées de l'organisation de ces modules : à quel point sont-ils propres à un système, un phénotype ou un contexte en particulier ? A quels points impactent-ils la distribution des effets des mutations et les mutations sélectionnées entre environnements et au cours de la trajectoire adaptative ? Pourquoi observe-t-on de l'évolution parallèle dans certains cas et peu dans d'autres ? L'existence de ces modules pourrait jouer un rôle important dans la contingence évolutive en restreignant l'espace phénotypique dans lequel l'adaptation peut progresser. Ces questions ont été abordées au cours des travaux de la thèse.

- Approches expérimentales

Plusieurs approches expérimentales sont possibles pour accéder à des distributions d'effets de mutations. Concrètement, aucune ne permet d'avoir accès directement à la distribution complète des mutations aléatoires telle que décrite dans le modèle. Faire abstraction de la sélection représente un gros défi expérimental et chaque méthode y parvient seulement partiellement. Brièvement, une première option consiste à générer des mutants en modifiant artificiellement le génome d'individus (via des insertions d'éléments transposables ou de duplications, des délétions de gènes ou de paires de bases) (pour revue voir, Martin and Lenormand 2006b; Bataillon and Bailey 2014). Ces méthodes ont l'avantage d'intégrer tous types d'effets des mutations y compris les létaux. Mais elles représentent une charge expérimentale importante et ne permettent pas, par exemple, d'apprécier totalement l'existence de potentiels modules mutationnels.

Un autre moyen d'éliminer la sélection est de se placer dans contexte où la dérive génétique domine. Ce principe est appliqué dans les expériences d'accumulation de mutations (pour revue voir Bataillon 2000). Cette méthode est facilement accessible expérimentalement mais présente les inconvénients suivants : les mutations létales ne sont pas représentées et surtout le nombre de mutations accumulées dans chaque lignée est inconnu de sorte que plusieurs pas

mutationnels sont mélangés dans la distribution générée. Par ces deux méthodes, on n'accède en général qu'à peu de mutations bénéfiques.

Finalement, une dernière méthode, et aussi celle utilisée dans les travaux de cette thèse, est de cibler des mutations avantageuses dans un environnement dans lequel le phénotype non-muté est létal (Kassen and Bataillon 2006; MacLean et al. 2010; Bataillon et al. 2011; Trindade et al. 2012). Cette méthode permet d'accéder seulement à un sous-échantillon de la distribution correspondant aux mutations bénéfiques dans l'environnement du cible. La méthode est simple et donc praticable à grande échelle et de faible coût. De plus, il est possible de formuler des hypothèses théoriques sur le biais généré par le criblage, et donc de corriger les prédictions en tenant compte de ce biais. Cette correction peut être implémentée à partir des prédictions théoriques du modèle de Fisher qui intègrent plusieurs environnements (Martin and Lenormand 2015).

Décrire et comparer les contraintes sélectives entre environnements

- Variations de l'environnement abiotique

Les fluctuations environnementales constituent une contrainte largement imprévisible des trajectoires évolutives des populations naturelles. L'impact d'une variation d'environnement sur la composition génétique de la population dépend à la fois de la durée d'exposition à cet environnement et de l'intensité de la sélection dans cet environnement. Une variation d'environnement ressentie comme peu intense affecte la population seulement lorsqu'elle est maintenue sur plusieurs générations et modifie en premier lieu la fréquence des allèles déjà présents à une certaine fréquence dans la population. Si la variation n'est pas maintenue elle n'a pas un rôle crucial dans l'émergence de nouveaux caractères adaptatifs, mais elle peut par contre jouer un rôle très important dans le maintien de la variabilité génétique des populations (par le simple fait de la fluctuation de la sélection ou par des stratégies de minimisation des risques ou « bet-hedging » par maintien de polymorphismes génétiques ; Philippi and Seger 1989; Beaumont et al. 2009). Dans le cas d'un changement ressenti comme fort, l'effet de la sélection peut être rapide et l'adaptation à court-terme peut reposer sur des allèles présents à très faibles fréquences dans les populations. Par exemple, un traitement antibiotique est ressenti comme un stress extrême pour une population bactérienne: tous les phénotypes susceptibles à l'antibiotique sont éliminés de la population à terme. S'il existe un ou des phénotypes résistants, ils envahissent très rapidement la population. Cet exemple illustre bien les variations d'effets qu'il peut y avoir entre différents contextes évolutifs et à quel point il est nécessaire de pouvoir

quantifier et comparer ces environnements pour comprendre les trajectoires évolutives. Dans le cas de plusieurs environnements pris au hasard (par exemple différentes espèces ou variétés de plantes exploitées par un ravageur), on ne voit *a priori* pas bien, comment classer ces environnements en fonction des contraintes sélectives ressenties par la population. Une alternative plus intuitive (et largement exploitée depuis longtemps par exemple dans Wilson and Bell 1990) pour comparer les contraintes entre différents environnements consiste à se placer le long d'un gradient environnemental. Cette option a été adoptée dans les expériences d'évolution réalisées au cours de la thèse.

- Compromis adaptatifs entre environnements

Une deuxième question qui se pose dans un contexte environnemental variable c'est à quel point est-il possible de s'adapter à plusieurs environnements en même temps ? Comment la valeur sélective d'une population dans un environnement varie le long de sa trajectoire adaptative dans un autre environnement ? Un large corpus d'expériences d'évolution en laboratoire montre que l'adaptation à long terme dans un environnement constant, conduit souvent à une spécialisation pour cet environnement (résumé dans Kassen 2002). La spécialisation va de pair avec l'existence de compromis adaptatifs dans d'autres environnements, c'est-à-dire qu'un phénotype optimal dans un environnement sera nécessairement sub-optimal dans un autre. Ces compromis émergent soit d'un antagonisme direct d'un caractère phénotypique entre différents environnements (par exemple une souris ne peut pas avoir à la fois un pelage clair et foncé qui lui permet d'être camouflé dans des environnements de différentes teintes), soit comme une conséquence indirecte des caractères adaptatifs (par exemple une mutation sur les enzymes de réPLICATION de l'ADN peuvent permettre à une bactérie de devenir résistante aux antibiotiques qui les ciblent mais ont un effet négatif sur le métabolisme de la cellule, qui est révélé en absence de l'antibiotique : le « coût » de la résistance). Ces compromis adaptatifs sont classiquement représentés dans des paysages adaptatifs « restreints » (où seulement un ou deux caractères phénotypiques sont représentés) par des positions différentes d'optimums phénotypiques définis par une fonction concave de fitness (généralement gaussienne) qui change selon l'environnement.

L'existence de compromis adaptatifs entre environnements (et donc de différents optimums phénotypiques dans le paysage) peut être facilement révélée par des expériences d'évolution en laboratoire. Par contre il est plus difficile de les mettre en évidence dans les populations naturelles et, même en laboratoire, il existe des cas où ces compromis ne sont pas révélés (Bennett and Lenski 2007; Hereford 2009; Gallet et al. 2014). Parmi les explications possibles à cela (détaillées dans l'introduction du chapitre 2), il y a le fait que ces compromis ne sont en fait

attendus que tardivement au cours de la trajectoire adaptative à un environnement, lorsque la population s'est optimisée pour son milieu de sélection. Une autre explication pourrait simplement être que ces compromis soient faibles et donc difficilement mesurables entre des environnements « proches ». [Encore une fois la nécessité de définir cette notion de *distance* entre environnement s'impose]. Ces situations peuvent être qualitativement illustrées dans un paysage adaptatif caricatural qui intègre plusieurs environnements comme représenté en figures 3 et 4. Plusieurs éléments importants en ressortent :

- D'abord la dynamique évolutive dans un environnement impose une dynamique dans l'autre environnement. La proportion de mutations bénéfiques dans les deux environnements considérés diminue au fur et à mesure que la population progresse vers un des optimums (figure 3). Cela implique concrètement que les mutations à la base de compromis sélectifs ont une plus grande probabilité d'être sélectionnées à proximité de l'optimum phénotypique (donc tardivement au cours de l'adaptation). Cela implique aussi, qu'en théorie, les distributions des effets sélectifs des mutations aléatoires d'un phénotype dans les deux environnements contiennent l'information pour replacer la population dans le paysage adaptatif. Cette théorie est quantifiée dans Martin et Lenormand (2015), sous la forme d'une distribution analytique qui dépend de paramètres de distances aux optimums et de l'angle entre les deux environnements à la position du génotype considéré. Cependant, la théorie ne tient pas compte des potentiels modules mutationnels explicités plus haut, de l'anisotropie du paysage ou d'une topographie de paysage plus complexe avec plusieurs pics dans un environnement.
- Deuxièmement, la figure 4 montre qu'il existe plusieurs façons de représenter des situations où les compromis adaptatifs sont faibles en supposant un phénotype bien adapté à un environnement. La première façon est de positionner les optimums proches dans le paysage. La deuxième façon est de considérer des optimums à une certaine distance mais d'introduire une variation de l'intensité de la sélection entre les environnements, telle que la variation de valeur sélective « nette » est faible. Concrètement, à quel point les variations d'environnements modifient l'une ou l'autre de ces caractéristiques? On peut se demander quelle est la part de ces différents effets (changement de l'optimum, ou de la force de la sélection) et s'il existe des cas extrêmes où seul un des effets prévaut? Plusieurs éléments de réflexions et de méthodologie autour de ces questions sont apportés dans les travaux de la thèse.

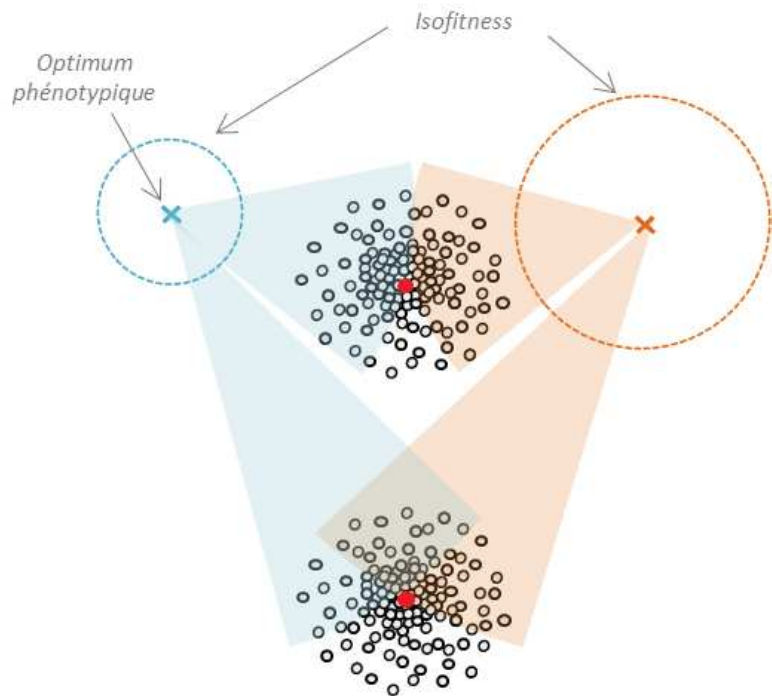


Figure 3 : Dynamique d'adaptation dans deux environnements dans un espace phénotypique à deux dimensions. La proportion de mutants (contours noirs) bénéfiques (représentés par les mutants inclus dans les faisceaux colorés associés aux environnements) dans les deux environnements diminue lorsque la lignée (point rouge) se rapproche d'un ou des optimum(s).

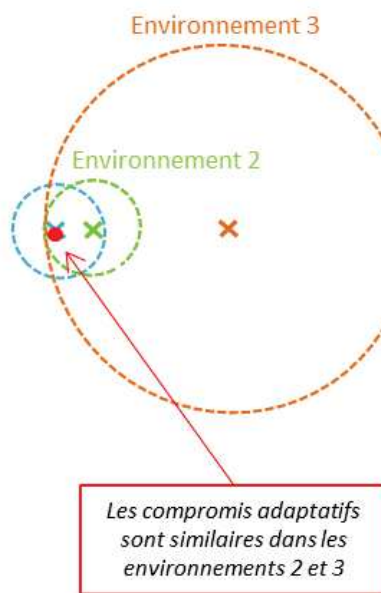


Figure 4 : Représentation des compromis adaptatifs dans un espace phénotypique à deux dimensions. Les croix représentent la position des optimums phénotypiques de différents environnements dans un espace phénotypique, et les cercles à un contour d'isofitness associé à l'environnement. La lignée (point rouge) adaptée à l'environnement 1 (bleu) montre des compromis adaptatifs de même ampleur dans les environnements 2 (vert) et 3 (orange).

- Environnement biotique au sein des lignées évolutives

Comme discuté plus haut dans l'introduction, la vision de l'environnement comme une composante uniquement abiotique passe à côté d'une composante majeure des pressions sélectives: les pressions biotiques générées par les interactions entre génotypes/populations/espèces. Ces interactions interviennent y compris dans l'évolution des lignées bactériennes en conditions contrôlées au laboratoire. Dans ce système, la forme dominante d'interaction est la compétition entre les génotypes qui émergent de différentes mutations dans une même lignée. En reprenant la décomposition caricaturale du processus de sélection périodique des lignées (Atwood et al. 1951; Barrick and Lenski 2013): d'abord des mutations aléatoires sont générées à partir d'un génotype, une partie est perdue par dérive génétique et les mutations bénéfiques restantes augmentent en fréquence par l'effet de la sélection. Les mutations de plus forts effets envahissent rapidement la population et se retrouvent en compétition les unes avec les autres. Cette compétition peut être maintenue pendant plusieurs générations entre des clones qui ont des valeurs sélectives proches. Pendant cette phase de compétition, de nouvelles mutations émergent dans les différentes lignées clonales. La sélection opère alors sur l'effet global des différents fonds génétiques. L'interférence clonale, c'est-à-dire le fait que des mutations qui ont un effet bénéfique soient éliminées lorsqu'elles sont associées à un fond génétique peu compétitif, est considéré comme freinant l'adaptation (par exemple dans Gerrish and Lenski 1998; De Visser and Rozen 2005; Fogle et al. 2008). Le même phénomène, ou effet « Hill-Robertson » se produit plus généralement dès lors que la recombinaison est limitée (Felsenstein 1974).

- Interactions de fréquence-dépendance et maintien de la diversité

Les attendus évolutifs sont plus complexes à décrire lorsque les interactions biotiques prennent une forme de sélection fréquence-dépendante. Dans ce cas la métaphore du paysage adaptatif classique perd beaucoup de sa pertinence. Il faudrait en effet considérer des paysages complexes, qui changent au fur et à mesure des changements de fréquence, formant des boucles de rétroactions difficiles à modéliser. La sélection fréquence-dépendance négative émerge le plus souvent d'interactions entre individus (Felsenstein 2017) qui peuvent être grossièrement classées entre :

- des causes écologiques : spécialisation pour différentes niches écologiques existantes dans l'environnement (par exemple différentes ressources), générées par un des protagonistes (bioproduits utilisés comme ressource ou bénéfices fournis), un des protagonistes est la

ressource de l'autre (prédatation, parasitisme, sélection apostatique incluant un troisième protagoniste).

- des causes comportementales : interactions favorisant différents types (sélection de parentèle, stratégies de minimisation des risques, « phénotypes tricheurs »)

Il est fort probable que la sélection fréquence-dépendance soit souvent impliquée par au moins une de ces causes dans les trajectoires évolutives de populations naturelles. Quelles en sont les conséquences ? En règle générale, la sélection fréquence-dépendante négative est vue comme un mécanisme assurant le maintien de la diversité (e.g. in Turner et al. 1996; Gigord et al. 2001; Weeks and Hoffmann 2008; Takahashi and Kawata 2013; Healey et al. 2016). A une certaine échelle temporelle, cette forme de sélection va en effet faire converger les partenaires de l'interaction (génotypes/populations/espèces, j'emploie le mot générique « type » ci-dessous) vers une fréquence intermédiaire d'équilibre. Cependant, à plus long terme, des processus d'innovation génétique (discuté tout au long de l'introduction) peuvent faire « pencher la balance » dans les deux sens: soit en renforçant la coexistence soit au contraire en donnant un avantage définitif à un des types sur les autres. Par exemple, les adaptations qui permettent à deux morphes de se spécialiser sur deux niches différentes peuvent tendre à maintenir la coexistence. Au contraire des adaptations phénotypiques inégales, par exemple sur une niche partagée, peuvent tendre à favoriser un type par rapport à l'autre. Il est probable que dans ce dernier cas, une rétroaction négative s'exerce en plus sur le taux d'adaptation du type désavantage dont les effectifs réduisent. Cela pourrait conduire à l'extinction de ce type. Encore une fois il est plus que probable que ces interactions soient régies par des dynamiques temporelles (degré de divergence entre les types) et environnementales (hétérogénéité du paysage qui définit les niches écologiques présentes; fluctuations environnementales qui interviennent dans le degré de spécialisation pour différent(e)s environnements/niches). Par exemple le cas d'un polymorphisme émergeant dans une population bien adaptée à une niche ancienne et le cas de deux espèces mis en présence d'un nouvel environnement peuvent s'avérer différents sur bien des aspects. Dans le premier cas le potentiel de divergence des populations sur l'exploitation de la niche ancienne est faible, en particulier lorsque les génotypes des deux types peuvent se recombiner. Au contraire dans le deuxième cas les divergences adaptatives sont favorisées par l'absence de recombinaison et des fonds génétiques très différents. Comment fonctionnent ces dynamiques d'adaptation ? A quel point sont-elles déterminées par l'environnement ? Peut-on prévoir quand les polymorphismes sont amenés à être maintenus ou non ? Les modèles d'adaptation qui prennent en compte le degré de complexité nécessaire pour répondre à ces questions sont encore rares. Il reste aussi beaucoup de contextes qui n'ont pas

été explorés expérimentalement: les expériences d'évolution ont encore beaucoup à nous dire sur tout ce qui se cache dans les observations de terrain.

Plan de la thèse

Les problématiques présentées dans cette introduction seront abordées dans les chapitres de la thèse à partir de résultats d'expériences d'évolution sur des bactéries dans des environnements antibiotiques. Malgré les spécificités de ce modèle biologique, nous tentons de garder une approche large et généralisable des processus évolutifs au travers des modèles théoriques utilisés. Cependant, les discussions se placent sur plusieurs niveaux en incluant également la question de la résistance aux antibiotiques. Cet aspect spécifique a été peu discuté dans l'introduction mais il se pose comme un bon exemple de processus évolutif et une illustration des intérêts concrets qui se cachent derrière ces approches fondamentales.

Chapitre 1: « *Fisher's geometrical model and the mutational patterns of antibiotic resistance* ». Ce chapitre porte sur les informations du paysage adaptatif reflétées par les effets sélectifs de mutants résistants criblés à différentes doses d'antibiotique.

Chapitre 2: « *Fitness trade-offs in the evolution of bacterial antibiotic resistance at different concentrations along a gradient* ». Ce chapitre présente l'analyse des profils de fitness le long d'un gradient de doses d'antibiotique, de lignées évolutives obtenues après évolution à différentes doses.

Chapitre 3: « *Mapping the topography of adaptive fitness landscapes across environments: An experimental landscape for bacterial adaptation across an antibiotic dose gradient* ». Dans ce chapitre les données de deux précédents chapitres sont utilisées pour reconstruire un paysage adaptatif intégrant les différents environnements (doses). A travers cet exemple nous proposons des méthodes générales pour reconstruire ce type de paysage.

Chapitre 4: « *Fast evolution of frequency-dependent selection between coexisting species of bacteria* ». Ce chapitre présente les résultats d'expériences de suivi d'une coévolution en laboratoire à long-terme entre deux bactéries sous sélection fréquence-dépendante.

Les grandes lignes de ces chapitres seront ensuite reprises dans la dernière partie de discussion et des perspectives à ces travaux seront présentées.

Fisher's geometrical model and the mutational patterns of antibiotic resistance across dose gradients

Harmand Noémie¹, Gallet Romain², Jabbour-Zahab Roula¹, Martin Guillaume³, Lenormand Thomas¹

1. UMR 5175 CEFE, CNRS - Université Montpellier - Université P. Valéry - EPHE, Montpellier Cedex 5, France
2. INRA - UMR BGPI, Cirad TA A-54/K Campus International de Baillarguet 34398 Montpellier Cedex 5, France
3. Institut des Sciences de l'Evolution de Montpellier, UMR CNRS-UM II 5554, Université Montpellier II, 34 095 Montpellier Cedex 5, France

Abstract

Fisher's geometrical model (FGM) has been widely used to depict the fitness effects of mutations. It is a general model with few underlying assumptions that gives a large and comprehensive view of adaptive processes. It is thus attractive in several situations, for example adaptation to antibiotics, but comes with limitations, so that more mechanistic approaches are often preferred to interpret experimental data. It might be possible however to extend FGM assumptions to better account for mutational data. This is theoretically challenging in the context of antibiotic resistance because resistance mutations are assumed to be rare. In this article, we show with *Escherichia coli* how the fitness effects of resistance mutations screened at different doses of nalidixic acid vary across a dose-gradient. We found experimental patterns qualitatively consistent with the basic FGM (rate of resistance across doses, gamma distributed costs) but also unexpected patterns such as a decreasing mean cost of resistance with increasing screen dose. We show how different extensions involving mutational modules and variations in trait covariance across environments, can be discriminated based on these data. Overall, simple extensions of the FGM accounted well for complex mutational effects of resistance mutations across antibiotic doses

Keywords

Escherichia coli, fitness cost, fitness landscape, adaptation, trade-offs



Fisher's geometrical model and the mutational patterns of antibiotic resistance across dose gradients

Noémie Harmand,^{1,2} Romain Gallet,³ Roula Jabbour-Zahab,¹ Guillaume Martin,⁴ and Thomas Lenormand¹

¹UMR 5175 CEFE, CNRS—Université Montpellier—Université P. Valéry—EPHE, Montpellier Cedex 5, France

²E-mail: noemie.harmand@cefe.cnrs.fr

³INRA—UMR BGPI, Cirad TA A-54/K Campus International de Baillarguet 34398 Montpellier Cedex 5, France

⁴Institut des Sciences de l'Evolution de Montpellier, UMR CNRS-UM II 5554, Université Montpellier II, 34 095 Montpellier cedex 5, France

Received April 5, 2016

Accepted October 25, 2016

Fisher's geometrical model (FGM) has been widely used to depict the fitness effects of mutations. It is a general model with few underlying assumptions that gives a large and comprehensive view of adaptive processes. It is thus attractive in several situations, for example adaptation to antibiotics, but comes with limitations, so that more mechanistic approaches are often preferred to interpret experimental data. It might be possible however to extend FGM assumptions to better account for mutational data. This is theoretically challenging in the context of antibiotic resistance because resistance mutations are assumed to be rare. In this article, we show with *Escherichia coli* how the fitness effects of resistance mutations screened at different doses of nalidixic acid vary across a dose-gradient. We found experimental patterns qualitatively consistent with the basic FGM (rate of resistance across doses, gamma distributed costs) but also unexpected patterns such as a decreasing mean cost of resistance with increasing screen dose. We show how different extensions involving mutational modules and variations in trait covariance across environments, can be discriminated based on these data. Overall, simple extensions of the FGM accounted well for complex mutational effects of resistance mutations across antibiotic doses.

KEY WORDS: *E. coli*, fitness cost, fitness landscape, adaptation, trade-offs.

Fitness landscape models have a long history in evolutionary biology, as they provide a rich and easily visualized topographical metaphor to describe adaptive processes. These landscapes take various forms (single peaked, multipeaked, rugged, moving, etc.) and focus on different quantities. Some follow a purely genotypic angle, directly assigning fitness values to specific genotypes (sequence space models in Maynard Smith 1970, NK models in Kauffman and Levin 1987; Kauffman and Weinberger 1989, “empirical” models in Weinreich et al. 2005, 2006, “house of cards” models in Gillespie 1983; Orr 2002, 2003). Others are phenotype based: genotypes determine phenotypes, which in turn determine fitness. These latter models are diverse: some borrow from quantitative genetics (Fisher 1930) others from “systems biology” (i.e., they represent organisms by explicitly modeling some integrated

phenotype such as metabolism, metabolic theory in Kacser and Burns 1973; flux balance analysis in Ibarra et al. 2002; Papp et al. 2004; Segre et al. 2005). These models are useful as they describe mutational inputs and therefore allow a complete description of the evolutionary process (mutation, selection) when coupled with standard population/quantitative genetics equations. However, they are difficult to calibrate and compare. Models inspired from “systems biology” take a realistic approach (sensu Levins 1966) but can be difficult to extrapolate beyond the context they were built for. For instance, metabolic theory concerns changes in metabolic pathways, but many organismal-level traits are not directly metabolic. On the contrary, models inspired from quantitative genetics take a more general approach, which make them more widely applicable. However, they are often neither

very precise in particular examples nor very realistic in terms of underlying traits and processes. (e.g., Fisher's geometrical model, Fisher 1930; Hartl and Taubes 1996; Orr 2000; Martin and Lenormand 2006a; Waxman 2006).

Recently, much effort has been devoted to obtain data on the fitness effects of mutations in many organisms (Eyre-Walker and Keightley 2007), which could be used to tease apart alternative models (Martin and Lenormand 2006a; Bataillon et al. 2011; Rokyta et al. 2011; Blanquart et al. 2014; Chou et al. 2014; Blanquart and Bataillon 2016). Fisher's geometrical model (hereafter FGM) is general and parsimonious in terms of parameters. An organism is modeled by a vector of several phenotypic trait values, each trait being under stabilizing selection around an optimum value. Mutational effects are then described by a multivariate change in these trait values. Thus, it provides an attractive baseline model to make testable predictions. For instance, Gaussian versions of this general model give relatively accurate predictions for the variation of the Distribution of Fitness Effects (hereafter DFE) among random mutations across environments (Martin and Lenormand 2006b), for the dominance of mildly deleterious mutations (Manna et al. 2011), for pairwise epistasis (Martin et al. 2007), or for fitness trajectories (Gordo et al. 2013; Perfeito et al. 2014). Yet, the FGM seems less successful in predicting observed epistasis patterns among resistance mutations (Blanquart and Bataillon 2016). As pointed out long ago, the FGM fails to predict genotypic parallel evolution despite overwhelming evidence of the phenomenon (Shull 1935; Lenormand et al. 2016), unless within-genome mutational heterogeneity (hereafter "modularity") is taken into account (Chevin et al. 2010). Modularity refers to the fact that the distribution of the phenotypic effects of mutations differs across different portions of the genome, these portions being called "modules". The FGM also fails to predict the dominance of mutations of large effect and the occurrence of lethals (Manna et al. 2011). Finally, various versions of the model may not be distinguishable from the sole shape of observed DFEs. For example, many correlated traits (anisotropic model) may yield the same DFE as a few uncorrelated ones (isotropic model) (Martin and Lenormand 2006a).

In practice, the FGM could be particularly useful to predict evolutionary responses in regimes where the standard quantitative genetics assumptions are not met. For instance, it includes responses to abrupt and intense environmental changes in natura (e.g., use of pesticide, antibiotics, pollution) where genetic variation for adaptation may be initially limiting. However, the basic FGM relies on a statistical description of fitness effects formulated in the context of a large number of possible phenotypic effects. This approach may be limiting in situations where only a handful of beneficial mutations are possible. Yet, such situations with strong selection pressures are particularly important to model and predict. In this case, a first option is to abandon the basic FGM

for other models. Another option would be to extend it to better capture the outcomes of such situations. As with any model extension, the difficulty remains in doing it in a disciplined manner that does not impair its fundamental interest (see e.g., Dawkins 2004), by minimally incorporating necessary extra ingredients. In this article, we investigate whether FGM-like models are sufficient and robust enough to accurately describe mutational patterns in very stressful environments. We used antibiotic resistance as empirical illustration, as it is one emblematic biological situation where the problem of predictability is most acute.

A fundamental appeal of the FGM is its ability to easily extrapolate mutational effects over genetic backgrounds and environments, thus providing a quantitative null model for adaptation in realistic/complex situations. Different genetic backgrounds are modeled by shifts in the position of the ancestral phenotype, while environmental variations are modeled by changes in phenotypic optima, as in quantitative genetics models (e.g., Duputié et al. 2012; Polechová and Barton 2015). Additionally, several other parameters of the FGM might vary across environments. (1) The overall intensity of selection may vary according to the strength of the environmental stress. (2) The magnitude and direction of mutational and selective covariances may change among environments. (3) The mutational contribution of different "modules" (as defined earlier) may vary among environments. We investigate these possibilities using experimental patterns of mutational effects of *Escherichia coli* resistant mutants screened at various doses of nalidixic acid (hereafter Nal). As a fluoroquinolone antibiotic, Nal blocks DNA replication by inhibiting the activities of gyrase and topoisomerase IV enzymes. Resistance mechanisms of *E. coli* to quinolone antibiotics have been intensely investigated (Hooper 1999; Hopkins et al. 2005; Jacoby 2005), notably using clinical isolates. Different chromosomal resistance mutations have been described in six genetic regions. Mutations in *gyrA*, *gyrB*, *parC*, or *parE* result in a decrease of the antibiotic affinity on targeted enzymes. Mutations in the *marOR* and *acrR* sequences, controlling the expression of membrane porins, result in a decrease of the uptake of the antibiotic in the cell or the increase of the efflux of the antibiotic out of the cell. Different studies showed that those mutations confer various degrees of resistance (Hane and Wood 1969; Zhou et al. 2000), but without providing an overall picture of their fitness effects across doses. In this study, we first show how the three FGM extensions presented earlier can be matched with specific mutational patterns. We then describe the mutational patterns experimentally observed along a Nal dose gradient, providing a comprehensive view of the fitness effects of Nal resistant mutants. We finally confront those patterns with the predictions formulated under extended-FGMs. This approach suggests that those limited extensions capture fairly complex (and sometimes unexpected) mutational patterns as observed in our data.

Experimental Methods

BACTERIAL STRAINS AND MEDIA

All strains are derived from *E. coli* strain REL4536, corresponding to the 10,000th generation of Lenski's long-term adaptation experiment to the medium DM25 (Lenski and Travisano 1994). The cyan fluorescent protein (CFP) and yellow fluorescent protein (YFP) genes were introduced separately in REL4536 chromosomal DNA to discriminate competing strains (see Gallet et al. 2012 for details). Preparation of Nal and media are detailed in Supplementary Material 1. Resistant mutants were screened on LBA-Nal petri-dishes and kept at -80°C in 15% glycerol. Competition assays were performed in fresh medium DM250 supplemented with Nal prepared weekly.

MUTANTS SCREEN AND MUTATION RATE

TO RESISTANCE

The MIC of REL4536-YFP strain was 2.6 $\mu\text{g.mL}^{-1}$ Nal under our conditions. Fluctuation tests (Lurias and Delbrück 1943) (Supplementary Material 2) were performed at 3, 5, 8, 12.5, and 20 $\mu\text{g.mL}^{-1}$ Nal (hereafter, referred to as screen doses) to screen for independent resistant mutations and to estimate the mutation rate toward resistance U_R at each screen dose with the P_0 estimator method (Lea and Coulson 1949) (Supplementary Material 3). From U_R data, we determined the corresponding proportion of new mutations conferring resistance, p_R , as $p_R = U_R/U$ where U is the genomic nonneutral mutation rate. We used $U = 0.0002$, estimated during *E. coli* exponential growth in LB in Kibota and Lynch (1996).

In fluctuation assays, mutations occur during the growth of the ancestral strain in the absence of Nal and are selected a posteriori on LBA Petri-dishes supplemented with the corresponding screen dose. Hence, the theoretical probability to screen double mutants is extremely low (Supplementary Material 4). Resistant mutants were screened based on their ability to form a visible colony after 48 hours on Nal-LBA Petri-dishes. 49, 60, 53, 60, and 20 resistant mutants among those screened at 3, 5, 8, 12.5, and 20 $\mu\text{g.mL}^{-1}$ Nal, respectively, were stored in glycerol stocks for subsequent competition experiments. Two successive fluctuation assays at 20 and 200 $\mu\text{g.mL}^{-1}$ Nal allowed the isolation of the highly resistant strain M200-CFP, with the resistance mutation 87Asn in the *gyrA* gene. It was stored, as well as the M200-YFP version (Supplementary Material 2), for later use as reference mutants in the competition experiments.

MUTANT SEQUENCING

A random subset of mutants (two-thirds) was sequenced at the *gyrA* gene, the most frequently observed genetic basis of Nal resistance in *E. coli*. The sequence covers most of the promoter and 32% of the *gyrA* gene, which includes all *gyrA* positions where resistance mutations have been observed previously (for

review see Hopkins et al. 2005) and particularly the complete quinolone resistance-determining region (Ala67-Gln106). Most known mutations occur in the latter region, which corresponds to the DNA-binding site (Yoshida and Bogaki 1990). PCR was performed on colonies, using the mix: 10 μL of 2X Phusion Master Mix (ThermoFisher Scientific, Waltham, MA), 1 μL of F-primer 5'-AGACAAACGAGTATATCAGGCA [*gyrA* sequence: -120pb to -101pb] and R-primer 5'-TTTACCAGTTCCGCAATCTTCTC [*gyrA* sequence: 823pb to 845pb], 6 μL sterile distilled water; the PCR program: 5' 95°C, 35 cycles of [1' 95°C, 1' 61°C, 2.5' 72°C], and 5' 72°C. Sequencing was performed by Eurofins mwg operon (Eurofins, Luxembourg). Mutations in *gyrA* gene were identified by comparative alignment against REL4536-YFP. Mutants were classified into two groups: *gyrA* (with a mutation in the sequenced part of *gyrA*) or non-*gyrA*.

COMPETITION EXPERIMENTS

For each resistant mutant (all marked YFP), four 24 hours competitions were performed: one against the ancestor (REL4536-CFP) in DM250 and three against the highly resistant strain M200-CFP in DM250 supplemented with 3, 8, or 12.5 $\mu\text{g.mL}^{-1}$ Nal (hereafter referred as measure dose). Using this resistant strain as a reference is necessary to perform competition in the presence of antibiotics, and is sufficient to capture variation in relative selection coefficients across doses. We assume that fitness effects are transitive, so that the difference among the selection coefficients of two mutants against M200-CFP reflects the selection coefficient between the two mutants, independently of the fitness of the reference mutant (this assumption has been shown to hold in a very similar experiment in Gallet et al. 2012).

Screen doses and mutant positions were randomized within microtiter plates among five series of experiments performed at different dates. Each initial mix was repeated twice independently, at two different dates (date replicates) and from each initial mix, two replicated competitions were performed (mix replicates). Two control replicates REL4536-CFP versus REL4536-YFP (resp. M200-CFP vs M200-YFP) were included in microtiter plates containing medium without (resp. with) antibiotic and included in statistical analyses (see detailed protocol in Fig. S1).

ESTIMATION OF SELECTION COEFFICIENTS

YFP and CFP fluorescence (F_Y and F_C , respectively) were used to estimate the log of competitor frequency ratio, based on a calibration curve. This curve was obtained using different mixes of REL4536-CFP and REL4536-YFP cultures in volume proportions ranging from 0% to 100%. After measuring each fluorescence F_Y and F_C , the relative numbers of YFP and CFP cells (n_Y and n_C) in each mix was estimated by counting 10^5 cells in a flow cytometer (Gallios, Beckman Coulter, Brea, CA) as detailed in Gallet et al. (2012). The following sigmoid curve model

(Supplementary Material 5) was then least-square adjusted (Mathematica 9.0, Wolfram Research, Champaign, IL) to the calibration data points:

$$\ln\left(\frac{F_Y}{F_C}\right) = \ln\left(\frac{1 + k_1 e^{\frac{n_Y}{n_C}}}{k_2 + k_3 e^{\frac{n_Y}{n_C}}}\right) \quad (1)$$

where k_1 , k_2 , and k_3 are estimated parameters of the calibration curve. The selection coefficient (s) per generation during a competition experiment was then computed directly as

$$s = \frac{1}{g} \left(\ln\left(\frac{n_{Y(T24)}}{n_{C(T24)}}\right) - \ln\left(\frac{n_{Y(T0)}}{n_{C(T0)}}\right) \right) \quad (2)$$

where the logarithm of cell number ratios was obtained by inverting the calibration equation (1) and using fluorescence measures at T0 and T24. This selection coefficient (per growth cycle) was scaled by $g = 6.64$, an approximation to the average number of divisions over a 24 h assay in DM250 without antibiotic.

A linear-mixed model (lmer in R 3.2.0, R Core Team) was performed on sequenced mutants to test for *measure dose*, *screen dose*, and *genetic basis* (i.e. *gyrA* vs non-*gyrA* mutants) as fixed effects and genotypes as well as plate-identity nested within date as random effects on selection coefficients, for all competitions including the controls. Model comparison and selection was performed based on AIC values (Table 1).

COST DISTRIBUTIONS ACROSS SELECTION DOSES

The DFE of mutants in the absence of antibiotics (so-called “cost” of resistance) refers to the distribution of selection coefficients of resistant mutants against their susceptible ancestor. The DFE was quantitatively analyzed by maximum likelihood, by fitting the following FGM theoretical predictions in multiple environments (Martin and Lenormand 2006a, 2008, 2015).

Assuming that the ancestor is optimal in the antibiotic-free environment, all mutants are deleterious in this environment as they are shifted from the optimum position. Then, under the FGM in n dimensions, the DFE among random mutations is a negative gamma distribution with shape $n/2$ (Martin and Lenormand 2006a, 2015). A similar DFE is expected among screened mutants, with a slightly smaller shape $(n - 1)/2$ and a shift toward deleterious effects by some “incompressible cost” (c_{min} , generally small). This incompressible cost corresponds to the fitness distance of the boundary of the screen zone to the optimum in the antibiotic-free environment (Martin and Lenormand 2015). In our case, for all screen doses, we thus expect cost distributions to follow a gamma distribution plus a minimal cost $c_{min} > 0$. The observed selection coefficients S were assumed to result from genetic effects s , following a displaced negative gamma distribution,

plus a measurement error, normally distributed with variance σ^2 that is

$$S|s \sim N(s, \sigma^2), \quad s \sim -\Gamma(a, \bar{c}/a, 1, c_{min}), \quad (3)$$

where $\Gamma(., ., ., .)$ is the generalized Gamma distribution as parameterized in Mathematica 9.0. Parameter a measures the shape of this distribution, \bar{c} its mean and c_{min} its location. We investigated whether these parameters varied with the *screen dose* and/or the *genetic basis* (*gyrA* vs non-*gyrA* mutants) and whether an incompressible cost was detectable. We only used data corresponding to sequenced mutants (so that they could be classified into *gyrA* or non-*gyrA* categories). The likelihood of this model was expressed analytically (Supplementary Material 6) and maximized numerically using Mathematica. Model selection was based on AIC ranking (Burnham and Anderson 2002). Goodness-of-fit was evaluated by randomly sampling 800 virtual datasets mimicking our data structure and simulated under the best model. The goodness-of-fit was estimated as the proportion of simulated datasets with a lower likelihood than the empirical one.

Results: Describing Resistance in Single-Peak Phenotype Landscape Models

Before explaining experimental results, we briefly describe predictions on mutational patterns expected under basic and extended versions of the FGM (see Martin and Lenormand 2006a, 2015; Orr 2006 for details). In FGM, phenotypes are defined by a combination of multiple continuous traits. Figure 1 illustrates landscapes with a phenotypic space in one dimension for simplicity. In a given environment, phenotypic traits are under Gaussian stabilizing selection, defining a global phenotypic optimum (single peak). In our experiment, we consider that the ancestor phenotype is close to the phenotypic optimum of the environment without antibiotic (because the strain REL4536 adapted to this environment for 10,000 generations). The position of the phenotypic optimum is thus necessarily shifted when antibiotic is present in the environment since the ancestor has very low fitness in antibiotic environments.

In the classic FGM (all cases of Fig. 1), mutation effects are identically and normally distributed around the ancestor phenotype. A mutation is represented by a shift from the ancestor position in phenotypic space. Furthermore, a “resistance mutation” in a given antibiotic environment, must lie in a region (hereafter referred to as “screen-zone”) where phenotypes have absolute fitness above some threshold corresponding to the limit of growth in that environment. The size and position of the screen zone is determined by the width of the fitness function (inversely proportional to the intensity of selection) and the optimum position

Table 1. Model simplification for selection coefficients of mutant and control competitions in presence of antibiotic among screen doses (SD), measure-doses (MD), and genetic basis (GB, i.e., *gyrA* or non-*gyrA* mutant).

Model	Fixed effects							ΔAIC
	SD	MD	GB	SD:MD	SD:GB	MD:GB	SD:MD:GB	
1	1	1	1	1	1	1	1	0
2	1	1	1	1	1	1	0	55.9
3	1	1	1	1	0	1	0	61.3
4	1	1	1	1	1	0	0	275.5
5	1	1	1	1	0	0	0	280.8
6	1	0	1	1	0	0	0	376.7
7	1	1	1	0	1	1	0	666.9
8	1	1	1	0	0	1	0	672.2
9	0	1	1	0	0	1	0	788.8
10	1	1	1	0	1	0	0	1837.8
11	1	1	1	0	0	0	0	1842.9
12	1	0	1	0	1	0	0	3111.6

Each line corresponds to a mixed model (lmer function, package lme4 in R 3.2.0) with random effects on genotype, date, and plate. For each model, the difference between Akaike information Criterions (ΔAIC) with the best model (model 1) allows model comparison.

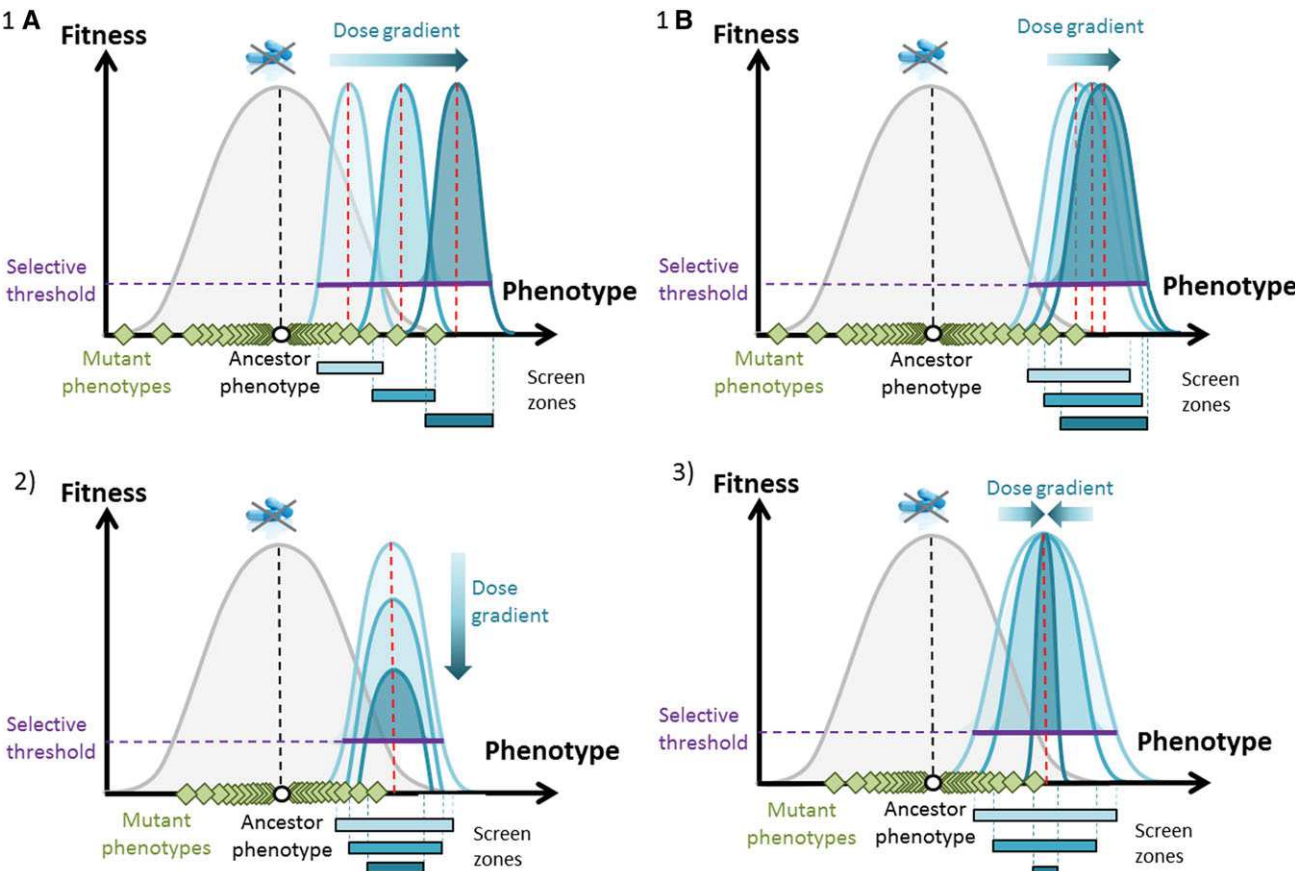


Figure 1. Scenarios of antibiotic dose effects on simple fitness landscapes. The ancestor phenotype (white dot) is optimal in the environment without antibiotic (fitness function given by the gray curve). Increasing antibiotic doses generate different fitness functions, indicated by increasingly dark blue curves. Screen dose may affect 1A–B the optimum, (2) the maximum, or (3) the curvature of the fitness function. The horizontal segment shows the threshold of positive growth. Phenotypic effects of random mutations (diamonds) are normally distributed around the ancestor phenotype. Resistant phenotypes can be screened within the phenotypic interval delimited by the growth threshold: the “screen zones”, indicated by horizontal segments below the x-axis, with the corresponding color of each dose.

at the screen dose. As commonly observed and confirmed in our data, resistant mutants remain relatively rare among random mutants, at all screen doses (Fig. 4). The scale of random mutation effects around the ancestor must thus be narrow relative to the distance to any antibiotic optimum. A corollary is that screened mutants will tend to accumulate in the region of the screen zone closest to the ancestral phenotype (left part of the segments in Fig. 1). Finally, in these conditions, the cost of a given resistance is determined by the distance between the mutant and the ancestral phenotype. In the following, we first present mutational patterns independently and specifically associated with the three FGM extensions that we consider, using simple and useful examples that are not necessarily connected to our data. Second, we present experimental results and discriminate landscape features associated with our case study using our experimental patterns.

EXTENSION 1: SELECTION INTENSITY VARIATION AMONG ENVIRONMENTS

In the basic FGM (cases 1a and 1b, Fig. 1), environmental variation is modeled by a shift in optima, everything else being equal. This is particularly useful to represent selection on an environmental gradient: optima gradually shift away from the optimum of the reference environment. However, other features of FGM could potentially vary along an environmental gradient: the maximal fitness may decrease with dose (case 2, Fig. 1) or the selection intensity may decrease with dose (case 3, Fig. 1). In these three extreme cases and their intermediates, the mutation rate toward resistance decreases with increasing screen dose. Case (2) is easily distinguished from (1) and (3) as it predicts that the relative fitness of mutants should stay identical across all measure doses (since the fitness function is just shifted and relative fitness is given by differences in Malthusian fitness). Cases (1) and (3) can also be distinguished on the basis of relative fitness patterns across doses, but it is more challenging. Case (1) already encompasses different situations depending on how the distance between optima scales with the width of fitness functions (intensity of selection), or simply how screen-zones overlap. If the distance between optima is large compared to the intensity of selection (case 1a, Fig. 1), a dose-specialization pattern arises across both measure doses and screen doses. In this case, mutants have their highest fitness in the dose where they were screened and they also have a higher fitness in this dose than mutants screened at other doses. Furthermore, no generalist mutants are selected, precisely because screen zones show little overlap. Alternatively, if the distance between optima is small compared to the intensity of selection (case 1b, Fig. 1), screen zones largely overlap: “generalist” mutants may be screened across widely differing doses. The average fitness of mutants should increase with the screen dose (for any measure dose), as mutants tend to cluster at the edge of their screen zone. The fitness of each mutant should also decrease with the

measure dose as they do not overshoot dose optima. Case 3, however, mimics patterns of case 1b, without involving changes in optima positions. Mutants screened at high doses (within the dark blue area) are closer to the optimum, and on average have a higher fitness at all measure doses than mutants screened at lower doses (within light blue areas). Screen zones fully overlap so that generalist mutants can also be obtained. Finally, as the fitness function is steeper at higher doses, mutant fitness profiles consistently decrease along measure doses.

EXTENSION 2: TRAIT-COVARIANCE VARIATION AMONG ENVIRONMENTS

Although presented in one dimension, the qualitative arguments above directly extend to multiple dimensions when considering an isotropic landscape (where all phenotypic traits are equivalent for mutation and selection), as represented in two dimensions in Figure 2A. Blue circles delimit screen zones for antibiotic environments and red dotted circles show isofitness curves in the antibiotic-free environment. In this case, as in all cases of Figure 1, the mean fitness cost of resistance mutations increases when screen dose increases. Anisotropy, whereby mutational and selective effects covary among traits (depicted by ellipses instead of circles on Fig. 2B), can alter this conclusion. If the covariances change across environments, fitness patterns also depend on variations in the favored directions of selection across doses. For example, on Figure 2B, the direction of ellipses is unchanged from the antibiotic-free (dashed) to a low antibiotic dose environment (light blue), but changes at a higher dose (dark blue). In this case, the low dose favors mutants along phenotypic directions that are strongly selected against, in the antibiotic-free environment, whereas high dose favors mutants along directions that are only weakly selected against, in the antibiotic-free environment. Thus, with the same optimum and the same selection intensity, these changes of covariance lead to a pattern of decreasing fitness costs with increasing screen dose.

EXTENSION 3: MODULAR MUTATIONAL VARIATION AMONG ENVIRONMENTS

In the basic FGM, total pleiotropy is assumed meaning that each mutation impacts all traits. “Modularity” is ignored so that mutation effects from distinct genetic targets are sampled in the same distribution. For instance, in Figure 3A, mutations on two parts of the genomes (dot and square) occur in the same phenotypic space and with the same distribution. A straightforward expectation in this case is that the proportion of dot versus square resistant mutants should stay constant at any screen dose (screen zones illustrated by the different grey contours). Note however, that this proportion, even if constant, can be strongly biased toward either square or dot mutants: the case where square mutants are less likely (smaller mutational target) is illustrated on Figure 3A.

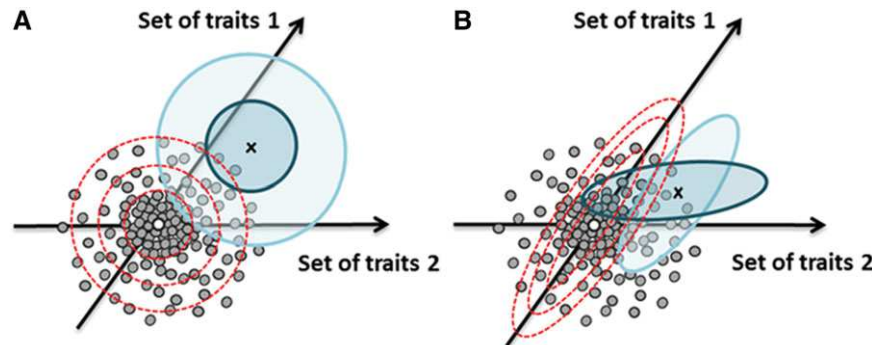


Figure 2. Isotropy versus anisotropy in fitness landscape models. The white dot marks the ancestor phenotype optimal in the nonantibiotic environment. Gray dots show mutant phenotypes arising from the ancestor. The cross indicates the unique optimal phenotype position in two doses of antibiotic (darker blue = higher dose) with circles (A) or ellipses (B) showing the corresponding screen zone. Dotted circles/ellipses illustrate isofitness curves in the environment without antibiotic. (A) An isotropic model yields patterns roughly similar to the 1D landscape in Fig. 1 case 2b. Anisotropic models (variations in selective covariance) may lead to variations in the resistant phenotypes screened at different doses.

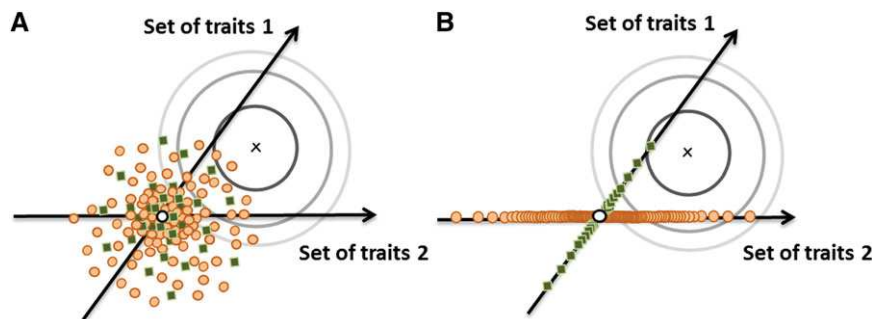


Figure 3. Modularity in fitness landscape models. The white dot marks the ancestor phenotype, optimal in the non-antibiotic environment. Orange dots and green squares represent mutant phenotypes arising from the ancestor in two different genes ("dot" and "square" genes, the latter is a larger target generating more mutants). The cross indicates the common optimal phenotype for three increasing doses of antibiotic (Fig. 1 case 3) illustrated by the gray circles showing the screen zone for each dose (indicated by the grayscale level). (A) Isotropic modules lead to a constant proportion of dotted and squared mutants screened at every screen dose. (B) Anisotropic modules may lead to variation in the proportion of dotted and squared mutants screened among screen doses. Here, the square gene is overrepresented at higher doses (although it is a smaller target).

A simple extension of this basic formulation is that the phenotypic effects of mutations occurring in different genomic regions are drawn in different distributions and possibly impact different subsets of traits. These regions can then be viewed as different "modules" (*sensu* Chevin et al. 2010). For instance, on Figure 3B, mutations on the dot and square modules occur in different phenotypic subspaces (i.e., only on the axes on the sketch, but more generally these axes represent hyperplanes in n dimensions). A straightforward expectation in this case is that the proportion of dot and square resistant mutants could further vary among screen doses if the optima are not equally distant to each subspace. For instance, if the screening optimum is closer to the square axis (as sketched on Fig. 3B), mutations in square modules should become overrepresented when selection intensity increases (screen zones are tightening on

Fig. 3B) or if optima positions become closer and closer to this axis (not shown).

Results: Experimental Patterns

THE PROPORTION OF RESISTANCE MUTATIONS DECREASES WHEN SCREEN DOSE INCREASES

The proportion of resistance mutations, P_R , decreased log-log linearly with the screen dose ($P_R = 0.00025 \text{ screen dose}^{-2.12}$, $R^2 = 0.98$) (Fig. 4). For the screen dose $3 \mu\text{g.mL}^{-1}$ Nal, which is just above the MIC, the probability of resistance is already very low (c.a. 5×10^{-5}), as expected given that any dose above the MIC is already very stressful. This probability then decreases sharply with increasing screen dose: at $20 \mu\text{g.mL}^{-1}$ Nal, our highest screen dose, it is two orders of magnitude lower (c.a. 5×10^{-7})

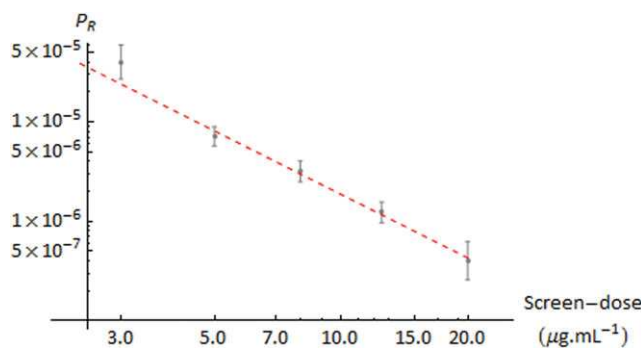


Figure 4. Inferred proportions of mutations providing nalidixic acid resistance among all nonneutral mutations with increasing screen doses in the *E. coli* ancestral strain REL4536. Gray dots and bars show maximum likelihood estimates from fluctuation assays and 95% confidence intervals. The dotted line shows the fitted log-log linear regression ($P_R = 0.00025 \text{ screen-dose}^{-2.122}$, $R^2 = 0.98$).

than at $3 \mu\text{g.mL}^{-1}$ Nal. The range of screen doses used thus covers a large underlying variation in terms of mutational target.

GYRASE A MUTATIONS ARE DIFFERENTIALLY SCREENED ALONG THE DOSE GRADIENT

Sequencing of the *gyrA* gene among mutants revealed 13 different non-synonymous substitutions, on ten nucleotides of the *gyrA* gene. These substitutions result in a change among eight different amino acids of the gyrase A protein (at positions 51, 55, 67, 81, 82, 83, 87, and 119), six of which (positions 51, 67, 81, 82, 83, 87) had already been detected in previous studies (Hopkins et al. 2005). As shown in Figure 5A, *gyrA* mutants occurred at every screen dose and their proportion increased with the screen dose (GLM, binomial error, LRT, $\chi^2_{(1)} = 70.8$, P -value $<< 10^{-6}$) from 24% to 100%. Several *gyrA* mutations were found at different screen doses. Three of them were consistently obtained across all screen doses (Fig. 5A, 83Leu, 87Tyr, 87Gly, hereafter “generalist” group), while some were only found at low (55Arg, 119Val, 51Val, “low” group), intermediate (67Ser, 83Ala, 87Ala, 81Cys, “intermediate” group) or high doses (87Asn, 82Gly, 119Glu, “high” group).

FITNESS RANKS ARE CONSERVED ACROSS MEASURE DOSES AND CORRELATE WITH SCREEN DOSE

We denote the set of selection coefficients of a given mutant across all measure doses, its “fitness profile”. Figure 5B shows the fitness profile of each *gyrA* mutation. A striking pattern is that fitness rank tends to be conserved across measure doses: the fittest mutants at a high measure dose ($12.5 \mu\text{g.mL}^{-1}$, here), tend to be the fittest at lower doses (3 and $8 \mu\text{g.mL}^{-1}$). This trend also holds among all mutants (Fig. S2). Within the *gyrA* mutants (Fig. 5B), fitness profiles further show that the mutations

found specifically at “low”, “intermediate”, and “high” screen doses (as mentioned in previous paragraph) consistently show low, intermediate, and high selection coefficients across all measure doses. Mutations consistently screened at all screen doses (the “generalist” group) provide high fitness across all measure doses, similarly to mutations from the “high” screen dose group.

SELECTION COEFFICIENTS DECREASE WITH MEASURE DOSE AND INCREASE WITH SCREEN DOSE

The best model describing the variation of selection coefficients included the effects of screen dose, measure dose, genetic basis, and their interactions (Table 1). This shows extensive G × E interactions across measure doses, and that the resistance mutations are significantly different among screen doses. Random effects were significant, indicating substantial genetic variation (genotype effect) for resistance within each screen dose and measure dose. Figure 6 illustrates the mean fitness profiles per screen dose. Over all mutants (Fig. 6A), the mean selection coefficient increases with screen dose within each measure dose and decreases with measure dose within each screen dose (Fig. 6B). These patterns also hold for mean selection coefficients within the *gyrA* and non-*gyrA* subgroups (Fig. 6C, D), but the decrease with measure dose is less pronounced among *gyrA* mutants. Fitness profiles of individual mutants (Fig. S2), show that this pattern also holds individually, and not only on average.

THE FITNESS PATTERN DIFFERS BETWEEN *gyrA* AND non-*gyrA* MUTANTS

The distribution of selection coefficients of the mutants becomes increasingly bimodal with increasing measure dose (bimodality is less rejected with increasing measure dose by Silverman tests: P -value = 0.006, 0.134, 0.593 for measure doses 3 , 8 , $12.5 \mu\text{g.mL}^{-1}$, respectively, Fig. 6B). This bimodality is well explained by the genetic basis of resistance (at $12.5 \mu\text{g.mL}^{-1}$, 87% of sequenced mutants with higher-than-average fitness are *gyrA* mutants, while only 12% of lower-than-average fitness mutants are *gyrA*). The mean selection coefficient of *gyrA* mutants is much higher than non-*gyrA* mutants at every measure dose (Fig. 6C, D) but few *gyrA* mutants show low fitness profiles (those screened at low doses) and similarly few non-*gyrA* mutants show high fitness profiles (Fig. 6C, D, Fig. S2). Finally, the pattern of increasing mean selection coefficient with screen dose (Fig. 6A) largely reflects the increasing proportions of *gyrA* mutants sampled at increasing screen doses (Fig. 5A).

COST DISTRIBUTIONS

The fitness effects of resistant mutants in the absence of antibiotics (costs of resistance) were analyzed, using shifted Gamma distributions based on previous FGM predictions (eq. 4). The four best models lie within less than 2 points of AIC (Table 2), and

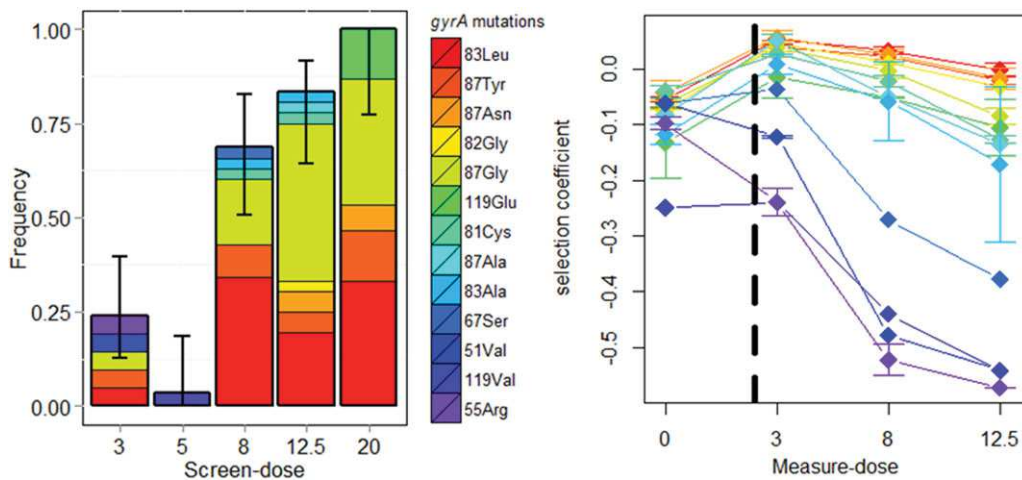


Figure 5. Nature, proportions, and fitness effects of *gyrA* mutations screened along a Nal dose gradient. (A) Contoured bars represent the proportion of mutants having a resistance mutation at the *gyrA* gene among all resistant mutants screened at five nalidixic acid screen doses (in $\mu\text{g} \cdot \text{mL}^{-1}$). Error bars represent the standard error associated with these proportions. Within bars, colored areas illustrate the different proportions of each type of *gyrA* mutation providing Nal resistance. The color gradient (from blue to red) follows the selection coefficient of mutants in competition with a reference competitor (M200-CFP) at $12.5 \mu\text{g} \cdot \text{mL}^{-1}$ Nal. Among all resistant mutants, 42, 31, 35, 37, and 17 mutants screened at dose 3, 5, 8, 12.5, and $20 \mu\text{g} \cdot \text{mL}^{-1}$ Nal, were sequenced at the *gyrA* gene, respectively. (B) Fitness profile across measure-doses (in $\mu\text{g} \cdot \text{mL}^{-1}$), for all *gyrA* mutation (bars give standard errors). The measure dose 0 (absence of Nal) should be considered separately from other measure doses (in $\mu\text{g} \cdot \text{mL}^{-1}$) as in the former case the reference competitor is the ancestor strain while it is the high dose resistant strain M200-CFP for all other measure doses (the black dotted line marks the separation).

only differ by the pattern of incompressible cost c_{min} . They all include: (i) fixed shape a across screen doses for *gyrA* mutants and screen dose dependent shape for non-*gyrA* mutants, and (ii) constant mean cost across screen doses but at lower level for *gyrA* mutants than for non-*gyrA* mutants (Tables 2, 3, Fig. 7B, C). The four best models included at least a nonzero c_{min} for *gyrA* mutants, and the best one assumed a nonzero c_{min} , constant across screen doses and equal between *gyrA* and non-*gyrA*. The distribution described by the best model is an adequate description of the data as 65% of simulated datasets based on these distributions had a lower likelihood than the observed dataset. Note that a different conclusion would be reached if the same data were analyzed without distinguishing *gyrA* and non-*gyrA* mutants (Table S1). In this case, the best model would show, quite unexpectedly, that the average cost is significantly decreasing with the screen dose (Tables S1, S2, Fig. 7A). Sequencing thus confirmed that this pattern is driven by the overrepresentation of *gyrA* mutants at high screen doses (Fig. 5A), rather than by variation in the selective properties of mutants within *gyrA* and non-*gyrA* groups across screen doses.

QUALITATIVE LANDSCAPE PROPERTIES EMERGING FROM EXPERIMENTAL RESULTS

A first observation from our experimental results is that there is ample (somewhat continuous) genetic variation for resistance, in each screen dose, for each measure dose, even only within the

gyrA mutants. Moreover, there is ample G × E interaction among resistance mutants. These observations are nicely captured by FGM models, which generate both G × E and variable mutational effects. Figure 8 shows three landscapes accounting for minimal extensions of FGM that are qualitatively consistent with all our experimental data. We now explain step by step how we can reach this conclusion.

- (1) The observation that the mutation rate toward resistance is low and decreasing with the screen dose is consistent with the three cases depicted on Figure 1. The magnitude of this decrease indicates that important features of the landscape must change among doses and that those changes follow a “monotonic” trend with increasing doses.
- (2) Extensive G × E interaction in the data clearly excludes the possibility that only the height of fitness peaks varies across doses (i.e., it excludes the case illustrated on case 2, Fig. 1).
- (3) The proportion of *gyrA* mutants strongly increases with the screen dose (Fig. 5A). This is consistent with models having different mutational modules (i.e., it excludes the case depicted on Fig. 3A), at least for *gyrA* and non-*gyrA*. The *gyrA* module corresponds here to a portion of the *gyrA* gene but this does not exclude the possibility that there are other submodules in this gene. Similarly, the non-*gyrA* module may be partitioned into further submodules, but this cannot be discriminated without characterizing the nature and genomic position of these mutations. The increase in *gyrA* mutants

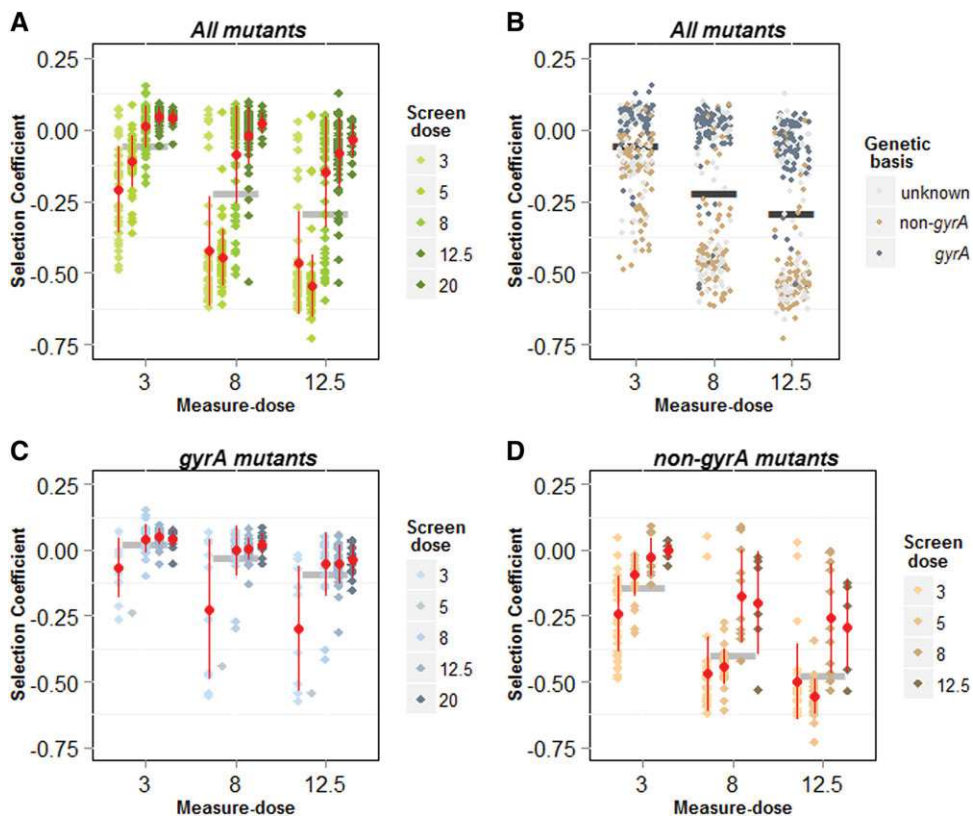


Figure 6. Fitness profiles across Nal measure doses (in $\mu\text{g.mL}^{-1}$) among all screened mutants (upper panel), sequenced mutants displaying (resp. lacking) a mutation in the *gyrase A* gene (lower left, resp. right, panel). Large gray dashes show the mean selection coefficient for each measure dose while in (A), (C), and (D), red dots and bars represent means and standard errors of selection coefficients for each screen dose (individual values indicated by color code and staggered at each measure dose). In (B), all screen doses are staggered randomly and the color code indicates the genetic basis: *gyrA*, non-*gyrA*, or not sequenced (“unknown”).

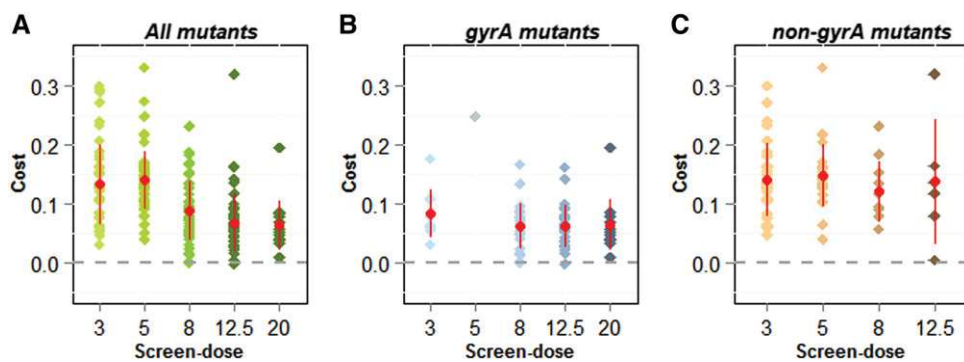


Figure 7. Effect of screen dose on fitness costs distribution. (cost = minus the selection coefficient of mutant relative to the ancestral sensitive strain, in the absence of antibiotic). Red dots and bars give the means and standard errors (A): among all screened mutants, (B) (resp. C) among sequenced mutants displaying (resp. lacking) a mutation in the *gyrA* gene.

with the screen dose also entails that the screen zones moves away from the axis corresponding to the non-*gyrA* module, with increasing screen dose. Finally, this observation entails that the mutational target of the non-*gyrA* module is larger than that of *gyrA*: when the screen zone covers both modules, at low screen dose, non-*gyrA* mutants largely predominate.

This is not very surprising as the *gyrA* module corresponds to mutations occurring in a single gene, whereas the non-*gyrA* module may cover the rest of the genome. The same interpretation is likely to hold with other fluoroquinolone antibiotics that have been shown to exhibit similar mutational patterns (Zhou et al. 2000).

Table 2. Model comparison for costs distribution among screen doses and genetic basis (*gyrA* or not-*gyrA*).

Model	Shape		Mean		Incompressible cost		<i>k</i>	LL	ΔAIC
	a_{gyrA}	$a_{non-gyrA}$	\bar{c}_{gyrA}	$\bar{c}_{non-gyrA}$	c_{min}^{gyrA}	$c_{min}^{non-gyrA}$			
1	1	dose	1	1	1	0	8	1619.57	0.00
2	1	dose	1	1	1	dose	8	1619.21	0.72
3	1	dose	1	1	1	1	12	1622.67	1.80
4	1	dose	1	1	1	1	9	1619.61	1.92
5	1	dose	1	dose	1		11	1621.32	2.50
6	1	dose	1	1	0		7	1615.26	6.62
7	1	dose	1	1	0	1	8	1615.65	7.84
8	1	1	1	1	1		6	1613.26	8.62
9	1	dose	dose	1	1		11	1613.47	18.20
10	1	dose	1	1	dose	1	12	1614.13	18.88
11	dose	dose	1	1	1		11	1612.58	19.98
12	1	dose	1		1		7	1600.20	36.74
Estimated parameters model 1	1.98	dose3: 2.55	0.051	0.132	0.0165				
		dose8: 8.83							
		dose12.5: 4.10							
		dose20 : 1.22							

Each line corresponds to one model following equation (4) with model parameters (a , \bar{c} , c_{min}) which are allowed to vary with screen dose (indicated by *dose*) or not (indicated by 1). Parameter c_{min} can vary with screen-dose ('dose') or not ('1') or be constrained to 0 ('0'). For each model the number of parameters estimated (*k*), the Log-Likelihood (LL) and the difference between Akaike Information Criterion with best model (ΔAIC) allow to compare models. Down: Estimated values of parameters in the best model (model 1).

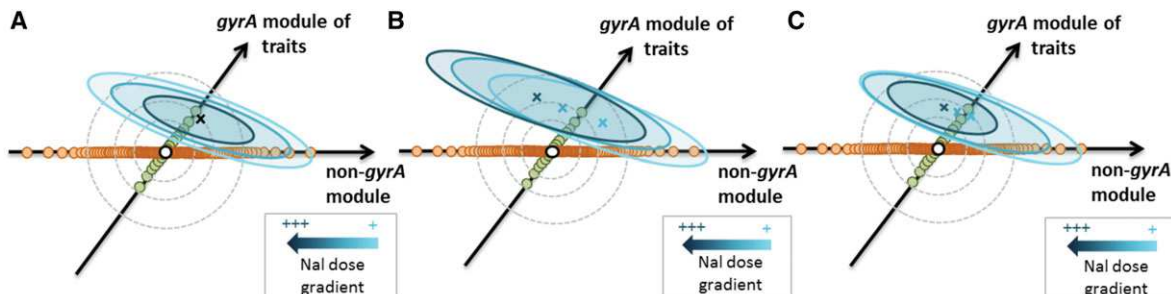


Figure 8. Extended Fisher's geometric models of fitness landscapes matching patterns of selection of nalidixic acid resistance in *E. coli* along a dose gradient. Dose variation entails (A) variation in selection intensity, (B) variation in optimum position, and (C) variation in both. Mutational modularity and selective anisotropy need to be integrated in the three landscapes to reproduce specific fitness patterns obtained experimentally. The three landscapes could in principle be discriminated by investigating patterns from experimental evolution.

- (4) A surprising observation is that the average cost of resistance decreases with the screen dose. This finding excludes isotropic models (i.e., cases illustrated on Fig. 2A), which predict the opposite trend for all cases depicted in Figure 1. It also excludes anisotropic models where the dominant direction is constant across all environments. Also, average costs within modules are constant across screen doses, so that the variation of cost with the screen dose was entirely attributable to the fact that *gyrA* mutants are preferentially screened at high dose, and exhibit low costs. This observation entails that selection is less intense along the phenotypic direction of the *gyrA* module in the absence than in the presence of antibiotics. In other words, the dominant direction of anisotropy in

the presence of antibiotics needs to be more or less orthogonal to the main direction of the *gyrA* module, so that *gyrA* have lower fitness costs than non-*gyrA* screened mutants.

- (5) We do not find a strong signature of specialization (i.e., mutants screened at low doses are not fitter at those doses than mutants screened at higher doses) and we observed "generalist" mutants. Hence, models with large shifts between optima among antibiotic environments are rejected (as case 1a, Fig. 1). The relative fitness data across doses can be well explained by variation in the curvature of the fitness function among those environments (case 3, Fig. 1, and Fig. 8A) or by small shifts between optima (case 1b, Fig. 1, and Fig. 8B) but these two models cannot be distinguished given that screen

zones largely overlap among environments in both cases or their intermediates (Fig. 8C). Despite this uncertainty, fitness patterns indicate that optimum position(s) is/are closer to the axis corresponding to the *gyrA* than to the non-*gyrA* module: *gyrA* mutants tend to have higher relative fitness at all measure doses than non-*gyrA* mutants. If optima vary (as in Fig. 8B, C), they must move away from the axis of the non-*gyrA* module when screen dose increases.

- (6) The distribution of selection coefficients is increasingly bimodal with increasing measure dose. This pattern can occur if *gyrA* mutants are relatively close to the optimum(s) so that their fitness slowly decreases when the fitness function becomes narrower or shifts with increasing measure dose. On the contrary, the fitness of the non-*gyrA* mutants strongly decreases with increasing measure dose if they are positioned further from the optimum(s), in the steepest part of the Gaussian fitness function.

Overall all the data are consistent with a relatively narrow range of simple fitness landscapes, as illustrated on Figure 8A–C. Compared to most basic version of FGM-like models, it is important to account for the existence of modules, the presence of anisotropy and its variation across environments. Yet, the more common ideas that selection intensity versus optimum positions vary across environments are very difficult to distinguish based on these data.

Discussion

EXTENDING FISHER'S GEOMETRICAL MODEL?

Phenotypic landscape models, like the Fisher's geometrical model (FGM), are often considered too simple to have more than just a heuristic value. Their generality, limited number of assumptions and ability to depict complex adaptation with a simple formalization offer however a robust approach to quantitatively model (mal)adaptation in a diversity of genetic backgrounds and environments (Martin et al. 2007; Bataillon et al. 2011; Sousa et al. 2012; Trindade et al. 2012). Yet, these FGM-like models, in their simplest formulations, also present important shortcomings and fail to account for several observed mutational patterns. It may be tempting therefore to simply throw away this category of models and turn to alternative modeling approaches, although they fail to provide the same level of generality (see Introduction). Another possibility is to see how FGM-like models can be minimally extended to account for empirical patterns of mutation and adaptation. What would the most parsimonious extensions be that would retain the generality of the approach, yet provide sufficient flexibility to account for empirical patterns? Some obvious modifications come to mind immediately, such as allowing for multiple peaks (Colegrave and Buckling 2005; Rozen et al. 2008; Szendro

et al. 2013) or non-Gaussian fitness functions (Peck et al. 1997; Martin and Lenormand 2006a; Gros et al. 2009). However, these extensions have not so far been shown to capture some of the empirical patterns that are not well predicted by the FGM, so they may not be the best starting points here. In contrast, some observations already point to extensions that are probably necessary in most cases. For instance, the occurrence of parallel evolution strongly points toward the existence of mutational modules (Chevin et al. 2010; Lenormand et al. 2016) and the observation of skewed distribution of fitness effects of random mutants points toward the occurrence of widespread selective/mutational covariance among traits (Martin and Lenormand 2006a). Hence, it would be a reasonable first step to see whether such extensions are generally sufficient or whether further modifications are required.

An important application of FGM-like models is to model adaptation across a range of possible environments. We wanted to determine whether patterns of mutations across environments can be explained by the variation of four simple features: (1) the optimum position, (2) the average strength of selection, (3) the contribution of different modules, (4) the traits covariances. These variations open a wide array of possible situations, and may be discriminated based on few specific qualitative patterns. Our data show that variation of mutational effects across antibiotic doses really requires (3) and (4). It also requires at least either (1) or (2), but our data cannot discriminate between the two possibilities. As far as we can conclude from our study, it is thus necessary to incorporate limited extensions to the basic FGM, which were already pointed out by previous data (modules, trait covariance). These extensions may not be necessary when considering random mutants sampled across a large number of modules even if those modules differ in their mutational covariances (Chevin et al. 2010). Similarly, different covariances among environments may average out when considering random mutants (Martin and Lenormand 2006b). Maybe because of these asymptotic behaviors, simple versions of the FGM can show a good fit to random mutant data (see Introduction). Considering the extreme tail of the distribution of fitness effects of mutations is however a situation where these asymptotic behaviors can fail. Screening mutants with a strong selective pressure necessarily biases toward this extreme tail, which can lead to discrepancies between data and simple random-mutants theory. In this case, it can nevertheless serve to reveal variation in modularity and covariance patterns, as we show. The latter are thus important to account not only for the occurrence of parallel evolution in FGM-like models (Chevin et al. 2010), but also for the effects of strongly screened mutants.

CONNECTING LANDSCAPE PROPERTIES WITH THE EFFECTS OF MUTATIONS

Although different landscape models should be discriminable based on data (Blanquart and Bataillon 2016), it is a priori not

trivial to make a one-to-one correspondence between the fitness effects of mutations and specific features of landscape models. In this study, we have shown how different extensions of the basic FGM (mutational modules, changes in phenotypic covariance, and in optimum or intensity of selection among environments) could be identified, at least qualitatively, based on specific data. Three important points emerge from this work, which could be considered in further studies.

First, it is important to match the predictions with the type of data at hand. For instance, we obtained mutants by screening them on a selective medium. We therefore focused on conditional distributions of fitness effects in FGM-like models (Martin and Lenormand 2015). Random mutants could also have been used, but the specific predictions would have to be changed accordingly. Second, discriminating features of landscape models may require various types of data. In this study for example, sequencing *gyrA* mutations in addition to fitness measurements, was necessary to better detect and characterize mutational modules. Yet, we could not clearly distinguish scenarios with different optima from those with different strength of selection across environments (Fig. 8) based on screened or random mutants. One possibility to discriminate these situations would be, for instance, to add data from experimental evolution. Adapting different strains to different doses for many generations should indicate, eventually, if a pattern of dose specialization emerges or not, which would discriminate the two possibilities. Third, data do not provide equal information to discriminate the different features of the landscape. For instance, the decrease in average fitness cost of mutants with increasing screen dose is hard to predict without changes in trait covariance. The occurrence of some dose specialists among mutants is difficult to interpret without having different optima among doses, etc.

In the general case, when FGM-like models are extended in a specific way, it is necessary to point toward key empirical patterns that would be hard to explain in the absence of this extension. Additional extensions of the FGM (non-Gaussian fitness functions, multiple peaks within environments) require investigation by setting specific tests and matching their predictions with the relevant data. Overall, we believe that this exercise helps setting the stage for more quantitative approaches. It points to the kind of summary statistics that may be useful in approaches such as ABC. It also points toward potential problems of identifiability of the parameters that may not be solved by a more quantitative approach (i.e., by fitting explicit analytical predictions to these data). For example, variations in optimum versus selection intensity are difficult to distinguish, as our analysis shows. However, a quantitative approach might be workable if properly investigated. Yet, given the dimensionality of the problem and the various possible extensions of FGM to be considered together, it is however likely to be a major endeavor.

ANTIBIOTIC RESISTANCE AND LANDSCAPE MODELS

Studying antibiotic resistance in the light of landscape models may serve several purposes. First, screening for resistance is a convenient option to retrieve many independent mutants (as already pointed out by Kassen and Bataillon 2006). Microbes allow efficient measurements of fitness across many environments (Elena and Lenski 2003) and a lot of information is available on the resistance mechanisms from intensive studies *in vitro* or on clinical isolates (Levy and Marshall 2004; Davies and Davies 2010). Such information is useful to identify genetic targets that potentially affect the same set of phenotypic traits and are thus good candidate modules. However, note that clinical isolates represent a nonrandom subset of resistant mutants (in terms of cost and effect) that evolved under specific ecological conditions. Yet, many *gyrA* resistance mutations detected in this study had been previously reported in clinical isolates. As our results and previous studies suggest, single mutations in the QRDR of *gyrA* confer high resistance to Nal associated with low cost (Lindgren et al. 2005). Those mutations are also a first step toward high-dose resistance to other fluoroquinolone antibiotics, which may explain why they are frequently found in clinical isolates. However, two mutations in our experiment were not reported previously (119Val, 55Arg). They were precisely the ones selected only at low doses, which might explain why they are absent from clinical isolates.

Second, the case of antibiotic resistance is *a priori* a situation that should really challenge the theory. The genetic basis of antibiotic resistance is often considered to be narrow, involving few loci and mutations. As a consequence, describing the fitness effects of individual mutants may be more useful (and simpler) than modeling a large set of mutants in a large and continuous phenotypic space. Our results show, however, that the range of screened mutations is quite large and diverse in their fitness effects, even considering a narrow genetic target (as the *gyrA* gene). Furthermore, we found that the fitness effects of screened mutants were well described by continuous gamma distributions, entirely consistent with landscape theory (Martin and Lenormand 2015). The proportion of resistance mutations (among all mutations) is very low and sharply decreases with the screen dose but this remains entirely compatible with landscape models where only the tails of mutant clouds are sampled upon screening (Martin and Lenormand 2015). Finally, our results showed that fairly complex and unexpected patterns can be well captured by relatively simple extensions of landscape models, for example a decreased average cost with increasing screen doses, or bimodal fitness effects distributions at high but not low measure doses. The finding that high resistance mutants exhibit lower fitness costs, even in the absence of compensatory evolution, is also important to emphasize, as resistance management strategies heavily depend on those relationships (Lenormand and Raymond 1998; Lenski 1998; Neve 2007; Ward et al. 2009). For this purpose, cost-resistance

relationships are probably more interesting to study within modules (or ideally individually) as they seem to strongly vary across modules.

Third, studying antibiotic resistance in the light of landscape models may significantly improve our understanding of adaptation across dose gradients in general. In evolutionary ecology, models of adaptation to different environments along a gradient typically assume stabilizing selection around different optima, all else being equal (Savolainen et al. 2013; Adrión et al. 2015). This view implies trade-offs across environments, as it is not possible to simultaneously be optimal in two distinct environments. In the field of antibiotic resistance (and pesticide resistance in general), this trade-off view is generally restricted to treated versus nontreated environments, and tends to ignore the possibility that adapting to a low dose may involve a different phenotypic optima than adapting to a higher dose. This is an important issue as (1) it can largely determine whether low doses can favor the emergence of strong resistance and (2) in natura, microorganisms adapt to a large panel of antibiotic concentrations, including low doses in polluted soils or water (Depledge 2011). The most common view in the field of antibiotic resistance is thus that different doses correspond to different intensities of selection, whereas the most common view in evolutionary ecology is that different environments correspond to different optima. These two views need to be reconciled, but our results show that it is difficult to discriminate these two extreme situations (and all intermediate cases) from data on screened mutants (Fig. 8). More experimental work, involving experimental evolution is necessary to solve this important issue.

ACKNOWLEDGMENTS

We would like to thank M.-P. Dubois for lab management, C. Duperray (IRB – Montpellier) and the Montpellier RIO Imaging platform. We thank J.-N. Jasmin, S. Bedhomme, P. Labbé, and T. Hindré for discussions. We also thank R. Lenski and D. Schneider for providing *E. coli* strains. This work was supported by a PhD grant from French ministry of research to NH, and the ANR SilentAdapt to T.L.

DATA ARCHIVING

The doi for our data is doi:10.5061/dryad.07850.

LITERATURE CITED

- Adrión, J. R., M. W. Hahn, and B. S. Cooper. 2015. Revisiting classic clines in *Drosophila melanogaster* in the age of genomics. *Trends Genet.* 31:434–444.
- Bataillon, T., T. Zhang, and R. Kassen. 2011. The distribution of fitness effects of new beneficial mutations in *Pseudomonas fluorescens*. *Biol. Lett.* 7:98–100.
- Blanquart, F., G. Achaz, T. Bataillon, and O. Tenaillon. 2014. Properties of selected mutations and genotypic landscapes under Fisher's geometric model. *Evolution* 68:3537–3554.
- Blanquart, F., and T. Bataillon. 2016. Epistasis and the structure of fitness landscapes: are experimental fitness landscapes compatible with Fisher's model? *Genetics* 203:847–862.
- Burnham, K. P., and D. R. Anderson. 2002. Model selection and multimodel inference. Springer-Verlag New York, New York.
- Chevin, L.-M., G. Martin, and T. Lenormand. 2010. Fisher's model and the genomics of adaptation: restricted pleiotropy, heterogenous mutation, and parallel evolution. *Evolution* 64:3213–3231.
- Chou, H.-H., N. F. Delaney, J. A. Draghi, and C. J. Marx. 2014. Mapping the fitness landscape of gene expression uncovers the cause of antagonism and sign epistasis between adaptive mutations. *PLoS Genet.* 10: e1004149.
- Colegrave, N., and A. Buckling. 2005. Microbial experiments on adaptive landscapes. *Bioessays* 27:1167–1173.
- Davies, J., and D. Davies. 2010. Origins and evolution of antibiotic resistance. *Microbiol. Mol. Biol. Rev.* 74:417–433.
- Dawkins, R. 2004. Extended phenotype—but not too extended. A reply to Laland, Turner and Jablonka. *Biol. Philos.* 19:377–396.
- Depledge, M. 2011. Reduce drug waste in the environment. *Nature* 478: 36.
- Duputié, A., F. Massol, I. Chuine, M. Kirkpatrick, and O. Ronce. 2012. How do genetic correlations affect species range shifts in a changing environment? *Ecol. Lett.* 15:251–259.
- Elena, S. F., and R. E. Lenski. 2003. Evolution experiments with microorganisms: the dynamics and genetic bases of adaptation. *Nat. Rev. Genet.* 4:457–469.
- Eyre-Walker, A., and P. D. Keightley. 2007. The distribution of fitness effects of new mutations. *Nat. Rev. Genet.* 8:610–618.
- Fisher, R. A. 1930. The genetical theory of natural selection. Oxford Clarendon Press, Oxford.
- Gallet, R., T. F. Cooper, S. F. Elena, and T. Lenormand. 2012. Measuring selection coefficients below 10^{-3} : method, questions, and prospects. *Genetics* 190:175–186.
- Gillespie, J. H. 1983. A simple stochastic gene substitution model. *Theor. Popul. Biol.* 23:202–205.
- Gordo, I., and P.R. Campos. 2013. Evolution of clonal populations approaching a fitness peak. *Biol. Lett.* 9:20120239.
- Gros, P.-A., H. Le Nagard, and O. Tenaillon. 2009. The evolution of epistasis and its links with genetic robustness, complexity and drift in a phenotypic model of adaptation. *Genetics* 182:277–293.
- Hane, M. W., and T. H. Wood. 1969. *Escherichia coli* K-12 mutants resistant to nalidixic acid: genetic mapping and dominance studies. *J. Bacteriol.* 99:238–241.
- Hartl, D. L., and C. H. Taubes. 1996. Compensatory nearly neutral mutations: selection without adaptation. *J. Theor. Biol.* 182:303–309.
- Hooper, D. C. 1999. Mechanisms of fluoroquinolone resistance. *Drug Resist. Updat.* 2:38–55.
- Hopkins, K. L., R. H. Davies, and E. J. Threlfall. 2005. Mechanisms of quinolone resistance in *Escherichia coli* and *Salmonella*: recent developments. *Int. J. Antimicrob. Agents* 25:358–373.
- Ibarra, R. U., J. S. Edwards, and B. O. Palsson. 2002. *Escherichia coli* K-12 undergoes adaptive evolution to achieve in silico predicted optimal growth. *Nature* 420:20–23.
- Jacoby, G. A. 2005. Mechanisms of resistance to quinolones. *Clin. Infect. Dis.* 41 (Suppl 2):S120–S126.
- Kacser, H., and J. A. Burns. 1973. The control of flux. *Biochem. Soc. Trans.* 23:341–367.
- Kassen, R., and T. Bataillon. 2006. Distribution of fitness effects among beneficial mutations before selection in experimental populations of bacteria. *Nat. Genet.* 38:484–488.
- Kauffman, S. A., and S. Levin. 1987. Towards a general theory of adaptive walks on rugged landscapes. *J. Theor. Biol.* 128:11–45.

- Kauffman, S. A., and E. D. Weinberger. 1989. The NK model of rugged fitness landscapes and its application to maturation of the immune response. *J. Theor. Biol.* 141:211–245.
- Kibota, T. T., and M. Lynch. 1996. Estimate of the genomic mutation rate deleterious to overall fitness in *E. coli*. *Nature* 381:694–696.
- Lea, D. E., and C. A. Coulson. 1949. The distribution of the numbers of mutants in bacterial populations. *Genetics*, 49:264–285.
- Lenormand, T., L.-M. Chevin, and T. Bataillon. 2016. Parallel evolution: what does it (not) tell us and why is it (still) interesting? *In* G. Ramsey, and C. H. Pence, eds. *Chance in Evolution*. University of Chicago Press, Chicago.
- Lenormand, T., and M. Raymond. 1998. Resistance management: the stable zone strategy. *Proc. R. Soc. London B* 265:1985–1990.
- Lenski, R. E. 1998. Bacterial evolution and the cost of antibiotic resistance. *Int. Microbiol.* 1:265–270.
- Lenski, R. E., and M. Travisano. 1994. Dynamics of adaptation and diversification: a 10,000 generation experiment with bacterial populations. *Proc. Natl. Acad. Sci. USA*, 91:6808–6814.
- Levins, R. 1966. The strategy of model building in population biology. *Am. Sci.* 54:421–431.
- Levy, S. B., and B. Marshall. 2004. Antibacterial resistance worldwide: causes, challenges and responses. *Nat. Med.* 10:S122–S129.
- Lindgren, P. K., L. L. Marcusson, D. Sandvang, N. Frimodt-møller, and D. Hughes. 2005. Biological cost of single and multiple norfloxacin resistance mutations in *Escherichia coli* implicated in urinary tract infections. *Antimicrob. Agents Chemother.* 49:2343–2351.
- Luria, E., and M. Delbrück. 1943. Mutations of bacteria from virus sensitivity to virus resistance. *Genetics* 28:491–511.
- Manna, F., G. Martin, and T. Lenormand. 2011. Fitness landscapes: an alternative theory for the dominance of mutation. *Genetics* 189:923–937.
- Martin, G. 2014. Fisher's geometrical model emerges as a property of complex integrated phenotypic networks. *Genetics* 197:237–255.
- Martin, G., S. F. Elena, and T. Lenormand. 2007. Distributions of epistasis in microbes fit predictions from a fitness landscape model. *Nat. Genet.* 39:555–560.
- Martin, G., and T. Lenormand. 2006a. A general multivariate extension of Fisher's geometrical model and the distribution of mutation fitness effects across species. *Evolution* 60:893–907.
- . 2006b. The fitness effect of mutations across environments: a survey in light of fitness landscape models. *Evolution* 60:2413–2477.
- . 2008. The distribution of beneficial and fixed mutation fitness effects close to an optimum. *Genetics* 179:907–916.
- . 2015. The fitness effect of mutations across environments: Fisher's geometrical model with multiple optima. *Evolution* 69:1433–1447.
- Maynard Smith, J. 1970. Natural selection and the concept of a protein space. *Nature* 225:563–564.
- Neve, P. 2007. Challenges for herbicide resistance evolution and management: 50 years after Harper. *Weed Res.* 47:365–369.
- Orr, H. A. 2000. Adaptation and the cost of complexity. *Evolution* 54:13–20.
- . 2002. The population genetics of adaptation: the adaptation of DNA sequences. *Evolution* 56:1317–1330.
- . 2003. A minimum on the mean number of steps taken in adaptive walks. *J. Theor. Biol.* 220:241–247.
- . 2006. The distribution of fitness effects among beneficial mutations in Fisher's geometric model of adaptation. *J. Theor. Biol.* 238:279–285.
- Papp, B., C. Pal, and L. D. Hurts. 2004. Metabolic network analysis of the causes and evolution of enzyme dispensability in yeast. *Nature* 429:661–664.
- Peck, J. R., G. Barreaut, and S. C. Heath. 1997. Imperfect genes, fisherian mutation and the evolution of sex. *Genetics* 145c:1171–1399.
- Perfeito, L., A. Sousa, T. Bataillon, and I. Gordo. 2014. Rates of fitness decline and rebound suggest pervasive epistasis. *Evolution* 68:150–162.
- Polechová, J., and N. H. Barton. 2015. Limits to adaptation along environmental gradients. *Proc. Natl. Acad. Sci. USA* 112:6401–6406.
- Rokyta, D. R., P. Joyce, S. B. Caudle, C. Miller, C. J. Beisel, and H. A. Wichman. 2011. Epistasis between beneficial mutations and the phenotype-to-fitness Map for a ssDNA virus. *PLoS Genet.* 7:e1002075.
- Rozen, D. E., M. G. J. L. Habets, A. Handel, and J. A. G. M. de Visser. 2008. Heterogeneous adaptive trajectories of small populations on complex fitness landscapes. *PLoS One* 3:e1715.
- Savolainen, O., M. Lasco, and J. Merilä. 2013. Ecological genomics of local adaptation. *Nat. Rev. Genet.* 14:807–820.
- Segrè, D., A. DeLuna, G. M. Church, and R. Kishony. 2005. Modular epistasis in yeast metabolism. *Nat. Genet.* 37:77–83.
- Shull, F. A. 1935. Weismann and Haeckel: One hundred years. *Science* 81:443–452.
- Sousa, A., S. Magalhães, and I. Gordo. 2012. Cost of antibiotic resistance and the geometry of adaptation. *Mol. Biol. Evol.* 29:1417–1428.
- Szendro, I. G., M. F. Schenk, and J. Franke. 2013. Quantitative analyses of empirical fitness landscapes. *J. Stat. Mech.* 2013:p.P01005.
- Trindade, S., A. Sousa, and I. Gordo. 2012. Antibiotic resistance and stress in the light of Fisher's model. *Evolution* 66:3815–3824.
- Ward, H., G. G. Perron, and R. C. Maclean. 2009. The cost of multiple drug resistance in *Pseudomonas aeruginosa*. *J. Evol. Biol.* 22:997–1003.
- Waxman, D. 2006. Fisher's geometrical model of evolutionary adaptation—beyond spherical geometry. *J. Theor. Biol.* 241:887–895.
- Weinreich, D. M., N. F. Delaney, M. A. Depristo, and D. L. Hartl. 2006. Darwinian evolution can follow only very few mutational paths to fitter proteins. *Science* (80-.). 312:2004–2007.
- Weinreich, D. M., R. A. Watson, and L. Chao. 2005. Perspective: sign epistasis and genetic constraint on evolutionary trajectories. *Evolution* 59:1165–1174.
- Yoshida, H., and M. Bogaki. 1990. Quinolone resistance-determining region in the DNA gyrase *gyrA* gene of *Escherichia coli*. *Anti microb. Agents Chemother.* 34:1271–1273.
- Zhou, J., Y. Dong, X. Zhao, S. Lee, A. Amin, S. Ramaswamy, J. Domagala, J. M. Musser, and K. Drlica. 2000. Selection of antibiotic-resistant bacterial mutants: allelic diversity among fluoroquinolone-resistant mutations. *J. Infect. Dis.* 182:517–525.

Associate Editor: D. Rozen

Handling Editor: M. Servedio

Supporting Information

Additional Supporting Information may be found in the online version of this article at the publisher's website:

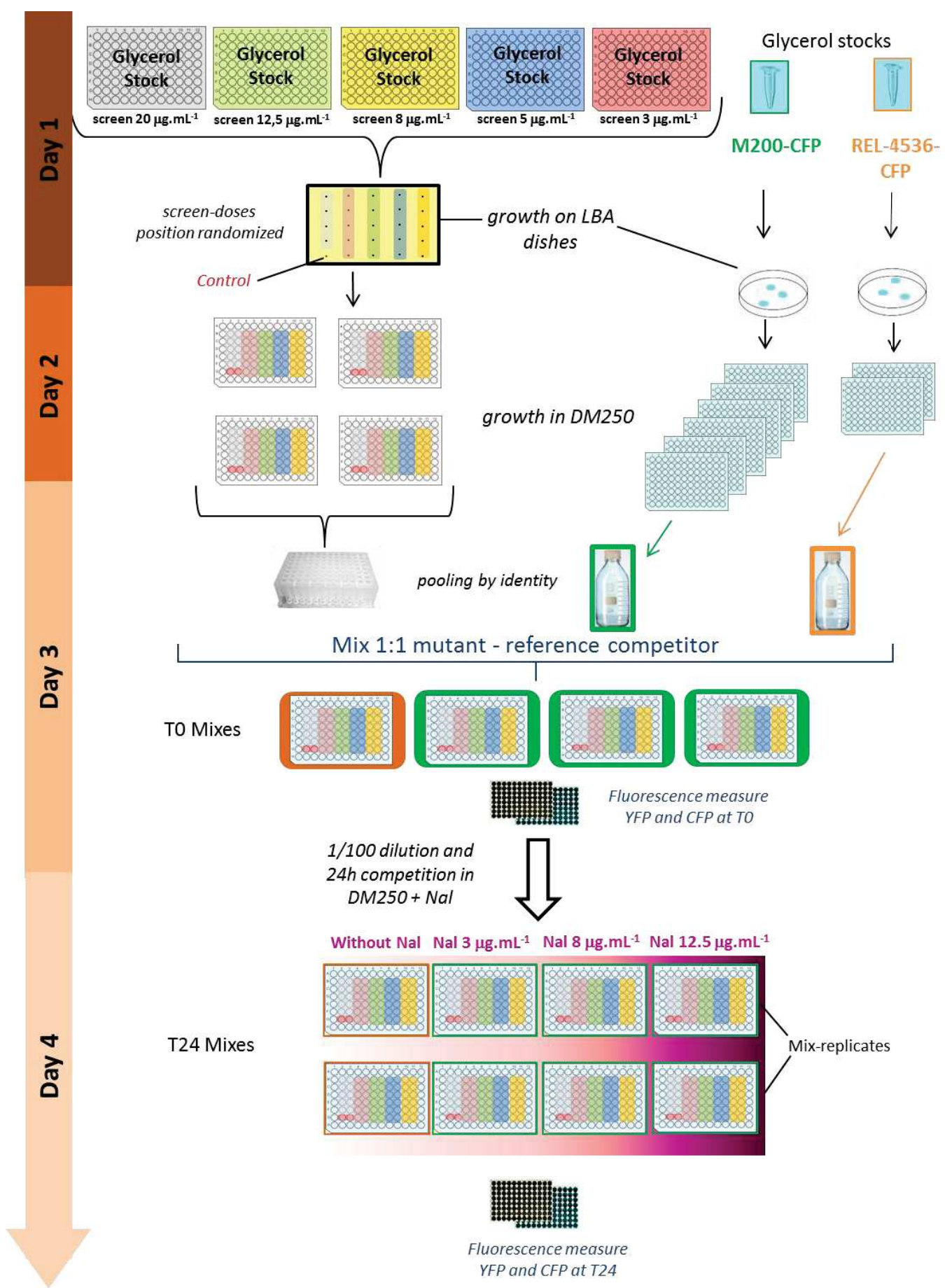
Figure S1: Detailed experimental protocol for competition assays

Figure S2: Selection coefficient per mutant

Table S1: Model comparison for costs distribution among screen-doses.

Table S2: Parameters estimated in the model best describing the distribution of costs of screened mutants among screen-doses.

Supplementary Figure 1: Detailed experimental protocol for competition assays



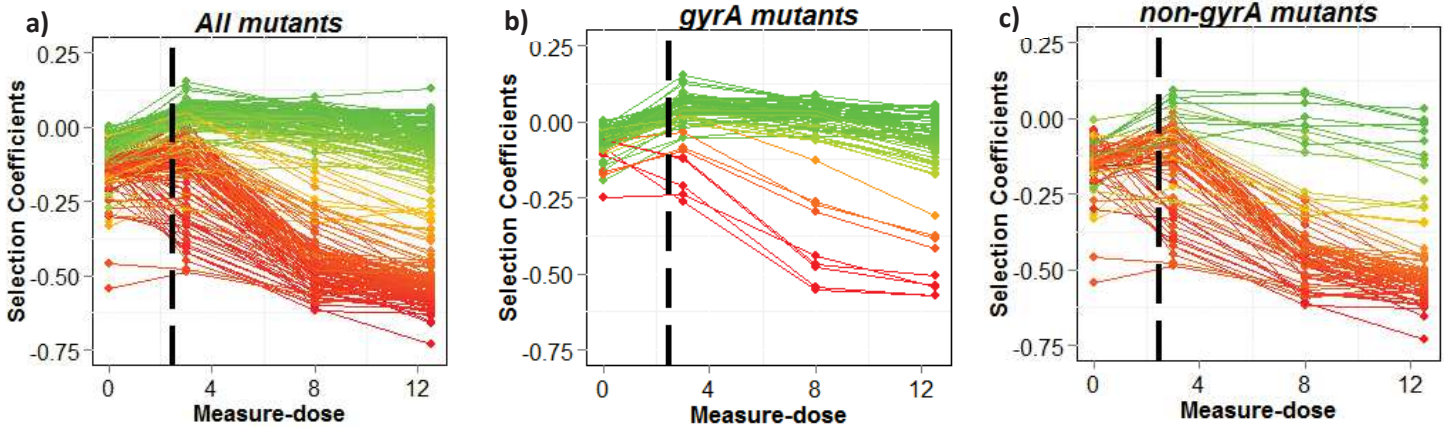
Day 1, mutants and reference strains (REL4536-YFP, REL4536-CFP, M200-YFP, M200-CFP) were taken from glycerol stocks, transferred on LBA plates and grown overnight at 37°C.

Day 2, each mutant was toothpick-transferred from LBA plates to a well in 96-well microplates containing 200 μ L DM0, then 5 μ L of each well were transferred to four replicate wells containing 200 μ L DM250 in four independent new 96-well microplates. In parallel, one colony of each reference strain was diluted into 60mL DM250 and distributed into several 96-well microplates. Microplates were covered with a BreathEasy film (Sigma-Aldrich, Saint-Louis, MO) for good oxygenation and contamination avoidance and incubated overnight at 37°C. Note that in all experiments involving cultures in 96-well microplates, the 36 exterior wells were filled with medium, but not used, as these wells are more exposed to evaporation.

Day 3, the four replicate wells used to grow each mutant were pooled into a single 1,5 mL well of a 96-well masterblock. All replicate cultures of the different reference competitors were also pooled into a single tube. For each mutant, four competition mixes were transferred to black 96-well microplates by mixing 100 μ L of the reference competitor and 100 μ L of mutant culture. The CFP and YFP fluorescence of these initial competition mixes (*i.e.* at time T0) were measured on a Tecan Infinite 200 (Tecan, Männedorf, Switzerland). Then, 2 μ L of each mix were transferred to two new black microplates containing 198 μ L of DM250 supplemented with 0, 3, 8 and 12.5 μ g.mL⁻¹ Nal. The plates were covered with a BreathEasy film and incubated 24h at 37°C.

Day 4, CFP and YFP fluorescence was measured, corresponding to the final point of the competition (*i.e.* at time T24).

Supplementary Figure S2: Selection coefficient per mutant



Fitness profiles across measure-doses for a) all mutants, b) *gyrA* mutants, c) non-*gyrA* mutants. The dotted black line figures the change of competitor (reference competitor is M200-CFP at measure-doses $3\mu\text{g/mL}^{-1}$, $8\mu\text{g/mL}^{-1}$ and $12.5\mu\text{g/mL}^{-1}$ Nal or the ancestral strain REL4536-CFP at measure-dose $0\mu\text{g/mL}^{-1}$). The color gradient (from red to green) reflects the value of the selection coefficient of corresponding mutant at measure-dose $12.5\mu\text{g/mL}^{-1}$ (from lower to higher values).

<i>a</i>	\bar{c}	c_{min}	<i>k</i>	<i>LL</i>	ΔAIC
<i>dose</i>	<i>dose</i>	1	11	1610.17	0.00
1	<i>dose</i>	<i>dose</i>	11	1608.94	2.46
<i>dose</i>	<i>dose</i>	0	10	1607.88	2.58
1	1	<i>dose</i>	7	1603.13	6.08
<i>dose</i>	<i>dose</i>	<i>dose</i>	15	1611.00	6.34
<i>dose</i>	1	<i>dose</i>	11	1606.96	6.42
1	<i>dose</i>	0	6	1600.79	8.76
1	<i>dose</i>	1	7	1600.89	10.56
<i>dose</i>	1	1	7	1591.66	29.02
<i>dose</i>	1	0	6	1581.67	47.00
1	1	0	2	1577.16	48.02
1	1	1	3	1578.04	48.26

Supplementary Table 1: Model comparison for costs distribution among screen-doses.

Each line corresponds to one model with model parameters (*a*, \bar{c} , c_{min}) which is allowed to vary with screen-dose (indicated by *dose*) or not (indicated by 1). Parameter c_{min} can vary with screen-dose ('*dose*') or not ('1') or be constrained to 0 ('0'). For each model the number of parameters estimated (*k*), the Log-Likelihood (*LL*), the difference between Akaike Information Criterions with best model (ΔAIC) were estimated and allowed to classify models.

	Screen-dose ($\mu\text{g.mL}^{-1}$)				
	3	5	8	12.5	20
a	1.93	7.32	1.57	0.97	1.19
\bar{c}	0.120	0.128	0.057	0.051	0.040
c_{min}			0.024		

Supplementary Table 2: Parameters estimated in the model best describing the distribution of costs of screened mutants among screen-doses. Parameters a , \bar{c} and c_{min} correspond to the shape, mean and incompressible cost respectively of the generalized Gamma distribution fitted.

Supplementary material 1: Antibiotic and culture media

Nalidixic acid (Nal) aliquots at 30 mg.mL⁻¹ were prepared in NaOH 300mM and filtered with a 0.45 µm filter. Aliquots were immediately used for screening experiments or kept at -20°C for competition experiments.

Nal resistant mutants were screened on LBA-Nal petri-dishes (lysogeny broth-Miller (LB): 10 g.L⁻¹ NaCl, 10 g.L⁻¹ tryptone, 5 g.L⁻¹ yeast extract; LBA= LB + 15g/liter agar) at desired Nal concentration. All strains were stored in 15% glycerol after 12h of growth in liquid LB supplemented with Nal at the desired concentration.

Davis minimal medium (DM0: 7 g.L⁻¹ KH₂PO₄.3H₂O, 2 g.L⁻¹ KH₂PO₄, 1 g.L⁻¹ (NH₄)₂SO₄, 0.5 g.L⁻¹ Na₃C₆H₅O₇, sterile water compensating exactly for evaporation after autoclaving; pH was set at 7.0) was used for competition assays. DM250 is DM0 supplemented with 1250 µL.L⁻¹ glucose 10%, 806 µL.L⁻¹ MgSO₄ [1M] and 1000 µL.L⁻¹ thiamine 0.2%. Finally Nal was added at the desired concentration. Fresh medium was prepared each week and kept protected from light at 4°C to prevent degradation of the thiamine and Nal.

Supplementary material 2: Experimental protocol for fluctuation tests

Starting from a few cells per well of REL4536-YFP, 288 independent overnight cultures were performed in three 96-well microtiter plates (37°C, 180 rpm), each well containing 200µL LB without antibiotic. After 12h of growth, the whole 200µL of each culture was plated on independent LBA Petri-dishes at a given screen-dose and incubated at 37°C for 72h. Hence, colonies from different Petri-dishes stem from independent spontaneous resistance mutations that occurred during the growth phase in the absence of selection pressure for resistant phenotypes. The number of Petri-dishes without visible colonies (n_0) among n plated in the fluctuation tests was picked to be used to estimate the mutation rate to resistance, U_R , with the P0 estimator (Lea and Coulson 1947) (described in Supplementary material 2). The resistant mutants were picked randomly from a colony on different non-empty Petri-dishes and stored at -80°C after an overnight culture in LB. We checked that mutants selected were also resistant in liquid medium DM250 by growing them during 12 hours starting from a 1/100 dilution in 4mL of DM250 supplemented with their corresponding Nal screen-dose.

The highly resistant mutant in YFP (M200-YFP) background, was obtained after two successive screens (at 20 then 200 µg.mL⁻¹ Nal, respectively. The YFP gene was then replace by the CFP gene in the M200 genetic background in order to obtain M200 in the two fluorescence colors. M200-YFP and M200-CFP were similarly stored at 80°C to be used as reference mutants in competition experiments.

Supplementary material 3: Estimation of mutation rate by maximum likelihood

The rate of mutations conferring resistance was estimated by the P_0 estimator (Luria and Delbrück 1943; Lea and Coulson 1947) from the fluctuation tests results. This method is the most robust to the confounding effects of any cost of resistance mutations during the initial growth phase (Jaeger and Sarkar 1995). Consider a pure birth process where divisions occur at rate $b N_t dt$ over dt arbitrary time units, where $N_t = N_0 e^{b t}$ is the population size at time t (ignoring stochasticity in the growth dynamics). The rate of production of new mutants is $U_R b N_t dt$ over the same period, where U_R is the per division rate of mutation to resistance. Over a full growth phase the total number of mutants arising is Poisson distributed $n_R \sim \text{Poisson} \left(b U_R \int_0^t N_\nu d\nu \right)$. The probability that no mutation arise during the growth phase is thus $p_0 = P(n_R = 0) = e^{-U_R \alpha}$ where $\alpha = b \int_0^t N_\nu d\nu = N_t - N_0$. As the culture is inoculated with a very small number of cells (estimated to roughly 10 cells with our protocol) and grows to a much higher population size, we approximate $\alpha \approx N_t$. If n independent cultures are plated on antibiotics, the number n_0 of plates yielding no visible resistant colonies is binomially distributed $n_0 \sim \text{Binomial}(n, p_0)$, ignoring limitations in plating efficiency (valid if the antibiotic is mainly bacteriostatic). The final population size N_t was estimated by many replicate plate counts of serial dilutions of independent wells: ignoring the variability in this estimate relative to that of U_R , we set $\alpha = \hat{N}_t = 4.46 \times 10^8$ cells (our estimate). The log-probability (log-likelihood \mathcal{LL}) of retrieving n_0 plates showing no visible colony out of a total of n wells plated is

$$\mathcal{LL}(n_0, n | U_R) = -n_0 U_R \alpha + (n - n_0) \ln(1 - e^{-U_R \alpha}) + \ln \left(\binom{n_0}{n} \right).$$

The maximum-likelihood estimate is thus $\hat{U}_R = \ln(n/n_0) / \alpha$, and the 95% confidence interval is given by the two values of $U = \hat{U}_R + \Delta U$ that decrease $\mathcal{LL}(n_0, n | U)$ by 2 around its maximum $\mathcal{LL}(n_0, n | \hat{U}_R)$. Assuming that the number of plates is sufficiently large (in our case several hundreds), that this confidence interval is small ($\Delta U \ll \hat{U}_R$) the likelihood can be linearized to leading order (order 2) in $\Delta U / \hat{U}_R$, which provides a simple expression for this interval: $\Delta U = 2\sqrt{1/n_0 - 1/n} / \alpha$.

Supplementary material 4: Probability of double mutants arising in the fluctuation test experiments

The occurrence of double mutants in a fluctuation assay is unlikely. Mutations occur during growth in the absence of the selective agent (Nal in our case) in fluctuation assays (p7 L146-147). In our case, if we consider the worst case scenario (at Nal screen-dose of 3 µg/mL where the rate of mutation to resistance is highest, *i.e.* where the chance to get a double mutant is highest), we have a rate of occurrence of resistance mutants of 10^{-8} . Because all these mutants carry at least one mutation, it provides a good estimate of the rate of mutation toward resistance in a single step. Hence, we would expect double mutant to occur at a rate close to 10^{-16} , which is too low to occur given the population sizes used in the assay (4.46×10^8).

Despite this computation, there might be a possibility that Nal resistance can be obtained only (or almost only) by double mutants. This unlikely scenario can also be ruled out with our data. The rate of double mutants must indeed be bounded by the genomic rate U of mutation (0.0002 in *E. coli* as shown in Kibota & Lynch, 1996. Noting p_R the proportion of mutations conferring Nal resistance among all mutations, the rate of occurrence of double mutants must be of the order of $(p_R U)^2$ in that case. Hence, for the lowest dose of Nal (3 µg/mL) where the problem of double mutants is potentially most acute, p_R must be at least 50% (square root of $10^{-8}/U^2$) to account for the rate of occurrence of resistance. This is unrealistic (50% of base pair in *E. coli* genome cannot be responsible for Nal resistance). In addition, previous literature on Nal resistance in *E. coli* confirm that single mutation usually suffice to be resistant in this range of doses (e.g. in Hughes and Lindgren 2003; Lindgren et al. 2005). Hence, our mutants are most probably single mutants.

Supplementary material 5: calibration model for fluorescence measures

Assuming some cross-talk (the instrument receives a small YFP signal due to CFP and vice-versa) when measuring CFP and YFP fluorescence in a mix of CFP and YFP cells and that fluorescence, in each color, is proportional to the density of each cell type in the well, the measured fluorescence F_C (resp. F_Y) of cells YFP (resp. CFP) is expressed as

$$\begin{aligned} F_Y &= a_1 n_Y + a_2 n_C \\ F_C &= b_1 n_C + b_2 n_Y \end{aligned} \quad (1)$$

with n_Y and n_C the number of cell YFP and CFP in the well, a_1 , (resp. a_2) the YFP fluorescence signal per YFP (resp. CFP) cells and b_1 , (resp. b_2) the CFP fluorescence signal per CFP (resp. YFP) cells. From (1) we deduce,

$$\begin{aligned} n_Y &= \frac{a_2 F_C - b_1 F_Y}{a_1 b_1 - a_2 b_2} \\ n_C &= \frac{b_2 F_Y - a_1 F_C}{a_1 b_1 - a_2 b_2} \end{aligned} \quad (2)$$

The ratio of cell number $x = n_Y/n_C$ can be expressed as a function of the ratio of fluorescence signals $y = F_Y/F_C$ as,

$$x = \frac{n_Y}{n_C} = \frac{k_1 y - 1}{k_2 - k_3 y} \quad (3)$$

with $k_1 = b_1/a_2$, $k_2 = a_1/a_2$, $k_3 = b_2/a_2$. Equation (2) of calibration curve model in the article corresponds to this last equation inversed and expressed in terms of log-ratios of fluorescence $\ln(y)$ vs. cell numbers $\ln(x)$:

$$\ln(y) = \ln\left(\frac{1 + k_1 e^{\ln(x)}}{k_2 + k_3 e^{\ln(x)}}\right) \quad (4)$$

Supplementary material 6: Expression of the Log-likelihood for cost distribution model

Mutant selection coefficients in the absence of antibiotics relative to the ancestor genotype (-cost) were analyzed after removing effects associated with the measurement protocol (weak-replicate and mix-replicate effects), keeping only the replicate/mutant estimates for each screen-dose. For a given screen dose D , denote $S_{ij}^D, \{i, j\} (j \in [1, k_i], i \in [1, n])$ the j^{th} replicate measurement of the selection of mutant i , relative to the ancestor, with k_i replicates for that mutant and n mutants analyzed in that dose. We fitted a generalized gamma, as parameterized in Mathematica 9.0 (shape a , scale \bar{c}/a , location c_{min}), to the cost distribution (\bar{c} being the mean of the cost distribution). Measurement error among replicates was assumed normally distributed: $S_{ij} \sim -c_i + e_{ij}$ with $c_i \sim \Gamma(a, \bar{c}/a, c_{min})$ and $e_{ij} \sim N(0, \sigma)$. For a given set of parameter values $\boldsymbol{\theta} = \{a, \bar{c}, c_{min}, \sigma\}$, the log-likelihood of the set of replicate mutant fitnesses in dose D was computed as

$$\mathcal{LL}_D(\boldsymbol{\theta}) = \sum_{i=1}^n \ln \left(\int_{c_{min}}^{\infty} f_{\Gamma} \left(a, \frac{\bar{c}}{a}, c_{min}; x \right) \prod_{j=1}^{k_i} f_N(\sigma; x + S_{ij}^D) dx \right)$$

where $f_{\Gamma}(a, \bar{c}/a, 1, c_{min}; x)$ and $f_N(\sigma; S)$ denote the probability density functions of the generalized Gamma distribution (as parameterized in Mathematica 9.0) and of the Normal distribution with mean 0 and standard deviation σ , respectively. The integral in the above expression can be further analytically expressed as

$$\begin{aligned} \phi(i, \boldsymbol{\theta}) &= \int_{c_{min}}^{\infty} f_{\Gamma} \left(a, \frac{\bar{c}}{a}, c_{min}; x \right) \prod_{j=1}^{k_i} f_N(\sigma; x + S_{ij}^D) dx \\ \phi(i, \boldsymbol{\theta}) &= C(k_i) A_i \left(\Gamma \left(\frac{a}{2} \right) HF1 \left(\frac{a}{2}, \frac{1}{2}, B_i^2 \right) + 2 B_i \Gamma \left(\frac{a+1}{2} \right) HF1 \left(\frac{1+a}{2}, \frac{3}{2}, B_i^2 \right) \right) \end{aligned}$$

where $HF1$ is the hypergeometric function, while the constants are

$$\begin{aligned} C(k) &= 2^{a-1-k/2} \frac{(\alpha/\sqrt{k})^a}{(\sigma\sqrt{\pi})^k \Gamma(a)} \\ A_i &= \exp \left(- \sum_{j=1}^{k_i} x_{ij}^2 \right) \\ B_i &= \left(\sum_{j=1}^{k_i} x_{ij} - \alpha \right) / \sqrt{k_i} \end{aligned}$$

with $x_{ij} = (S_{ij} - c_{min}) / (\sqrt{2}\sigma)$ and $\alpha = a\sigma / (\sqrt{2}\bar{c})$. The log-likelihoods of data from mutants independently screened at different doses were then summed up. Depending on the model, their fitted

parameters $\boldsymbol{\theta}_D$ varied across screen doses D or not. Over screen doses ranging from $D = 1$ ($3 \mu\text{g.ml}^{-1}$) to $D = 5$ ($20 \mu\text{g.ml}^{-1}$), the likelihood of the full dataset was computed as

$$\mathcal{LL}(\boldsymbol{\theta}_1, \dots, \boldsymbol{\theta}_5) = \sum_{D=1}^5 \mathcal{LL}_D(\boldsymbol{\theta}_D)$$

Likelihood maximization was performed either separating *gyrA* mutants from non-*gyrA* mutants into two independent datasets or keeping all mutants sequenced in a single dataset. Maximum Log-likelihood values from models separating *gyrA* and non-*gyrA* mutants were summed up to allow comparison with models including all sequenced mutants. For each model, estimated parameters are detailed in Table 2 and Supplementary Table 1.

Fitness trade-offs in the evolution of bacterial antibiotic resistance at different concentrations along a gradient

Harmand Noémie¹, Gallet Romain², Martin Guillaume³, Lenormand Thomas¹

1. UMR 5175 CEFÉ, CNRS - Université Montpellier - Université P. Valéry - EPHE, Montpellier Cedex 5, France
2. INRA - UMR BGPI, Cirad TA A-54/K Campus International de Baillarguet 34398 Montpellier Cedex 5, France
3. Institut des Sciences de l'Evolution de Montpellier, UMR CNRS-UM II 5554, Université Montpellier II, 34 095 Montpellier Cedex 5, France

Abstract

Antibiotics are found at many concentrations in microorganisms habitats. This context has to be taken into account to understand and manage the evolution of antibiotic resistance. A central tenet of evolutionary ecology is that different ecological conditions select for distinct adaptations. This view has been largely emphasized by measuring fitness trade-offs among well adapted phenotypes across environments. For this reason, the cost of antibiotic resistance, the trade-off between treated and non-treated environments, stands as a central element in resistance management strategies. This classical view however neglects that trade-offs may occur pervasively throughout dose gradients. In this study, we evolved experimentally resistant lines of *Escherichia coli* at different antibiotic concentrations during 400 generations and measured their relative fitness across the dose gradient. Our results reveal rapid specialization for the dose of evolution consistent with a model with different phenotypic optima for different antibiotic concentrations. Those results also provide a general explanation for variability observed in the costs of resistance. Finally, few replicates revealed historical contingency for which trajectories were explained without considering multiple fitness peaks per environment, as usually done.

Keywords

Experimental evolution, *Escherichia coli*, specialization, historical contingency, fitness landscape

Introduction

The massive use of antibiotics since the 1950's greatly improved standards of living in our societies but lead to an explosion in the number of resistant phenotypes in microorganisms (World Health Organization 2014). Besides being naturally excreted by microorganisms, antibiotics are also massively used for medical, agronomical, veterinary and industrial purposes. The occurrence of antibiotics is most often associated to gradients of concentrations (hereafter doses). Within the body of treated animals or humans, the antibiotic molecules are differentially absorbed, distributed and eliminated resulting in large variations of doses (Levison and Levison 2009). These gradients also occur in the environment. Antibiotic molecules easily diffuse over long distances and pollute soils and water (Thiele-Bruhn 2003; Kümmerer 2009; Depledge 2011). Thus, from hospitals or farms to rivers or soils, a very large panel of antibiotic molecules is present at varying doses.

A central tenet of evolutionary ecology is that different ecological conditions select for distinct adaptations, *i.e.* diverging phenotypes. This view applies to gradual ecological changes. For instance, the beak size and shape of Darwin finches evolve differentially depending on the size and the toughness of the seeds available in their environment (Grant and Grant 1999). The ultimate cause of this phenomenon is simply that different "solutions" are optimal for different "problems". This view is directly associated with the idea that there are trade-offs to adapt to distinct ecological conditions, *e.g.* it is not possible to simultaneously have a small and large beak. Considering that different trait values are optimal in different environments is tantamount to assuming fitness trade-offs across ecological conditions.

Evolution in heterogeneous environments in the presence of trade-offs has been extensively studied but is not straightforward. The degree of adaptation expected to evolve depends on the spatial and temporal context, the mode of population density regulation, the strength of trade-offs and the genetic architecture of the traits involved in adaptation. It may result in the evolution of 'specialist' strategies, 'generalist' strategies or in a coexistence of the two (Bell 1997; Kassen 2002; Lenormand 2002; Ravigne et al. 2009; Débarre and Gandon 2010). While local adaptation, specialization, and trade-offs have been widely documented, they are not always found when investigated in natural populations (reviewed in Hereford 2009). Apart from technical issues (precision on fitness measures), trade-offs may be undetectable because 1) they are hidden by large variations in fitness caused by unconditionally deleterious or beneficial mutations, 2) they are weak because they have been attenuated by a long history of adaptation (environments considered are not outside the current range of well tolerated conditions) (Gallet et al. 2014), 3) environments do not really represent different 'problems' of nature. Another

difficulty is that natural populations were most often exposed to a complex set of ecological conditions in the past, which makes it difficult to link adaptive traits with specific environmental conditions. Experimental evolution using microbes in controlled conditions has become essential to address these issues (Bell 1997; Kassen 2002; Elena and Lenski 2003; Garland and Rose 2009; Jansen et al. 2013). With this approach, highly adapted phenotypes can be obtained in response of defined selective pressures, which can be used to reveal fitness trade-offs among various environments.

Several evolution experiments have measured such trade-offs by estimating the difference in relative fitness between evolved lines and their ancestor in several environments. For example, specialization has been investigated across different temperatures (e.g. on bacteriophage in Bull et al. 2000, on *E.coli* in Bennett and Lenski 2007), luminosity levels (on *Chlamydomonas* in Reboud and Bell 1997), nutrient sources (on *E.coli* in Cooper and Lenski 2000; *Pseudomonas fluorescens* in Bataillon et al. 2011), or pH (on *E.coli* in Hughes et al. 2007; Gallet et al. 2014). Measuring fitness along an environmental gradient, rather than a set of unrelated environments, is of particular interest because it allows scanning large environmental variation ranges with a quantified “distance” between habitats and estimate whether levels of adaptation can be understood and predicted in reference to this “distance”.

Trade-offs also have a major role in the evolution of antibiotic/pesticide resistance. They are classically measured by evaluating the “fitness cost” of resistance alleles relative to a susceptible allele in the absence of antibiotic (Lenski 1998; Andersson and Levin 1999; Ward et al. 2009; Sousa et al. 2012). From an evolutionary perspective, the magnitude of the cost of resistance determines the rate at which the frequency of resistance mutation decreases in the absence of antibiotic. It also determines the frequency at which resistance mutations are maintained at selection-mutation or selection-migration balance. It is thus a crucial parameter for management strategies (Bonhoeffer et al. 1997; Lenormand and Raymond 1998; Andersson 2006; Hall et al. 2015). A major limitation of this classical view is, nevertheless, that studies of trade-offs have been restricted to the conditions of absence versus presence of antibiotic, and not throughout dose gradients.

Strikingly, it is even assumed (at least implicitly) that there are no trade-off to adapt to different (non-zero) doses of antibiotic or pesticide. The presence of antibiotic determines a single fitness peak, and doses modulate the intensity of selection around that peak. As a consequence, low dose environments (meaning doses under the Minimum Inhibitory Concentration (MIC)) have been argued to strongly favor the emergence of high dose resistances in natural conditions (Gullberg et al. 2011; Andersson and Hughes 2012). Such low doses could favor the emergence

of resistance by providing small fitness advantages to resistance phenotypes which would (1) allow them to persist and remain available upon exposure to a higher dose (reservoir effect) or (2) allow the occurrence of additional mutations conferring resistance levels that would hardly be achieved in a single step (multiple hit effect). Implicit in this view is the fact that mutations favorable at low dose confer some advantage at higher dose (so that a multiple hit effect can occur) and that, perhaps to a lesser extent, high-dose resistances are also favorable at low dose (so that a reservoir effect occur). This view contrasts with the classical view of evolutionary ecology where trade-offs are pervasive and different environments correspond to different fitness peaks and select for different phenotypes (e.g. Darwin's finches). Because of these different views, it remains very unclear how adaptation proceeds along dose gradients (Gullberg et al. 2011; Hermsen et al. 2012; Milesi et al. 2016), which is a critical issue to understand long-term adaptation at different antibiotic doses, and obviously to determine the extent to which reservoir and multiple hit effects are important.

In a previous study, we investigated mutational and selective patterns across antibiotic dose gradients (Harmand et al. 2016). We screened resistant single mutants in different antibiotic doses and measured their fitness effects across a dose gradient. With these data, we showed that resistance to different doses mobilizes distinct mutational modules, i.e. distinct genetic targets with distinct phenotypes and fitness effects. Yet, these mutational patterns did not allow discriminating whether different doses correspond to different phenotypic optima or not. As in natural populations, screened resistant mutants in the lab may be far from the phenotypic optimum of their selective environment, making it difficult to detect fitness trade-offs among doses (Bataillon et al. 2011a; Martin and Lenormand 2015). To circumvent this limit, we experimentally evolved resistant lines of *Escherichia coli* at five doses of nalidixic acid (Nal) for 400 generations in order to 'push' them closer to their optimal phenotype. We measured the relative fitness of the lines in five Nal doses, before and after evolution. Our results reveal pervasive fitness trade-offs across environments: different doses selected for distinct optimal phenotypes. Surprisingly, adaptation to those distinct optima also revealed historically contingent adaptive trajectories. We show that these trajectories can be explained without considering multiple peaks, as usually done. Overall, our results call for more realistic models of resistance evolution in heterogeneous dose conditions.

Material and methods

- Bacterial strains

All mutants in the experiments were derived from the *E.coli* strain REL4536, corresponding to the 10,000th generation of Lenski's long term adaptation experiment (LTEE) to Davis minimal medium DM25 (Lenski and Travisano 1994). REL4536 is susceptible to nalidixic acid (Nal) with a MIC experimentally estimated at Nal 2.6. All Nal doses are given in $\mu\text{g.mL}^{-1}$, but these units will not be repeated below. Cyan and yellow fluorescent proteins (CFP, YFP) genes were previously introduced in REL4536 and REL606 (the ancestral strain of Lenski's LTEE) chromosomal DNA in order to perform competitions (Gallet et al. 2012). The resulting fluorescent strains REL4536 and REL606 are termed 10K-CFP, 10K-YFP and 0K-CFP, 0K-YFP in the following.

To obtain the evolution lines, six resistant 10K-YFP mutants were randomly chosen from each of three sets of single mutants, obtained in Harmand et al. (2016) using fluctuation assays at doses 3, 8 and 20 ('Mutants Nal' 3, 8 and 20 on Fig. 1). 'Mutants Nal' 100 and 200 could not be obtained in one fluctuation assay, as the resistance mutation rate is too low at these doses (at dose 20, this rate is already as low as 5.10^{-7}). They were obtained via an additional fluctuation assay (same protocol as in Harmand et al 2016), at doses 100 and 200 respectively, starting from 20 independent mutants obtained from the previous screen at dose 20. Six "double" mutants obtained in this way at dose 100 and 200, were used to start the corresponding evolution lines. We refer to them, here and below, as "double" mutants for convenience, as they are very likely to carry two new mutations, but we cannot formally exclude that they carry more mutations. Overall (Fig. 1), we obtain 30 evolution lines: 6 independent lines per 5 doses (at which they were screened). Our reference competitor for all competitions was the strain ref-CFP, used in (Harmand et al. 2016), which is a mutant from the set screened at dose 200 (distinct from the lines used for evolution).

The protocol of the fluctuation assays are detailed in (Harmand et al. 2016). Briefly, several cultures were initiated with few cells of the relevant ancestor and incubated 12h at 37°C in 200 μL LB medium without antibiotic (lysogeny broth-Miller (LB): 10 g.L⁻¹ NaCl, 10 g.L⁻¹ tryptone, 5 g.L⁻¹ yeast extract). Each culture was then plated on LB-Agar supplemented with Nal at the desired concentration and incubated 36h at 37°C. Each mutant belongs to one colony randomly picked from one non-empty plate.

- Antibiotic and culture media

Experimental evolution and competitions were performed in Davis minimal medium (DM0: 7 g.L⁻¹ KH₂PO₄.3H₂O, 2 g.L⁻¹ KH₂PO₄, 1 g.L⁻¹ (NH₄)₂SO₄, 0.5 g.L⁻¹ Na₃C₆H₅O₇, sterile water compensating exactly for evaporation after autoclaving; pH was set at 7.0) supplemented with 1250 µL.L⁻¹ glucose 10%, 806 µL.L⁻¹ MgSO₄ [1M] and 1000 µL.L⁻¹ thiamine 0.2%. This medium, (hereafter DM250) corresponds to the DM25 medium used in the LTEE, with ten times more glucose. The addition of glucose increases bacterial carrying capacity and allows for more accurate fluorescence measurements, but leads to very similar fitness measures in the LTEE (Cooper et al. 2001; Gallet et al. 2017). We thus assumed that REL4536 is well adapted to DM250, so that the dominant selective pressure during the experiment is the antibiotic. This assumption was checked by monitoring fitness variations of control lines in absence of antibiotics (see below). Fresh medium DM250 supplemented with Nal was prepared weekly and kept protected from light at 4°C to prevent degradation of the thiamine and Nal.

- Experimental evolution

The 30 evolution lines underwent independent experimental evolution at the Nal concentration at which they were screened (denoted ‘evolution dose’ 3, 8, 20, 100 or 200, Fig. 1). Six control lines were evolved in the absence of Nal (evolution dose 0): two were initiated with the strain 10K-CFP, two with 0K-CFP and two with 0K-YFP. The two 10K-CFP lines are expected to show limited adaptation to DM250 while the four 0K-YFP and CFP lines are expected to show adaptation trajectories reproducing that observed in the LTEE (Lenski and Travisano 1994; Wiser et al. 2013).

All lines were distributed into four 24-wells lidded microplates with 1ml medium per well, with the six Nal concentrations allocated in each plate. Inoculated wells were alternated with non-inoculated wells following a checkered pattern, to control for contaminations. The plates were incubated at 37°C, 200 rpm in a water-saturated atmosphere (sealed box). Every 24h, 10 µL of the cultured lines were transferred to new wells containing 1mL of fresh medium and incubated in the same conditions. Every two weeks, all lines were stored as glycerol stocks. The protocol was applied during two months corresponding to ~400 generations of evolution (as 1/100 dilution corresponds to $g = 6.64$ generations during exponential growth in DM250 for the strain REL4536). In the following, T_{ini} refers to the initial time of evolution, after the mutant screen, and T_{fin} refers to the final time of evolution (Fig. 1).

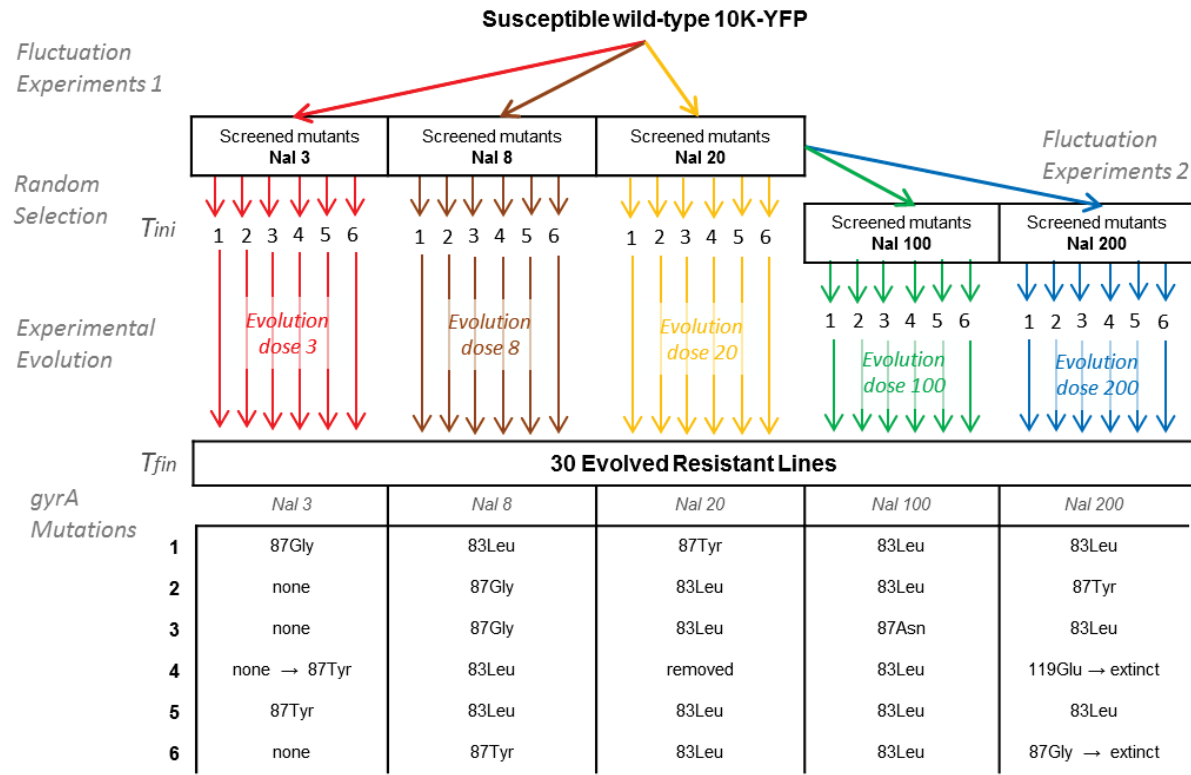


Figure 1: Schematic experimental protocol. In the upper part, mutants screen and experimental evolution in different doses of Nal ($\mu\text{g/mL}$) are represented by the colored arrows. Six experimental lines were evolved in each dose from a random selection of resistant mutants. Down, the sequenced resistance mutation in the *gyrA* gene at T_{ini} as well as at T_{fin} (only line 4 in Nal 3 changed between T_{ini} and T_{fin}).

- Sequencing

All lines were sequenced at the *gyrA* gene at T_{ini} and T_{fin} . This sequence covers most of the promoter and 32% of the *gyrA* gene and its complete quinolone resistance-determining region (Hopkins et al. 2005). PCR were performed on colonies, using the mix: 10 μL of 2X Phusion Master Mix, (ThermoFisher Scientific, Waltham, MA), 1 μL of F-primer 5'-AGACAAACGAGTATATCAGGCA [position in *gyrA* sequence: -120pb to -101pb], 1 μL of R-primer 5'-TTTACCAGTTCCGCAATCTTCTC [position in *gyrA* sequence: 823pb to 845pb], 8 μL sterile distilled water; and the PCR program: 5' 95°C, 35 cycles of [1' 95°C, 1' 61°C, 2.5' 72°C] and 5' 72°C]. Sequencing was performed by Eurofins mwg operon (Eurofins, Luxembourg). Mutations in *gyrA* gene were identified by comparing the mutant sequences to that of the wild-type strain 10K-YFP.

- Competition experiments

Competitions experiments were performed from glycerol stocks at T_{ini} and T_{fin} . For each mutant (YFP), we performed five competitions in DM250 at doses 3, 8, 20, 100 and 150 (denoted ‘measure dose’ or ‘MD’) against the resistant mutant ref-CFP. This provides a “fitness profile” across the measure dose gradient, for a given line. The measure dose 150 was preferred to dose 200 (corresponding to the highest ED) because the latter highly inhibited the growth of the reference competitor, such that fluorescence measurements were close to the detection limit. A sixth competition was performed in DM250 in the absence of antibiotic, against the strain 10K-CFP, to measure the fitness cost of resistance relative to the susceptible ancestor.

Competition assays were performed as follow. 1:1 volumic ratio competition mixes were prepared from saturated cultures. Fluorescence signals of these mixes were measured on a Tecan Infinite 200 (Tecan, Männedorf, Switzerland) prior to the competition (t_0). Competitions were initiated by inoculating 2 μL of the competition mix into 200 μL of DM250 (and a given dose of Nal). Fluorescence signals were measured again after 24h of growth (t_{24}) in the same conditions as the evolution experiment (37°C, 250 rpm, water saturated atmosphere). Each competition was repeated at least three times at different dates. We assumed that fitness effects were transitive between genotypes competing in the same dose. Deviation from transitivity as measured in Gallet et al. (2012) for strains competing in similar experimental conditions are very small (10^{-3} at most in these experiments).

The selection coefficient per generation associated with each competition was estimated as:

$$s = \frac{1}{g} \left(\log \left(\frac{n_{\text{YFP}}}{n_{\text{CFP}}} \right)_{t_{24}} - \log \left(\frac{n_{\text{YFP}}}{n_{\text{CFP}}} \right)_{t_0} \right) \quad (1)$$

with $\frac{n_{\text{YFP}}}{n_{\text{CFP}}}$ the ratio of frequencies of YFP and CFP cells estimated from the ratio of YFP on CFP fluorescences in the mix using an experimental calibration curve. The constant $g = 6.64$ is used to scale per generation. It approximates the number of divisions, assuming full regrowth from a dilution by 1/100 over a 24h assay. We denote “fitness” the selection coefficient of a line relative to the reference strain ref-CFP, and “fitness cost” the selection coefficient of a line relative to the ancestor 10K-CFP (for measures in the absence of antibiotics).

- Statistical analysis

We analyzed fitness variations between measure doses (MD), evolution doses (ED) and initial vs. final time. A linear mixed model (lmer in R 3.2.0, R Core Team) was used, with fixed effects (1)

“ED” (5 doses), (2) “MD” (5 doses), *time* (T_{ini} and T_{fin}) and “*MutID*” the identity of the initial resistance mutation (5 different mutations in the *gyrA* and 1 extra level combining all non-*gyrA* mutations). Random effects included *lineID* (line identities), plate and date of the competition assay. We investigated whether the lines adapted to the antibiotic (effect of *time*) differently across evolution and measure doses (*time.MD.ED*). We also checked whether the initial mutation impacts the adaptation trajectory and pattern (any interactions including *MutID*). In this analysis, ED and MD effects are evaluated on average across evolutionary and technical replicates. The models including (or not) the various possible interactions were compared based on their AIC.

In order to illustrate how each line evolved in more details, we also conducted the same analysis with *lineID* as a fixed effect and dropping *ED* and *MutID*. This analysis included control lines and competitions at dose zero. The effects estimated for each line in each MD (averaged across technical replicates) at one time of evolution were used to plot the results in Figs. 2, 3, 5 and Supp. Fig. 2. This last analysis was also used to estimate the fitness changes between T_{ini} and T_{fin} of each line in each MD (Fig. 4) and test whether it was different from zero (pairwise comparisons performed with mvt adjustment from lsmeans R package).

Results

- Control lines

Selection coefficients of lines 10K-CFP neither vary significantly over time in DM250 (*P-values* = 0.399) nor between replicates (*P-value* = 0.772) (Supp. Fig. 1). This result confirms that the ancestral strain is already well adapted to DM250. Hence potential variations in fitness on evolution lines result predominantly from adaptations to the presence of Nal. The differential cost of the fluorescence markers obtained in 10K-YFP versus 10K-CFP competitions was estimated at -0.03 (*P-value* < 0.01). All selection coefficients below were corrected for this cost.

The selection coefficients of 0K lines in competition versus 10K, show a significant increase through *time* (*P-value* < 10^{-4}) due to adaptation to experimental conditions (Supp. Fig. 1). The 0K-YFP and CFP lines were not mutually different (*P-values* > 0.1), except one of the 0K-YFP lines that differed from the three others at the 400th generations of evolution due to a fitness jump (*P-value* = 0.006). This fitness trajectory is consistent with that expected from the similar 400 generations evolution in DM25 in the LTEE (Lenski and Travisano 1994). These results confirm that the ten-fold increase in glucose in DM250 does not cause substantial differences in evolutionary trajectories compared to those observed in DM25 to which the ancestor REL4536

has adapted for 10'000 generations in the LTEE (Cooper et al. 2001; Gallet et al. 2017).

- Resistance mutations in the *gyrA* gene

Among the 30 evolving lines, three different *gyrA* mutations (83Leu, 87Tyr and 87Gly) and some non-*gyrA* mutations were initially sampled across the sets of single resistant mutants screened at the doses 3, 8 and 20 (Fig. 1). Evolution lines at ED100 and 200 were initiated with resistant mutants screened in two-steps fluctuation tests, which are most probably double mutants. However, all those mutants showed only a single mutation within the *gyrA* sequence (83Leu, 87Asn, 87Tyr or 119Glu).

Two lines evolving at ED200 (initiated from *gyrA* mutants 87Gly and 119Glu) went extinct early in the evolution experiment. One of the lines evolving at ED20 proved to be initially polymorphic for the *gyrA* resistance mutation. This line was removed from later analysis in order to avoid confusion in the data interpretation. In other lines, no additional mutations than the ones detected at T_{ini} were detected in the *gyrA* sequence at T_{fin} . Among the four lines without *gyrA* mutations initially, only one line fixed a *gyrA* mutation (87Tyr) during the evolution experiment.

Fixed effects															ΔAIC
ED	MD	T	GB	ED:MD	ED:T	MD:T	ED:GB	MD:GB	T:GB	ED:MD:T	ED:T:GB	MD:T:GB	ED:MD:GB	ED:MD:T:GB	
1	1	1	1	1	1	1	1	1	1	0	1	1	1	0	0
1	1	1	1	1	1	1	1	1	1	1	0	1	1	0	1
1	1	1	1	1	1	1	1	1	1	1	0	1	1	1	13
1	1	1	1	1	1	1	1	1	1	0	0	1	1	0	32
1	1	1	1	1	1	1	1	1	1	1	0	0	1	0	32
1	1	1	1	1	1	1	1	1	1	1	0	1	0	0	34
1	1	1	1	1	1	1	1	1	1	0	1	1	1	0	34
1	1	1	1	1	1	1	1	1	1	1	1	1	0	0	102
1	1	1	1	1	1	1	1	1	1	1	1	0	1	0	103
1	1	0	1	1	0	0	1	1	0	0	0	0	1	0	589
1	1	1	0	1	1	0	0	0	0	1	0	0	1	0	604
0	1	1	1	0	0	1	0	1	1	0	0	1	0	0	667
1	0	1	1	0	1	0	1	0	1	0	1	0	0	0	1702

Table 1: Global analysis of selection coefficients. Each line represents a mixed model including (1) or not (0, shaded) an effect of the evolution dose (ED), the measure dose (MD), the time of evolution (T = T_{ini} or T_{fin}), the genetic basis of initial resistance (GB, the identity of the *gyrA* mutation or no *gyrA* mutation) and all possible interactions. The line identity and the date and plate of competition were considered as random effects in all models. Models are ranked based on their difference in AIC value compared with the best model (first line).

- Analysis of selection coefficients across doses

Selection coefficients of the different lines, at different MD, and at initial and final evolution time, were analyzed with different mixed-models (Table 1). The best model includes the triple interaction *ED.MD.Time*. This indicates that lines (1) evolved differently depending on the ED and (2) changed in fitness profiles across MD. The quadruple interaction, that includes also *mutID*, was not significant indicating that these changes did not strongly depend on the first mutational step. As expected, there was no effect of the *ED* at T_{ini} for ‘single mutants’ once *mutID* was taken into account (since at T_{ini} , the differences between lines are a priori only due to *mutID*). However at T_{fin} , *MD*, *ED* and *mutID* all have significant effects on selection coefficients. Assuming that all lines ultimately reached a common phenotypic optimum (across evolution doses (ED)), neither *ED* nor the genetic basis of resistance (*mutID*) should remain significant. This result thus suggests that lines have not reached the same optimal phenotype, neither among nor within ED.

- Adaptation to the different dose of antibiotic

In order to determine if, as expected, lines adapted to their ED, selection coefficients of each line were compared between T_{ini} and T_{fin} , at the dose to which they evolved. In all cases, this fitness change was positive or not significantly different from zero (Fig. 2). In the case of lines evolved at ED200, for technical reasons the fitness change was measured at MD150, which was not their ED, but here too, fitness changes were positive or not significantly different from zero.

The magnitude of the fitness increase in the ED was negatively correlated with the selection coefficient of the line at T_{ini} (*P-value* < 10⁻⁴), with a significant effect of the genetic module of resistance (*i.e.* mutation in the *gyrA* gene or not) on the intercept (*P-value* = 0.002) (Fig. 2). The lines showing the lowest fitness change were also the most adapted lines at T_{ini} .

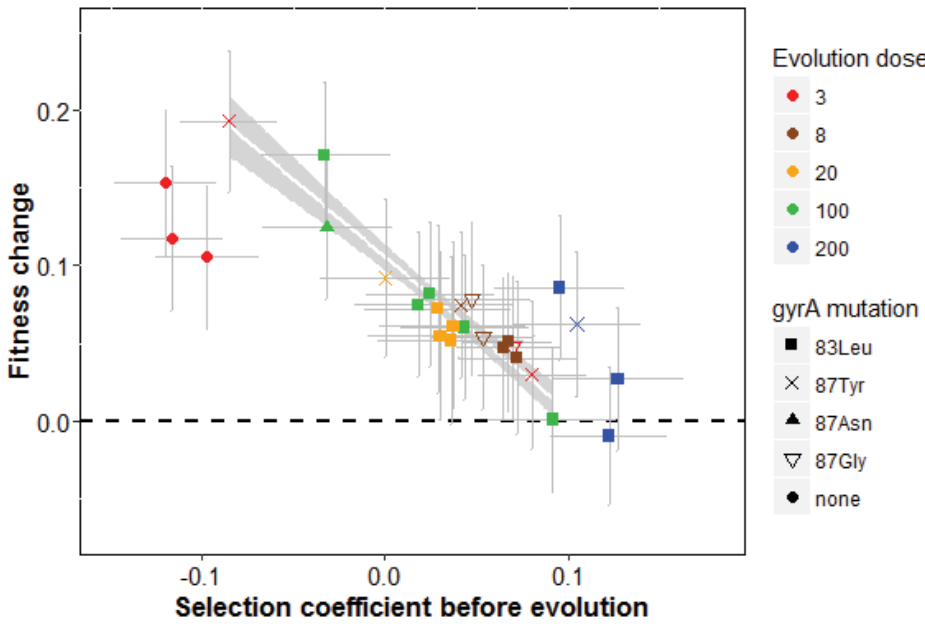


Figure 2: Fitness change per resistant line after 400 generations of evolution vs. initial fitness in the measure dose corresponding to the evolution dose (lines evolved at dose 200 were measured in dose 150, so were not included in the model). Symbols indicate the *gyrA* mutations sequenced in each line while colors indicate the dose at which they were selected. The best model yields different intercepts for non-*gyrA* lines (*circles*) and *gyrA* lines (all other symbols and the corresponding model indicated by the grey zone). Error bars represent standard errors of the mean estimates among replicate measures.

- Fitness trade-offs across evolution doses and evolution of specialization

Specialization was analyzed by comparing the selection coefficients, measured in each MD, of the lines evolved at different ED. The fitness effects of lines are directly comparable within the same MD, but not across MD, as a part of the variation across MD could be caused by fitness changes of the reference line across MD. To avoid this confusion, the fitness effects are scaled to range between 0 and 1 in each MD on Fig. 3 (unscaled values are shown on Supp. Fig. 2). Thus, only the position of the maximum and the shape/curvature of the functions are meaningful when comparing patterns of specialization across different MD. The three lines that did not have a *gyrA* mutation at T_{fin} , showed large differences of fitness profiles compared with *gyrA* lines evolving at the same dose (ED3) (Supp. Fig. 2). They were not included in the average effects represented on Fig. 3 for comparison with other ED. We discuss more precisely these three non-*gyrA* lines below.

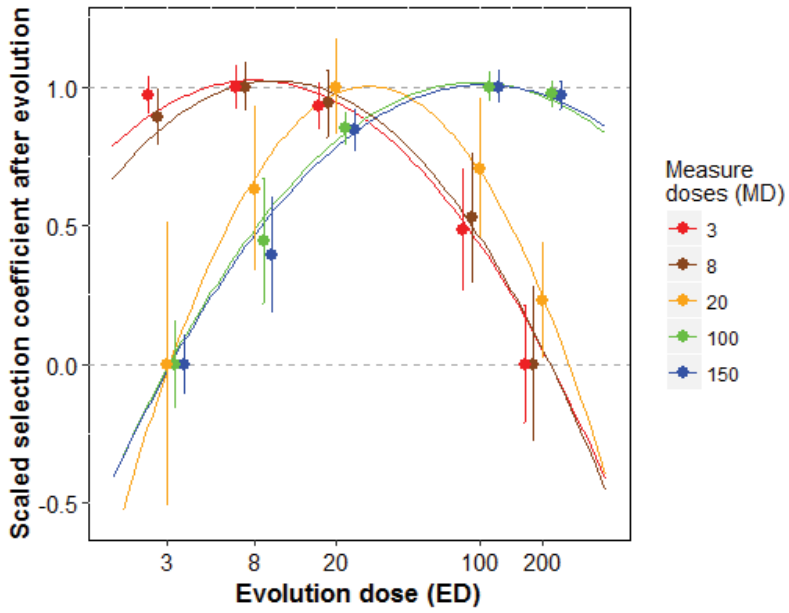


Figure 3: Final fitness profiles of *gyrA* resistant lines across evolution doses. Mean selection coefficients and standard deviations are scaled to range between 0 and 1 within each measure dose (see legend), for clarity of comparison (unscaled selection coefficients per lines included non-*gyrA* lines are showed in Supp. Fig. 2). For each measure dose, traits of the corresponding color show the fitted parabolic functions of the log-evolution dose.

In each MD, the selection coefficients of evolved lines are well fitted by a quadratic function of the log-ED ($\Delta AIC=27$ compared to a model including a factorial effect of ED, Fig. 3 and Supp. Fig. 2). The relative fitness of resistant mutants shows a simple and predictable pattern across evolution doses, with the curvatures being surprisingly similar, on a log-concentration scale. Importantly, the fitted maxima changes across MD and correspond to the ED, at MD 8, 20 and 100. At these three doses, the evolved line reaching the highest fitness is the one that evolved in this dose. This general pattern is still observed at MD3 and MD150, but the maximum is similar that observed at MD8 and MD100, respectively. These results show that there are strong fitness trade-offs on the phenotypic traits related to the resistance at low (3, 8), intermediate (20) and high (100, 200) Nal doses.

- Fitness variation during evolution

The pattern of specialization shown on Fig. 2 was not present at T_{ini} , just after the screen of the first mutation(s). It evolved over the course of the experiment. To see this, we illustrate on Fig. 4 the fitness changes (between T_{ini} and T_{fin}) of each line at all MD (see also Harmand et al. 2017 for the fitness pattern of screened mutants). A positive fitness change in a given MD indicates that

the line adapted to this MD (even though it evolved at another dose), and conversely a negative value indicates ‘de-adaptation’. On average, the lines evolved at low ED (3, 8 and 20) show an adaptation (or no change) in all MD, suggesting that evolving at low dose is beneficial for resistance at high dose. However, it is important to note that despite this adaptation, those lines show low fitness at T_{fin} at high doses (100 and 150). A different pattern is observed for lines evolved at high doses. While they adapted to their ED, they tended to ‘de-adapt’ to low doses. This same pattern is found when comparing the fitness of ED 100 and 200 double-mutants with the fitness of single mutants (of other ED) sharing the same *gyrA* mutation at T_{ini} . This comparison (not shown) indicates that the second mutation in these double mutants already caused a decrease in fitness at MD3 and 8. Finally, Fig. 4 shows that average fitness changes follow a regular pattern across both increasing ED and MD including dose zero. This observation suggests that evolving at different doses involved progressing toward the same phenotypic direction but with different optimal targets, which seems to be placed regularly along the dose gradient.

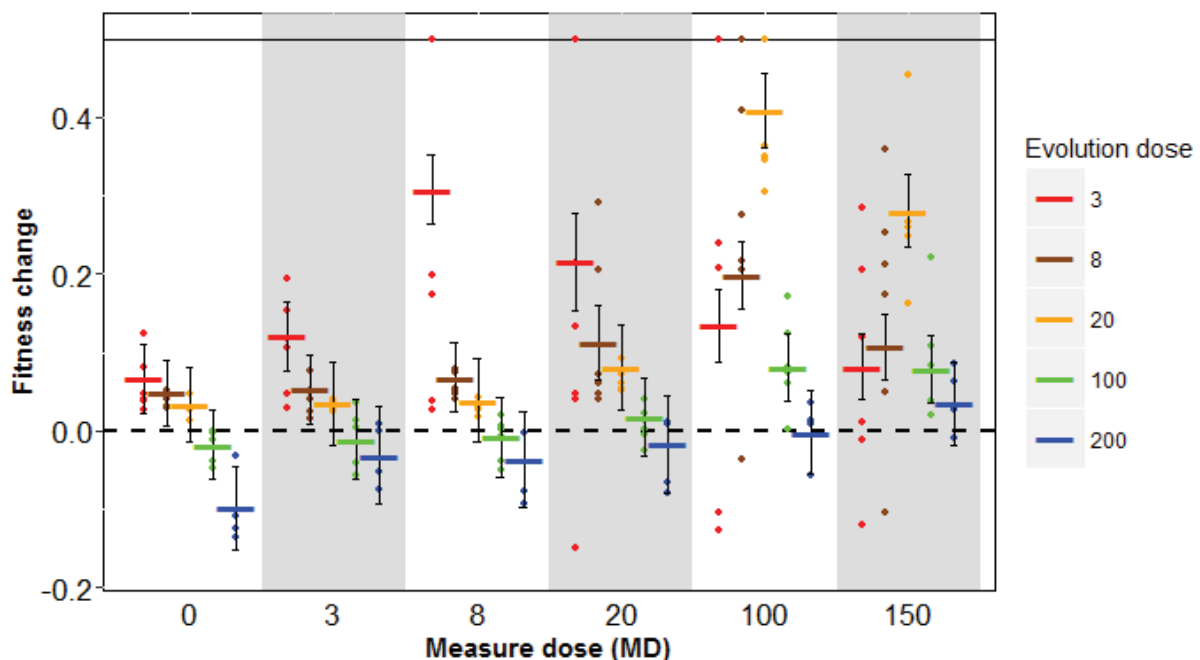


Figure 4: Fitness change of resistant lines after 400 generations of evolution at different measure doses (x-axis) and evolution doses (colors) of Nal antibiotic in $\mu\text{g}/\text{mL}$. Horizontal bars represent the mean values with their standard errors considering all lines evolved at the same dose. Dots are mean values for each different line. Positive values of fitness change indicate an adaptation to the measure dose whereas negative values stand for a counter-adaptation. The black horizontal line at 0.5 represent the superior limit; for the clarity of the figure, dots with values outside this range are represented on the line.

- Influence of initial mutational steps

The identity of the initial *gyrA* mutations (e.g. 83Leu) did not predict their evolutionary trajectory: they diverged after evolving at different ED. At T_{fin} , their fitness profiles across doses are completely different and are more similar to fitness profiles of lines evolved at the same ED but with a different initial resistance mutation (Supp. Fig. 2). Dose-specialization pattern is little influenced by the first mutational step, at least within the *gyrA* module: there is little historical contingency in this case. The situation is different when comparing lines with or without *gyrA* mutations evolved at ED3. The fitness profiles of the latter show a very different adaptive trajectory, showing much less adaptation in their ED, and lower fitness at every MD than *gyrA* lines also evolved at ED3 (Supp. Fig. 2). Here, there is a very strong signal of historical contingency on the first mutational step. Furthermore, sequencing revealed that three of these four non-*gyrA* lines did not fix a *gyrA* mutation later, during the experiment. This is *a priori* odd given the high fitness benefit of *gyrA* mutations and the high fitness eventually achieved with lines initially started with a *gyrA* mutation. Hence, we observe strong historical contingency across but not within modules.

- Evolution of the cost of resistance

At T_{ini} , all resistance mutants were costly and the costs were variable among the different resistance mutations (Fig. 5). It was also variable among ‘double’-mutants of ED100 and 200, even when they carried the same *gyrA* mutation. The change in cost between T_{ini} and T_{fin} was negatively correlated with the ED (pP -value $<10^{-6}$, MD 0 on Fig. 4). Adaptation to high ED led to an increase in the fitness costs of resistance. On the contrary, adaptation to low ED (3, 8, 20) led to smaller costs, suggesting that initial mutations were overshooting. At T_{fin} , the *gyrA* lines are increasingly costly with higher ED (filled black circles on Fig. 5). The non-*gyrA* lines (present only at ED3) have generally higher costs than the *gyrA* lines (see also Harmand et al. 2016), which leads to a higher mean cost at ED3 than ED8 or 20.

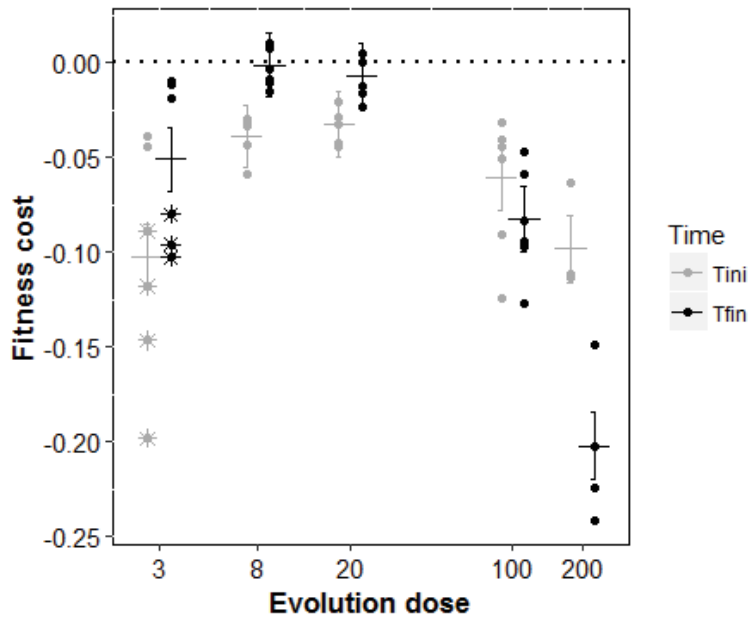


Figure 5 : Evolution of the cost of resistance across Nal doses. Horizontal bars represent the mean values with standard errors for lines evolved at the same dose. Dots are mean values for each different *gyrA* line before and after 400 generations of evolution in antibiotic whereas stars indicate the non-*gyrA* lines.

Discussion

In order to investigate the existence of fitness trade-offs among adaptive traits at different antibiotic concentrations, we experimentally evolved resistant lines of *E.coli*. Our results show that lines diverged after 400 generations and specialized to their evolution dose, revealing the existence of pervasive fitness trade-offs in adaptation to different doses of an antibiotic gradient.

- Fitness landscape along a gradient of antibiotic doses

The occurrence of fitness trade-offs strongly supports the idea that doses can be considered as different “environmental conditions” or different selective constraints in terms of adaptation. Using the well-known representative metaphor of adaptive fitness landscape, this means that the phenotypic position of the fitness peak is changing along the dose-gradient. The fitness profiles of our evolved lines also appear to be remarkably regular along the dose gradient, suggesting that it should be possible to make prediction for other ED than the ones we use. The optimal MD very consistently tracks the ED and fitness is monotonously decreasing from the optimum as shown by quadratic relationships with log-concentration of the antibiotic (Fig. 3). These results

provide evidence for modeling adaptation along ecological gradients using a gradual shift in phenotypic optimum as often assumed (e.g. Lynch and Lande 1993; Kirkpatrick and Barton 1997). This finding does not exclude variations in the selection intensity across doses (Harmand et al. 2017), but such variation alone, without a variation in the position of the peak, would not account for our data.

Some patterns of adaptation between lines, within each evolution dose, are also consistent with previous observations in other environments and microbial experiments. In particular, the net adaptive change scales linearly with initial maladaptation (Fig. 2). This “rule of declining adaptability” (Couce and Tenaillon 2015) which is known to be predicted by simple fitness landscape models (Couce and Tenaillon 2015; Martin and Roques 2016), seems to also apply in our dataset. Overall, this study suggests that evolution across antibiotic dose gradients may be captured, at least qualitatively, by classic evolutionary ecology concepts and peak shift models.

- Consequences for the evolution of resistance

From a practical point of view, the existence of different phenotypic optima regularly arranged along a dose-gradient has several implications. First, selection at low and intermediate doses can indeed promote adaptive steps toward high resistance (consistent with a reservoir effect). Second, phenotypes evolved at intermediate dose are better adapted to high doses than phenotypes evolved at low dose (consistent with multiple hit effect). Third, long term selection at low dose will not result in high fitness (meaning optimal phenotypes) at high dose, and reciprocally, long-term selection at high dose will not select for high-fitness phenotypes at low dose. These conclusions have important implications for understanding and modeling the evolution of resistance in the field under heterogeneous conditions.

To our knowledge, no previous study has clearly established the pattern of dose-specialization so far. Many studies have investigated resistance mutants from clinical isolates (several examples reported in Davies and Davies 2010). However, as is often the case when studying natural populations, the context (and dose) in which those mutants evolved is usually unknown and potentially complex. These situations can therefore hardly reveal the occurrence of trade-offs across doses. Second, some studies focused on short-term antibiotic resistance from screened mutants (Thulin et al. 2015; Harmand et al. 2017). In general, this short-term evolution cannot easily reveal trade-offs across environmental conditions, especially when the initial type is highly maladapted (Bataillon et al. 2011; Martin and Lenormand 2015), as it is the case for resistance when starting from a susceptible wild-type. Last, studies that used long term evolution of resistance often focused on the evolution of the cost of resistance, *i.e.* the trade-off between

absence vs. a given dose of antibiotic (reviewed by Melnyk et al. 2015) and/or did not assay directly fitness across doses (*e.g.* Gullberg et al. 2011; Hughes and Andersson 2012). While it is clear that such studies provide key insight for resistance management, studying fitness variations across full gradients and in particular low doses is probably critical to develop accurate management models.

Because of the occurrence of shifted optima across doses, the long-term cost of resistance largely differs between the doses in which it evolves (Fig. 5). Previous studies have highlighted that fitness costs are highly variable (*e.g.* depending on mechanisms) and difficult to predict in a general way (Melnyk et al. 2015; Vogwill and Maclean 2015). Our results show that taking into account different dose-environments is a key element (see also Westhoff et al. 2017). Because low dose optima are closer to dose zero than high dose optima, the dynamics of cost evolution can be opposite depending on the dose. We found a negative correlation between the fitness cost changes and the evolution dose (Fig. 4). At low dose, initial costs are quickly compensated, suggesting that the first mutational step overshot the phenotypic optimum at low ED. After compensation, they become very small, as expected since selection intensity has to be much lower around the ED0 optimum than around optima with antibiotics. At high dose however, costs increase. The presence of different optima across doses explains this pattern and can thus provide a powerful conceptual framework to understand the large variability of fitness costs observed previously in long term studies.

- Historical contingency of adaptive trajectories

'Historical contingency' or 'mutation-order' effects have been widely discussed in the literature to describe the dependence of adaptive trajectories on initial conditions (Elena and Lenski 2003; Lenormand et al. 2009, 2016; Lobkovsky and Koonin 2012). Our results show that the pattern of specialization at final time is not dependent on the identity of the first *gyrA* mutation. However, we find strong historical contingency at ED3 where some initial mutational steps are non-*gyrA* mutations and exhibit very different adaptive trajectories and different final fitness profile across MD. Such pattern is typically interpreted with multiple fitness peaks and the stochastic occurrence of mutations bringing the population in the attraction basin of different peaks. However, our study points to a different and new interpretation. The study of the fitness effects among screened mutants in Harmand et al. (2017) revealed the occurrence of mutational modules (*i.e.* different subsets of phenotypic traits are affected by the mutations among different modules) and selective covariances across traits in this system. In such a situation, mutation order effects can occur even with a single fitness peak, and the hypothesis of multiple peaks is not necessary. Such a scenario is illustrated in Fig. 6. Because of selective covariances, the

fixation of a mutation in one module may shift the phenotype in such a way that most mutations in all modules become deleterious ('blocking' effect on Fig. 6). In this scenario, progress towards the phenotypic optimum would then require a series of very small effects mutations in both modules, which is likely to be extremely slow. This secondary phase of slow progress towards the optimum is qualitatively different from the situation expected with multiple peaks (where a secondary peak shift may occur after a long stasis). This difference should allow, in principle, to test the two alternative models. Interestingly, this phenomenon might be quite general after a period of fast adaptation. For instance, in the LTEE, populations are still adapting slowly after 50 000 generations (Wiser et al. 2013), consistently with a scenario where mutational modules, combined with selective covariance strongly limit the rate of adaptation (Fig. 6).

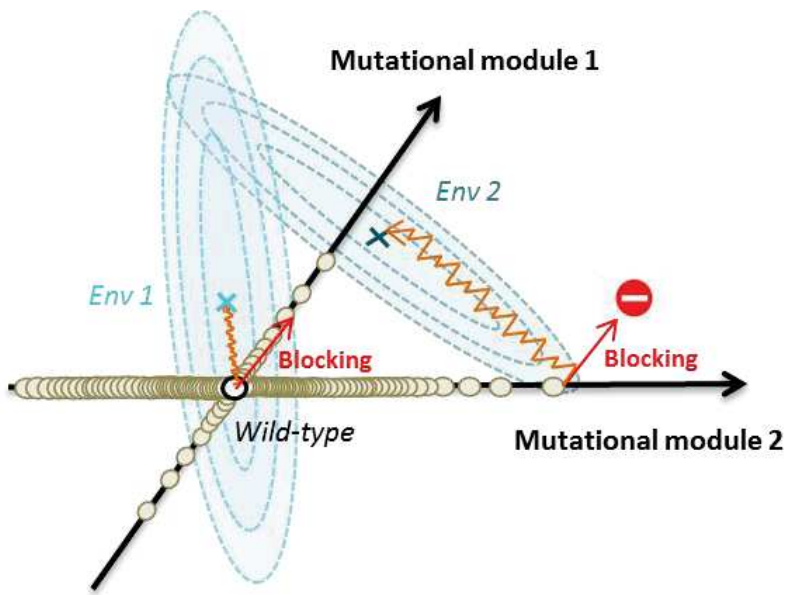


Figure 6: Schematic fitness landscape illustrating the 'blocking' effects in a single peak landscape with selective covariance and mutational modularity. The landscape is represented as a contour plot of the fitness functions of two different environments (Env1 and Env2), with crosses being the fitness optima and dotted ellipses as isofitness contours. Beige dots symbolizes random mutants of the wild-type (white dot) distributed on two mutational modules.

Overall, our results show that the evolution of resistance along antibiotic dose gradients is consistent with classic evolutionary models of adaptation on ecological gradients, where each environment corresponds to one peak. The observed patterns of adaptation and maladaptation are fully consistent with the occurrence of dose-dependent optima and show pervasive trade-offs across doses. The few cases showing historical contingency and mutation order effects, can still be explained in this context. Elaborating these peak shift models are likely to be important to improve resistance management models and include the impact of low doses of antibiotics that

are now ecologically widespread.

Acknowledgements

We thank M.-P. Dubois and R. Zahab for lab management and the Montpellier Ressources Imagerie (MRI) platform. We also wish to thank S. Bedhomme, P. Labbé, T. Hindré and N. Bierne for discussions. The original strain RELB 4536 was kindly provided by Richard Lenski's lab. This work was supported by a PhD grant from French ministry of research to NH, and the ANR SilentAdapt to T.L.

References

- Andersson, D. I. 2006. The biological cost of mutational antibiotic resistance: any practical conclusions? *Curr. Opin. Microbiol.* 9:461–5.
- Andersson, D. I., and D. Hughes. 2012. Evolution of antibiotic resistance at non-lethal drug concentrations. *Drug Resist. Updat.* 15:162–72. Elsevier Ltd.
- Andersson, D. I., and B. R. Levin. 1999. The biological cost of antibiotic resistance. *Curr. Opin. Microbiol.* 2:489–93.
- Bataillon, T., T. Zhang, and R. Kassen. 2011. Cost of adaptation and fitness effects of beneficial mutations in *Pseudomonas fluorescens*. *Genetics* 189:939–949.
- Bataillon, T., T. Zhang, and R. Kassen. 2011b. The distribution of fitness effects of new beneficial mutations in *Pseudomonas fluorescens*. *Biol. Lett.* 7:98–100.
- Bell, G. A. C. 1997. Experimental evolution in *Chlamydomonas*. I . Short-term selection in uniform and diverse environments. *Heredity (Edinb)*. 78:490–497.
- Bennett, A. F., and R. E. Lenski. 2007. An experimental test of evolutionary trade-offs during temperature adaptation. *PNAS* 104:8649–8654.
- Bonhoeffer, S., M. Lipsitch, and B. R. Levin. 1997. Evaluating treatment protocols to prevent antibiotic resistance. *Proc Natl Acad Sci U S A* 94:12106–12111.
- Bull, J. J., M. R. Badgett, and H. A. Wichman. 1988. Big-benefit mutations in a bacteriophage inhibited with heat. 942–950.
- Chevin, L. M., R. Lande, and G. M. Mace. 2010. Adaptation, plasticity, and extinction in a changing environment: Towards a predictive theory. *PLoS Biol.* 8:1–8.
- Cooper, V. S., A. F. Bennett, and R. E. Lenski. 2001. Evolution of thermal dependence of growth rate of *Escherichia coli* populations during 20,000 generations in a constant environment. *Evolution (N. Y.)*. 55:889–896.
- Cooper, V. S., and R. E. Lenski. 2000. The population genetics of ecological specialization in evolving *Escherichia coli* populations. *Nature* 407:10–13.
- Couce, A., and O. A. Tenaillon. 2015. The rule of declining adaptability in microbial evolution experiments. *Front. Genet.* 5:1–6.

- Davies, J., and D. Davies. 2010. Origins and evolution of antibiotic resistance. *Microbiol. Mol. Biol. Rev.* 74:417–33.
- Débarre, F., and S. Gandon. 2010. Evolution of specialization in a spatially continuous environment. *J. Evol. Biol.* 23:1090–9.
- Depledge, M. 2011. Reduce drug waste in the environment. *Nature* 478:36.
- Elena, S. F., and R. E. Lenski. 2003. Evolution experiments with microorganisms: the dynamics and genetic bases of adaptation. *Nat. Rev. Genet.* 4:457–469.
- Gallet, R., T. F. Cooper, S. F. Elena, and T. Lenormand. 2012. Measuring selection coefficients below 10^{-3} : method, questions, and prospects. *Genetics* 190:175–86.
- Gallet, R., Y. Latour, B. S. Hughes, and T. Lenormand. 2014. The dynamics of niche evolution upon abrupt environmental change. *Evolution* 68:1257–69.
- Gallet, R., C. Violle, N. Fromin, R. Zahab, B. Enquist, and T. Lenormand. 2017. The evolution of bacterial size: the internal diffusion-constraint hypothesis. *ISME* in press.
- Garland, T. J., and M. R. Rose. 2009. Experimental Evolution. University of California press, Berkeley, Los Angeles, London.
- Grant, P., and R. Grant. 1999. The ecology and evolution of Darwin's finches. Princeton, NJ: Princeton University Press.
- Gullberg, E., S. Cao, O. G. Berg, C. Ilbäck, L. Sandegren, D. Hughes, and D. I. Andersson. 2011. Selection of resistant bacteria at very low antibiotic concentrations. *PLoS Pathog.* 7:1–9.
- Hall, A. R., D. C. Angst, K. T. Schiessl, and M. Ackermann. 2015. Costs of antibiotic resistance - separating trait effects and selective effects. *Evol. Appl.* 8:261–72.
- Harmand, N., R. Gallet, R. Jabbour-Zahab, G. Martin, and T. Lenormand. 2017. Fisher's geometrical model and the mutational patterns of antibiotic resistance across dose gradients. *Evolution (N. Y.)*. 71:23–37.
- Hereford, J. 2009. A quantitative survey of local adaptation and fitness trade-offs. *Am. Nat.* 173:579–588.
- Hermsen, R., J. B. Deris, and T. Hwa. 2012. On the rapidity of antibiotic resistance evolution facilitated by a concentration gradient. *Proc. Natl. Acad. Sci. U. S. A.* 109:10775–80.

- Hopkins, K. L., R. H. Davies, and E. J. Threlfall. 2005. Mechanisms of quinolone resistance in *Escherichia coli* and *Salmonella*: recent developments. Int. J. Antimicrob. Agents 25:358–73.
- Hughes, B. S., A. J. Cullum, and A. F. Bennett. 2007. Evolutionary adaptation to environmental pH in experimental lineages of *Escherichia coli*. Evolution 61:1725–34.
- Hughes, D., and D. I. Andersson. 2012. Selection of resistance at lethal and non-lethal antibiotic concentrations. Curr. Opin. Microbiol. 15:555–60. Elsevier Ltd.
- Jansen, G., C. Barbosa, and H. Schulenburg. 2013. Experimental evolution as an efficient tool to dissect adaptive paths to antibiotic resistance. Drug Resist. Updat. 16:96–107. Elsevier Ltd.
- Kassen, R. 2002. The experimental evolution of specialists, generalists, and the maintenance of diversity. 15:173–190.
- Kirkpatrick, M., and N. H. Barton. 1997. Evolution of a species range. Am. Nat. 150:1–23.
- Kümmerer, K. 2009. Antibiotics in the aquatic environment - A review -Part I. Chemosphere 75:417–434.
- Lenormand, T. 2002. Gene flow and the limits to natural. Trends Ecol. Evol. 17:183–189.
- Lenormand, T., L.-M. Chevin, and T. Bataillon. 2016. Parallel evolution: What does it (not) tell us and why is it (still) interesting?
- Lenormand, T., and M. Raymond. 1998. Resistance management : the stable zone strategy. Proc. R. Soc. London B 265:1985–1990.
- Lenormand, T., D. Roze, and F. Rousset. 2009. Stochasticity in evolution. Trends Ecol. Evol. 24:157–165.
- Lenski, R. E. 1998. Bacterial evolution and the cost of antibiotic resistance. Int. Microbiol. 1:265–70.
- Lenski, R. E., and M. Travisano. 1994. Dynamics of adaptation and diversification: a 10,000-generation experiment with bacterial populations. Proc Natl Acad Sci USA 91:6808–6814.
- Levison, M. E., and J. H. Levison. 2009. Pharmacokinetics and pharmacodynamics of antibacterial agents. Infect Dis Clin North Am. 23:791–797.
- Lobkovsky, A. E., and E. V. Koonin. 2012. Replaying the tape of life: Quantification of the

predictability of evolution. *Front. Genet.* 3:1–8.

Luo, N., S. Pereira, O. Sahin, J. Lin, S. Huang, L. Michel, and Q. Zhang. 2005. Enhanced in vivo fitness of fluoroquinolone-resistant *Campylobacter jejuni* in the absence of antibiotic selection pressure. *Proc. Natl. Acad. Sci. United States Am.* 102:541–546.

Lurias, E., and M. Delbrück. 1943. Mutations of bacteria from virus sensitivity to virus resistance. *Genetics* 28:491–511.

Lynch, M., and R. Lande. 1993. Evolution and extinction in response to environmental change. Pp. 234–250 in *Biotic Interactions and Global Change*.

Martin, G., and T. Lenormand. 2015. The fitness effect of mutations across environments: Fisher's geometrical model with multiple optima. *Evolution (N. Y.)*. 69:1433–47.

Martin, G., and L. Roques. 2016. The non-stationary dynamics of fitness distributions: asexual model with epistasis and standing variation. *Genetics* 1–37.

Melnyk, A. H., A. Wong, and R. Kassen. 2015. The fitness costs of antibiotic resistance mutations. *Evol. Appl.* 8:273–283.

Metcalf, C. J. E. 2016. Invisible trade-offs : Van Noordwijk and de Jong and life-history evolution. *Am. Nat.* 187:3–5.

Milesi, P., T. Lenormand, C. Lagneau, and E. Myl. 2016. Relating fitness to long-term environmental variations in natura. *Mol. Ecol.* 25:5483–5499.

Ravigne, V., U. Dieckmann, and I. Olivieri. 2009. Live where you thrive : joint evolution of habitat choice and local adaptation facilitates specialization and promotes diversity. *Am. Nat.* 174:E141–E169.

Reboud, X., and G. Bell. 1997. Experimental evolution in *Chlamydomonas* . III . Evolution of specialist and generalist types in environments that vary in space and time. *Heredity (Edinb).* 78:507–514.

Schoustra, S. E., A. J. M. Debets, M. Slakhorst, and R. F. Hoekstra. 2006. Reducing the cost of resistance; experimental evolution in the filamentous fungus *Aspergillus nidulans*. *J. Evol. Biol.* 19:1115–1127.

Sousa, A., S. Magalhães, and I. Gordo. 2012. Cost of antibiotic resistance and the geometry of adaptation. *Mol. Biol. Evol.* 29:1417–28.

Thiele-Bruhn, S. 2003. Pharmaceutical antibiotic compounds in soils - a review. *J. plant Nutr. soil Sci.* 166:145–167.

Thulin, E., M. Sundqvist, and D. I. Andersson. 2015. Amdinocillin (mecillinam) resistance mutations in clinical isolates and laboratory-selected mutants of *Escherichia coli*. *Antimicrob. Agents Chemother.* 59:1718–1727.

Van Noordwijk, A. J., and G. De Jong. 1986. Acquisition and allocation of resources: their influence on variation in life history tactics. *Am. Nat.* 128:137–142.

Vogwill, T., and R. C. Maclean. 2015. The genetic basis of the fitness costs of antimicrobial resistance: A meta-analysis approach. *Evol. Appl.* 8:284–295.

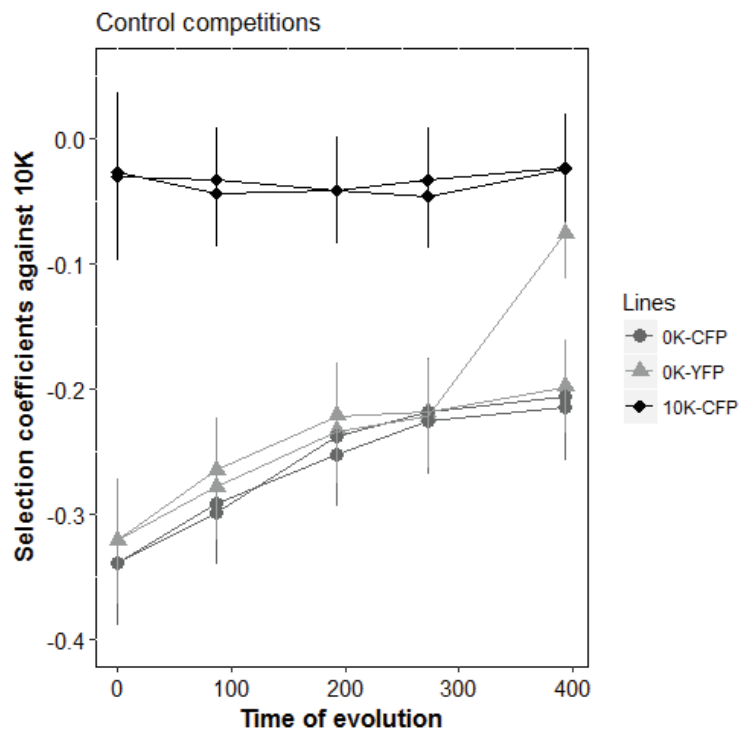
Ward, H., G. G. Perron, and R. C. Maclean. 2009. The cost of multiple drug resistance in *Pseudomonas aeruginosa*. *J. Evol. Biol.* 22:997–1003.

Westhoff, S., T. Van Leeuwe, Z. Zhang, G. Van Wezel, and D. Rozen. 2017. The evolution of no-cost resistance at sub-MIC concentrations of streptomycin in *Streptomyces coelicolor*. *ISME* 1–11. Nature Publishing Group.

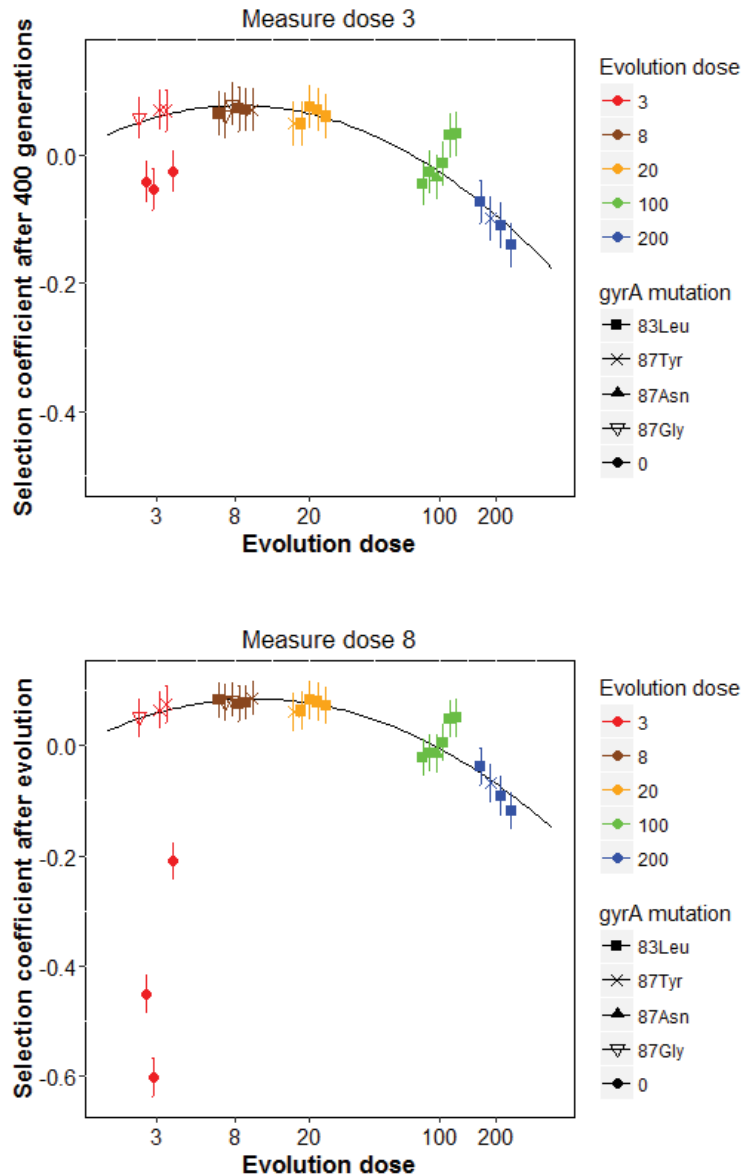
Wiser, M. J., N. Ribeck, and R. E. Lenski. 2013. Long-Term dynamics of adaptation in asexual populations. *Science* (80-.). 342:1364–1367.

World Health Organization. 2014. Antimicrobial resistance global report on surveillance.

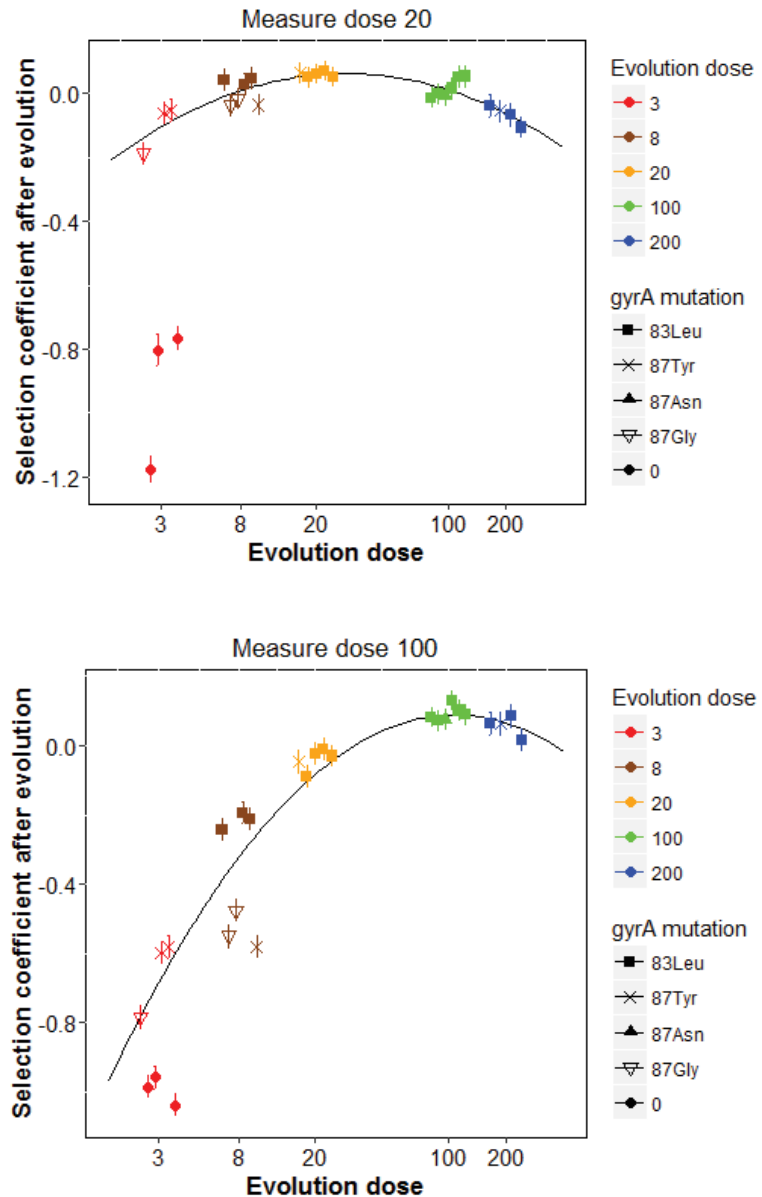
Supplementary Figures



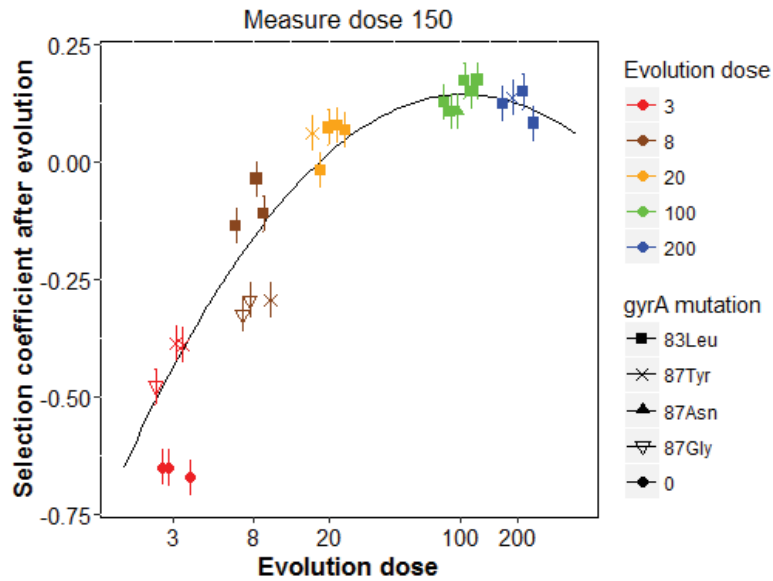
Supplementary Figure 1: Selection coefficients of control lines evolved in the absence of antibiotic in competition against the non-evolved wild-type 10K-YFP (or 10K-CFP in the case of 0K-YFP lines).



Supplementary Figure 2: Selection coefficients of evolved lines in the five measure doses. Symbols indicate the initial resistance mutations while colors indicate the evolution dose. Second order polynomials of the log evolution dose were fitted on *gyrA* lines only (black line). Error bars represent standard errors among replicates. Values of selection coefficients are not comparable among different measure doses as the competitor strain fitness is varying among Nal measure doses (e.g. higher selection coefficients in measure dose 150 than in measure dose 100 are due to a decrease in fitness of the competitor between dose 100 and 150).



Supplementary Figure 2 (cont.): Selection coefficients of evolved lines in the five measure doses. Symbols indicate the initial resistance mutations while colors indicate the evolution dose. Second order polynomials of the log evolution dose were fitted on *gyrA* lines only (black line). Error bars represent standard errors among replicates. Values of selection coefficients are not comparable among different measure doses as the competitor strain fitness is varying among Nal measure doses (e.g. higher selection coefficients in measure dose 150 than in measure dose 100 are due to a decrease in fitness of the competitor between dose 100 and 150).



Supplementary Figure 2 (cont.): Selection coefficients of evolved lines in the five measure doses. Symbols indicate the initial resistance mutations while colors indicate the evolution dose. Second order polynomials of the log evolution dose were fitted on *gyrA* lines only (black line). Error bars represent standard errors among replicates. Values of selection coefficients are not comparable among different measure doses as the competitor strain fitness is varying among Nal measure doses (e.g. higher selection coefficients in measure dose 150 than in measure dose 100 are due to a decrease in fitness of the competitor between dose 100 and 150).

Mapping the topography of adaptive fitness landscapes across environments

An experimental landscape for bacterial adaptation across an antibiotic dose gradient

Harmand Noémie¹, Martin Guillaume^{2*}, Lenormand Thomas^{1*}

1. UMR 5175 CEFE, CNRS - Université Montpellier - Université P. Valéry - EPHE, Montpellier Cedex 5, France
2. Institut des Sciences de l'Evolution de Montpellier, UMR CNRS-UM II 5554, Université Montpellier II, 34 095 Montpellier cedex 5, France

* Contributed equally

Abstract

The adaptive landscape metaphor has been considerably used and refined since its first formulation by Wright in 1932. It has guided many adaptive theories. However even now it has still not entirely taken the leap between theory and reality. An increasing number of studies describe phenotype-to-fitness or genotype-to-fitness maps that assimilate to the very local and precise maps needed for a nice hiking weekend (short adaptive time scales). However with such maps, the general information to plan a travel across the whole country (long-term adaptation) is missing, unless we have the entire collection of those maps. We propose new empirical methods to take some distance with the local topography and reveal global adaptive landscape on long-term adaptation. Those methods involve empirical data retrieved from short and long-term experimental evolution and relative fitness estimations across various environmental conditions. Our results showed that it is possible to map the global topography of a landscape and even that the map extends well to more than one environment opening large opportunities to plan future adaptive travels.

Introduction

The concept of “adaptive landscape” has been immensely influential to shape evolutionary thinking (Gavrilets 2004, 2010; Orr 2005). Since Fisher and Wright, such landscapes have been central to build theories of adaptation and speciation (e.g. in Simpson 1944; Lande 1975; Kauffman and Levin 1987; Hartl and Taubes 1996; Gavrilets 1997, 2004, Orr 1998, 2000a). Adaptive landscape models are particularly useful as they can encapsulate many important and complicated features of the adaptive processes (the role of historical contingency, the context-dependent effect of mutations, various forms of GxG and GxE interactions, the composition of adapting populations, several time scales). Different fitness landscapes can be considered. In Wright’s original concept of ‘adaptive landscape’, a population-level quantity (allele *frequencies* at multiple loci) is mapped to another population-level quantity (population mean fitness). In modern genotypic or phenotypic fitness landscapes, a fitness value is directly assigned to a (multivariate) genotype or phenotype. Genotypic-fitness landscapes have been intensely studied, for instance to reveal patterns of epistasis, in particular the occurrence of ruggedness and multiple fitness peaks in sequence space (Weinreich et al. 2005). They are however very difficult to extrapolate over different environments (Hartl 2014). Phenotypic landscape models were mainly derived as a heuristic to conceptualize adaptation and mutation (Fisher 1930) and later used to model adaptation at sets of quantitative traits. In a population version, mean phenotype is mapped onto mean fitness (Lande 1975) or in an individual version, each phenotype is assigned a distinct fitness (Hartl and Taubes 1998; Orr 1998; Waxman and Welch 2005; Martin and Lenormand 2006a). This type of landscape can be easily extended to model different environments, where selection favors different optima. This is therefore the approach we use in this paper.

Phenotype-to-fitness landscapes in single environments have been widely used to model adaptation (reviewed in Orr 2005), speciation (Barton 2001; Chevin et al. 2014; Fraïsse et al. 2016), parallel evolution (Chevin et al. 2010; Lenormand et al. 2016) but also to empirically and quantitatively analyze selection on particular phenotypes (starting with Lande and Arnold 1983) or distributions of mutation fitness effects (reviewed in Tenaillon 2014). In the context of multiple peaks/environments, they have also been used in a qualitative sense to discuss empirical data, notably in the case of mutational effects (Martin and Lenormand 2006b; Harmand et al. 2016) or in cases of adaptive radiations (Schluter 2000; Benkman 2003; Seehausen 2004; Hendry et al. 2006; Keepers and Martin 2014). Yet, to date, few attempts have been made to draw a global ‘topography’ (as defined in Arnold et al. 2001) connecting the fitness peaks associated with different environments on the same landscape. The existing attempts,

even if involving detailed measurements, remain qualitative (e.g. Rueffler et al. 2004). Thus, even if the study of fitness landscape have brought a series of important and robust global insights on the process of adaptation (Hartl 2014), we still largely ignore if adaptive landscapes are good models to *quantitatively* describe the processes of adaptation and if they can be used to represent selective pressures over several environments. Such representation would prove very powerful to extrapolate evolving trajectories in various scenarios.

Inferring phenotypic fitness landscapes from data can be extremely challenging. For instance, studying a limited set of phenotypic traits (their pattern of genetic covariance and multivariate selection) can reveal some aspects of fitness surfaces (Schluter and Nychka 1994; Gimenez et al. 2009) may not be sufficient to identify critical features of the fitness landscape. It is indeed very difficult to *a priori* sample the most important traits for adaptation, and even less so across different environments. Only studying fitness over sets of mutations (their fitness effect, alone and in various combinations) is a useful alternative for this purpose, but it may only reveal a very partial and imprecise view of underlying fitness landscapes, at least in any single environment (Blanquart and Bataillon 2016). In this paper, we take a different approach to reveal the global topography of fitness landscapes by using experimental evolution where different lines adapt to different peaks (environments). We develop a method, where the pattern of fitness of these evolved lines measured across the different environments inform on the global underlying topography of those peaks, if such a topography exists at all. As a check, we specifically use populations adapting to different environments along a gradient. Indeed, if the method is correct, we expect the topography of these fitness peaks to be regular with respect to this gradient, and the whole pattern of fitness data, across lines and environments, to be well-fitted by the inferred landscape.

A first step of the method is to clearly define the topographical elements that will be considered in the landscape. Different mutational and selective properties might be expected to vary across environments, which may be represented by different fitness landscape features (number of peaks, their shape, location etc). Yet, those features are potentially numerous and it is important to consider the simplest and most general ones and only incorporate model complexity when there is sufficient statistical support. The question of the number of peaks within each environment is particularly important. From the parsimony argument just presented, it would be recommended to first consider that each environment corresponds to one peak, and see if the data can be explained in this way. This assumption is a major simplification, but may not be as restrictive as it seems. Peaks may be far apart (relative to the effect size of mutations), such that considering only one local peak is a very good approximation. Multiple peaks are most often invoked when they are close to each other and when, consequently, adaptive trajectories can

show important levels of historical contingency. Depending on the occurrence of a sequence of mutations, populations may climb one peak or another, generating much uncertainty. Hence, if there are multiple peaks, landscape models are likely to be much less powerful, requiring more parameters, and achieving worse prediction. This simplification is also at the core of most of the evolutionary ecology literature regarding niche evolution and range expansion, where an environmental gradient is assumed to continuously shift a single optimum over space (e.g. Levins 1966; Lynch and Lande 1993; Kirkpatrick and Barton 1997b; Polechová et al. 2009). ‘Evidence’ for multiple peaks usually consists in observing diverging adaptive trajectories, strong patterns of epistasis or the occurrence of some lethal hybrid or recombinant phenotypes (Whitlock et al. 1995; Elena and Lenski 2003; Weinreich et al. 2005; Cutter 2012; Kondrashov and Kondrashov 2015). Importantly, all these patterns can also be obtained in single-peaked landscapes (Coyne et al. 1997; Gavrilets 1997; Martin et al. 2007; Manna et al. 2011; Crona et al. 2013; Harmand et al. in prep.). Hence, the requirement for multiple peaks needs to be taken with caution, especially if simpler models provide similar qualitative agreement with the data. More quantitative tests seem to be needed to tell apart these different models.

Even if we consider that each environment corresponds to one peak, several important landscape features can vary across environments (Harmand et al. 2016, in prep.). Most obviously, the position of the peak can change, as expected if adaptation to different environments involves some phenotypic trade-offs. The intensity of selection and the pattern of selective covariance around each peak can also change, reflecting e.g. habitat quality, and the precise combination of favorable traits in different environments. Variation in the intensity of selection around each peak and shift in peak position can lead to the same fitness variation. Hence, these two features are not easy to distinguish with empirical data (Harmand et al. 2016). In addition, when selective covariances vary across environments, they can largely influence the distribution of available beneficial mutations. This is particularly important when mutation is ‘modular’ (i.e. when mutations in some module, for instance a gene, only affect a subset of traits, Chevin et al. 2010). In this case, adaptation to different environment may recruit beneficial mutations from different modules (Chevin et al. 2010; Harmand et al. 2016; Lenormand et al. 2016), making the interpretation of fitness data even more difficult across those environments.

In a previous study, we qualitatively investigated the fitness landscapes of *Escherichia coli* adapting to different doses of antibiotic (nalidixic acid, hereafter Nal). We observed the occurrence of strong trade-offs across environments, as expected with the occurrence of different peaks (Harmand et al. in prep.). We also observed different mutational modules and variation in the pattern of selective covariance across environments (Harmand et al. 2016). These qualitative observations were not sufficient to determine if a simple peak topography

could quantitatively capture all the data. In this paper, we investigate whether it is possible to quantitatively calibrate and map the topography of the fitness landscape associated to those environments. We show which method can be used for mapping, and the different kinds of data that can be used for this purpose.

We show that a robust topography can be inferred, which capture the most part of the fitness variation in our experimental results. We also show that there is a curvature in the position of peaks in phenotypic space, which contradicts naïve views of adaptation along environmental gradients. Overall, we demonstrate that fitness peaks are more than a metaphor: they can be quantitatively mapped across environments.

Material and methods

- Overview

The landscape model estimation was performed in two steps relying on different methods to estimate the relative positions of peaks and selection intensities. Both methods are directly inspired from a true topographical approach and are based on the principle of ‘triangulation’, where the position of a point can be determined knowing its distance to three fixed points. The first method uses measures of relative fitness of experimental lines evolved in different environmental conditions. We used it to estimate the location and shape of fitness peaks in antibiotic environments (Fig. 1). The second method uses the distribution of fitness effects of mutations measured across different environments. We used it to estimate the location and shape of the peak without antibiotic (Fig. 1). We present these two methods to show that different sets of data can be used for mapping. We also combined them in order to provide more refined mapping where the data was sufficient to estimate extra parameters. More specifically, in the first part, we used a basic mapping where only the mean selection intensity among all phenotypic directions is estimated. In the second part, we used a more refined mapping to show how it is possible to account for variation in selective covariances across environments. The experimental methods are those already described in our previous studies (Harmand et al. 2016, in prep.), and summarized below.

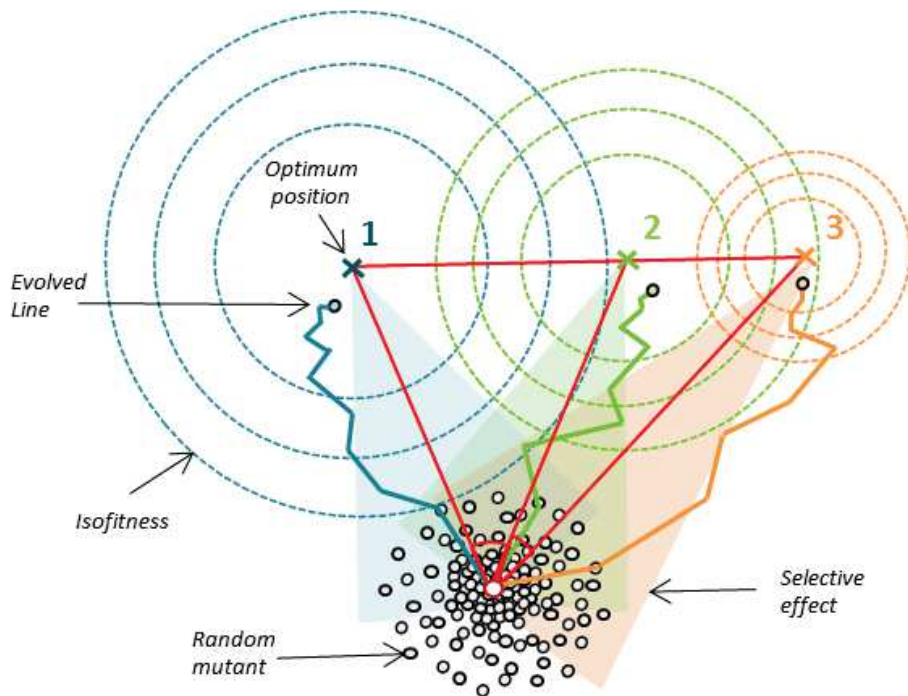


Figure 1: Schematic overview of the method. Dots represent the phenotype of the wild-type (red contour), random single mutants (white with black contours) and lines evolved in three different environments (blue, green and orange with black contours) on a phenotypic plane. Crosses represent the phenotypic optima in environments 1, 2 and 3 and dotted circles figure isofitness for 3 fitness values assuming quadratic fitness functions (of increasing selection intensities from 1 to 3) associated with the different environments. The colored sectors of disks indicate the portion of beneficial random single mutants (those lying within those sectors) in the corresponding environment.

Experimental methods

- Screen of resistant mutants and experimental evolution

Resistant mutants and evolved lines are those already described in Harmand et al. (in prep.). Briefly, Nal resistant mutants originated from the same *E. coli* strain, that previously evolved for 10 000 generations in DM25 and which was transformed with a YFP fluorescent marker. Collections of resistant mutants were obtained from fluctuation tests performed at five different Nal concentrations: 3, 5, 8, 12.5, 20 µg/mL. An additional fluctuation test on resistant mutants screened at 20 µg/mL allowed to screen resistant mutants at Nal 100 and 200 µg/mL.

Six mutants were randomly selected from the mutant collections screened at 3, 8, 20, 100 and 200 µg/mL to initiate experimental lines of evolution in DM250 supplemented with Nal at the same concentration as the mutant's screen dose. Those lines were maintained during ~400 generations of evolution, transferring 2 µL of culture in 1 mL of fresh medium daily. Samples were taken at regular times of evolution and kept in glycerol at -80°C for later competition experiments. Two third of the collections of mutants as well as the resistant lines at 400 generations were sequenced at the *gyrA* gene in order to look for resistance mutations in this specific gene target and check for cross-contaminations among evolved lines.

After 400 generations of evolution, the resistant lines coevolved with another bacterial strain (*Citrobacter freundii*) for 1000 additional generations in the same medium and conditions. The *E.coli* lines evolved for 1400 generations in Nal were included in the fitness assays in order to know if lines were still adapting after the 400 generations of evolution.

- Competition assays

Competitions experiments were performed on evolved lines at six different Nal concentrations: 0, 3, 8, 20, 100 and 150 µg/mL, as well as on the collections of resistant mutants at Nal 0, 3, 8 and 12.5 µg/mL (see protocols in Harmand et al. 2016, in prep.). In the absence of Nal, the competitions were performed between the YFP-marked lines/mutants and the CFP-marked susceptible ancestral strain. In presence of Nal the competitions were performed between the YFP-marked lines/mutants and a CFP-marked resistant reference mutant, which was screened at Nal 200 µg/mL (with two successive fluctuation experiments as described before). The competitions were performed during 24h starting from a mix of saturated cultures of YFP and CFP strains (at equal volume) diluted in proportion 1/100 in fresh competition medium. The selection coefficients per generation were estimated as the change in frequencies of YFP against

CFP cells during the competition, divided by the number of generations occurring during the growth cycle. Each measure of selection coefficient was replicated at least two times (four times at generation 400).

Selection coefficients at generations 0, 200, 400 and 1200 were used to reconstruct the fitness trajectory of each evolving lines in their evolution dose. The analytical expression describing the expectation for such adaptive trajectory from a clonal population under Fisher's Geometrical Model (FGM) assumptions (described after) is given in equation 12 of Martin and Roques 2016. This expression was fitted by maximum likelihood to the selection coefficient measures assuming a normal error among replicates.

Landscape topographical methods

- Topographical variations among antibiotic environments

In this first part, the relative distances and selection intensities among peaks were jointly estimated from the relative fitness of experimental lines (against a *reference* competitor) evolved in four antibiotic doses and measured across the same four antibiotic doses. The model relies on three major assumptions. First, relative fitness are assumed to be transitive among genotypes. This assumption has been experimentally tested on the same experimental system proved to be reasonably accurate (Gallet et al. 2012). The selection coefficient of a line i in competition with the *reference* strain in the environment j is thus expressed as the difference of their absolute Malthusian fitness: $s_{i,j} = m_{i,j} - m_{\text{reference},j}$. Second, we assume a landscape where Malthusian fitness (m) is an isotropic multivariate quadratic function of phenotype, with maximal value $m_{\max,j}$ at the phenotypic optimum of environment j associated with an average variance $\frac{1}{\lambda_j}$ (as in FGM). The parameter λ_j represents the mean strength of selection intensity on the adaptive traits in environment j , with larger λ_j standing for stronger selection intensity. Under this FGM, the Malthusian fitness $m_{i,j}$ of a phenotype evolved in the dose-environment i (hereafter 'evolution doses') and measured in the dose-environment j (hereafter 'measure dose') is a quadratic function of its phenotypic distance to the optimal phenotype $d_{i,j}$ as $m_{i,j} = m_{\max,j} - \frac{1}{2}\lambda_j d_{i,j}^2$ (Martin and Lenormand 2006a, 2008). The last assumption is that the experimentally evolved lines were close to the optimal phenotype of their evolution dose-environment. More precisely, we assume that their phenotypic distance to the optimum, in their evolution dose, is negligible compared to the phenotypic distance to the same optimum, for lines evolved in alternative evolution doses ($d_{j,j} \ll d_{i,j}$). Combining those three hypotheses, we

consider the difference $\Delta s_{i,j}$ between the selection coefficients of a phenotype evolved in dose i and one evolved in dose j , both measured in the same measure dose j . It is given by

$$\Delta s_{i,j} = s_{j,j} - s_{i,j} = m_{j,j} - m_{i,j} \approx \frac{1}{2} \lambda_j d_{i,j}^2 \quad (1)$$

From this equation, the distance between optima can be measured directly from observed $\Delta s_{i,j}$ recalling that we assume each line i or j to be close to optimal in its evolution dose.

Alternative models for the optima positions can then be tested. Here, we opted for three embedded models where optima can either be aligned, disposed along a second order polynomial or independently distributed on a plane. Note that even this last model imposes some constraint if the dimensionality of the whole phenotypic space is more than two. To test between models, the squared phenotypic distances $d_{i,j}^2$ between optima, were expressed in terms of the 2D Euclidian coordinates $\{x_i, y_i\}$ and $\{x_j, y_j\}$ of these optima, within a phenotypic plane, for each model:

Linear model: $d_{i,j}^2 = (y_j - y_i)^2$,

Curved model: $d_{i,j}^2 = (y_j - y_i)^2 + a (y_j^2 - y_i^2)^2$, (2)

Plane model: $d_{i,j}^2 = (y_j - y_i)^2 + (x_j - x_i)^2$

where x_i, x_j, y_i, y_j, a , are parameters to be estimated from the set of $d_{i,j}^2$ measurements (from (1)), for each pair of evolution doses (i, j) with measure dose j .

In order to comply as best as possible to the third assumptions (evolved lines should be close to their phenotypic optimum), we performed pairwise comparisons with test adjustments between fitness measures of the lines evolved in the same dose. We kept only the lines with the best s in their evolution dose and all lines that were not significantly different from this best value. This corresponds to 3, 3, 2 and 2 lines among six in the evolution doses 3, 8, 20 and 100, respectively.

Without loss of generality, we set the position of the optimum of dose 3 at the origin of the phenotypic plane and its selection intensity at 1, so that all distances and selection intensities were estimated relatively to those values. The models parameters were estimated by maximizing the likelihood of the experimental data across the four dose-environments, assuming a landscape given by equations (1) and (2) and a normal error distribution. Linear, curved and independent models were compared based on their AIC score. We included

constrained versions of those models where the selection intensities do not vary across environments and the positions of optima are functions (linear or log) of the antibiotic dose. Confidence intervals of the estimates were estimated within 1.92 points to the maximum.

- Angles between optimal directions and the wild-type position

This part of the analysis relies on the distributions of fitness effects (DFEs) of single-mutants measured across different environments. The method assumes an isotropic quadratic fitness function as previously and additionally that the phenotypic effects of mutations are drawn into an isotropic multivariate normal distribution n dimensions. We analyzed the effect of a deviation from these assumptions in the specific case of mutational modules (as described in our experimental system) via simulations (*ongoing work*).

According to Martin and Lenormand (2015, equation 6), under the FGM assumptions, the angle between the directions towards two different environmental optima, from the position of a given ancestor phenotype/genotype, can be inferred from the correlation of the fitness effects of random mutants from this genotype, measured in each environment. When the ancestor genotype is strongly maladapted to both environments, as we assume here, this correlation directly gives the cosine of the angle between optimum directions. Correlation can be measured using relative or absolute fitness data, and is unaffected (scale-free) by differences ($\lambda_i \neq \lambda_j$) in the strength of selection between environments. Here, we use screened mutants, rather than random ones, the former being much simpler to obtain experimentally.

The DFE of screened mutants is a biased sample of all random mutants. This bias is however predictable, as is detailed in Appendix (we briefly summarize the method below). First, by definition, screened mutations are all beneficial in the screening environment. Antibiotic environments are often used as screening environments, as in this study. In this case, the DFE is largely biased toward large beneficial fitness effects, as mutations are sampled on the basis of their positive growth in this antibiotic environment, while their ancestor decays (so that “screening” is possible). Thus, only the mutants showing a detectable growth (i.e. a fitness higher than a “growth threshold” value) are sampled. Second, the mutations of smaller effects are expected to show a lower probability to form a visible colony, from a single cell (due to random extinction of the lineage) than mutations of larger effects. This further biases the DFE of screened mutants toward higher fitness values.

Under the FGM hypotheses and with the ancestor highly maladapted to both environments, the bivariate DFE of random mutants in two environments (hereafter i and j) can be approximated

by a bivariate normal distribution of means μ_i , μ_j variances σ_i^2 , σ_j^2 and correlation ρ_{ij} (Martin and Lenormand 2015a). Let environment i be the screening-environment, then the DFE of screened mutants will be semi-truncated above a minimal “growth threshold” in this environment. This “growth threshold” imposes higher bias at higher dose, a screening level measured by a parameter α_i , see Appendix. This parameter was inferred, for each screen dose, from the corresponding proportion p_i of mutants resistant to the dose considered. This proportion was itself obtained from the per-division rate of mutation to resistance at that dose (determined by the $P0$ estimator method on the fluctuation assays, see Harmand et al. 2016), divided by the total genomic mutation rate, taken to be $U \approx 0.001$ per division for E.coli in exponential growth (Kibota and Lynch 1996).

Given a known screening level (p_i in dose i) and a correlation ρ_{ij} of the parent distribution, the correlation ρ_{ij}^* in the truncated sample from a bivariate Gaussian can be predicted, using results from “hidden-truncation models” (Arnold et al. 1993). The correlation ρ_{ij}^* of the fitness effects, in doses i and, of mutants resistant to dose i , can then be expressed as a function of α_i and ρ_{ij} . Finally, we further correct for the stochastic extinction of resistance mutations during growth on the agar plate (from a single cell to a visible colony), and its effect on the observed correlation among screened mutants. Overall, we obtain an analytical expression for ρ_{ij} , as a function of the observed correlation ρ_{ij}^{**} of the DFEs in i and j among mutants screened at dose i . This expression is then inverted to estimate ρ_{ij} and thus the angle ϕ_{ij} from the observed correlation ρ_{ij}^{**} and proportion of screened mutants p_i .

This method was applied to determine the angles between the susceptible ancestral strain and the dose-environments 3, 8 and 12.5 in the landscape. ρ^{**} was directly obtained from the values of s of screened mutants measured across the dose-environments (described before). Two types of cross-validations of this inference measures were performed. First, we checked that the angle inferred from the correlation between i and j using mutants screened in dose i were consistent with that estimated from mutants screened in dose j . Second, we checked that the angle between dose-environments 3 and 12.5 corresponded to the sum of the two other angles (angle between 3 and 8, and angle between 8 and 12.5). This last pattern is expected to arise only if the three optima (of doses 3, 8 and 12.5) lie within a plane (a two dimensional subspace within the whole n -dimensional phenotypic space).

- Characterization of the zero dose-environment

The zero dose-environment was not included in the topographical analysis presented above. For this environment, we dispose of two topographical pieces of information. First, the fitness of the different lines (evolved at different doses) in this zero-dose environment. Second, as explained in the previous paragraph, angles between the directions towards the peaks of three dose-environments, from the position of the wild type (i.e. from a position close to the zero dose optimum). Hence, we opted here to combine this information to estimate extra-parameters. Our previous qualitative results on this experimental system strongly suggested that selective covariances were varying between the zero dose-environment and the other dose-environments (Harmand et al. 2016). We quantitatively tested this qualitative inference by introducing those covariances. Hence, this environment illustrates how different kind of data can be used to refine mapping.

The position of the dose zero optimum was determined considering that the positions of the other optima were aligned (as found above). Assuming that the ancestral strain is close to the zero dose-environment optimum, we infer its position (i.e. its coordinates (x_0, y_0) in the phenotypic plane of the optima) by triangulation (Fig. 2). Specifically, we used the following system:

$$\begin{cases} \tan(\phi_k) = \frac{y_0}{x_0} \\ \tan(\phi_k + \phi_{3,8}) = \frac{y_0 + y_8}{x_0} \\ \tan(\phi_k + \phi_{3,12.5}) = \frac{y_0 + y_{12.5}}{x_0} \end{cases} \quad (3)$$

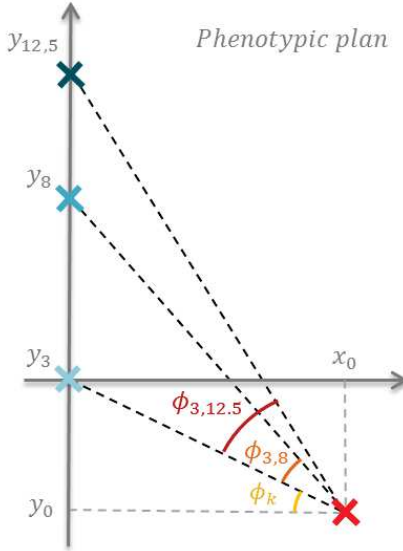


Figure 2: Schematic representation of the triangulation of equation (3) (the same notations are used). Crosses indicate the optima position of Nal dose-environments 3, 8 and 12.5 (following the blue gradient) and dose-environment 0 (red).

with ϕ_k corresponding to the angle between the direction of the orthogonal projection of the wild-type position on the line of the optimum positions and the direction of optimum position of dose 3 and $\phi_{3,8}$ (resp $\phi_{3,12,5}$) the angle between directions of optima at doses 3 and 8 (resp. 3 and 12.5) from the wild-type position. The y_i correspond to the coordinates of optimum at dose i (obtained from the previously described analysis). Figure 2 illustrates the geometry of this problem of triangulation and reports the different angles and positions with their notation.

In order to test for the occurrence of selective covariances at dose zero, we assumed a bivariate Gaussian fitness function of mean $m_{max,0}$, variances $\frac{1}{\lambda_{0x}}$ and $\frac{1}{\lambda_{0y}}$ associated with x and y axis directions, respectively, and a correlation coefficient ρ . At dose zero the selection coefficients were directly measured against the wild-type (assumed close to the optimum) such that:

$$s_{i,0} = m_{max,0} - m_{i,0} \sim - \frac{1}{2(\rho^2 - 1)} (\lambda_{0x} (x_i - x_0)^2 + \lambda_{0y} (y_i - y_0)^2 - 2\rho (x_i - x_0)(y_i - y_0) \sqrt{\lambda_{0x}} \sqrt{\lambda_{0y}}) \quad (4)$$

The parameters λ_{0x} , λ_{0y} and ρ were estimated from this equation by maximizing the likelihood with the replicated measures of selection coefficients of the evolved lines in dose zero, assuming a normal error distribution. The model with covariances was compared with a model without covariances (setting $\rho = 0$ and $\lambda_0 = \lambda_{0x} = \lambda_{0y}$) on the basis of their AIC score.

- Reconstruction of the trajectories on the fitness landscape

The screened mutants and the evolving lines at different time point were positioned under the best landscape model, by triangulation, using their selection coefficients across the different dose-environments. For each strain, the phenotypic distances to each dose-optimum were expressed from equation (1) using the fitted landscape parameters (optima positions and selection intensities). Their coordinates were then estimated by triangulation, by maximizing the likelihood across the dose-environments and assuming a normal error distribution among replicated fitness measures.

Results

- Adaptation to the dose-environments

The relative fitness of the evolved lines across generations show a good agreement with adaptive trajectories toward the same phenotypic optimum in each dose-environment (Sup.Fig. 1) (additional measures and replicates at generations 200 and 1200 are ongoing). Those trajectories are also consistent with the approach to an optimum, as expected under the FGM assumptions. At generation ~ 400 , the fitness values seem to reach a stable fitness value at doses 8 and 100. At doses 3 and 20, the fitness is still increasing after generation 400 but not much compared to the previous adaptation. These results are consistent with our assumptions that the evolved lines were already close to an optimum in their dose-environment at generation 400.

- Optima and intensities of selection in presence of antibiotics

We investigated the topography of the fitness landscape across antibiotic dose-environments in a phenotypic plane from experimental fitness measures of evolved lines. Table 1 shows the models comparison. The best model includes variations of the optima positions in one direction of the plane as well as variations of selection intensities among the dose-environments. In particular, the parameters estimated under this model indicate that dose-environments are aligned following an increasing dose order, as we would *a priori* expect. Interestingly, the phenotypic distance between optima positions linearly scaled with the log-dose value ($R^2=0.98$)

(Figure 3a and 4). This relationship was not particularly expected (in fact, it is precisely this kind of information that is extremely difficult to obtain *a priori*), but it demonstrates a strong regularity in variations along the dose gradient. Similarly, the selection intensity associated with the dose-environments increases monotonically, also almost linearly with the log-dose value ($R^2=0.97$) (Figure 3b and 4). Such log-dose linearity was also observed previously on the proportion of beneficial mutations arising in the different dose-environments of selection (Harmand et al. 2016). Together, those results suggest that the underlying adaptive topography is very regular and robustly captured by our method.

Distance model	Optima Coordinates (x, y)					Selection Intensities (λ)				LL	k	ΔAIC
	dose 3	dose 8	dose 20	dose 100	curve c	dose 3	dose 8	dose 20	dose 100			
$d(y)$	0	1	1	1	0	0	1	1	1	173.64	7	0.00
$d(y, c y^2)$	0	1	1	1	1	0	1	1	1	173.69	8	1.90
$d(x, y)$	0	2	2	2	0	0	1	1	1	175.16	10	2.97
$d(\log\text{-dose})$	0	0	0	0	0	1	1	1	1	141.74	5	59.79
$d(dose)$	0	0	0	0	0	1	1	1	1	53.76	5	235.77
$d(x, y)$	0	2	2	2	0			0		38.85	7	269.59

Table 1: Models comparison for optima positions and selection intensities of the antibiotic dose-environments. The 10 first columns indicate the number of parameters estimated ($0 = \text{fixed parameter}$) in the corresponding model (lines) of equation (1). LL is the log-likelihood value, k the number of parameters and ΔAIC the difference in Akaike Information Criterion with the best model (first line) associated with each model.

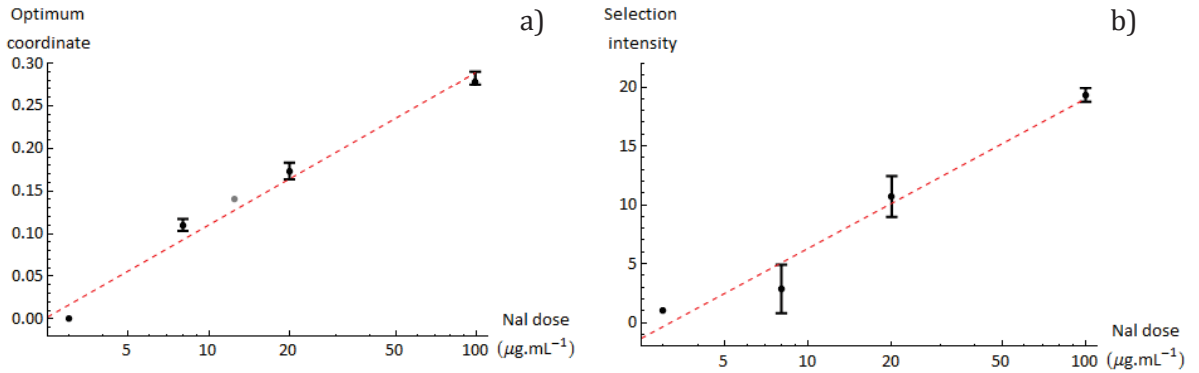


Figure 3: Parameters estimated in the best model (aligned optima) for optima positions and selection intensities described in Table 1. Error bars indicate the confidence intervals of the parameter values. The position of the optima (left panel) and selection intensities scale linearly with the log-dose of antibiotic.

- Estimations of the angles between optimal directions from the susceptible wild-type

The angles estimated from the bivariate DFE of the screened mutants are shown on Figure 4. The values are reasonable consistent between the same angles estimated from the different sets of mutants. Indeed, we can independently estimate the same angle (e.g. between environment 1 and 2) with mutants screened in either environment 1 or environment 2. The confidence intervals nicely include the two estimates for the larger angle value $\theta_{3-12.5} \sim 17^\circ$. For the two other angle values, the replicated values estimated and their confidence interval do not overlap, but replicated estimates are nevertheless quantitatively close, especially when compared with the overall angle differences among environments (13.9° and 8.7° are the replicated estimates for θ_{3-8} , 2.4° and 4.9° for $\theta_{8-12.5}$). In addition, the sum of the angles values θ_{3-8} and $\theta_{8-12.5}$ falls very close to the value estimated for the angle $\theta_{3-12.5}$. This shows that the angle method is remarkably robust, especially considering that it rests on several assumptions and simplifications. In particular, it rests on analytical results that ignore mutational modularity. The extent to which modularity impacts these predictions depends on the number of such modules and the phenotypic directions of those modules with respect to the alignment of optima. With multiple modules, this effect is however probably negligible (*Sup.Mat. in progress*).

The different angles estimated were quite small. This indicates that antibiotic optima stand in a similar phenotypic direction from the wild-type position. This is consistent with the continuity detected in optima positions if extended to the zero dose-environment. In the case where the zero-dose would be also aligned with other optima, the angles value should be 0° . Our estimations however indicate that the wild-type is shifted from the alignment of Nal optima.

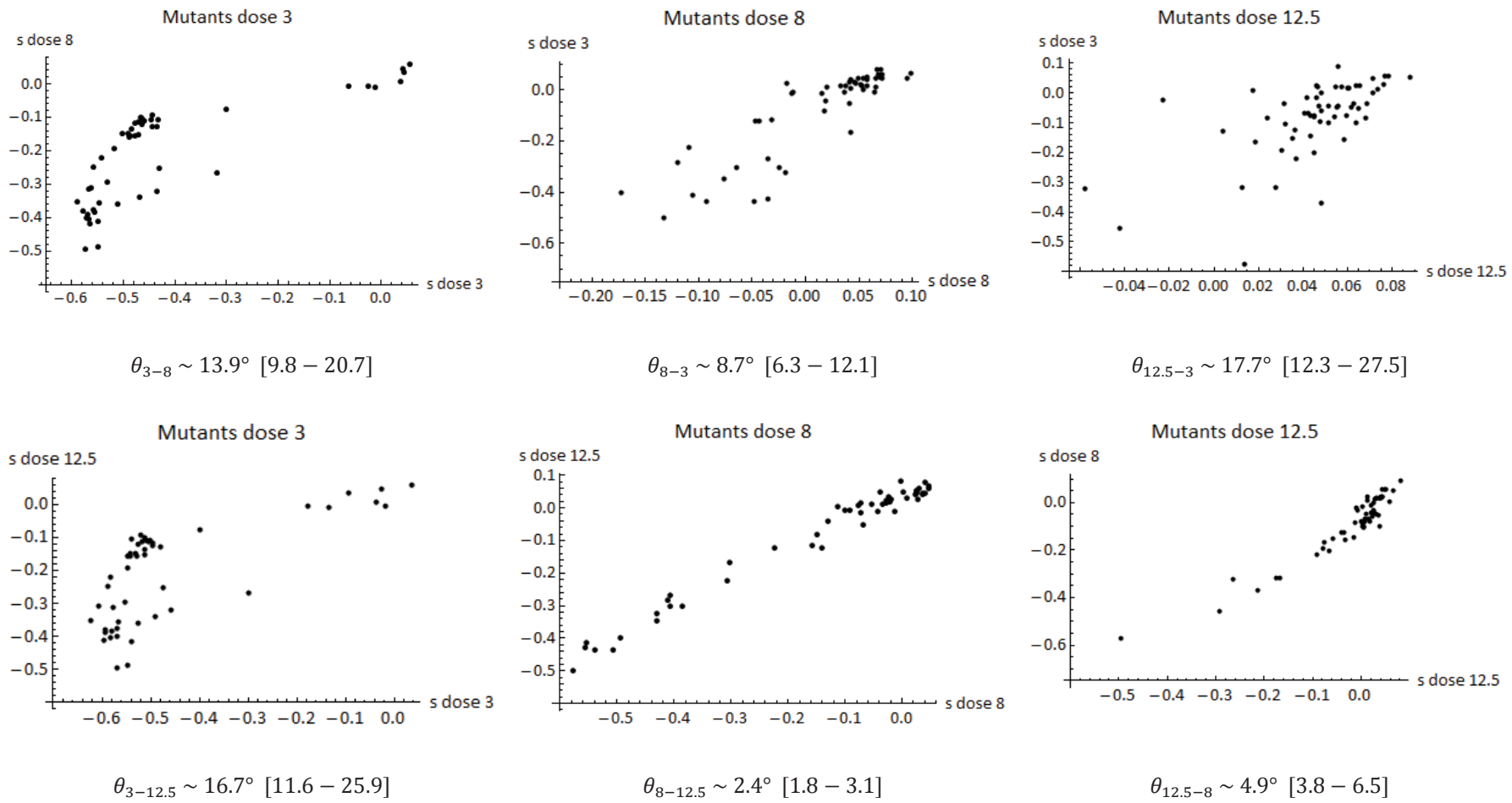


Figure 4: Correlation of the fitness effects of screened mutants among dose-environments 3, 8 and 12.5 and estimated angles. Dots correspond to mean values for two replicated measures of selection coefficients of screened mutants in the dose indicated in the title of each graph against the reference competitor at the dose indicated on axes. The angle values and confidence intervals estimated from each correlation are indicated below each graph.

- Characteristics of the zero dose-environment

Angle estimation errors were not directly taken into account in the analysis of the peak topography at dose zero. However three independent analyses were performed with mean, minimal and maximal angles values in order to show how much the result were impacted by this uncertainty (Fig. 5). In the three cases, the optimum position of the dose zero is globally in the continuity of the dose gradient, prior to dose 3. The distance between doses 0 and 3 is close to the one between doses 3 and 100. With the minimal angle values, the dose 0 is almost aligned with the antibiotic whereas it is shifted in the two other cases. Those results show that the positions of the optima show a curvature at least between dose 0 and 3.

The fitness function associated with the dose zero was modeled as a bivariate Gaussian function allowing for selective covariances between the two phenotypic directions of the plane. Consistently with our previous qualitative inference (Harmand et al. 2016), the model with covariance was strongly favored over an isotropic model ($\Delta AIC = 13.3$) (Table 2). In the best model, there is strong selective covariance. The two axes of the isofitness ellipse exhibit very different selective intensity. The first axis points toward the optimum at dose 8 and exhibits weak selection (much weaker than selection intensity measured around other Nal optima). The other direction (orthogonal to the first), exhibits much more intense selection, of the same order than the intensity of selection measured around Nal20 optimum. Finally, estimates based on the minimal and maximal bounds for the angles do not strongly alter these conclusions and the resulting landscape (Fig. 5).

Model	Angles model						
	Min		Mean		Max		
	Values	LL	Values	LL	Values	LL	
<i>Selective covariances</i>	λ_{0x}	18.42		0.47		0.14	
	λ_{0y}	0.10	96.43	0.07	96.43	0.12	96.43
	ρ	-0.986		-0.990		-0.981	
<i>Isotropic selection</i>	λ_0	0.45	89.34	0.31	87.79	0.35	87.38

Table 2: Model for selection intensity in dose-environment zero (from Equation 4). Min, Mean and Max columns refer to the model estimated with the minimal, the mean and the maximal angle values. For each column the parameter values estimated (column Values) and the log-likelihood (LL) are given.

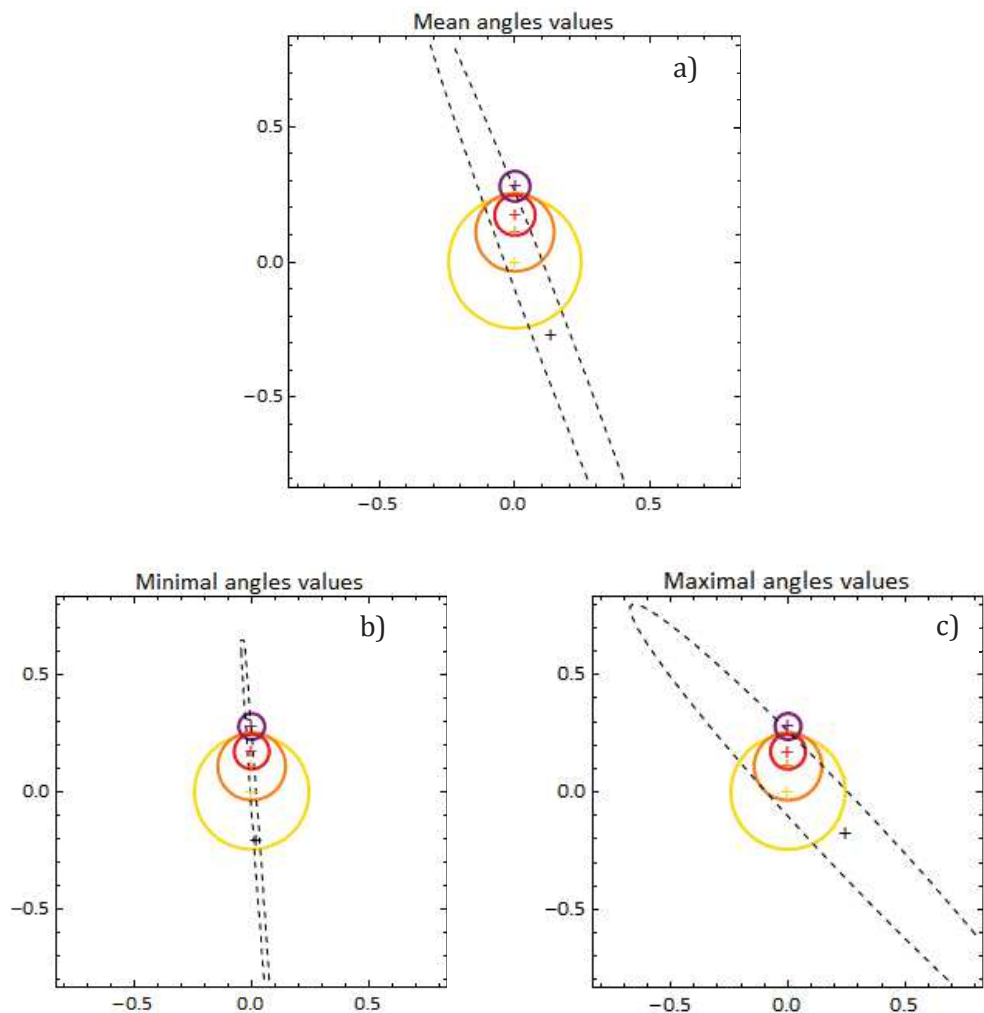


Figure 5: Estimated landscape models with the mean (a), minimal (b) and maximal (c) angle values for dose 0 position. Crosses indicate the optima positions in the phenotypic plane for dose 0 (black), 3 (yellow), 8 (orange), 20 (red) and 100 $\mu\text{g/mL}$ (purple). The circles correspond to the isofitness line of value 0.03 for all environment considered (color code).

- Adaptive trajectories

The fitted landscape model (Fig. 5) was used to place the initial mutants and evolved lines of the experimental evolution based on their fitness values across the dose-environments. The goodness-of-fit is illustrated on Figure 6 showing the regression of the experimental fitness values (with replicates) of all lines in all dose-environments against their estimated values in the model. The slope of this regression is not significantly different of 1 and the intercept close to 0 showing a very good agreement between the data and the model. This is a strong validation that this landscape is robust and captures well the fitness effects of resistant phenotypes across all the dose-environments. Figure 7 shows the estimated positions of each strain on the landscape.

The initial resistant mutants (blue dots) fall pretty close to the Nal3 and Nal8 optima (except the non-*gyrA* lines). This is consistent with a fitness threshold imposed by the screen of resistant mutants (inferring the positions of all the screened mutants obtained in Harmand et al. 2016 would be interesting to establish this point with more data, this is ongoing work). As expected, for each line, the phenotypes get closer to the optimum of their evolution dose after experimental evolution (colored triangles), with some variation among the different lines. Overall, the fitted landscape captures very well the trajectories of the *gyrA* lines. However, the fitted position of the non-*gyrA* lines is very unexpected. Those lines occurred only at low doses (3 and 8) (Harmand et al. 2016). Their inferred positions overshoot by far the optimum at dose 100. Similarly, the non-*gyrA* mutants were qualitatively inferred to be located in a very different position compared to *gyrA* mutants in Harmand et al. 2016. More work is needed to understand the geometry of this problem and determine whether the qualitative solution proposed in this previous study could be implemented to improve the landscape geometry proposed here.

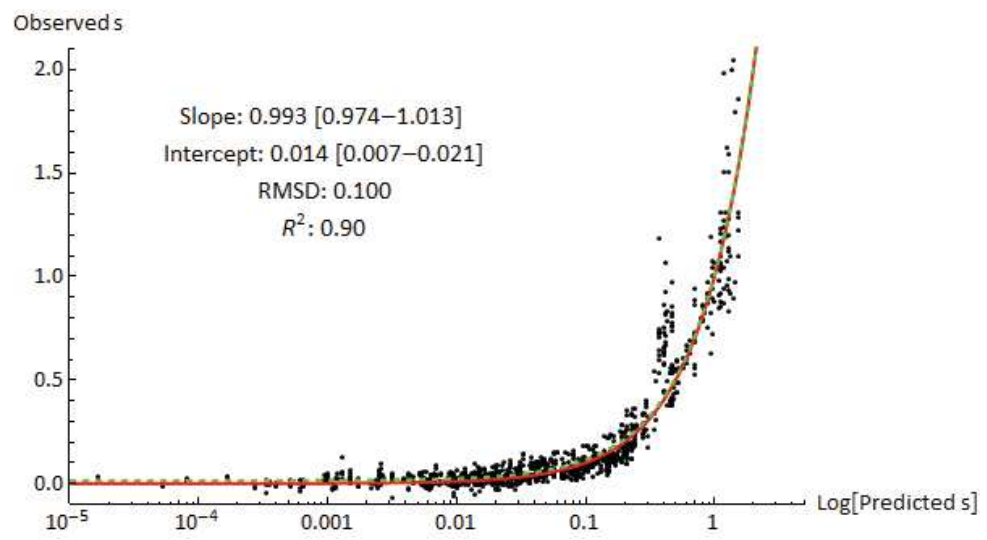


Figure 6: Regression observed values (with replicates) versus fitted values (in log for clarity) in the model with covariances (with mean angle values). Red line corresponds to the $x=y$ regression and green dashed line to the fitted regression (with parameters indicated on the graph).

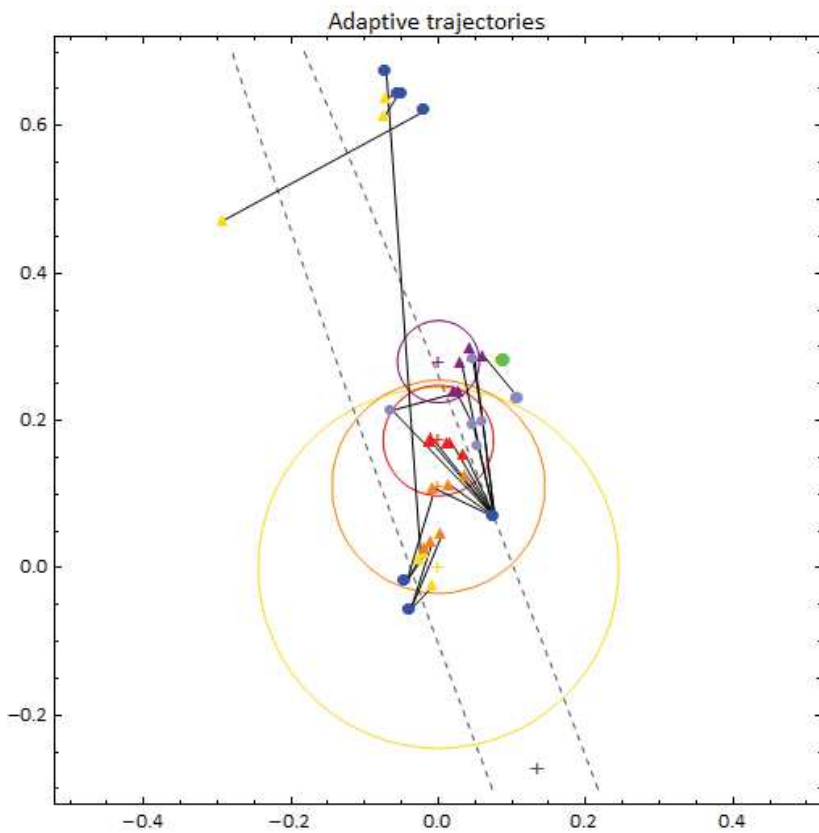


Figure 7: Adaptive trajectories of evolved lines in the landscape model. Crosses indicate the optima positions in the phenotypic plane for dose 0 (grey), 3 (yellow), 8 (orange), 20 (red) and 100 $\mu\text{g/mL}$ (purple). The circles correspond to the isofitness line of value 0.03 for all environment considered (color code). Dots correspond to the inferred position of screened single (darkblue), (presumably) double (lila) mutants and the reference competitor (green). Colored triangles correspond to the inferred position of evolved lines in the evolution dose of the corresponding color. Black lines link the corresponding mutant and evolved line. The four mutants up in the graph correspond to the four non-*gyrA* mutants poorly positioned in the landscape.

Discussion

- Ongoing work

In this manuscript, I presented robust results, but several (technical) improvements are planned before the submission of the paper.

First, we plan to write a global model to estimate all parameters of the landscape in a single round. This should give the benefit to test more reliably scenarios including the dose zero, like for example the curvature of optima positions along the gradient.

Second, we plan to estimate the positions of all the screened mutants obtained in Harmand et al. 2016 in the landscape. This would give deeper insight in the mutational properties and allow discussing the occurrence of mutational modules. We also planned to investigate from simulations how mutational modules can affect the angle predictions from the correlation effects of screened mutants across environments.

Finally, we plan to perform simulations of the experimental evolution on the estimated landscape and compared it with the experimental results.

- Mapping principles

In this paper, we presented two promising methods to infer global topographies of adaptive landscapes across different environments. The two methods lead to consistent and precise estimations of the selective properties associated with five environments along a gradient. We obtained clear, regular and continuous patterns of variation following the gradient: the optimum position shifts along a slightly curved trajectory in the phenotypic space and the selection intensity increases almost log-linearly with the dose.

The first topographical method requires well adapted phenotypes to the different environments considered. They can be obtained from experimental evolution with short generation-time biological models, such as microorganisms (Kassen 2002; Elena and Lenski 2003; Garland and Rose 2009). Alternatively, those phenotypes could be sampled *in natura* from an environment where they are assumed to be well adapted (e.g. specialized parasites on a specific host-environment). The relative fitness among all phenotypes are then measured across all environments. Those measures are taken as estimations of the distances among optima positions. As shown in this study, the method is also robust to the use of an intermediate phenotype of reference, against which the relative fitness is measured, provided fitness is

transitive or nearly so. This method present several advantages: it involves few hypotheses (adapted phenotypes close to the optimum and the form of the fitness function) and few parameters. It turns out to be very robust. It allowed to detect small shifts and to test whether optima were aligned or not. Other configurations could be easily tested and implemented, which would be particularly insightful when studying environments that have no *a priori* special relationships (e.g. different temperature versus pH, or different hosts for parasites etc.). However it provides only averaged selective properties associated with each environment: it does not allow to detect selective covariances. It is also more difficult to use when phenotypes are lethals in some environments. For example, in this study it was not possible to performed competitions against the phenotype adapted to dose 0 in the antibiotic environments (since this phenotype is lethal in presence of antibiotic). There is thus a limitation in the environmental range that can be considered.

The second topographical method relies on correlations among fitness effects of random mutants across environments. This method has a great potential since it allows to infer optima positions directly from fitness data available at a short time scale. As demonstrated in this paper, the general theory can easily account for specific sets of mutants (we used here screened mutants, but other kinds of mutants could be used). In principle, it could even be extended to work on phenotypes directly sampled from a population. However, such extension would have to account with the selective history and possibly other evolutionary processes (migration, drift...), which is likely to represent an important challenge in most cases. This method relies on important simplifications, notably constant mutational and selective effects on all phenotypic directions under selection. Consequently, the inferences may be biased if these assumptions are not met. In particular, more work would be necessary to evaluate the effect of mutational modules and other cases in which the predictions are expected to lead to wrong estimations of the optima positions.

We showed that combining those methods allows to compensate for some of the weaknesses just mentioned. For instance, we could map the zero dose-environment, even if the phenotypes close to this optimum are lethals in the other environments and cannot be reliably used to measure fitness in competition. Combining these methods also allow to refine some of the inference. For instance, we combined them in this study to estimate selective covariances in the zero dose-environment. Finally, the context of environmental gradients proved pertinent, to build a landscape topography and check the reliability of the results. Our results align well with the general intuition that optima in a gradient should be monotonously organized. Such regularity shows that there is great potential for extrapolating and predicting the properties of all other environments on the gradient within the range of doses that we studied.

The inferred landscape model is very close to the qualitative predictions that were formulated looking at general patterns of fitness (Harmand et al. 2016). We believe that this preliminary step was important to guide the present analysis. First, it suggested which topographical elements would probably have to be incorporated to obtain a reliable landscape. Second, it guided our choice to test for the possible occurrence of strong selective covariances at dose zero. Indeed, we found extremely strong statistical support for those covariances, confirming our previous interpretation.

- Understanding adaptation along gradients

The shift in optimum positions among environments along a gradient has been often emphasized in ecology. It encapsulates the idea of fitness trade-offs that cannot be resolved by long-term adaptation (reviewed in Kassen 2002). In contrast, short-term adaptation, like the first adaptive steps toward antibiotic resistance, are often associated with strong differences of selective effects among environments but neglects the occurrence of fitness trade-offs among doses, so that a single adaptive peak is considered (Baquero and Negri 1997; Gullberg et al. 2011; Oz et al. 2014; Hughes and Andersson 2015). Here we show that both views incorporate only partial features of the global topography that can conciliate patterns considered at different time-scales. Environmental gradient should be considered with both variations in optimum positions and selection intensity (as already suggested in Arnold et al. 2001). This reveals crucial to model more precisely how evolution proceed on gradients.

In addition, our representation of the gradient suggests a curvature in the positions of the optima. The impact of such curvature has been little explored theoretically. It is important to insist on its underlying biological meaning. In some circumstances, adaptation to more extreme conditions can be well represented by a shift in trait values. For instance, adaptation to escape a faster predator can be achieved by larger running muscles. However, at some point, it may not be possible to increase running speed by this mechanism (e.g. because of physical limitations or other constraints) and another adaptive strategy may evolve instead (camouflage, other defense or movement strategy etc). For instance, if camouflage evolves, costly muscle mass may evolve back to lower values. In trait space, this corresponds to a curvature in the position of phenotypic optima. In the case of antibiotic resistance, exactly the same general phenomenon can occur. For instance, the best solution to adapt to low dose of antibiotic may be the overexpression of channels that excrete the antibiotic outside the cell. With increased antibiotic dose, more of these channels may be required (corresponding to a progress in the same phenotypic direction). At some point, however, cell membrane may become too permeable, preventing to increase further excretion rate without compromising cell homeostasis. In this case, change in another

trait may be required to adapt to higher dose, for example with a mutation at the antibiotic target gene. Once this trait starts evolving, there is no need to overexpress excretion channels. This scenario will lead to a complete turnaround of the positions of optima in the phenotypic space. This interpretation is only hypothetical and illustrative, but showing that phenotypic optima can exhibit a curvature in phenotypic space, as in our results, points to a less naïve view of adaptation along gradients. Adapting to more extreme conditions does not necessarily lead to the evolution of more extreme traits.

- Interest and limits of the adaptive landscapes

This study showed that several environmental “adaptive peaks” can be characterized and mapped on the same adaptive landscape. This opens important perspectives to understand how environmental conditions drive different evolving strategies. It would be particularly insightful to see how different, *a priori* unrelated, environmental variables (temperature, pH, another antibiotics etc.) could be mapped together. With this approach, it might be possible to determine in a quantitative way the adaptive challenges represented by different environments for different, possibly distant species. Furthermore, it is possible to quantify the distance of a population to various optimum positions and thus to really classify the environments on a scale of “adaptability” for each specific phenotype mapped. Such tool can prove useful for direct applications in agronomy for example to understand adaptation of pathogens to different host-plants or medical applications like illustrated here to understand the evolution of antibiotic resistance or the emergence of viral diseases. They are also a promising approach to model realistic adaptive trajectories in heterogeneous contexts of fluctuating, brutal or gradual environmental change.

In many evolutionary situations, adaptive landscapes with a simple topography (and the corresponding theory) may not be very useful, or even misleading. For instance, evolution by genetic conflicts may require more complex topographies (e.g. Connallon and Clark 2014). The occurrence of frequency-dependent selection may require to consider moving landscapes (Arnold et al. 2001; Rueffler et al. 2004). Runaway evolution may require to consider topographies with fitness ridges (e.g. Lande 1981). Nevertheless, many situations of adaptation may still be well captured by simple landscapes. Adaptive landscape models incorporate the full process of adaptation within a unified framework. If well calibrated, they have the potential to make adaptive predictions at different time-scales and reconcile the discordance between short-term versus long-term observations. They also have the potential to extrapolate adaptive trajectories in different environments. Because of their generality, they are likely to be central to develop a much needed quantitative and predictive evolutionary theory.

Acknowledgements

We thank M.-P. Dubois and R. Zahab for lab management and the Montpellier Ressources Imagerie (MRI) platform. The original strain RELB 4536 was kindly provided by Richard Lenski's lab. This work was supported by a PhD grant from French ministry of research to NH, and the ANR SilentAdapt to T.L.

References

- Arnold, B. C., R. J. Beaver, R. A. Groeneveld, and W. Q. Meeker. 1993. The nontruncated marginal of a truncated bivariate normal distribution. *Psychometrika* 58:471–488.
- Arnold, S. J., M. E. Pfrender, and J. A. G. 2001. The adaptive landscape as a conceptual bridge between mico- and macroevolution. *Genetica* 112–113:9–32.
- Baquero, F., and M.-C. Negri. 1997. Selective compartments for resistant microorganisms in antibiotic gradients. *BioEssays* 19:731–736.
- Barton, N. H. 2001. The Role of Hybridization in Evolution. *Proc. Am. Philos. Soc.* 10:551–568.
- Benkman, C. W. 2003. Divergent Selection Drives the Adaptive Radiation of Crossbills. *Evolution* (N. Y). 57:1176–1181.
- Blanquart, F., and T. Bataillon. 2016. Epistasis and the structure of fitness landscapes : are experimental fitness landscapes compatible with Fisher’s model ? *Genetics* 203:847–862.
- Chevin, L. M., G. Decorzent, and T. Lenormand. 2014. Niche dimensionality and the genetics of ecological speciation. *Evolution* (N. Y). 68:1244–1256.
- Chevin, L. M., G. Martin, and T. Lenormand. 2010. Fisher’s model and the genomics of adaptation: Restricted pleiotropy, heterogenous mutation, and parallel evolution. *Evolution* (N. Y). 64:3213–3231.
- Connallon, T., and A. G. Clark. 2014. Evolutionary inevitability of sexual antagonism. *Proc. Biol. Sci.* 281:20132123.
- Coyne, J. A., N. H. Barton, and M. Turelli. 1997. A critique of Sewell Wright’s shifting balance theory of evolution. *Evolution* (N. Y). 51:643–671.
- Crona, K., D. Greene, and M. Barlow. 2013. The peaks and geometry of fitness landscapes. *J. Theor. Biol.* 317:1–10. Elsevier.
- Cutter, A. D. 2012. The polymorphic prelude to Bateson-Dobzhansky-Muller incompatibilities. *Trends Ecol. Evol.* 27:209–218.
- Elena, S. F., and R. E. Lenski. 2003. Evolution experiments with microorganisms: the dynamics and genetic bases of adaptation. *Nat. Rev. Genet.* 4:457–69.

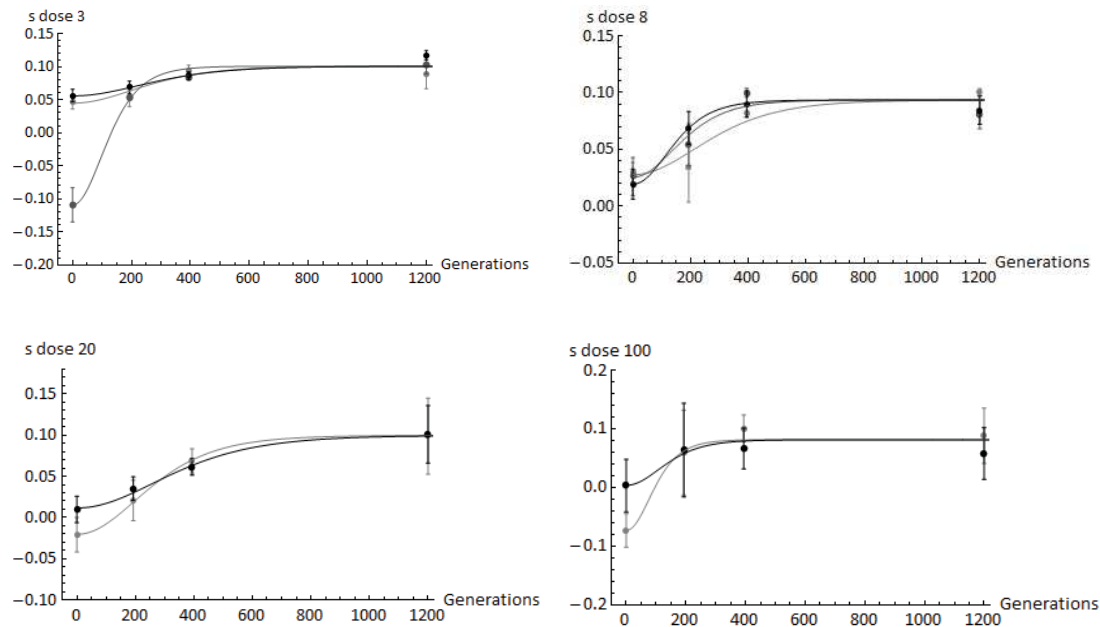
- Fisher, R. a. 1930. The Genetical Theory of Natural Selection. *Genetics* 154:272.
- Fraïsse, C., P. A. Gunnarsson, D. Roze, N. Bierne, and J. J. Welch. 2016. The genetics of speciation: Insights from Fisher's geometric model. *Evolution (N. Y.)*. 70:1450–1464.
- Gallet, R., T. F. Cooper, S. F. Elena, and T. Lenormand. 2012. Measuring selection coefficients below 10^{-3} : method, questions, and prospects. *Genetics* 190:175–86.
- Garland, T. J., and M. R. Rose. 2009. Experimental Evolution. University of California press, Berkeley, Los Angeles, London.
- Gavrilets, S. 1997. Evolution and speciation on holey adaptive landscapes. *Trends Ecol. Evol.* 12:307–312.
- Gavrilets, S. 2004. Fitness landscapes and the origin of species. Princeton University Press.
- Gavrilets, S. 2010. High-Dimensional Fitness Landscapes and Speciation. P. in Evolution - the extended synthesis. MIT Press Scholarship.
- Gimenez, O., A. Grégoire, and T. Lenormand. 2009. Estimating and visualizing fitness surfaces using mark-recapture data. *Evolution (N. Y.)*. 63:3097–3105.
- Gullberg, E., S. Cao, O. G. Berg, C. Ilbäck, L. Sandegren, D. Hughes, and D. I. Andersson. 2011. Selection of resistant bacteria at very low antibiotic concentrations. *PLoS Pathog.* 7:1–9.
- Harmand, N., R. Gallet, R. Jabbour-Zahab, G. Martin, and T. Lenormand. 2016. Fisher's geometrical model and the mutational patterns of antibiotic resistance across dose gradients. *Evolution (N. Y.)*. 23–37.
- Harmand, N., R. Gallet, G. Martin, and T. Lenormand. n.d. Fitness trade-offs in the evolution of bacterial antibiotic resistance along a dose gradient.
- Hartl, D. L. 2014. What can we learn from fitness landscapes? *Curr. Opin. Microbiol.* 21:51–57. Elsevier Ltd.
- Hartl, D. L., and C. H. Taubes. 1996. Compensatory nearly neutral mutations : selection without adaptation. *J. Theor. Biol.* 182:303–309.
- Hartl, D. L., and C. H. Taubes. 1998. Towards a theory of evolutionary adaptation. *Genetica* 102–3:525–533.

- Hendry, A. P., P. R. Grant, B. Rosemary Grant, H. a Ford, M. J. Brewer, and J. Podos. 2006. Possible human impacts on adaptive radiation: beak size bimodality in Darwin's finches. *Proc. Biol. Sci.* 273:1887–1894.
- Hughes, D., and D. I. Andersson. 2015. Evolutionary consequences of drug resistance: shared principles across diverse targets and organisms. *Nat. Rev. Genet.* 16:459–471. Nature Publishing Group.
- Kassen, R. 2002. The experimental evolution of specialists , generalists , and the maintenance of diversity. *J. Evol. Biol.* 15:173–190.
- Kauffman, S. A., and S. Levin. 1987. Towards a general theory of adaptive walks on rugged landscapes. *J. Theor. Biol.* 128:11–45.
- Keepers, K. G., and A. P. Martin. 2014. Fitness landscape of sympatric pupfishes a useful tool for visualizing speciation. *Mol. Ecol.* 23:2144–2145.
- Kibota, T. T., and M. Lynch. 1996. Estimate of the genomic mutation rate deleterious to overall fitness in *E.coli*. *Nature* 381:694–696.
- Kirkpatrick, M., and N. H. Barton. 1997. Evolution of a species range. *Am. Nat.* 150:1–23.
- Kondrashov, D. A., and F. A. Kondrashov. 2015. Topological features of rugged fitness landscapes in sequence space. *Trends Genet.* 31:24–33. Elsevier Ltd.
- Lande, R. 1981. Models of speciation by sexual selection on polygenic traits. *Proc. Natl. Acad. Sci. U. S. A.* 78:3721–3725.
- Lande, R. 1975. Natural selection and random genetic drift in phenotypic evolution. *Evolution (N. Y.)*. 30:314–334.
- Lande, R., and S. Arnold. 1983. The measurement of selection on correlated characters. *Evolution (N. Y.)*. 37:1210–1226.
- Lenormand, T., L.-M. Chevin, and T. Bataillon. 2016. Parallel Evolution: What does it (not) tell us and why is it (still) interesting? *P. in Chance in Evolution*.
- Levins, R. 1966. The strategy of model building in population biology.
- Lynch, M., and R. Lande. 1993. Evolution and extinction in response to environmental change.

- Manna, F., G. Martin, and T. Lenormand. 2011. Fitness landscapes: an alternative theory for the dominance of mutation. *Genetics* 189:923–37.
- Martin, G., R. Aguilée, J. Ramsayer, O. Kaltz, O. Ronce, P. T. R. S. B, and R. Aguile. 2013. The probability of evolutionary rescue : towards a quantitative comparison between theory and evolution experiments. *Philos. Trans. R. Soc. Lond. B. Biol. Sci.* 368.
- Martin, G., S. F. Elena, and T. Lenormand. 2007. Distributions of epistasis in microbes fit predictions from a fitness landscape model. *Nat. Genet.* 39:555–60.
- Martin, G., and T. Lenormand. 2006a. A general multivariate extension of Fisher's geometrical model and the distribution of mutation fitness effects across species. *Evolution* 60:893–907.
- Martin, G., and T. Lenormand. 2008. The distribution of beneficial and fixed mutation fitness effects close to an optimum. *Genetics* 179:907–916.
- Martin, G., and T. Lenormand. 2006b. The fitness effect of mutations across environments: a survey in light of fitness landscape models. *Evolution (N. Y.)*. 60:2413–2477. Wiley Online Library.
- Martin, G., and T. Lenormand. 2015. The fitness effect of mutations across environments: Fisher's geometrical model with multiple optima. *Evolution (N. Y.)*. 69:1433–1447.
- Martin, G., and L. Roques. 2016. The Non-stationary Dynamics of Fitness Distributions: Asexual Model with Epistasis and Standing Variation. *Genetics* 1–37.
- Orr, H. A. 2000. Adaptation and the cost of complexity. *Evolution (N. Y.)*. 54:13–20.
- Orr, H. A. 2005. The genetic theory of adaptation: a brief history. *Nat. Rev. Genet.* 6:119–27.
- Orr, H. A. 1998. The population genetics of adaptation: the distribution of factores fixed during adaptive evolution. *Evolution (N. Y.)*. 52:935–949.
- Oz, T., A. Guvenek, S. Yildiz, E. Karaboga, Y. T. Tamer, N. Mumcuyan, V. B. Ozan, G. H. Senturk, M. Cokol, P. Yeh, and E. Toprak. 2014. Strength of selection pressure is an important parameter contributing to the complexity of antibiotic resistance evolution. *Mol. Biol. Evol.* 31:2387–2401.
- Polechová, J., N. Barton, and G. Marion. 2009. Species' range: adaptation in space and time. *Am. Nat.* 174:E186–204.

- Rueffler, C., T. J. M. Van Dooren, and J. A. J. Metz. 2004. Adaptive walks on changing landscapes: Levins' approach extended. *Theor. Popul. Biol.* 65:165–178.
- Schlüter, D. 2000. The ecology of adaptive radiation. Oxford Series in Ecology and Evolution.
- Schlüter, D., and D. Nychka. 1994. Exploring fitness surfaces. *Am. Nat.* 143:597–616.
- Seehausen, O. 2004. Hybridization and adaptive radiation. *Trends Ecol. Evol.* 19:198–207.
- Simpson, G. G. 1944. Tempo and Mode in Evolution. New York: Columbia Univ. Press.
- Tenaillon, O. 2014. The Utility of Fisher's Geometric Model in Evolutionary Genetics. *Annu. Rev. Ecol. Evol. Syst.* 45:179–201.
- Waxman, D., and J. J. Welch. 2005. Fisher's Microscope and Haldane's Ellipse. *Am. Nat.* 166:447–457.
- Weinreich, D. M., R. a Watson, and L. Chao. 2005. Perspective: Sign epistasis and genetic constraint on evolutionary trajectories. *Evolution* 59:1165–1174.
- Whitlock, M. C., P. C. Phillips, F. B.-G. Moore, and S. J. Tonsor. 1995. Multiple fitness peaks and epistasis. *Annu. Rev. Ecol. Syst.* 26:601–629.

Supplementary Figure



Sup.Fig 1: Fitness trajectories of the experimental lines selected to build the landscape, evolved in the four antibiotic doses 3, 8, 20 and 100 $\mu\text{g}/\text{mL}$ of Nal antibiotic. [To be completed with more time-data and replicates]. Means (dots) and standard errors among measure replicates. Lines show the fit of the trajectories under the FGM assumptions considering the same maximal value for all line within a dose.

Appendix

1. Measuring distances between optima:

Under the classic form of the FGM that we use, the malthusian fitness $m_{i,j}$ of any line i , when measured in dose j , is a quadratic function of the distance $d_{i,j}$ between the line's phenotype and the optimum in dose j : $m_{i,j} = m_{max,j} - 1/2 \lambda_j d_{i,j}^2$, where $m_{max,j}$ is the maximum fitness in measure dose j . Let $m_{ref,j}$ be the fitness of the reference strain in dose j , the selection coefficient $s_{i,j}$ of line i in measure dose j is measured relative to this reference, which corresponds to a difference between their Malthusian fitnesses: $s_{i,j} = m_{i,j} - m_{ref,j}$. The difference between selection coefficients of two lines i and j (the latter having evolved in the measure dose j) is

$$\Delta s_{i,j} = s_{j,j} - s_{i,j} = m_{j,j} - m_{i,j} = \frac{1}{2} \lambda_j (d_{i,j}^2 - d_{j,j}^2) \approx \frac{1}{2} \lambda_j d_{i,j}^2 , \quad (\text{A1})$$

Where the approximation on the right hand side of Eq.(A1) neglects $d_{j,j}^2 \ll d_{i,j}^2$ and corresponds to Eq. (1) in the main text. The measure $\Delta s_{i,j}$ is independent of the reference line's fitness or of the maximal fitness in the measure dose j .

2. Measuring the angle between the direction to each optimum from the ancestor

Bivariate DFE among random mutants: Consider an FGM in n dimensions, with selection strengths λ_i and λ_j in environments i and j . The ancestor background from which mutations arise has Malthusian fitness $m_{0,i}$ (resp. $m_{0,j}$) in environments i (resp. j). The angle between the phenotypic direction to each optimum, from the ancestor phenotype is denoted ϕ_{ij} , and its cosine is denoted $\rho_{ij} = \cos(\phi_{ij})$. Consider the joint distribution of mutation fitness effects $\{s_i, s_j\}$, relative to their ancestor, in a pair of environments $\{i, j\}$. This distribution has known general form, when considering random mutations (Martin & Lenormand 2015). We extend this result to allow for different strengths of selection in each environment ($\lambda_i \neq \lambda_j$), as assumed in the main text. Define $s_o^i = m_{max,i} - m_{0,i}$ (resp. $s_o^j = m_{max,j} - m_{0,j}$) the fitness distance from the ancestor, to the optimum in environment i (resp. j). Define also the scaled fitness distances $\epsilon_i = 2s_o^i/(n \lambda_i)$ and $\epsilon_j = 2s_o^j/(n \lambda_j)$. The joint distribution of $\{s_i, s_j\}$ is characterized by its cumulant generating function (CGF), which is obtained as a straightforward extension of Eq. (5) in (Martin & Lenormand 2015):

$$C_{s_i, s_j}(t_i, t_j) = \frac{n}{2} \left(\frac{b}{1+a} - \ln(1+a) \right) .$$

$$a = \lambda_i t_i + \lambda_j t_j \text{ and } b = \lambda_i^2 t_i^2 \epsilon_i + 2 \rho \lambda_i \lambda_j t_i t_j \sqrt{\epsilon_i \epsilon_j} + \lambda_j^2 t_j^2 \epsilon_j$$
(A2)

We assume that the background is maladapted to both environments, which means that $\epsilon_i, \epsilon_j \gg$

1. An asymptotic series of Eq.(A2), for large $\epsilon \gg \lambda t$ yields a bivariate Gaussian approximation:

$$C_{s_i, s_j}(t_i, t_j) \underset{\epsilon \gg \lambda t}{\approx} \frac{n}{2} b ,$$
(A3)

Which is the CGF of a centered bivariate normal distribution

$$\begin{pmatrix} s_i \\ s_j \end{pmatrix} \sim N \left(\begin{pmatrix} 0 \\ 0 \end{pmatrix}, \begin{pmatrix} v_i & \rho_{ij} \sqrt{v_i v_j} \\ \rho_{ij} \sqrt{v_i v_j} & v_j \end{pmatrix} \right) ,$$
(A4)

With means zero, variances ($v_i = n \lambda_i^2 \epsilon_i, v_j = n \lambda_j^2 \epsilon_j$) in each environment and correlation $\rho_{ij} = \cos(\phi_{ij})$. The latter thus provides information on the angle between directions towards each optimum, from the ancestor.

We assume that the growth rates $\{r_i, r_j\}$ of mutants, measured in each dose (i and j), are approximately linearly related to their corresponding measured selection coefficients, relative to our reference strain: $r_i = k_1 s_i + k_2$ and $r_j = l_1 s_i + l_2$, for some constants (k_1, k_2, l_1, l_2) . In the simplest demographic model, $k_1 = 1$ and $k_2 = -m_{ref,i}$ the fitness of the reference strain in dose i (and the same goes for dose j), but we only require a general form of linearity. The bivariate distribution of growth rates is then also Gaussian (from Eq.(A4)), and we can write a general form:

$$\begin{pmatrix} r_i \\ r_j \end{pmatrix} \sim N \left(\begin{pmatrix} \mu_i \\ \mu_j \end{pmatrix}, \begin{pmatrix} \sigma_i^2 & \rho_{ij} \sigma_i \sigma_j \\ \rho_{ij} \sigma_i \sigma_j & \sigma_j^2 \end{pmatrix} \right) ,$$
(A5)

With some means (μ_i, μ_j) , variances (v_i, v_j) and the same correlation ρ_{ij} (correlation is unchanged by any linear function).

Bivariate DFE among resistant mutants: Our data are not based on random mutants but on screened mutants, which are a biased subsample of all random mutants. Mutants screened at

dose i must first be resistant at this dose, i.e. they must show positive growth ($r_i > 0$). Their selection coefficient must thus lie above some threshold $s_i \geq b_i$. The proportion of all mutants that is resistant in dose i , in the Gaussian approximation used here (Eq.(A5)), is given by

$$p_i = P(s_i > b_i) = P(r_i > 0) = \frac{1}{2} \left(1 + \operatorname{erfc} \left(\frac{\alpha_i}{\sqrt{2}} \right) \right), \quad (\text{A6})$$

Where $\operatorname{erfc}(.)$ is the complementary error function and $\alpha_i = \mu_i/\sigma_i$ is a composite parameter that measures the level of screening: it increases with lower p_i (i.e. stronger screening, leading to less resistant mutants). This parameter can be estimated from a measure of the frequency of resistance mutations, as

$$\alpha_i = -\sqrt{2} \operatorname{erfc}^{-1} (2(1-p_i)). \quad (\text{A7})$$

The effect of truncation inherent to screening on the correlation of fitness effects can be studied directly on normalized variables, as correlation is scale-free. Define the normalized growth rates

$$\begin{pmatrix} u = (r_i - \mu_i)/\sigma_i \\ v = (r_j - \mu_j)/\sigma_j \end{pmatrix} \sim N \left(\begin{pmatrix} 0 \\ 0 \end{pmatrix}, \begin{pmatrix} 1 & \rho_{ij} \\ \rho_{ij} & 1 \end{pmatrix} \right). \quad (\text{A8})$$

The CGF of the bivariate distribution of $\{u, v\}$ is given by $C_{uv}(x, y) = (x^2 + y^2 + 2\rho_{ij}xy)/2$. Resistance to dose i ($r_i > 0$) then implies a truncation of u above $u > -\mu_i/\sigma_i = \alpha_i$. From known results on hidden truncation models, the CGF of the normalized distribution after truncation above some level α_i (indicated by a star) is (from eq. (7) in Arnold, 1993)

$$C_{uv}^*(x, y) = \frac{1}{2} (x^2 + y^2 + 2\rho_{ij}xy) + \log \left(\frac{1 + \operatorname{erf} \left(\frac{y - \alpha_i + \rho_{ij}x}{\sqrt{2}} \right)}{\operatorname{erfc} \left(\frac{\alpha_i}{\sqrt{2}} \right)} \right). \quad (\text{A9})$$

From that expression, the correlation ρ_{ij}^* within resistant mutants is simply obtained by taking derivatives of the CGF at $x = y = 0$. More precisely, setting $\varphi(\alpha) = \sqrt{\pi e^{\alpha^2}} \operatorname{erfc}(\alpha/\sqrt{2})$, we have

$$\rho_{ij}^* = \frac{\partial_{x,y} C_{uv}^*(0,0)}{\sqrt{\partial_x^2 C_{uv}^*(0,0) \partial_y^2 C_{uv}^*(0,0)}} = \rho_{ij} \sqrt{\frac{\sqrt{2} \alpha_i \varphi(\alpha_i) + \varphi(\alpha_i)^2 - 2}{\varphi(\alpha_i)^2 + \rho_{ij}^2 (\sqrt{2} \alpha_i \varphi(\alpha_i) - 2)}}. \quad (\text{A10})$$

We see that the observed correlation ρ_{ij}^* among resistant mutants is entirely determined by that among random mutants ρ_{ij} and the measurable screening level parameter α_i (Eq.(A7)).

Bivariate DFE among screened mutants: Finally, an additional correction may be used to better describe the screening process. When plated onto a selective agar plate (with antibiotic at dose i), we expect that not all single resistant cells on the plate will grow to produce a visible colony (a large population). Some will get extinct stochastically during their early growth, i.e. have limited ‘plating efficiency’, in fluctuation assay terminology. This may affect the distribution of screened mutants and hence the observed correlation of their selection coefficients across doses. We model this effect using a classic Feller diffusion approximation {Feller, 1951 #2746} for the stochastic growth of a cell. This approximation states that the probability $\pi(r_i)$ for a single cell with growth rate r_i to avoid stochastic loss is proportional to this growth rate: $\pi(r_i) \propto r_i$ for any resistant mutant with $r_i > 0$. Rigorously, this is in general accurate as long as the probability is relatively small ($\pi(r_i) \ll 1$), but it typically proves robust even for relatively strongly growing mutants (Martin et al. 2013).

Considering this plating efficiency, screened mutants (“**”) are themselves a biased subsample of all resistant mutants (“*”). The moment generating function (MGF) of $\{u, v\}$ among screened mutants is the exponential of the CGF. It is readily obtained as a conditional expectation weighted by the probability of non-extinction and thus satisfies:

$$M_{uv}^{**}(x, y) = \frac{\mathbb{E}_{u,v}(e^{x u + y v} \pi(r_i) | u > \alpha_i)}{\mathbb{E}_{u,v}(\pi(r_i) | u > \alpha_i)}, \quad (\text{A11})$$

With $\pi(r_i) = k r_i = k (\sigma_i u + \mu_i)$, for some constant $k > 0$, and $\mathbb{E}_{u,v}(\cdot)$ an expectation taken over the bivariate distribution of $\{u, v\}$. We note that $\mathbb{E}_{u,v}(u e^{x u + y v} | u > \alpha_i) = \partial_x M_{uv}^*(x, y)$ and $\mathbb{E}_{u,v}(e^{x u + y v} | u > \alpha_i) = M_{uv}^*(x, y)$, where $M_{uv}^*(x, y) = e^{C_{uv}^*(x, y)}$ is the MGF of $\{u, v\}$ among resistant mutants. We now focus on the CGF of $\{u, v\}$ among screened mutants and get, after rearranging:

$$C_{uv}^{**}(x, y) = \log(M_{uv}^{**}(x, y)) = \log(\partial_x e^{C_{uv}^*(x, y)} - \alpha_i e^{C_{uv}^*(x, y)}) + K, \quad (\text{A12})$$

For some constant K and with $C_{uv}^*(x, y)$ given by Eq.(A9). The same approach as in Eq.(A10) with $C_{uv}^{**}(x, y)$ instead of $C_{uv}^*(x, y)$ then yields the correlation ρ_{ij}^{**} among screened resistant mutants as

$$\rho_{ij}^{**} = \rho_{ij} \sqrt{\frac{4 - 3\sqrt{2} \alpha_i \varphi(\alpha_i) + (\alpha_i^2 - 1) \varphi(\alpha_i)^2}{2(1 + \rho_{ij}^2) - \sqrt{2} \alpha_i (2 + \rho_{ij}^2) \varphi(\alpha_i) + (\alpha_i^2 - \rho_{ij}^2) \varphi(\alpha_i)^2}}. \quad (\text{A13})$$

This relationship is then inverted numerically, to infer ρ_{ij} (and thus the angle $\phi_{ij} = \cos^{-1}(\rho_{ij})$) from the observed correlation ρ_{ij}^{**} among screened mutants and the measurable screening level parameter α_i (inferred via Eq.(A7)).

Fast evolution of frequency-dependent selection between coexisting bacteria species

Harmand Noémie¹, Valentine Federico¹, Thomas Hindré², Lenormand Thomas¹

1. UMR 5175 CEFÉ, CNRS - Université Montpellier - Université P. Valéry - EPHE, Montpellier Cedex 5, France
2. UMR 5163, CNRS - Université Joseph Fourier, F-38041 Grenoble, France.

Abstract

The long-term maintenance of polymorphisms can be explained by several mechanisms. One of the most powerful is negative frequency-dependent selection on genotypes, populations, or species. Negative frequency-dependent selection (NFDS) can emerge from several types of ecological and behavioral interactions that are widespread in natural populations. In the field, the detection of NFD interactions are often rapidly taken as a proof of long-term coexistence at the frequency equilibrium. In contrast, tracking coevolutions in the laboratory can prove efficient to study how NFDS evolves as populations adapt, and what is susceptible to reinforce or disrupt coexistence. We recorded the coevolution of two bacterial types during 870 generations along a gradient of different environmental conditions. These bacteria show initially strong asymmetries both in their ecological characteristics and in their adaptation to environmental conditions. The results indicate a fast evolution of negative frequency-dependent selection patterns, driven by adaptation of the less well-adapted bacteria to the experimental conditions. Yet, the coexistence was successfully maintained due to a strong curvature of the NFDS profile. These findings show that NFDS does not entail a stable frequency equilibrium and provides an explanation for the long-term maintenance of some species at very low frequencies.

Keywords

Experimental coevolution, *Escherichia coli*, *Citrobacter freundii*, Nalidixic acid, polymorphism

Introduction

Astounding biodiversity can be observed at different scales: from locus to species, from newly emerging polymorphism to trans-specific polymorphisms maintained for millions of years (e.g. in Devier et al. 2009). Understanding the maintenance of such diversity among species (coexistence in communities) and within species (genetic polymorphism) is a long-standing question in ecology and evolution. Various mechanisms can explain stable coexistence by balancing selection against other forces, such as migration or mutation (listed in Débarre and Lenormand 2011). However, a very powerful way to maintain long-term coexistence or polymorphism is when selection itself operates in a frequency-dependent manner, favoring rare types. With such negative frequency-dependent selection (NFDS), by definition, a small frequency perturbation below (resp. above) the equilibrium frequency leads to positive (resp. negative) selection, bringing the system back to its equilibrium point and ensuring stability (Lewontin 1958; Haldane and Jayakar 1963; Ayala and Campbell 1974; Bell 2008; Felsenstein 2017). Apart from selection on allele caused by overdominance in diploids, NFDS can emerge from a diversity of underlying ecological mechanisms: (1) It can occur when different types specialize on different limiting resources and density is locally regulated, as in Levene's model (Levene 1953; Hedrick 1978; Ravigné et al. 2004; Bürger 2010). (2) It can occur when trade-offs occur between traits or life-stages involved in the exploitation of the same resource (Heino et al. 1997; Bonsall 2006). (3) It can result from a modification of the resource/environment by one type which directly benefits a second type (e.g. by making the resource more easily accessible as with producer/scrounger strategies (Barnard and Sibly 1981), or by generating a secondary resource in cross-feeding (Rosenzweig et al. 1994; Treves et al. 1998; Doebeli 2002; Plucain et al. 2014) or other facilitation situations (Thijs et al. 1994; Dugatkin et al. 2005; Kelsic et al. 2015)). (4) The different types can themselves be resources for specialized predators or parasites (Clarke 1962; Oaten and Murdoch 1975; Borghans et al. 2004; Olendorf et al. 2006). (5) The behavior of a third party (predator, parasite, mutualist) can specifically benefit rare types, such as in the case of apostatic selection (Joron and Mallet 1998; Borghans et al. 2004; Fincke 2004). (6) Interactions between individuals can be more favorable when they involve different types (e.g. as with mating types, sexes) (e.g. Gross 1996; Sinervo and Lively 1996; Penn and K 1999; Reusch et al. 2001) or favor rare types (such as cheaters in public good games) (e.g. O'Connell and Johnston 1998; Gigord et al. 2001; Cordero and Polz 2014).

Finding NFDS in field or laboratory experiments provides a robust explanation for the origin and maintenance of a polymorphism. It requires measuring how relative fitness varies when the competing types are manipulated to be at different frequencies. In addition, the system can be

shown to be at selective equilibrium by demonstrating that the observed frequency is close to the frequency at which the two types have equal fitness. Such findings are usually taken as a strong argument for the stability and likely long-term persistence of the observed polymorphism, as long as environmental conditions remain unchanged (e.g. in Turner et al. 1996; Gigord et al. 2001; Weeks and Hoffmann 2008; Takahashi and Kawata 2013; Healey et al. 2016). This view neglects the fact that frequency-dependent patterns of selection can evolve, even under constant environmental conditions, which could undermine polymorphism maintenance in the long term. Observing a short-term and local equilibrium is not a guarantee of long-term stability. Similar shortcuts are frequently made in similar contexts. For instance, overdominance does not really guarantee long-term polymorphism: a duplication combining overdominant alleles could arise, and fix to suppress the segregation load and the original polymorphism (Haldane 1954).

At first sight, the mechanism of negative frequency dependence applies equally well to alleles at a locus (within a species) as it does to species in a community. And indeed, the basic theoretical models are virtually indistinguishable in the two cases (Levin 1988; Mazancourt and Dieckmann 2004). However, there might be an important difference between long-term coexistence among alleles or among species. The genomes of different species can diverge at multiple loci, which might lead to a faster destabilization of NFDS. This destabilization effect could be particularly strong between two already divergent species, since they are more likely to exhibit different rates of adaptation than very recently diverged species. In contrast, within a sexual species, recombination will homogenize the genetic backgrounds of loci maintained by NFDS, which will strongly limit this effect. Hence, we could expect polymorphism maintained by NFDS to persist longer among alleles in a sexual species than among species, and longer between recently-diverged than anciently-diverged species.

When two types are maintained by NFDS, each can still adapt to the surrounding environmental conditions, and to the presence of the competitor. Hence, the pattern of NFDS itself can evolve through time, which may change the condition and degree of coexistence (Rozen and Lenski 2000; Svensson et al. 2005; Maddamsetti et al. 2015). For example, let us consider two asexual microbial strains coexisting by NFDS in fixed conditions (e.g. in the laboratory). If one strain acquires an adaptive mutation but not the other, the NFDS pattern and the frequency equilibrium is expected to change in favor of this strain. As the other strain is becoming less frequent, and with a lower population size, it might be less likely to acquire a beneficial mutation (since this probability scales linearly with population size). Hence, the stochastic occurrence of independent beneficial mutations in each strain may destabilize the polymorphism (i.e. lead to the extinction of one of the strains, as in Maddamsetti et al. 2015), and this effect might be

amplified by demographic feedbacks. In Fig. 1, this process is illustrated by changes in the intercept of the NFDS profile. However, long-term coexistence may be also promoted if evolution strengthens the interaction between the types. When the slope of the NFDS profile becomes more negative, this reinforces the stability of the equilibrium with respect to frequency perturbations, and protects the polymorphism from larger evolutionary variation in the intercept. Hence, long-term coexistence depends on whether the slope or the intercept of the NFDS profile evolves more quickly. Furthermore, the evolution of the interaction may change the shape of the profile itself. As explained above, different non-exclusive mechanisms can lead to NFDS, and combine when an interaction evolves. In particular, the shape of the profile near 0 and 1 can strongly impact long-term persistence of the polymorphism. If one species / strain / allele exhibits a fast non-linear increase in selection coefficient when rare, it is much more likely to escape long-term extinction. Graphically, when NFDS is linear as in Fig. 1a, a change of intercept strongly displaces the equilibrium frequency value, whereas with curved profile as in Fig. 1b, polymorphism can be maintained for much longer times upon perturbation of the intercept.

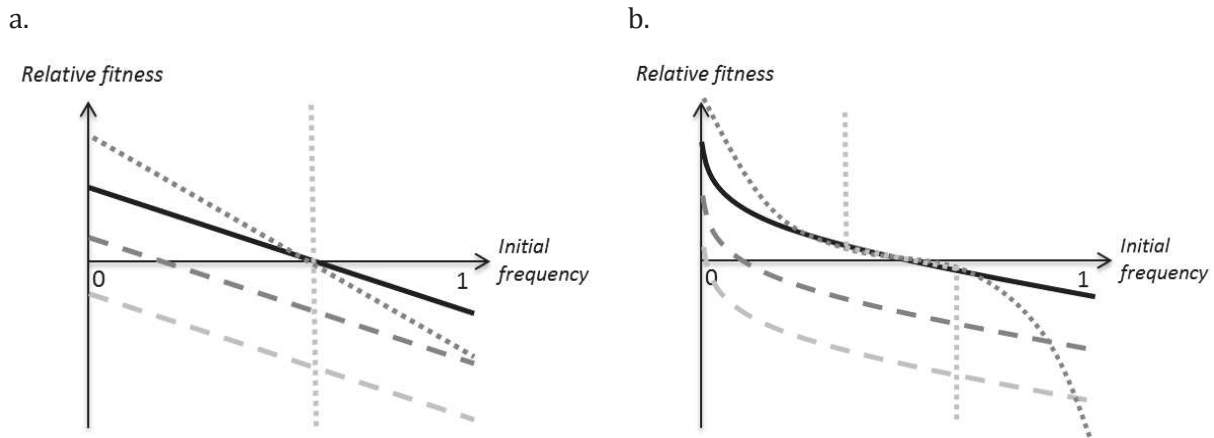


Figure 1: Scenarios of evolution of negative frequency-dependent interactions maintaining or disrupting polymorphism. Black lines represent a hypothetical linear (a) or non-linear (b) NFDS at time t . The gray gradient shows the evolution of this NFDS in a scenario where the NFDS is reinforced (dotted lines), and ultimately results in ‘private’ niches for each morph, or a scenario where unbalanced evolution leads to decreasing frequency of one morph (dashed lines) and may ultimately disrupt the polymorphism (light grey dashed line in a).

The stability and evolution of NFDS profiles has been much more extensively studied for interactions within species than for interactions across species. The long-term persistence of polymorphic alleles in sexual species has been repeatedly demonstrated and can last hundreds of millions of years (Takahata and Nei 1990; Devier et al. 2009; Karasov et al. 2014; Těšicky and Vinkler 2015). In parallel, several studies using experimental evolution on bacteria have

demonstrated that emerging polymorphism can arise and last for tens of thousands of generations in constant environments (Turner et al. 1996; Rainey and Travisano 1998; Friesen et al. 2004; Rozen et al. 2007; Blount et al. 2012; Plucain et al. 2014; Maddamsetti et al. 2015; Healey et al. 2016). However, in these cases, and despite persistence, it is apparent that the maintenance of polymorphism is quite precarious. The independent occurrence of beneficial mutations in the different lineages causes important variations in the intercept of NFDS profiles (and consequently important fluctuations in equilibrium frequencies). There is, however, a strong ascertainment bias in these studies, as all lost polymorphisms are less likely to be detected and studied. This is exemplified by the study of (Maddamsetti et al. 2015) who found traces of such lost NFDS polymorphism among de novo emerging strains of *E. coli*. In contrast, the evolution of NFDS in divergent species has received much less attention. As explained above, there are good reasons to expect that NFDS profiles should be even less stable in such cases. However, it is also possible that different species start with steeper NFDS profiles, and already present specialized or interaction-stabilizing traits, making their long-term coexistence more likely. To address this question, we study the long-term coexistence between two divergent bacteria species. We also investigate whether different abiotic conditions change the outcome of this coevolution, as would be expected if different environments represent different adaptive challenges to the two coevolving species.

Material and methods

- Overview

In our experiment, NFDS occurs between nalidixic acid (Nal) resistant *Escherichia coli* (hereafter *E. coli* or *E*) strains and *Citrobacter freundii* (hereafter *C. freundii* or *C*) strains. *E. coli* is well adapted to the experimental conditions in the absence of *C. freundii*, whereas the experimental conditions are new for *C. freundii* strains. The two strains coevolved during 870 generations at five different Nal concentrations. Variations of the NFDS profiles were investigated by performing competitions at initial and final time points of the coevolution as well as through time-shift competitions between evolved and initial strains.

- Medium and antibiotic

Experimental coevolution and competitions assays were performed in Davis minimal medium (DM: 7 g.L⁻¹ KH₂PO₄.3H₂O, 2 g.L⁻¹ KH₂PO₄, 1 g.L⁻¹ (NH₄)₂SO₄, 0.5 g.L⁻¹ Na₃C₆H₅O₇, sterile water compensating exactly for evaporation after autoclaving; pH set at 7.0) supplemented with 1250

$\mu\text{L.L}^{-1}$ glucose 10%, $806 \mu\text{L.L}^{-1}$ MgSO₄ [1M] and $1000 \mu\text{L.L}^{-1}$ thiamine 0.2% (medium referred to as DM250). DM250 thus contains c.a. 1.2 times more citrate than glucose. Nal was added to the medium at the desired concentration from aliquots at 30 mg.mL^{-1} diluted in NaOH 300mM. Fresh medium was prepared each week and kept protected from light at 4°C.

- Strains

44 *E. coli* lines were initiated from Nal-resistant mutants of the strain REL4536 of Lenski's LTEE line, evolved in DM250 for 10.000 generations. These mutants express constitutively yellow fluorescent proteins (see details in Gallet et al. 2012, Harmand et al. in prep.). Prior to the coevolution, eight lines were allowed to evolve for approximately 400 generations in DM250 at each of five different Nal concentrations ($5 \times 8 = 40$ lines): 3, 8, 20, 100 and 200 $\mu\text{g/mL}$. Four lines also adapted in the absence of Nal.

The *C. freundii* initial strain was obtained from an external contamination (this strain has never been used in the lab) of the glycerol stock that was used for storing *E. coli* evolution lines. It was identified from the absence of fluorescence of colonies when plated on petri dishes and a diauxic growth curve in the presence of glucose and citrate. Sequencing and alignment of the 16S ribosomal DNA revealed them as *C. freundii*. No other contaminants were detected (the presence of Nal and well-adapted *E. coli* probably reduced the chance of invasion by other potential contaminants). Sequencing of highly variable 16S regions III and VI of *C. freundii* were performed to control for genetic variability of *C. freundii* among the initial lines. No differences were observed.

- Experimental coevolution

The 44 *E. coli* and *C. freundii* mixes from glycerol stocks were cultured in 1mL DM250-Nal at different concentrations: 0, 3, 8, 20, 100 and 200 $\mu\text{g/mL}$ (eight coevolving lines in each concentration but four at concentration 0) at 37°C, 250 rpm and transferred daily with a dilution rate 1:100 for ~870 generations. The mixes were stored at regular intervals of the coevolution. The relative frequencies of *E. coli* and *C. freundii* strains were estimated for each line at c.a. 0, 200, 550 and 870 generations of coevolution by flux cytometry. 100 000 cells of the corresponding co-culture were analyzed to estimate the frequency of YFP-fluorescent cells in the mix.

- Strain isolation

E. coli and *C. freundii* strains were isolated based on metabolic differences between the two species: *C. freundii* can grow on citrate only, which *E. coli* cannot do, whereas *E. coli* is resistant to streptomycin (Str), but *C. freundii* is not. Mixes were cultured for 24h at 37°C both in DM-Nal without glucose and in DM250-Nal-Str. The cultures were then diluted and plated in order to obtain isolated colonies after overnight growth at 37°C. We checked that colonies from the culture in DM250-Nal-Str were all fluorescent, contrary to the colonies from the DM-Nal cultures. Cells from six different colonies from each culture were collected and stored for later experimentation.

- Competitions

Two coevolved lines from the intermediate Nal concentration 20 µg/mL were selected to investigate variations in the NFDS during coevolution. For each line, we performed four different series of competitions: 1) *E. coli* against *C. freundii* at the initiation of coevolution (*E0* and *C0*, respectively), 2) *E. coli* against *C. freundii* after 870 generations of coevolution (*E8* and *C8*), 3) *E0* against *C8*, and 4) *E8* against *C0*. The first two series should indicate whether the interaction changed during coevolution, while the last two should indicate how each species contributed to that change. *E* and *C* strains were first cultured separately in DM250-Nal20 for 12h in the same conditions as the experimental evolution. The cultures were then mixed in 1mL wells with a large range of different volumic frequencies (t0 mixes). 10 µL of those mixes were transferred to 1 mL of DM250-Nal20 and allowed to compete for 24h at 37°C, 250 rpm (t24 mixes). Frequencies of *E* and *C* cells in the t0 and t24 mixes were estimated by flux cytometry measures, counting 100 000 cells.

- Characterization

In order to investigate the mechanism of NFDS, we inoculated the *C0*, *E0*, *C8* and *E8* strains in several conditions (at a 1:100 volumic ratio) and recorded the optical density and fluorescence YFP throughout a 24h growth cycle at 37°C. Growth curves were obtained in the conditions of the experimental evolution (DM250-Nal20). In order to test for cross-feeding interactions, we also inoculated *C* strains in a filtrate of the growth medium of an *E* strain (but in medium without citrate) and vice-versa. We also recorded growth at 6 different citrate concentrations ranging from 0 to 2 times the concentration in DM250 for *E* and *C*, from a pair evolved in each Nal dose before and after the coevolution. This experiment allowed us to investigate the effect of the citrate and Nal doses on strains.

Results

- NFDS profiles evolved rapidly and consistently across abiotic conditions

The two species were still (detectably) coexisting in 39 out of the 44 coevolution lines at generations 200, 550 and 870 (Fig. 2). A clear NFDS profile was present at generations 0 and 870 of the coevolved lines selected for competition experiments (Fig. 3). This NFDS is most likely involved in the long-term coexistence of those 39 coevolved lines. In the five remaining lines (1 at Nal 0, 2 at Nal 3, 1 at Nal 100 and 1 at Nal 200); >98% cells were typed as YFP throughout the coevolution. It is however difficult to conclude whether or not *C.freundii* is present at low frequencies in these replicates, as a few non-fluorescent *C* cells cannot be easily distinguished from background noise. Some plating done on these lines did not reveal the presence of *C* either.

Figures 2 and 3 show that the NFDS profiles changed dramatically in the coevolved lines. The shape of the profile presents a distinctive curvature near the fixation points (near frequency = 0 or 1). This shape was not strongly changed through time, but shifted significantly downwards (which is analogous to a change in intercept), resulting in a much lower equilibrium frequency of *E* at the final compared to initial time points (Fig. 2). This pattern is shown more generally on Fig. 1: the equilibrium frequency of *E. coli* tends to decrease through time (following the gray gradient lines). In addition, this decrease is very consistently more pronounced at increasing Nal concentrations.

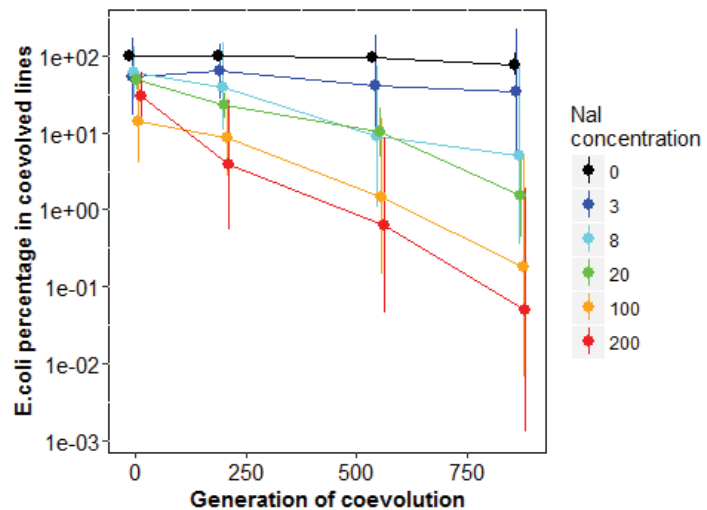


Figure 2: Evolution of the proportion of *E. coli* against *C. freundii* throughout the coevolution at different antibiotic concentrations (colors). Mean values and standard deviations are calculated per antibiotic dose (8 lines per dose but 4 in Nal0), the values per line are shown in Supp. Fig. 1. The values were estimated from samples of 100 000 cells in which the proportion of YFP fluorescent cells was estimated.

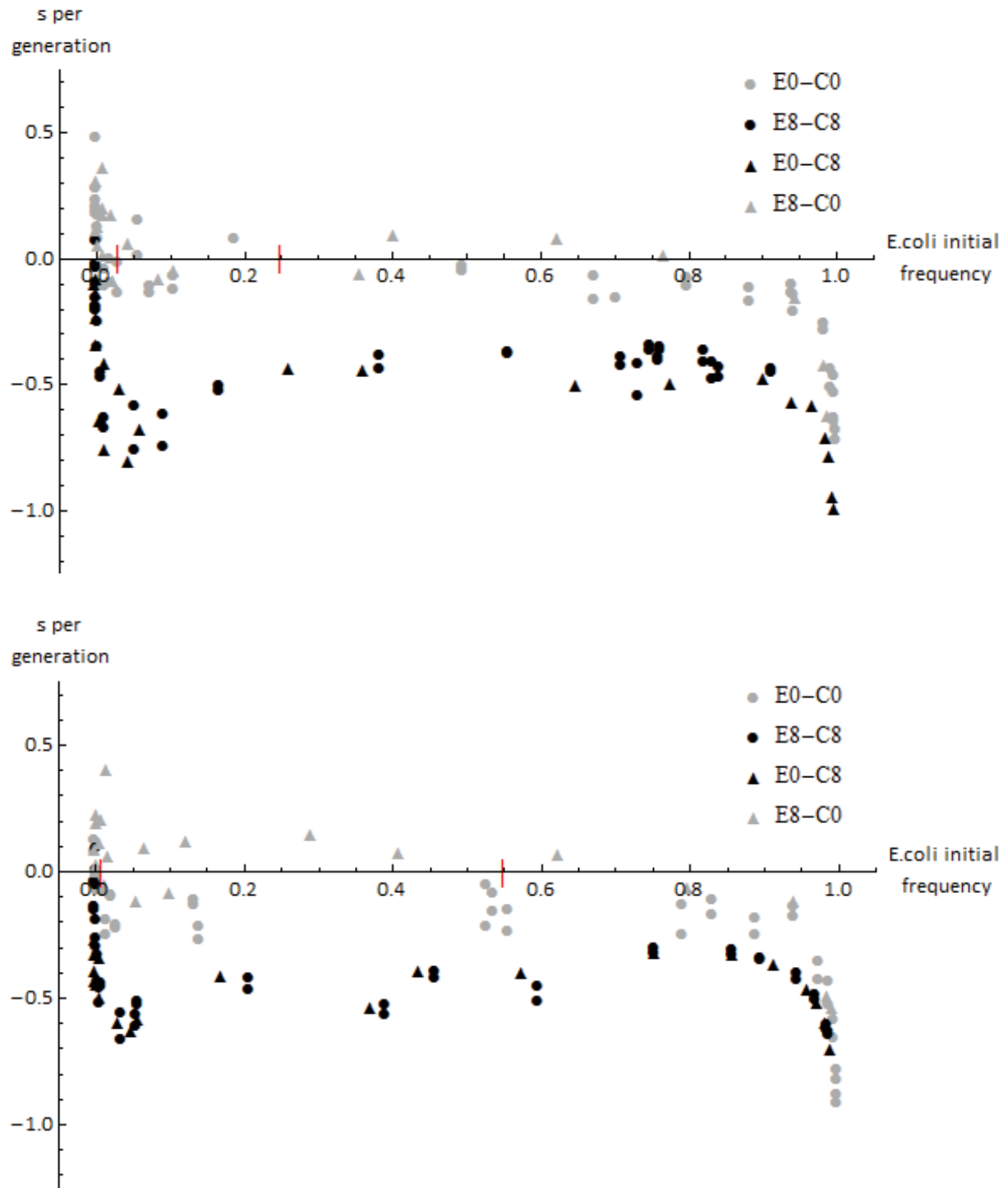


Figure 3: Negative frequency-dependent selection profiles between *E. coli* (*E*) and *C. freundii* (*C*) at initial (0) (grey dots) and final time (8) (black dots) of the coevolution for two sets of co-evolved lines, evolved in

DM250 at Nal concentration 20 µg/mL. Triangles represent the crossed-time competitions. Each point is the selection coefficient of one competition. Red marks on the x-axis represent the frequency of *E* measured in the mixes at initial (higher values) and final time (lower values) of the coevolutions.

- Evolution of frequency-dependence is driven by the adaptation of *C*

We performed competitions at generation 0, 200 and 870 and time-shifted competitions in order to assign specific patterns of variation in NFDS profiles to *E* or *C* evolution. Competitions between *E*0 and *C*8 should indicate whether *C* evolution was responsible for the change in NFDS profiles, and the reciprocal competition should measure how much of the pattern was due to evolution of *E*.

Figure 3 shows that cross-competition NFDS profiles overlap almost entirely with profiles obtained from contemporary competitions at the initial and final time points: the *E*8-*C*0 profile is nearly identical to the *E*0-*C*0 profile, indicating that *E* did not evolve and therefore that nearly all the evolutionary changes occurred in *C*. Consistent with this finding, *C*8-*E*0 profiles are nearly identical to the *E*8-*C*8 profile, indicating also that most evolutionary change occurred in *C* and almost none in *E*. Hence, the variation of the NFDS is almost entirely imputable to the evolution of *C*. The shapes of the NFDS profiles at initial and final time are very similar. The main difference is an overall shift downwards, as would be expected if *C* accumulated many more unconditionally beneficial mutations over this time period. Here unconditionally refers to mutations that confer the same fitness advantage at all frequencies of *C* versus *E*. However, this interpretation is not correct. At intermediate time (generation 200), the NFDS profiles show a very different shape (see NFDS profiles at generation 200 in Fig. 4). They are only shifted downwards for large starting frequencies of *E*, not for small frequencies. The same pattern holds for the two cases investigated. The growth curves of isolated *C* and *E* strains (Fig. 5) confirm that *C* was adapting rapidly during coevolution (e.g. by reducing its lag time for citrate consumption) whereas *E* showed no obvious adaptation to the abiotic conditions.

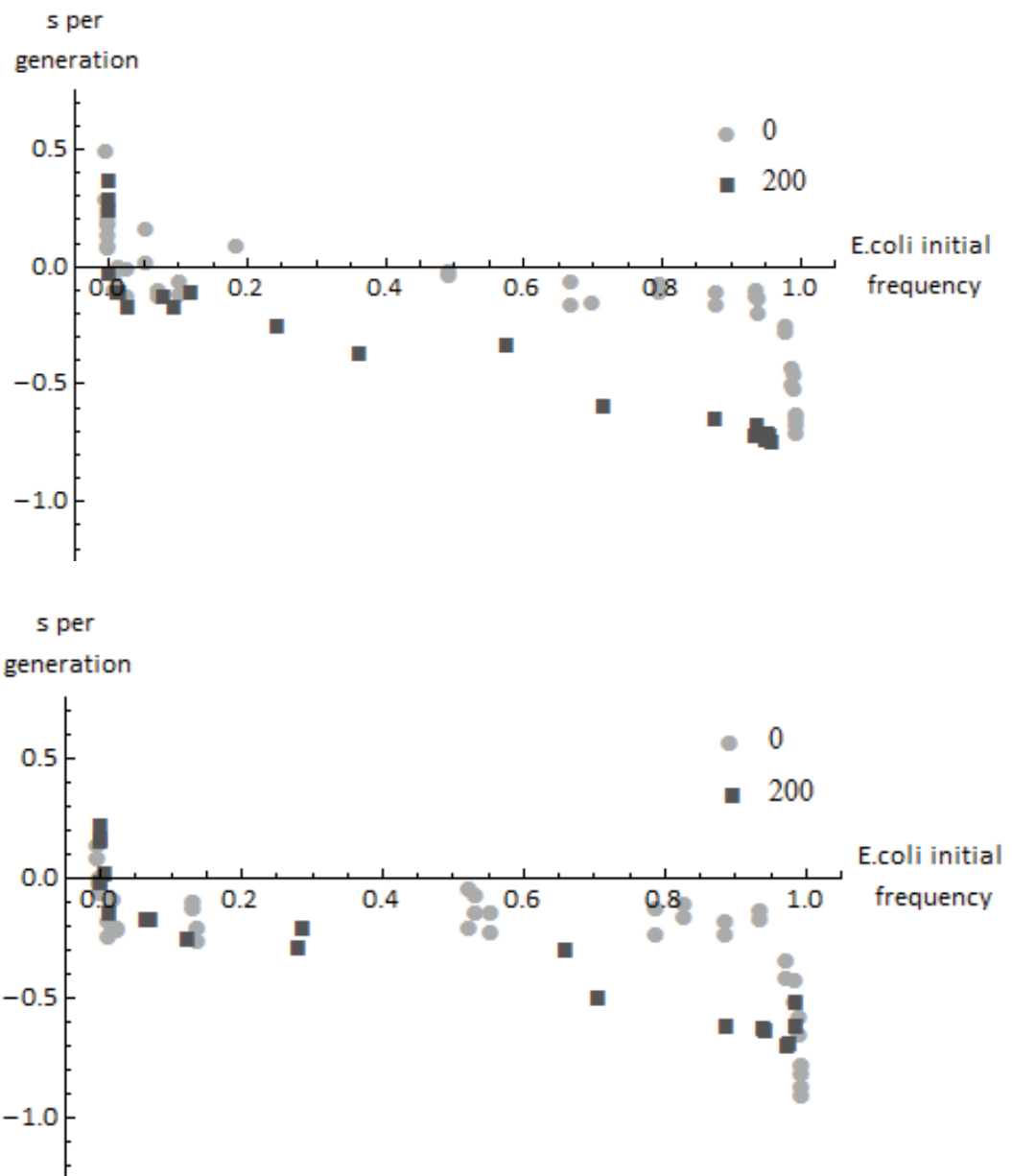


Figure 4: Transient deformation of the NFDS profile at generation 200 (dark grey squares) compared to generation 0 (light grey dots). This deformation is not visible at generation 870 (not represented here for clarity, see Fig. 3).

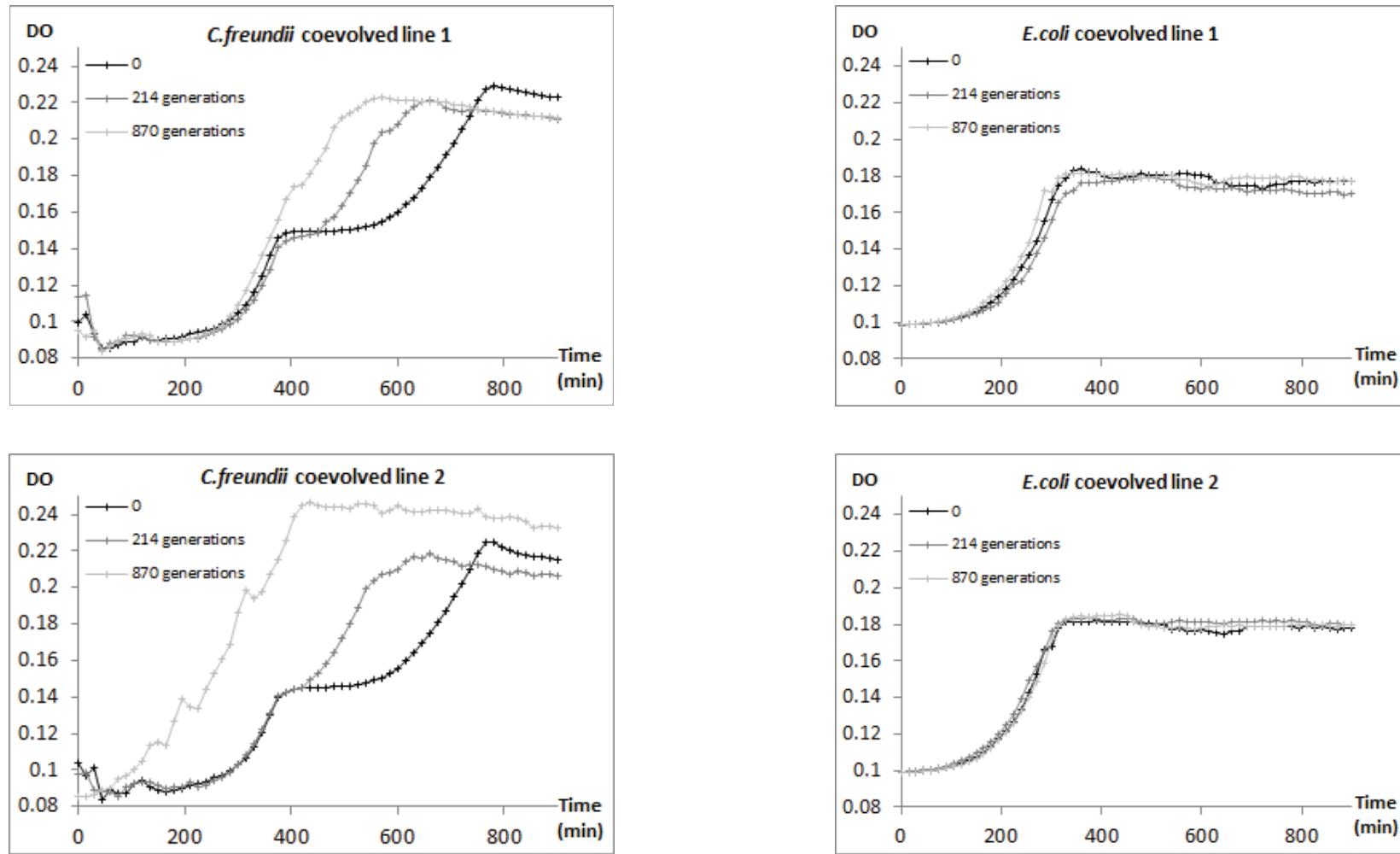


Figure 4: Representative growth curves of isolated lines of *E. coli* and *C. freundii* in DM250-Nal20 throughout the coevolution (grey gradient). Growth curves were repeated four times, resulting in very similar curves, but for the clarity of the figure we selected one representative set. The optical density (DO) was measured at regular intervals of 10 minutes and each dot corresponds to one measure.

- Ecological context of the frequency-dependent selection

Neither *C* nor *E* can grow in the filtrated medium produced after a growth cycle of the other strain. This indicates that they do not excrete byproducts that the other strain can consume. Note that this observation does not rule out the possibility that some metabolic byproducts are excreted and then reabsorbed and consumed later (e.g. acetate produced can be temporarily excreted).

Figure 6 shows a linear relationship between the citrate concentration in the medium and the density of *C* cells (filled triangles). This indicates that the citrate is used as a resource for *C*. This relationship did not change on average during the coevolution (compare Fig. 6a & b), but the different lines seem to diverge around the initial value. This increased variance across lines is clearly visible at 100%, 150% and 200% citrate (Fig. 6). This variance could be caused by differences in the metabolic efficiency when converting glucose, citrate or both. *E* shows a maximal carrying capacity at 100% citrate (i.e. the concentration corresponding to that of the experimental evolution medium). At other citrate concentrations, this carrying capacity is smaller, but the difference is modest in all cases. This small variation does indicate that citrate plays a role in *E* metabolism, but not as a resource. It is used either directly as a secondary metabolite or indirectly on chemical properties of the medium (e.g. pH buffering). The effect of citrate concentration on *E* carrying capacity did not change between the initial and the final time point of the coevolution. Finally, the citrate concentration in the medium does not affect the first growth phase of *C* (open triangles on Fig. 6a). This is consistent with the consumption of glucose as the first resource. Compared to *E*, *C* has a lower efficiency on glucose at initial time of the coevolution. Additional citrate compensates the resulting difference in cell densities from a concentration 0.25 times the one in the evolution medium. The same comparison was not possible at the final time point as the lag at switching time was hardly detectable for most lines.

Overall, these results again suggest that various phenotypic changes occurred for *C* lines but not for *E* during the coevolution. The results also show that the efficiencies of the two strains on the two resources are different: *E* seems to consume glucose more efficiently, but cannot use citrate as a resource, whereas the growth of *C* seems to be less efficient in glucose, but is compensated by a metabolic switch that allows the consumption of citrate.

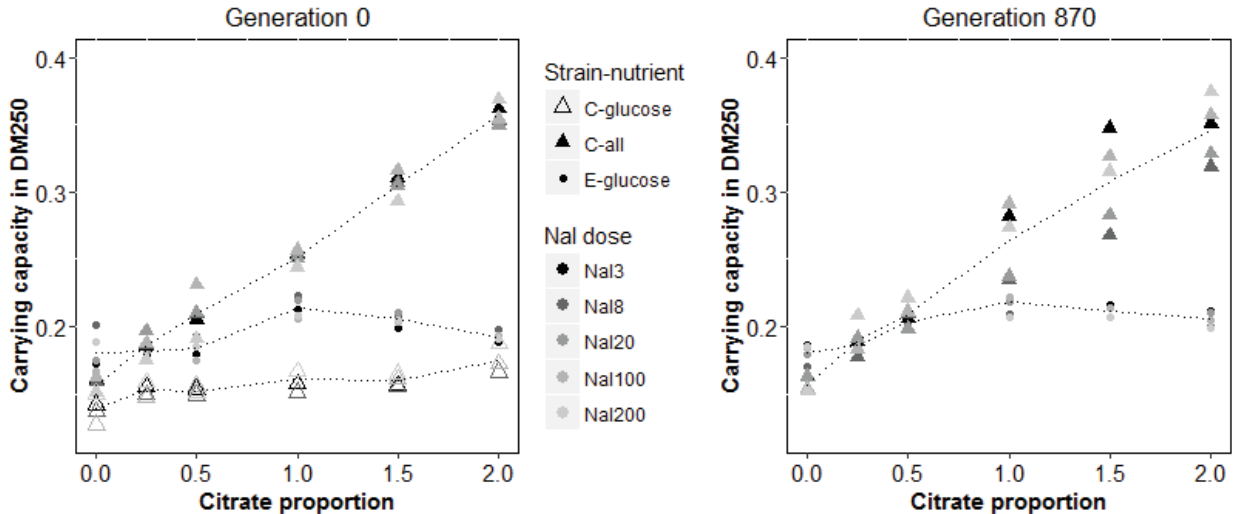


Figure 5: Effect of citrate concentration (normalized such that 1 corresponds to the concentration used for experimental evolution) on isolated lines of *E. coli* (dots) and *C. freundii* (triangles) in DM250-Nal20. The average optical density is used as a measure of the carrying capacity of each strain in the medium. For *E*, there is a single plateau, and the final optical density indicates the carrying capacity during the stationary phase. For *C*, there is a diauxic growth curve: the optical density at the first and second plateau is indicated by open and filled triangles, respectively. At the final time point of the coevolution (right panel), the first plateau was not identifiable due to a very short lag time, so only the second plateau is shown.

Discussion

- NFDS does not entail long term coexistence

The first striking result obtained in this experiment is that patterns of frequency dependent selection can evolve quickly, on a scale of hundreds of generations, and that this variation strongly alters the conditions for coexistence. The frequency of *E. coli* (*E*) observed in the different lines decreased quickly as the pairs coevolved, driving *E* close to extinction after 870 generations. At this final time point, however, *E* still persisted at low frequency, and it was still maintained by negative frequency dependent selection.

The dynamics of the system are governed by two time scales. At the first time scale, which is probably on the order of tens of generations at most, the relative frequencies of *E* and *C* equilibrate at the point where their fitness is equal, as given by the NFDS profiles. At the second time scale, on the order of hundreds of generations, this NFDS profile evolves by the occurrence and spread of mutations in *E* and *C*. This scenario is different from the NFDS dynamics observed

between newly diverging lines in the course of the Lenski's LTEE (Rozen and Lenski 2000; Gac et al. 2012; Plucain et al. 2014). In those studies, *de novo* polymorphism occurred after 6 000 generations of adaptation of *E. coli* to the experimental conditions and the two lineages were maintained for more than 30 000 generations after diverging, with a slow change in NFDS profiles. There is a major difference between this case of coevolution and ours, in the degree of similarity of the coevolving genotypes. With *de novo* polymorphism the coevolving strains are initially identical, save for a handful of mutations at most. In our case, *E* and *C* are genetically largely divergent. One consequence of this divergence is that the two strains can show very different potential for adaptation to the environment. In our experiment *E* was initially relatively well adapted to the environment (due to 10 000 generations of evolution in similar conditions in DM250, and then ~500 generations in DM250-Nal). Because adaptation most often shows a pattern of diminishing return (Lenski and Travisano 1994; Elena and Lenski 2003), *E* was probably already close to its phenotypic optimum, with little prospect of important and rapid improvement to the abiotic conditions. In contrast, *C* had probably not been previously exposed to serial batch culture in minimal medium (although the history of this strain cannot be established). The exposure to these new conditions probably triggered several fast and large adaptive steps. Consistent with this interpretation, no changes were observed for *E* lines, while *C* showed extensive adaptation. Yet, different rates of adaptation to the abiotic conditions between *E* and *C* are clearly not a sufficient explanation for all the results. The NFDS profile was mainly shifted downwards between the initial and final time points. This pattern would be expected if unconditionally beneficial mutations accumulated in *C*. However, NFDS profiles at intermediate time (generation 200) showed that their shape changed transitorily, indicating that the interaction between the two species evolved.

A second striking result of our experiments is that the NFDS profiles show extensive curvature near the fixation points. This indicates that the fitness advantage of each species becomes very large when very rare. This pattern can considerably extend long-term coexistence. Indeed, with such a pattern, a stable point may still persist with large variations in intercept and strong asymmetrical adaptation. This type of NFDS profile may be more typical of already-divergent species, which may have predating specialized traits that allow them to exploit 'private' niches. In our experiment, this pattern of NFDS prevented the extinction of *E* in most replicates, despite considerable asymmetrical adaptation of *C*. It also leads to stable persistence at very low frequency of *E* in many cases. The persistence of rare species in communities is often difficult to understand, as they should be very vulnerable to stochastic perturbations. The occurrence of a sharply increasing selective advantage at very low frequencies, as demonstrated in our case, could explain these observations. This increased persistence timespan may provide sufficient

time for further niche specialization, and eventually stabilization of interactions among coevolving competitors. Continuing our experiments would be interesting in order to determine whether such outcome can take place before the loss of polymorphism caused by asymmetrical adaptation.

Overall, we found conflicting effects of NFDS patterns on long-term coexistence. First, rates of adaptation can be very asymmetrical between species engaged in NFDS interactions. This is a strong destabilizing effect, which is certainly representative of many natural situations. For example, asymmetric evolution is largely expected to occur among species with strongly divergent genomes, but also among populations that were temporarily isolated or brought into contact secondarily or during an invasion event. Even without such asymmetry, NFDS profiles can evolve, and their observation at any given point does not guarantee long-term coexistence, even if the different competing types are at their selective equilibrium. Second, NFDS profiles across divergent species can present non-linear patterns that protect strongly against extinction of the competing types. Hence, the evolutionary dynamics of NFDS appear to be qualitatively different among divergent species than among emerging polymorphisms.

- Mechanisms underlying the NFDS and the maintenance of *E. coli* at very low frequencies

Different biological mechanisms can lead to NFDS, and they can be difficult to tease apart (see Introduction). In our case study, many possibilities can be ruled out (e.g. effect of parasites or predators) and some possibilities are worth discussing. First, NFDS can emerge from environmental heterogeneity (mainly represented here by different resources) provided that relevant fitness trade-offs exist among the different niches, as suggested in Levene's model (Levene 1953; Ravigné et al. 2004). It is a good candidate mechanism in this study since both glucose and citrate can be used in the medium, and are carbon sources on which respectively *E* and *C* are known to be specialized. In particular, *E* does not usually consume citrate under aerobic conditions, due to the repression of the gene coding for the citrate transporter (Dimroth 2013), but *C* does. Second, additional niches can be created by the strains themselves, when one strain provides an asymmetrical benefit to the other strain. This situation includes cases of cross-feeding interactions (Rosenzweig et al. 1994; Treves et al. 1998; Doebeli 2002; Plucain et al. 2014) and 'detoxification' of the environment (Dugatkin et al. 2005; Kelsic et al. 2015). In all cases, it is essential that this benefit (excretion of nutrients, elimination of toxic molecules) also has a beneficial effect for the strain that provides it (e.g. excretion prevents the accumulation in the cell of a molecule that could inhibit its metabolism, even if it can be used as a nutrient later on). Third, the coexistence can rely on different strategies of exploitation of the same resource

via a trade-off between the uptake efficiency and the energetic conversion of this resource. In Appendix 1, we describe how these mechanisms can be formalized. Finally, a combination of these mechanisms can occur. For example we can easily imagine that a strain which consumes the resource rapidly but with low efficiency (third mechanism) is prone to excrete byproducts, which provides an opportunity for cross-feeding interactions (second mechanism).

The NFDS profiles alone do not allow us to definitively infer mechanisms, however the form of the interaction and its pattern of deformation in time can point toward more likely hypotheses. We investigated this by modeling different competition scenarios of two strains in experimental conditions similar to ours. We present this model more fully in Appendix 1. Briefly, the growth curve of each type is modeled by a lag phase followed by an exponential phase, until the available resource is depleted. Time to resource depletion is computed by summing the resource consumed by the competitors (using conversion parameters) until it reaches a threshold (corresponding to the available resource). Diauxic growth is simply modeled by adding a lag and a growth phase on the second resource. A parameter is introduced to allow switching to resource 2 before resource 1 is depleted. The parameters of this model were set to best fit our system (described in Appendix 1), and calibrated to correspond to the specific growth rates and lag times of the two strains exploiting each resource, the quantity of the resource, the initial cell number and the efficiency of utilization of each resource. Figure 7 illustrates the NFDS profiles expected under the three different mechanisms.

First (Fig. 7a), we investigated the case where two types can coexist when exploiting the same resource. This can occur when one type is specialized on growth rate while the other one is specialized on conversion efficiency. The ‘efficient converter’ can be favored when rare, possibly leading to NFDS with an internal equilibrium, provided the conversion advantage is large. This is illustrated in Fig. 7a with increased conversion efficiency compared to a baseline. This mechanism is not very likely in our case, as it requires very large differences in conversion efficiency, which are not apparent on the individual growth curves. It also does not reproduce the observed NFDS patterns well, and does not account for diauxic growth in *C*.

Second (Fig. 7b), we investigated cases involving competition on two resources. We consider a baseline situation where the lag and growth parameters of *C* and *E* were set as identical in glucose and where citrate was only consumed by *C*. *C* has a general advantage, and a particularly large advantage when it is rare, provided by the ‘private’ niche on citrate, as observed in our results. Lighter gray curves on Fig. 7b illustrate how NFDS can emerge when *E* is favored either by a lower lag time or by an increased growth rate on glucose (changing these two parameters has the same qualitative effect). This situation is similar to a Levene model with *E* as a better

competitor on glucose, and C as a better competitor on citrate. However, in this simple model, contrary to our observations, there is no strong non-linearity of the NFDS profile when E is rare.

Third (Fig. 7c), we investigated the same case as above, except that $C. freundii$ switches to citrate before glucose is depleted. This might occur if there is a selection pressure on C to switch to citrate earlier and if the metabolic activity on glucose is, as is likely, reduced after the onset of this switch. The selection pressure for an early switch may be caused by competition for citrate within C alone, independently of the presence of E . With such an early switch, the glucose niche is divided into two sub-niches: one where C and E are competing and one that supports E exclusively. This last sub-niche corresponds roughly to the amount of glucose left at the time of C 's citrate-switch. This switch could be triggered in response to a reduced concentration of glucose (Wang et al. 2015). Fig. 7c illustrates the shapes of the NFDS profiles that emerge in this scenario, when E is favored either by a lower lag time or by an increased growth rate on glucose (again, changing these two parameters has the same qualitative effect). These patterns are generally consistent with the NFDS profiles we observe (Fig. 3). This scenario is also consistent with the observation that the lag phase between the glucose-phase and the citrate-phase was strongly reduced in C during coevolution (Fig. 4). More generally, such a mechanism is of great interest because it can lead to long term coexistence at very low frequencies. Adaptation of the competitor (*i.e.* a shifting intercept), as in our experiment, reduces the equilibrium frequency, but cannot drive the rare type to extinction due to small 'private' niches generated by trade-offs. This might be a common mechanism of long-term coexistence. This scenario also points to the importance of investigating NFDS profiles at extreme frequencies.

Overall, this modeling approach provides a clarification of the different possible mechanisms for generating NFDS in our system (and other similar system involving experimental evolution of microbes in constant environments). It shows that not all kinds of NFDS profiles can be obtained under all scenarios. It provides a key to interpreting those profiles, and points to the most promising candidate mechanisms in our particular situation. Yet, in our case, the modeling approach could not help identify the mechanism generating the non-monotony of the NFDS profiles observed in Fig. 3 at intermediate frequencies (the frequency-dependence seems to be weakly, but consistently positive between frequency 0.2 and 0.8 in the profiles investigated). More investigations may be required to interpret this specific feature, particularly on the cumulative effects of several mechanisms.

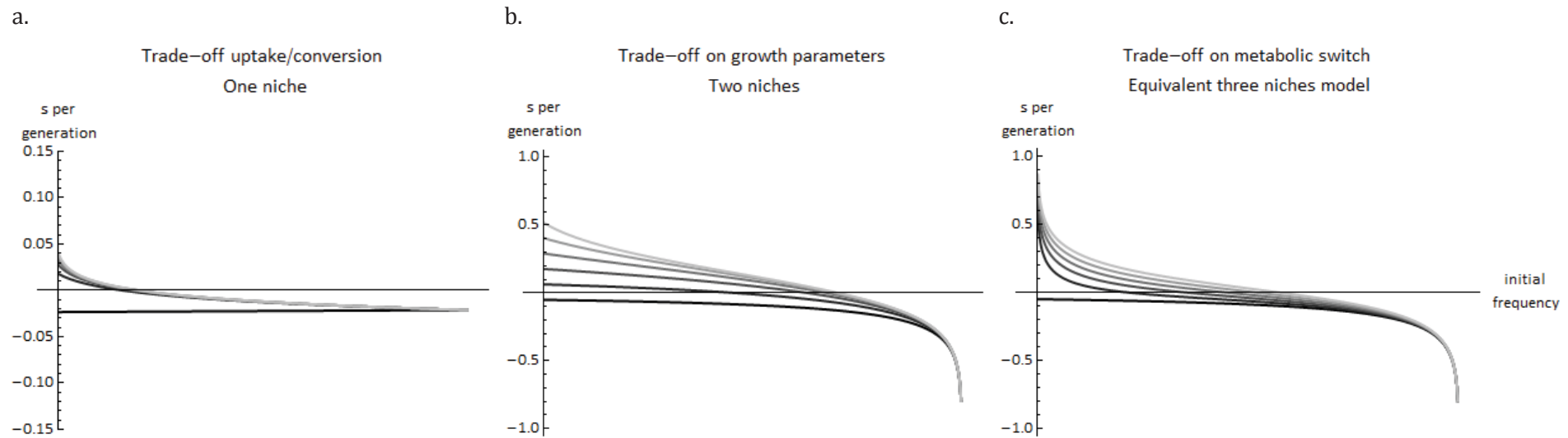


Figure 7: Frequency-dependent interactions obtained by modeling competition with different trade-off scenarios between two resources. In (a) and (b) the black line represents competitions where two strains have equivalent properties in one resource and only one strain can consume the other resource (this strain has an initial frequency of $1-x$). The gray gradient represents a variation in one trait: (a) the efficiency of resource consumption, (b) the quantity of resource left at switching time. In (c) only one resource is considered and one strain initially has a growth advantage over the other (black line). The grey gradient represents a gradual increase of the efficiency of the less competitive strain's energetic conversion.

- NFDS evolution across environments

The evolution of NFDS patterns in our experiment was strongly influenced by abiotic environmental conditions (here the concentration of Nal). The patterns of variation are remarkably repeatable and regular with respect to the gradient of Nal concentration. The importance of environmental conditions in the emergence or maintenance of biotic interactions has already been pointed out in other experiments (e.g. in Hansen and Hubbell 1980; Healey et al. 2016). These observations suggest that the environmental context can have a large influence on the long-term patterns of NFDS. This would be easily interpretable if such environmental variation was related to the mechanism of coexistence, for instance the proportion of the different available resources (glucose or citrate). But this is not the case: the environmental variable playing such a strong role is the concentration of the antibiotic, which seems entirely unrelated to the mechanism of coexistence and orthogonal to the issue of resource utilization. There are two kinds of possible explanations for this pattern. First, the variation in this environmental variable could interfere, for a fortuitous reason, with the mechanism of coexistence. Second, it could represent an asymmetrical handicap for one of the two species. We can propose an example of a possible mechanism for each of these general ideas.

For the ‘fortuitous case’, it may be possible that the mechanism of Nal resistance interferes with resource usage. For example, some (loss-of-function) mutations on the citrate synthase, the enzyme allowing for the degradation of citrate in the Krebs cycle, have been shown to enhance the production of generalist efflux pumps. Presumably, the expression of these pumps is triggered by an excess of intermediate metabolites (here: citrate) in the cytosol. Fortuitously, these pumps can export the Nal molecules from the cell, which can confer some resistance to cells (Helling and Kukora 1971; Lakshmi and Helling 1976; Helling et al. 2002). Hence, the evolution of Nal resistance in *E* could occur by loss-of-function of the citrate synthase. This would not prevent glucose processing through glycolysis, but would lead to a lower metabolic efficiency and to citrate excretion, both unfavorable effects when competing with *C*. This path to resistance would not occur in *C* as the citrate metabolism is vital for this species.

For the ‘handicap’ scenario, it may be possible that Nal represents an asymmetrical challenge for *C* and *E*. For instance, contrary to *E*, *C* may be mostly unaffected by the presence of Nal (e.g. because of reduced uptake or a Nal-proof gyrase target). Some tests (not shown) tended to indicate that *C* growth rate is not affected at all by the range of antibiotic concentrations used in our experiment (i.e. up to 200 µg/mL). Indeed, some *C. freundii* clinical isolates consistently proved to be resistant to very high Nal doses, reaching minimal inhibitory concentrations (MIC) > 1 600 µg/mL (Aoyama et al. 1988). In contrast, the growth rate of *E* is reduced with increasing

Nal concentration in this range. Assuming that the antibiotic concentration linearly increases the lag time of *E* or decreases its growth rate (without affecting *C*), the NFDS profiles should present a regular shift in favor of *C* with increasing Nal concentrations (scenario modeled in Supp. Fig. 2). Irrespectively of the exact underlying mechanism, our results show that environmental conditions that are a priori unrelated to the mechanism of coexistence can seriously impact the evolutionary outcome and maintenance of NFDS interactions.

Conclusion

Overall, our results indicate that it is important to take the potential evolution of NFDS profiles into consideration before drawing conclusions on the long-term maintenance of a polymorphism. These variations can occur on a relatively short time scale (hundreds of generations). They can be largely influenced by asymmetrical adaptive potential, genetic backgrounds, or susceptibility to environmental conditions. Conversely, we also show that NFDS profiles can be largely non-linear near fixation, which tends to buffer these effects and maintain coexistence, even if one species is only maintained at low frequency. This experimental system offers the possibility to study the impact of biotic interactions on patterns of adaptation to abiotic conditions, and vice-versa. For example, it would be interesting to know to what extent the presence of *C. freundii* changed the adaptation of *E. coli* to the antibiotic environment. Such considerations are rarely considered when investigating the evolution of antibiotic resistance, despite the large opportunities for such interactions among pathogen microorganisms.

Acknowledgments

We thank M.-P. Dubois and R. Zahab for lab management and the Montpellier Ressources Imagerie (MRI) platform. We also wish to thank E. Lievens for very helpful suggestions on the manuscript and R. Gallet, G. Martin, S. Bedhomme, P. Labbé, and N. Bierne for discussions. The original strain RELB 4536 was kindly provided by Richard Lenski's lab. This work was supported by a PhD grant from French ministry of research to NH, and the ANR SilentAdapt to T.L.

References

- Aoyama, H., K. Fujimaki, K. Sato, T. Fujii, M. Inoue, K. Hirai, and S. Mitsuhashi. 1988. Clinical isolate of *Citrobacter freundii* highly resistant to new quinolones. *Antimicrob. Agents Chemother.* 32:922–924.
- Ayala, F. J., and C. A. Campbell. 1974. Frequency-dependent selection. *Annu. Rev. Ecol. Syst.* 115–138.
- Barnard, C. J., and R. M. Sibly. 1981. Producers and scroungers: A general model and its application to captive flocks of house sparrows. *Anim. Behav.* 29:543–550.
- Bell, G. 2008. Selection the mechanism of evolution. Oxford University Press.
- Blount, Z. D., J. E. Barrick, C. J. Davidson, and R. E. Lenski. 2012. Genomic analysis of a key innovation in an experimental *Escherichia coli* population. *Nature* 489:513–8. Nature Publishing Group.
- Bonsall, M. B. 2006. Longevity and ageing: appraising the evolutionary consequences of growing old. *Philos. Trans. R. Soc. Lond. B. Biol. Sci.* 361:119–135.
- Borghans, J. A. M., J. B. Beltman, and R. J. De Boer. 2004. MHC polymorphism under host-pathogen coevolution. *Immunogenetics* 55:732–739.
- Bürger, R. 2010. Evolution and polymorphism in the multilocus Levene model with no or weak epistasis. *Theor. Popul. Biol.* 78:123–138. Elsevier Inc.
- Clarke, B. 1962. Balanced polymorphism and the diversity of sympatric species. Pp. 47–70 in N. D, ed. Systematics Association, Oxford.
- Cordero, O. X., and M. F. Polz. 2014. Explaining microbial genomic diversity in light of evolutionary ecology. *Nat Rev Microbiol* 12:263–273. Nature Publishing Group.
- Débarre, F., and T. Lenormand. 2011. Distance-limited dispersal promotes coexistence at habitat boundaries: reconsidering the competitive exclusion principle. *Ecol. Lett.* 14:260–6.
- Devier, B., G. Aguileta, M. E. Hood, and T. Giraud. 2009. Ancient trans-specific polymorphism at pheromone receptor genes in basidiomycetes. *Genetics* 181:209–223.
- Dimroth, P. 2013. Molecular basis for bacterial growth on citrate or malonate. *EcoSalPlus* 1–36.

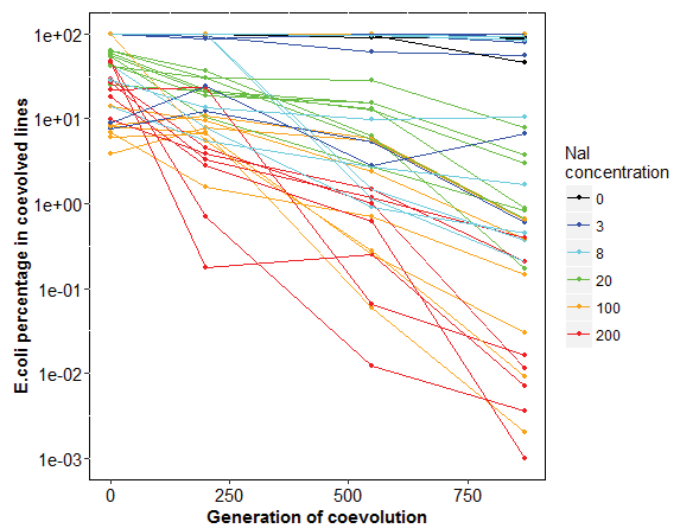
- Doebeli, M. 2002. A model for the evolutionary dynamics of cross-feeding polymorphisms in microorganisms. *Popul. Ecol.* 44:59–70.
- Dugatkin, L. A., M. Perlin, J. S. Lucas, and R. Atlas. 2005. Group-beneficial traits, frequency-dependent selection and genotypic diversity: an antibiotic resistance paradigm. *Proc. Biol. Sci.* 272:79–83.
- Elena, S. F., and R. E. Lenski. 2003. Evolution experiments with microorganisms: the dynamics and genetic bases of adaptation. *Nat. Rev. Genet.* 4:457–69.
- Felsenstein, J. 2017. Theoretical evolutionary genetics.
- Fincke, O. M. 2004. Polymorphic signals of harassed female odonates and the males that learn them support a novel frequency-dependent model. *Anim. Behav.* 67:833–845.
- Friesen, M. L., G. Sacher, M. Travisano, and M. Doebeли. 2004. Experimental Evidence for Sympatric Ecological Diversification Due To Frequency-Dependent Competition in *Escherichia Coli*. *Evolution (N. Y.)*. 58:245.
- Gac, M. Le, J. Plucain, T. Hindré, R. E. Lenski, and D. Schneider. 2012. Ecological and evolutionary dynamics of coexisting lineages during a long-term experiment with *Escherichia coli*. *Proc. Natl. Acad. Sci.* 109:9487–9492.
- Gallet, R., T. F. Cooper, S. F. Elena, and T. Lenormand. 2012. Measuring selection coefficients below 10^{-3} : method, questions, and prospects. *Genetics* 190:175–86.
- Gigord, L. D., M. R. Macnair, and a Smithson. 2001. Negative frequency-dependent selection maintains a dramatic flower color polymorphism in the rewardless orchid *Dactylorhiza sambucina* (L.) Soo. *Proc. Natl. Acad. Sci. U. S. A.* 98:6253–6255.
- Gross, M. R. 1996. Alternative reproductive strategies and tactics: diversity within sexes. *Trends Ecol. Evol.* 11:92–98.
- Haldane, J. B. S. 1954. Biochemistry of genetics. London: George Alien & Unwin, Ltd.
- Haldane, J. B. S., and S. D. Jayakar. 1963. Polymorphism due to selection of varying direction. *J. Genet.* 58:237–242.
- Hansen, S. R., and S. P. Hubbell. 1980. Single-nutrient microbial competition: qualitative agreement between experimental and theoretically forecast outcomes. *Science (80-.).* 207:1491–1493.

- Healey, D., K. Axelrod, and J. Gore. 2016. Negative frequency-dependent interactions can underlie phenotypic heterogeneity in a clonal microbial population. *Mol. Syst. Biol.* 12:877.
- Hedrick, P. W. 1978. Genetic variation in a heterogeneous environment. V. Spatial heterogeneity in finite populations. *Genetics* 89:389–401.
- Heino, M., J. A. J. Metz, and V. Kaitala. 1997. Evolution of mixed maturation strategies in semelparous life histories: the crucial role of dimensionality of feedback environment. *Philos. Trans. R. Soc. B Biol. Sci.* 352:1647–1655.
- Helling, R. B., and J. S. Kukora. 1971. Nalidixic Acid-Resistant Mutants of *Escherichia coli* Deficient in Isocitrate Dehydrogenase. *J. Bacteriol.* 105:1224–1226.
- Helling, R., B. Janes, and H. Kimball. 2002. Toxic waste disposal in *Escherichia coli*. *J. ...* 184:3699–3703.
- Joron, M., and J. L. B. Mallet. 1998. Diversity in mimicry: Paradox or paradigm? *Trends Ecol. Evol.* 13:461–466.
- Karasov, T. L., J. M. Kniskerb, L. Gao, B. DeYoung, J. Ding, U. Dubiella, R. O. Lastra, S. Nallu, F. Roux, R. W. Innes, L. G. Barrett, R. R. Hudson, and J. Bergelson. 2014. The long-term maintenance of a resistance polymorphism through diffuse interactions. *Nature* 512:436–440.
- Kelsic, E. D., J. Zhao, K. Vetsigian, and R. Kishony. 2015. Counteraction of antibiotic production and degradation stabilizes microbial communities. *Nature* 521:516–519.
- Lakshmi, T. M., and R. B. Helling. 1976. Selection for citrate synthase deficiency in icd mutants of *Escherichia coli*. *J. Bacteriol.* 127:76–83.
- Lenski, R. E., and M. Travisano. 1994. Dynamics of adaptation and diversification: a 10,000-generation experiment with bacterial populations. *Proc Natl Acad Sci U S A* 91:6808–6814.
- Levene, H. 1953. Genetic Equilibrium When More Than One Ecological Niche is Available Howard. *Am. Nat.* 87:331–333.
- Levin, B. R. 1988. Frequency-dependent selection in bacterial populations. *Philos. Trans. R. Soc. Lond. B. Biol. Sci.* 319:459–472.
- Lewontin, R. C. 1958. A General Method for Investigating the Equilibrium of Gene Frequency in a Population. *Genetics* 43:419–34.

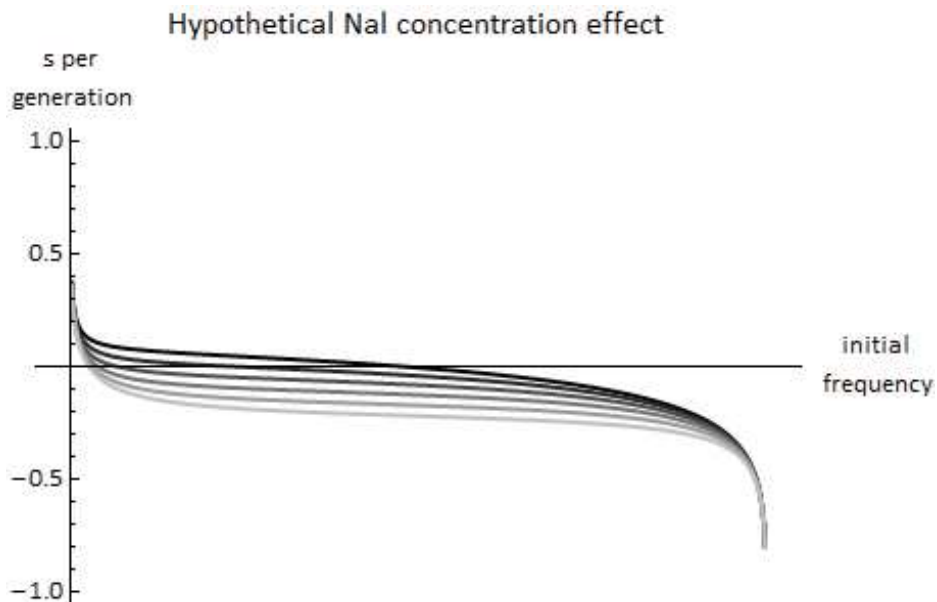
- Maddamsetti, R., R. E. Lenski, and J. E. Barrick. 2015. Adaptation, clonal interference, and frequency-dependent interactions in a long-term evolution experiment with *Escherichia coli*. *Genetics* 200:619–631.
- Manhart, M., B. V Adkar, and E. I. Shakhnovich. 2016. Tradeoffs between microbial growth phases lead to frequency-dependent and non-transitive selection. *BioRxiv*, doi: <http://dx.doi.org/10.1101/096453>.
- Mazancourt, C. de, and U. Dieckmann. 2004. Trade-Off Geometries and Frequency-Dependent Selection. *Am. Nat.* 164:765–778.
- O'Connell, L. M., and M. O. Johnston. 1998. Male and Female Pollination Success in a Deceptive Orchid, a Selection Study. *Ecology* 79:1246–1260.
- Oaten, A., and W. W. Murdoch. 1975. Functional response and stability in predator-prey systems. *Am. Nat.* 109:289–298.
- Olendorf, R., F. H. Rodd, D. Punzalan, A. E. Houde, C. Hurt, D. N. Reznick, and K. a Hughes. 2006. Frequency-dependent survival in natural guppy populations. *Nature* 441:633–636.
- Penn, D. J., and P. W. K. 1999. The Evolution of Mating Preferences and Major Histocompatibility Complex Genes. *Evolution (N. Y.)* 153:145–164.
- Plucain, J., T. Hindré, M. Le Gac, O. Tenaillon, S. Cruveiller, C. Médigue, N. Leiby, W. R. Harcombe, C. J. Marx, R. E. Lenski, and D. Schneider. 2014. Epistasis and allele specificity in the emergence of a stable polymorphism in *Escherichia coli*. *Science (80-.).* 343:1366–1369.
- Rainey, P. B., and M. Travisano. 1998. Adaptive radiation in a heterogeneous environment. *Nature* 394:69–72.
- Ravigné, V., I. Olivier, and U. Dieckmann. 2004. Implications of habitat choice for protected polymorphisms. *Evol. Ecol. Res.* 6:125–145.
- Reusch, T. B. H., M. A. Häberli, P. B. Aeschlimann, and M. Milinski. 2001. Female sticklebacks count alleles in a strategy of sexual selection explaining MHC polymorphism. *Nature* 414:300–302.
- Rosenzweig, R. F., R. R. Sharp, D. S. Treves, and J. Adams. 1994. Microbial evolution in a simple unstructured environment: Genetic differentiation in *Escherichia coli*. *Genetics* 137:903–917.

- Rozen, D. E., and R. E. Lenski. 2000. Long-Term Experimental Evolution in *Escherichia coli*. VIII. Dynamics of a Balanced Polymorphism. Am. Nat. 155:24–35.
- Rozen, D. E., L. McGee, B. R. Levin, and K. P. Klugman. 2007. Fitness costs of fluoroquinolone resistance in *Streptococcus pneumoniae*. Antimicrob. Agents Chemother. 51:412–416.
- Sinervo, B., and C. M. Lively. 1996. The rock-paper-scissors game and the evolution of alternative male strategies. Nature 380:240–243.
- Svensson, E. I., J. Abbott, and R. Härdling. 2005. Female polymorphism, frequency dependence, and rapid evolutionary dynamics in natural populations. Am. Nat. 165:567–576.
- Takahashi, Y., and M. Kawata. 2013. A comprehensive test for negative frequency-dependent selection. Popul. Ecol. 55:499–509.
- Takahata, N., and M. Nei. 1990. Allelic genealogy under overdominant and frequency-dependent selection and polymorphism of major histocompatibility complex loci. Genetics 124:967–978.
- Těšický, M., and M. Vinkler. 2015. Trans-Species Polymorphism in Immune Genes: General Pattern or MHC-Restricted Phenomenon? J. Immunol. Res. 2015:838035.
- Thijs, H., J. R. Shann, and J. D. Weidenhamer. 1994. The effect of phytotoxins on competitive outcome in a model system. Ecology 75:1959–1964.
- Treves, D. S., S. Manning, and J. Adams. 1998. Repeated evolution of an acetate-crossfeeding polymorphism in long-term populations of *Escherichia coli*. Mol. Biol. Evol. 15:789–97.
- Turner, P. E., V. Souza, and R. E. Lenski. 1996. Tests of ecological mechanisms promoting the stable coexistence of two bacterial genotypes. Ecology 77:2119–2129.
- Wang, J., E. Atolia, B. Hua, Y. Savir, R. Escalante-Chong, and M. Springer. 2015. Natural variation in preparation for nutrient depletion reveals a cost-benefit tradeoff. PLoS Biol. 13:1–31.
- Weeks, A. R., and A. a Hoffmann. 2008. Frequency-dependent selection maintains clonal diversity in an asexual organism. Proc. Natl. Acad. Sci. U. S. A. 105:17872–17877.

Supplementary Figures:



Supplementary Figure 1: Evolution of the proportion of *E. coli* against *C. freundii* throughout the coevolution at different concentrations of antibiotic (colors). Lines connect the dots of values for each coevolving line. These values were estimated from samples of 100 000 cells in which the proportion of YFP fluorescent cells was estimated.



Supplementary Figure 2: Hypothetical model scenario for the Nal dose effect on the interactions between the two strains in our experiment. Lighter lines represent an increasing lag time (decreasing growth rate gives similar results) of *E. coli* to consume glucose compared to *C. freundii*.

Appendix: Resource-based models for the occurrence of NFDS

x	E initial frequency
N_0	Initial cell number
λ	Lag time
r	Growth rate
T_{sat2}	Times of resource 2 depletion
$T_{switch} + \Delta T$	Times of resource 1 depletion
T_{switch}	Time of metabolic switch
R_1, R_2	Quantities of resource 1, 2
$R_{1switch}$	Quantity of resource triggering metabolic switch from resource 1 to resource 2
Y	Energetic efficiency of resource use

Notations and meaning of parameters

The following model is inspired by Manhart et al. 2016. We considered a case where two bacterial strains (E and C) are in competition in a medium containing two resources. The strain E consumes only one resource (denoted R_1) and the strain C consumes first the resource R_1 and then switches toward the other resource (denoted R_2). The competition lasts until both resources have been depleted. The consumption of a resource results in three phases for the population dynamics: a lag phase, an exponential phase and a stationary phase when the resource is exhausted. The expressions for the growth functions of E and C across those phases are thus:

$$N_E(t) = \begin{cases} x N_0, & 0 \leq t \leq \lambda_E \\ x N_0 e^{r_E (t - \lambda_E)}, & \lambda_E < t < T_{switch} + \Delta T \\ x N_0 e^{r_E (T_{sat1} + \Delta T - \lambda_E)}, & t \geq T_{switch} + \Delta T \end{cases} \quad (1)$$

For E and

$$N_C(t) = \begin{cases} (1-x) N_0, & 0 \leq t \leq \lambda_{C1} \\ (1-x) N_0 e^{r_{C1} (t - \lambda_{C1})}, & \lambda_{C1} < t < T_{switch} \\ (1-x) N_0 e^{r_{C1} (T_{switch} - \lambda_{C1})}, & T_{switch} \leq t \leq T_{switch} + \lambda_{C2} \\ (1-x) N_0 e^{r_{C1} (T_{switch} - \lambda_{C1}) + r_{C2} (t - \lambda_{C2})}, & T_{switch} + \lambda_{C2} < t < T_{switch} + T_{sat2} \\ (1-x) N_0 e^{r_{C1} (T_{switch} - \lambda_{C1}) + r_{C2} (T_{sat2} - \lambda_{C2})}, & t \geq T_{switch} + T_{sat2} \end{cases} \quad (2)$$

For C . The amount of resource consumed at time of switch can be expressed from the cell numbers at this time and the efficiency parameters as:

$$\begin{aligned}
 R_{1switch} &= \frac{N_E(T_{switch})}{Y_E} + \frac{N_C(T_{switch})}{Y_{C1}} \\
 R_1 - R_{1switch} &= \frac{N_E(T_{switch} + \Delta T) - N_E(T_{switch})}{Y_E} \\
 R_2 &= \frac{N_C(T_{switch} + T_{sat,C2})}{Y_{C2}}
 \end{aligned} \tag{3}$$

The selection coefficient of the competition is defined as:

$$\begin{aligned}
 s &= \log\left(\frac{N_E(T_{switch} + \Delta T)}{N_C(T_{switch} + T_{sat2})}\right) - \log\left(\frac{N_E(0)}{N_C(0)}\right) \\
 &= r_E(T_{switch} + \Delta T - \lambda_E) + r_{C1}(T_{switch} - \lambda_{C1}) + r_{C2}(T_{sat2} - \lambda_{C2})
 \end{aligned} \tag{4}$$

This equation is used to introduce s in the expressions for $R_{1switch}$ and $R_1 - R_{1switch}$ in (3). This is done by replacing the term $r_E(T_{switch} - \lambda_E)$ by $s + r_{C1}(T_{switch} - \lambda_{C1}) + r_{C2}(T_{sat2} - \lambda_{C2}) - r_E \Delta T$. The system (3) is then solved for T_{switch} , ΔT and T_{sat2} and the resulting expressions are replaced in the expression of s in (4). This equation is finally solved numerically in Mathematica 9, to obtain s values corresponding to different parameter values. The table below indicates the baseline numerical values used for all parameters $(x, R_1, R_{1switch}, R_2, Y_E, Y_{C1}, Y_{C2}, N_0, r_E, r_{C1}, r_{C2}, \lambda_E, \lambda_{C1}, \lambda_{C2})$.

Parameter	Numerical Value	Comment
x	From 0 to 1	Frequency of E
R_1	1390	Proportions corresponding to the molar proportions in the medium DM250
$R_{1switch}$	1390	
R_2	1700	
$Y_E = Y_{C1}$	3000	Energetic production (equivalent ATP) for 1 molecule of glucose $\sim 3 \times$ energetic production for 1 molecule citrate
Y_{C2}	1000	
N_0	1000	Order of magnitude of initial population inoculum in our batch cultures
$r_E = r_{C1}$	0.38	Baseline value corresponding to the observed
r_{C2}	0.40	Value that does not affect the result in this context because only C consumes the resource 2
$\lambda_E = \lambda_{C1}$	0	Baseline value corresponding to an absence of a clear lag observed on growth on glucose, for both E and C
λ_{C2}	3	Value that does not affect the result in this context because only C consumes the resource 2

Table 1. Parameter baseline values

Discussion et perspectives

Au cours de cette thèse, nous avons cherché à décrire et modéliser les déterminants des trajectoires adaptatives de lignées bactériennes dans différents environnements. Les chapitres de la thèse reflètent plusieurs étapes du processus évolutif, mais également plusieurs niveaux de réflexion sur la façon d'intégrer des observations expérimentales dans un modèle capable de décrire l'ensemble d'un processus évolutif. Les modèles de paysages adaptatifs se sont révélés de très bons candidats. De manière fortuite, cette thèse illustre également leurs limites dans la prise en compte complète d'un contexte écologique réel. Le dernier chapitre montre en partie à quel point les expériences de laboratoire et les approches de modélisation utilisées ici restent éloignées du contexte évolutif des environnements naturels. Les travaux de la thèse montrent également que les limites des paysages sont loin d'être figées. Il y a encore un gros potentiel dans les paysages adaptatifs pour intégrer des niveaux de complexité, décrypter les informations « cachées » des données empiriques et reproduire des trajectoires évolutives dans des contextes de plus en plus réalistes.

L'introduction de cette thèse mettait en avant plusieurs objectifs: 1) comprendre comment la variabilité génétique intervient dans l'adaptation, 2) décrire et comparer les effets de la sélection entre différents environnements, 3) comprendre si et comment tous ces éléments s'intègrent dans un paysage adaptatif, 4) intégrer une composante biotique au contexte évolutif. L'approche multi-environnementale utilisée pour y répondre s'est révélée, de mon point de vue, très intéressante. Intuitivement, on se rend bien compte que décrire quelque chose de complexe en le regardant sous plusieurs angles plutôt qu'un seul permet de mieux apprécier sa complexité. De la même manière en démultipliant les observations expérimentales sur plusieurs environnements, des patrons intéressants ont pu être révélés. En complément l'approche par le gradient environnemental a permis de « classer » et d'extrapoler les observations. Le résultat de cette démarche expérimentale, est que nous avons récupéré beaucoup de petites pièces d'un très grand puzzle. Une partie stimulante du travail de thèse a donc été de commencer à reconstituer des bouts de ce puzzle, présentés au travers des chapitres de la thèse. Dans cette discussion, je reprends d'abord rapidement les éléments expérimentaux révélés dans la thèse. Tous ces éléments mis bout-à-bout se sont montrés à la fois complémentaires et cohérents pour raconter « l'histoire » des trajectoires dans un paysage adaptatif multi-environnemental et dans le contexte de la coexistence entre espèces. Je discute ensuite quelques points abordés rapidement dans les chapitres de la thèse ainsi que des perspectives pour prolonger ces études.

La variabilité génétique à travers plusieurs environnements

- Les distributions des effets des mutations criblées dans l'antibiotique (et à plus forte raison les distributions bivariées de ces effets dans différents environnements) ont permis de révéler des modules mutationnels, validés par une approche génétique.
- Les coûts des mutations de résistance à l'intérieur de ces modules suivent une distribution gamma peu variable avec l'environnement. En revanche la contribution relative des modules aux mutations criblées varie régulièrement le long du gradient. Cela conduit à ce qu'un des modules contribue plus aux mutations criblées quand on tend vers des doses plus fortes du gradient.
- Le taux de mutation vers la résistance montre une décroissance très régulière le long du gradient.
- Ces résultats sont cohérents avec une distribution modulaire d'effets phénotypiques des mutations (comme décrite dans Chevin et al. 2010) et d'une fonction de fitness qui se décale dans le paysage (du fait à la fois d'un optimum qui « s'éloigne » avec la dose et d'une intensité de sélection qui croît avec la dose dans l'espace phénotypique) de telle sorte que, en augmentant la dose de cible, on récupère des mutations dont les effets phénotypiques sont de plus en plus extrêmes.

Que révèle l'approche multi-environnementale sur les variations d'effets sélectifs entre environnements

- Les distributions d'effets des mutants criblés permettent de détecter des variations sélectives entre environnements (*c.f.* paragraphe précédent) mais ne permettent pas d'identifier la cause de ces variations : variation de la position de l'optimum ou bien de l'intensité de sélection associées à chaque environnement.
- L'évolution à long terme dans différents environnements couplée à des mesures de fitness dans ces différents environnements permet de révéler à la fois des compromis adaptatifs et des variations d'intensité de sélection mais surtout de les quantifier (sous certaines hypothèses).

- Sachant que les positions d'optimums varient entre environnements (et sous les autres hypothèses du modèle géométrique de Fisher), les corrélations entre les distributions d'effets de mutations permettent d'estimer la distance du phénotype ancêtre aux optimums de différents environnements (mais là encore l'influence des modules mutationnels est importante à prendre en compte).
- Les caractéristiques mutationnelles couplées aux mesures de fitness (à court ou/et long terme) permettent de détecter des directions sélectives préférentielles et de quantifier ces covariances sélectives. Ces covariances sélectives prennent une importance particulière lorsque l'on veut comparer plusieurs environnements puisqu'elles peuvent varier entre environnements.

Comment les interactions avec les autres espèces s'intègrent dans la dynamique évolutive

- Les interactions de fréquence-dépendance évoluent en cohérence avec la fixation de mutations avantageuses dans l'un et l'autre des types en interaction.
- Les paramètres qui définissent l'évolution vers un renforcement ou au contraire une rupture de la coexistence incluent les caractéristiques environnementales et le potentiel d'évolution des types dans cet environnement.
- Les compromis adaptatifs peuvent favoriser le maintien de la diversité notamment en dégageant des très petites niches qui assurent le maintien de types à très faible fréquences.

Retour sur les multiples effets des modules mutationnels

Comme discuté dans l'introduction, l'évolution parallèle (génétique) a été présentée très tôt et à répétition comme une observation allant à l'encontre d'une hypothèse de pléiotropie universelle des mutations (Shull 1935; Lenormand et al. 2016). Nos résultats apportent une confirmation expérimentale robuste à cela dans le sens où l'on montre que l'évolution parallèle observée n'est pas uniquement due à une sélection par le crible (Bailey et al. 2016). L'évolution parallèle émerge dans notre cas (et c'est probablement largement extrapolable à d'autres cas de résistance) de la présence des modules mutationnels. Il est bien attendu qu'elle soit encore plus

accentuée dans des populations soumises à la sélection (les mutations qui ont les effets sélectifs les plus forts sont sur-représentées). On peut noter que seules quelques-unes des mutations *gyrA* décrites dans notre étude sont régulièrement citées dans les résistances cliniques (Jacoby 2005). Toutefois, de nombreux autres effets sont susceptibles d'intervenir dans la sélection de ces isolats cliniques (milieu intra-hôte, hétérogénéités spatiales et temporelles etc.). Si les effets des modules mutationnels ont déjà été considérés dans cette adaptation à court terme, ils sont par contre largement négligés à plus long terme (par exemple on considère rarement leur potentiel à créer des contraintes d'accessibilité de certains sous-espaces phénotypiques dans un paysage).

Dans notre étude, le nombre de modules mutationnels associés à des phénotypes résistants (mutations de forts effets) est faible à forte dose : un seul gène est mobilisé pour toutes les mutations de résistance. Dans ce contexte, les modules imposent un nombre de «voies» réduit pour s'adapter entraînant une certaine prévisibilité du premier pas mutationnel. Les mutations impliquées dans le deuxième pas mutationnel et les suivants peuvent potentiellement être tirées d'un plus grand nombre de modules mutationnels (associés à des effets phénotypiques moins grands) et les modules mobilisés ne sont pas nécessairement les mêmes que ceux impliqués dans le premier pas mutationnel. Dans le cas de la résistance aux antibiotiques en général, les mutations impliquées dans l'évolution compensatoire montrent une diversité génétique plus importante et des effets phénotypiques moins importants que les mutations de résistance (Szamecz et al. 2014; Qi et al. 2016; Dettman et al. 2017). Nos données expérimentales ne nous permettent pas d'apprécier le parallélisme génétique qui intervient dans l'évolution secondaire de nos lignées (mais aucune mutation *gyrA* n'a été sélectionnée après le crible initial) ni à quel point la modularité mutationnelle s'exprime après le premier pas mutationnel. Par contre, l'évolution à long-terme indique clairement que les trajectoires ont conduit (par la même voie mutationnelle ou par des voies différentes) à un phénotype similaire parmi les lignées *gyrA* dans un même environnement. Au contraire, les lignées non-*gyrA* n'ont pas atteint, sur le même pas de temps, le même phénotype final que les *gyrA*. Tout au long de la thèse, ces lignées non-*gyrA* en particulier nous ont beaucoup interrogés sur la question des « blocages » adaptatifs. A elles seules, elles ont remis en cause plusieurs hypothèses du modèle de base des effets de la sélection et sont donc particulièrement intéressantes. Elles ont en plus un intérêt bien concret puisqu'elles représentent probablement une importante proportion des mutations sélectionnées à des doses très faibles (inférieures à la MIC) d'antibiotique : leur taux de mutation est déjà largement plus important que celui des mutations *gyrA* à la plus faible dose d'antibiotique utilisée dans nos expériences (supérieure à la MIC). De manière intéressante, elles restent très « mauvaises » à forte dose même après des centaines de générations d'évolution. A ce point de la

thèse (et de mon point de vue) le mystère plane encore beaucoup sur ces lignées (elles représentent le principal élément non cohérent du paysage adaptatif reconstruit). Typiquement, elles pourraient être interprétées comme une preuve de l'existence de deux pics de fitness, séparés par une vallée adaptative. Dans la thèse nous montrons qu'il existe des scénarios alternatifs à l'existence de plusieurs pics adaptatifs, qui émergent directement de l'existence des modules mutationnels, pour expliquer ces situations de « blocages » adaptatifs. Les rôles des modules mutationnels ainsi que des covariances sélectives ont été pour l'instant largement sous-considerés dans les trajectoires évolutives à long terme. En perspective, il me semble donc important de se demander à quel point ces éléments peuvent générer des blocages adaptatifs. Des contributions à la fois théoriques et expérimentales (combien de modules interviennent dans l'évolution à plus long terme? Est-ce que les lignées non-*gyrA* peuvent être « débloquées »?), complétées par des approches de génomique, permettraient de préciser les effets des modules.

De mon point de vue, cette question de blocages adaptatifs se pose également dans le prolongement de notre expérience d'adaptation des lignées expérimentales (*gyrA* comprises) à leur dose d'antibiotique : à quel point est-t-il possible de s'adapter à une dose différente et de « défaire » ou « re-compenser » les compromis adaptatifs entre doses? Est-ce que cette évolution est plus ou moins facile que lorsqu'il n'y a pas eu d'évolution compensatoire à une dose (par exemple à partir des mutants criblés)? A quel point la «distance» environnementale influence-t-elle ces résultats? Est-ce que les éléments décrits dans le paysage adaptatif rendent bien compte de ces nouvelles trajectoires? Ces questions peuvent être abordées, à la fois avec un intérêt pour leur application en terme de gestion des résistances et dans le prolongement des problématiques de cette thèse, à partir des lignées expérimentales produites.

Enfin, si l'argument d'un blocage adaptatif ne suffit pas à démontrer l'existence de plusieurs pics adaptatifs (à proximité), il paraît important de se demander quels seraient les arguments expérimentaux qui permettraient de conclure sur ce point. De mon point de vue, la question reste assez ouverte : qualitativement on peut penser que les contraintes mutationnelles génèrent un patron d'adaptation ralenti qui, même faible, devrait être détectable (e.g. Wiser et al. 2013), alors que sous l'hypothèse de plusieurs pics, les trajectoires devraient atteindre un plateau de fitness très stable lorsqu'un pic est atteint et éventuellement augmenter brusquement si une perturbation de l'équilibre mutation-sélection permet de traverser une vallée et d'atteindre un autre pic. Cependant si les modules et les covariances créent des blocages, il est possible qu'à un certain point de progression de l'adaptation, un déblocage puisse aussi s'opérer. La conséquence serait une augmentation brusque de la fitness et donc un patron similaire au paysage à plusieurs pics. Ces hypothèses encouragent à prolonger l'évolution

expérimentale des lignées (et mutants) non-*gyrA* et à analyser plus finement la trajectoire de fitness associée à ces lignées.

Caractériser et comparer des environnements

Les résultats de la thèse font ressortir que différents environnements peuvent être décrits et comparés sur la base de deux caractéristiques générales : les distances phénotypiques entre les optimums et l'intensité de la sélection qui peut être vue comme un degré de tolérance des écarts phénotypiques à l'optimum. Plutôt que d'englober ces deux informations dans une notion commune de « stress » environnemental, nous mettons en avant des critères pour les distinguer. L'information du déplacement des optimums se trouve dans l'existence de compromis adaptatifs. L'information d'une variation de l'intensité de sélection se trouve dans la comparaison des différences de fitness associées à ces compromis entre les environnements. En l'absence d'une comparaison inter-environnements la valeur du compromis adaptatif ne permet par contre pas de distinguer les deux composants.

Concrètement ces informations existent dans plusieurs études expérimentales pour lesquelles des compromis entre environnements ont été mesurés dans des populations bien adaptées (*e.g.* Bennett and Lenski 2007; Hughes et al. 2007; Gallet et al. 2014; Schick et al. 2015). La méthode proposée dans la thèse pourrait donc permettre de reconstituer d'ores et déjà plusieurs autres paysages adaptatifs inter-environnements et de les comparer. Notamment, dans notre étude les caractéristiques du gradient de dose d'antibiotique sont étonnamment reliées à des variations log-linéaire avec la dose d'antibiotique. Il est peu probable que cette variation soit généralisable (peut-être à certains autres antibiotiques ou composants toxiques?) mais il serait par exemple intéressant de les comparer avec les variations générées sur d'autres gradients tels que la température, le pH, etc., qui sont des composantes cumulables de l'environnement (par exemple dans le cas des bactéries, le pH est variable entre les organes d'un hôte sous traitement antibiotique). Dans le cas des bactéries, d'autres stress environnementaux que les antibiotiques peuvent sélectionner des phénotypes résistants (Baharoglu et al. 2013; Rodríguez-Verdugo et al. 2013). Il peut être intéressant de voir à quel point les propriétés sélectives de plusieurs composantes environnementales se recouvrent dans un paysage adaptatif et donc quels sont précisément les conditions favorables à l'évolution de ces phénotypes. Ces perspectives font tout de même ressortir plusieurs limites.

Un point largement limitant à court terme est que les méthodes développées pour le moment supposent que les optimums soient tous inclus dans une ou deux dimensions de l'espace phénotypique. Il est quasiment certain que plus de dimensions phénotypiques seront

nécessaires pour décrire des paysages adaptatifs multi-gradients. La méthode pourrait *a priori* facilement être étendue dans un espace de plus grande dimension, cependant on perdrat alors l'intérêt visuel du paysage adaptatif. La formulation mathématique du paysage reste très intéressante pour explorer le paysage mais je pense qu'il sera important de développer en parallèle des méthodes de visualisation de « morceaux » représentatifs des paysages globaux. Cet aspect visuel et donc intuitif des paysages est en partie garant d'un intérêt croissant pour leur utilisation en tant qu'outil pour interpréter et prévoir des trajectoires évolutives expérimentales ou sur le terrain. Des limitations existent cependant à une autre échelle et sont partiellement discutées dans la partie suivante.

Vers une intégration du contexte écologique

Un autre point limitant de l'utilisation de ces modèles est qu'ils décrivent pour l'instant des contextes évolutifs très simplifiés. Il y a bien sûr un intérêt très important à comprendre de façon isolée les propriétés sélectives directement associées à une composante environnementale. Cependant les données de terrain et les expériences d'évolution (cette thèse y compris) montrent de plus en plus que les assemblages écologiques dans lesquels les populations évoluent sont bien plus complexes. De la même manière qu'un paysage adaptatif peut capter des interactions complexes entre des bases génétiques et des traits phénotypiques, il devient nécessaire de savoir relier un ensemble complexe et quasi-infini de composantes environnementales aux propriétés sélectives de cet ensemble.

Des modèles alternatifs aux paysages adaptatifs intègrent une partie de ce contexte (mais au détriment d'une précision sur la description des bases génétiques de l'adaptation) en tenant compte par exemple des effets des flux de gènes entre habitats hétérogènes (*e.g.* Kirkpatrick and Barton 1997; Polechová et al. 2009; Duputié et al. 2012), des interactions écologiques et/ou comportementales au sein des communautés (*e.g.* Austin 2002; DeAngelis and Grimm 2014). On note cependant que les aspects plus basiques des propriétés sélectives entre environnements décrits dans cette thèse (*i.e.* la variation des phénotypes optimaux et de l'intensité de sélection), sont rarement pris entièrement en compte dans ces approches. De mon point de vue, il serait pertinent d'intégrer ces deux composantes aux modèles évolutifs, à la fois ceux d'écologie évolutive qui prennent en compte seulement un déplacement des optimums le long d'un gradient environnemental et ceux d'évolution de la résistance qui négligent les compromis adaptatifs à différentes doses. Cela ne devrait pas pour autant limiter l'intérêt de ces modèles. A l'inverse, les paysages adaptatifs gagneraient à mieux intégrer et décrire différents effets sélectifs. Par exemple, ils pourraient assez facilement intégrer les effets des variations

d'intensité de sélection sur le maintien d'une certaine variance génétique dans une population. Ces effets peuvent notamment se révéler importants pour comprendre les trajectoires évolutives dans des environnements variables dans le temps ou l'espace.

Finalement, deux projets développés pendant ces années de thèse m'ont permis de sortir de la vision caricaturale de la trajectoire adaptative d'une population isolée dans un paysage. Un de ces projets correspond au dernier chapitre de la thèse, où la réalité écologique a repris par elle-même le dessus sur le contexte artificiel du laboratoire. Le deuxième projet est en cours et n'a pas été développé comme chapitre de la thèse. Il met en avant l'architecture génétique comme une composante sélective importante pour l'évolution de populations sexuées dans un environnement spatialement hétérogène. J'aborderai rapidement les questions soulevées dans ce projet car elles se placent directement dans une perspective d'intégration et de compréhension des rôles du contexte écologique dans les trajectoires évolutives.

Importance des interactions biotiques

D'abord, l'intrusion de *C. freundii* nous a montré que même notre milieu de culture ultra-optimisé de laboratoire n'est pas UN environnement, mais une composante de plusieurs niches écologiques. Cela a été démontré à répétition dans un contexte expérimental similairement limité (Rainey and Travisano 1998; Blount et al. 2012b). Ces résultats laissent seulement entrevoir la multiplicité des niches qui peuvent exister dans des environnements naturels. Dans la métaphore du paysage adaptatif, cela implique que *C. freundii* et *E. coli* s'adapteraient à différents pics dans notre cas, mais surtout que la position des pics pourrait être dynamique par la fixation de mutations qui permettent d'accéder à de nouvelles niches, et selon la dynamique d'adaptation de l'autre espèce.

Ensuite, cette coévolution nous amène à reconSIDérer le paysage adaptatif construit. Les propriétés sélectives des bactéries l'une sur l'autre imposent d'ajouter une couche de complexité et une dynamique en lien avec la fréquence, au paysage. Cette forme de paysage me paraît pour le moment assez abstraite et également beaucoup moins intuitive que celles utilisées jusqu'ici. Son analyse empirique requerrait en outre de définir et mesurer de nouveaux paramètres décrivant l'interaction biotique. Reste qu'il est très important de se demander à quel point il est différent de s'adapter dans un environnement isolé et dans une communauté bactérienne par exemple, où la sélection fréquence-dépendante est certainement omniprésente.

Ce « nouveau » système expérimental ouvre des perspectives pour répondre à des problématiques à la fois sur l'évolution et le maintien de la coexistence d'espèce mais aussi sur le rôle de cette coexistence dans les trajectoires évolutives. Par exemple, il serait intéressant de

comparer la trajectoire évolutive de *E. coli* en présence ou en absence de *C. freundii* (et l'inverse) ainsi que dans des environnements antibiotiques ou non, en présence ou non de citrate dans le milieu. Outre le fait de répondre à la question du potentiel mécanisme de la coexistence, ces expériences pourraient aider à comprendre comment les objectifs évolutifs sont déplacés par chacun de ces éléments, et enfin de considérer leurs applications, en termes d'utilisation de probiotiques dans la gestion de la résistance par exemple.

Flux de gènes et adaptation dans des environnements hétérogènes

Un contexte écologique se définit en plus de ces interactions biotiques par une composante spatiale, c'est-à-dire qu'un environnement fait souvent partie d'un continuum environnemental (à part dans certains cas comme par exemple une île) le long duquel les individus ou gamètes, et donc les gènes, circulent. Pour des populations sexuées bien adaptées à un environnement, les flux de gènes provenant de populations adaptées à d'autres environnements vont représenter un fardeau à l'adaptation (d'intensité variable selon le contexte, voir Lenormand 2002 pour une description détaillée). Ce fardeau est issu de la recombinaison entre les génomes sélectionnés dans l'environnement considéré et des génomes adaptés à un autre environnement. En théorie, on peut montrer que dans une poche environnementale donnée, il existe une limite (dépendante des taux de migration des individus entre environnements et des effets sélectifs des allèles adaptatifs à l'extérieur et à l'intérieur de la poche) en dessous de laquelle ce fardeau devient trop lourd et empêche totalement la population de s'adapter (Nagylaki 1975; Lenormand 2002). A partir du modèle décrit dans l'annexe 1 de la thèse, nous avons pu valider cette observation sur la base de simulations de populations évoluant sur plusieurs dizaines de milliers de générations. Dans ce contexte évolutif, l'architecture des gènes (c'est-à-dire leur localisation sur un chromosome) joue un rôle important dans l'adaptation (Yeaman and Whitlock 2011; Yeaman 2013, 2015; *dans ces études le modèle considère deux "îles" avec des optimums phénotypiques différents entre lesquelles les populations migrent alors que le modèle que nous utilisons intègre une poche environnementale dans un continuum spatial*, voir annexe 1). En effet, lorsque les bases génétiques de l'adaptation sont très regroupées sur le chromosome, elles sont *a priori* moins susceptibles d'être dissociées lors d'événements de recombinaison que si elles sont réparties sur l'ensemble du chromosome. Par la même logique, un allèle de fort effet phénotypique serait plus avantageux (pour résister à la recombinaison) que plusieurs allèles de plus petits effets phénotypiques dont l'effet total est équivalent. Dans ce contexte, on peut s'attendre à ce que des architectures génétiques adaptatives très agrégées (par exemple des îlots génétiques adaptatifs) soient sélectionnées. Nos simulations montrent que ce n'est pas forcément le cas (voir aussi Yeaman 2013). Notamment la substitution d'une mutation d'effet phénotypique équivalent mais mieux placée sur le chromosome impose un état transitoire maladaptatif (d'autant plus fort que

l'effet phénotypique de la mutation est fort) qui peut bloquer l'évolution vers des structures génétiques très agrégées. Nos simulations montrent que les populations évoluent plutôt vers des architectures génétiques avec un niveau intermédiaire d'agrégation : les allèles de petits effets phénotypiques se substituent (l'état transitoire est seulement légèrement maladaptatif) et tendent vers des structures génétiques où ils sont agrégés entre eux et autour de ceux de forts effets alors que les allèles de forts effets ne se substituent pas (l'état transitoire est hautement maladaptatif). Plusieurs paramètres du modèle sont encore en cours d'exploration pour valider ces résultats et cette interprétation. Malgré cela, cette étude illustre une autre couche de complexité qu'il peut être nécessaire d'intégrer pour comprendre des trajectoires évolutives dans des environnements naturels.

Conclusion

Pour conclure, beaucoup de pièces du puzzle que nous avons récupérées au cours de la thèse ont pu être rassemblées et mises en cohérence au travers de la métaphore du paysage adaptatif. Notre première analyse des résultats expérimentaux sur l'adaptation à court terme s'est montrée bien cohérente avec les résultats expérimentaux de l'adaptation à long terme des lignées bactériennes. Le modèle de paysage adaptatif utilisé (inspiré du modèle géométrique de Fisher) intègre bien à la fois les patrons de fitness mesurés à différents temps évolutifs mais aussi à travers différents environnements. Ces résultats confortent largement l'utilisation de ces paysages comme modèles purement théoriques mais permettent aussi de faire un pas supplémentaire pour les relier à des applications empiriques. Pour aller dans ce sens, nous avons vu qu'il reste plusieurs éléments (en particulier les modules mutationnels et les covariances sélectives) qui mériteraient d'être plus amplement considérés et explorés. Finalement, les processus évolutifs décrits dans les modèles de paysages adaptatifs s'accordent bien avec les expériences d'évolution en laboratoire. En théorie, les paysages permettent d'extrapoler des trajectoires évolutives sous divers autres scénarios contextuels. Leurs utilisations sur le terrain se heurtent néanmoins à une forme de complexité environnementale peu prise en compte dans ces modèles, émergeant d'un contexte écologique. Ce contexte écologique est de mieux en mieux intégré dans des modèles alternatifs aux paysages, qui proposent ainsi des approches complémentaires pour décortiquer les mécanismes évolutifs à l'œuvre dans les populations naturelles.

Bibliographie

- Achaz, G., A. Rodriguez-Verdugo, B. S. Gaut, and O. Tenaillon. 2013. The reproducibility of adaptation in the light of experimental evolution with whole genome sequencing. Pp. 211–231 in Ecological genomics.
- Angilletta, M. J., and M. W. Sears. 2011. Coordinating theoretical and empirical efforts to understand the linkages between organisms and environments. *Integr. Comp. Biol.* 51:653–661.
- Arnold, S. J., M. E. Pfrender, and J. A. G. 2001. The adaptive landscape as a conceptual bridge between mico- and macroevolution. *Genetica* 112–113:9–32.
- Atwood, K. C., L. K. Schneider, and F. J. Ryan. 1951. Periodic Selection in *Escherichia Coli*. *Proc. Natl. Acad. Sci.* 37:146–155.
- Austin, M. P. 2002. Spatial prediction of species distribution: An interface between ecological theory and statistical modelling. *Ecol. Modell.* 157:101–118.
- Ayala, F. J., and C. A. Campbell. 1974. Frequency-dependent selection. *Annu. Rev. Ecol. Syst.* 115–138.
- Baharoglu, Z., G. Garriss, and D. Mazel. 2013. Multiple pathways of genome plasticity leading to development of antibiotic resistance. *Antibiotics* 2:288–315.
- Bailey, S. F., F. Blanquart, T. Bataillon, and R. Kassen. 2016. What drives parallel evolution? *BioEssays* 1600176:1–9.
- Bank, C., R. T. Hietpas, J. D. Jensen, and D. N. A. Bolon. 2015. A Systematic Survey of an Intragenic Epistatic Landscape. *Mol. Biol. Evol.* 32:229–238.
- Barrick, J. E., and R. E. Lenski. 2013. Genome dynamics during experimental evolution. *Nat. Rev. Genet.* 14:827–839.
- Barton, N. H. 2001. The Role of Hybridization in Evolution. *Proc. Am. Philos. Soc.* 10:551–568.
- Barton, N. H., and J. B. Coe. 2009. On the application of statistical physics to evolutionary biology. *J. Theor. Biol.* 259:317–324.
- Bataillon, T. 2000. Estimation of spontaneous genome-wide mutation rate parameters: Whither beneficial mutations? *Heredity*. 84:497–501.
- Bataillon, T., and S. F. Bailey. 2014. Effects of new mutations on fitness: insights from models and data. *Ann. N. Y. Acad. Sci.* 1320:76–92.
- Bataillon, T., T. Zhang, and R. Kassen. 2011. Cost of adaptation and fitness effects of beneficial mutations in *Pseudomonas fluorescens*. *Genetics* 189:939–949.

- Beaumont, H. J., J. Gallie, C. Kost, G. C. Ferguson, and P. B. Rainey. 2009. Experimental evolution of bet hedging. *Nature* 462:90–93.
- Bell, G. 2008. Selection the mechanism of evolution. Oxford University Press.
- Bennett, A. F., and R. E. Lenski. 2007. An experimental test of evolutionary trade-offs during temperature adaptation. *PNAS* 104:8649–8654.
- Blanquart, F., and T. Bataillon. 2016. Epistasis and the structure of fitness landscapes : are experimental fitness landscapes compatible with Fisher 's model ? *Genetics* 203:847–862.
- Blount, Z. D. 2016. History's windings in a flask: microbial experiments into evolutionary contingency. *P. in Chance in evolution.*
- Blount, Z. D., J. E. Barrick, C. J. Davidson, and R. E. Lenski. 2012a. Genomic analysis of a key innovation in an experimental *Escherichia coli* population. *Nature* 489:513–518.
- Blount, Z. D., J. E. Barrick, C. J. Davidson, and R. E. Lenski. 2012b. Genomic analysis of a key innovation in an experimental *Escherichia coli* population. *Nature* 488:513–518.
- Chevin, L. M., G. Decorzent, and T. Lenormand. 2014. Niche dimensionality and the genetics of ecological speciation. *Evolution (N. Y.)*. 68:1244–1256.
- Chevin, L. M., R. Lande, and G. M. Mace. 2010a. Adaptation, plasticity, and extinction in a changing environment: Towards a predictive theory. *PLoS Biol.* 8.
- Chevin, L. M., G. Martin, and T. Lenormand. 2010b. Fisher's model and the genomics of adaptation: Restricted pleiotropy, heterogenous mutation, and parallel evolution. *Evolution (N. Y.)*. 64:3213–3231.
- Coyne, J. A., N. H. Barton, and M. Turelli. 1997. A critique of Sewell Wright's shifting balance theory of evolution. *Evolution (N. Y.)*. 51:643–671.
- Davies, J., and D. Davies. 2010. Origins and evolution of antibiotic resistance. *Microbiol. Mol. Biol. Rev.* 74:417–33.
- DeAngelis, D. L., and V. Grimm. 2014. Individual-based models in ecology after four decades. *F1000Prime* 6:1–6.
- De Visser, J. A. G. M., and D. E. Rozen. 2005. Limits to adaptation in asexual populations. *J. Evol. Biol.* 18:779–788.
- Dettman, J. R., N. Rodrigue, S. E. Schoustra, and R. Kassen. 2017. Genomics of Compensatory Adaptation in Experimental Populations of *Aspergillus nidulans*. *G3* 7:427–436.
- Dittmar, E. L., C. G. Oakley, J. K. Conner, B. Gould, and D. Schemske. 2016. Factors influencing the effect size distribution of adaptive substitutions. *Proc. R. Soc. B* 283:20153065.
- Duputi, A., F. Massol, I. Chuine, M. Kirkpatrick, and O. Ronce. 2012. How do genetic correlations affect species range shifts in a changing environment? *Ecol. Lett.* 15:251–259.

- Elena, S. F., and R. E. Lenski. 2003. Evolution experiments with microorganisms: the dynamics and genetic bases of adaptation. *Nat. Rev. Genet.* 4:457–69.
- Felsenstein, J. 1974. The evolutionary advantage of recombination. *Genetics* 78:737–756.
- Felsenstein, J. 2017. Theoretical evolutionary genetics.
- Fisher, R. a. 1930. The Genetical Theory of Natural Selection. *Genetics* 154:272.
- Fogle, C. A., J. L. Nagle, and M. M. Desai. 2008. Clonal interference, multiple mutations and adaptation in large asexual populations. *Genetics* 180:2163–2173.
- Fraïsse, C., P. A. Gunnarsson, D. Roze, N. Bierne, and J. J. Welch. 2016. The genetics of speciation: Insights from Fisher's geometric model. *Evolution (N. Y.)* 70:1450–1464.
- Gallet, R., Y. Latour, B. S. Hughes, and T. Lenormand. 2014. The dynamics of niche evolution upon abrupt environmental change. *Evolution* 68:1257–69.
- Garland, T. J., and M. R. Rose. 2009. Experimental Evolution. University of California press, Berkeley, Los Angeles, London.
- Gavrilets, S. 1997. Evolution and speciation on holey adaptive landscapes. *Trends Ecol. Evol.* 12:307–312.
- Gavrilets, S. 2004. Fitness landscapes and the origin of species. Princeton University Press.
- Gavrilets, S. 2010. High-Dimensional Fitness Landscapes and Speciation. P. in Evolution - the extended synthesis. MIT Press Scholarship.
- Gerrish, P. J., and R. E. Lenski. 1998. The fate of competing beneficial mutations in an asexual population. *Genetica* 102/103:127–144.
- Gigord, L. D., M. R. Macnair, and a Smithson. 2001. Negative frequency-dependent selection maintains a dramatic flower color polymorphism in the rewardless orchid *Dactylorhiza sambucina* (L.) Soo. *Proc. Natl. Acad. Sci. U. S. A.* 98:6253–6255.
- Gonzalez, A., O. Ronce, R. Ferriere, and M. E. Hochberg. 2012. Evolutionary rescue: an emerging focus at the intersection between ecology and evolution. *Philos. Trans. R. Soc. Lond. B. Biol. Sci.* 368:20120404.
- Gordo, I., and P. R. Campos. 2013. Evolution of clonal populations approaching a fitness peak. *Biol Lett* 9:20120239.
- Gould, S. 1989. Wonderful life: The burgess shale and the nature of History. W. W. Norton.
- Haldane, J. B. S., and S. D. Jayakar. 1963. Polymorphism due to selection of varying direction. *J. Genet.* 58:237–242.
- Hartl, D. L. 2014. What can we learn from fitness landscapes? *Curr. Opin. Microbiol.* 21:51–57. Elsevier Ltd.

- Healey, D., K. Axelrod, and J. Gore. 2016. Negative frequency-dependent interactions can underlie phenotypic heterogeneity in a clonal microbial population. *Mol. Syst. Biol.* 12:877.
- Hendry, A. P., T. J. Farrugia, and M. T. Kinnison. 2008. Human influences on rates of phenotypic change in wild animal populations. *Mol. Ecol.* 17:20–29.
- Hereford, J. 2009. A quantitative survey of local adaptation and fitness trade-Offs. *Am. Nat.* 173:579–588.
- Hietpas, R. T., J. D. Jensen, and D. N. a Bolon. 2011. Experimental illumination of a fitness landscape. *Proc. Natl. Acad. Sci. U. S. A.* 108:7896–7901.
- Hughes, B. S., A. J. Cullum, and A. F. Bennett. 2007. Evolutionary adaptation to environmental pH in experimental lineages of *Escherichia coli*. *Evolution (N. Y.)*. 61:1725–1734.
- Hwang, S., S.-C. Park, and J. Krug. n.d. Genotypic complexity of Fisher's geometric model. *Genetics*, doi: 10.1534/genetics
- Iwasa, Y. 1988. Free fitness that always increases in evolution. *J. Theor. Biol.* 135:265–281.
- Jacob, F. 1977. Evolution and tinkering.
- Jacoby, G. a. 2005. Mechanisms of resistance to quinolones. *Clin. Infect. Dis.* 41 Suppl 2:S120-6.
- Kassen, R. 2002. The experimental evolution of specialists , generalists , and the maintenance of diversity. *J. Evol. Biol.* 15:173–190.
- Kassen, R., and T. Bataillon. 2006. Distribution of fitness effects among beneficial mutations before selection in experimental populations of bacteria. *Nat. Genet.* 38:484–8.
- Kimura, M. 1965. A stochastic model concerning the maintenance of genetic variability in quantitative characters. *Proc. Natl. Acad. Sci.* 54:731–736.
- Kimura, M. 1983. The neutral theory of molecular evolution. Cambridge University Press, New York.
- Kirkpatrick, M., and N. H. Barton. 1997. Evolution of a species' range. *Am. Nat.* 150:1–23.
- Koonin, E. V. 2012. The logic of chance: the nature and origin of biological evolution. Pearson Education, Inc.
- Labbé, P., C. Berticat, A. Berthomieu, S. Unal, C. Bernard, M. Weill, and T. Lenormand. 2007. Forty years of erratic insecticide resistance evolution in the mosquito *Culex pipiens*. *PLoS Genet.* 3:2190–2199.
- Labbé, P., N. Sidos, M. Raymond, and T. Lenormand. 2009. Resistance gene replacement in the mosquito *Culex pipiens*: Fitness estimation from long-term cline series. *Genetics* 182:303–312.
- Lande, R., and S. Arnold. 1983. The measurement of selection on correlated characters. *Evolution*

(N. Y). 37:1210–1226.

Lässig, M., V. Mustonen, and A. M. Walczak. 2017. Predicting evolution. *Nat. Ecol. Evol.* 1:77. Macmillan Publishers Limited.

Lawson, C. R., Y. Vindenes, L. Bailey, and M. van de Pol. 2015. Environmental variation and population responses to global change. *Ecol. Lett.* 18:724–736.

Le Gac, M., and M. Doebeli. 2010. Epistasis and frequency dependence influence the fitness of an adaptive mutation in a diversifying lineage. *Mol. Ecol.* 19:2430–2438.

Lenormand, T. 2002. Gene flow and the limits to natural selection. *Trends Ecol. Evol.* 17:183–189.

Lenormand, T., L.-M. Chevin, and T. Bataillon. 2016. Parallel Evolution: What does it (not) tell us and why is it (still) interesting? P. in *Chance in Evolution*.

Lenormand, T., D. Roze, and F. Rousset. 2009. Stochasticity in evolution. *Trends Ecol. Evol.* 24:157–165.

Lenski, R. E., and M. Travisano. 1994. Dynamics of adaptation and diversification: a 10,000-generation experiment with bacterial populations. *Proc Natl Acad Sci U S A* 91:6808–6814.

Levins, R. 1966. The strategy of model building in population biology.

Levy, S. B., and B. Marshall. 2004. Antibacterial resistance worldwide: causes, challenges and responses. *Nat. Med.* 10:S122–9.

Lewontin, R. C. 1958. A General Method for Investigating the Equilibrium of Gene Frequency in a Population. *Genetics* 43:419–34.

Lobkovsky, A. E., and E. V. Koonin. 2012. Replaying the tape of life: Quantification of the predictability of evolution. *Front. Genet.* 3:1–8.

Lynch, M., and R. Lande. 1993. Evolution and extinction in response to environmental change.

Lynch, M., and B. Walsh. 1998. Genetics and analysis of quantitatives traits. Sinauer Associates, Sunderland, MA.

MacLean, R. C., and A. Buckling. 2009. The distribution of fitness effects of beneficial mutations in *pseudomonas aeruginosa*. *PLoS Genet.* 5.

MacLean, R. C., G. G. Perron, and A. Gardner. 2010. Diminishing returns from beneficial mutations and pervasive epistasis shape the fitness landscape for rifampicin resistance in *Pseudomonas aeruginosa*. *Genetics* 186:1345–1354.

Maddamsetti, R., R. E. Lenski, and J. E. Barrick. 2015. Adaptation, Clonal Interference, and Frequency-Dependent Interactions in a Long-Term Evolution Experiment with *Escherichia coli*. *Genetics* 200:619–31.

- Mangel, M. 1991. Adaptive Walks on Behavioral Landscapes and the Evolution of Optimal Behavior by Natural-Selection. *Evol. Ecol.* 5:30–39.
- Manna, F., G. Martin, and T. Lenormand. 2011. Fitness landscapes: an alternative theory for the dominance of mutation. *Genetics* 189:923–37.
- Martin, G., S. F. Elena, and T. Lenormand. 2007. Distributions of epistasis in microbes fit predictions from a fitness landscape model. *Nat. Genet.* 39:555–60.
- Martin, G., and T. Lenormand. 2006a. A general multivariate extension of Fisher's geometrical model and the distribution of mutation fitness effects across species. *Evolution* 60:893–907.
- Martin, G., and T. Lenormand. 2008. The distribution of beneficial and fixed mutation fitness effects close to an optimum. *Genetics* 179:907–916.
- Martin, G., and T. Lenormand. 2006b. The fitness effect of mutations across environments: a survey in light of fitness landscape models. *Evolution (N. Y.)*. 60:2413–2477. Wiley Online Library.
- Martin, G., and T. Lenormand. 2015. The fitness effect of mutations across environments: Fisher's geometrical model with multiple optima. *Evolution (N. Y.)*. 69:1433–1447.
- Martin, G., and L. Roques. 2016. The Non-stationary Dynamics of Fitness Distributions: Asexual Model with Epistasis and Standing Variation. *Genetics* 1–37.
- Matuszewski, S., J. Hermisson, and M. Kopp. 2014. Fisher's geometric model with a moving optimum. *Evolution (N. Y.)*. 68:2571–2588.
- McCandlish, D. M., and A. Stoltzfus. 2014. Modeling Evolution Using the Probability of Fixation: History and Implications. *Q. Rev. Biol.* 89:225–252.
- Nagylaki, T. 1975. Conditions for the existence of clines. *Genetics* 595–615.
- Orgogozo, V. 2015. Replaying the tape of life in the twenty-first century. *Interface Focus* 5:20150057.
- Orr, H. A. 2003. A minimum on the mean number of steps taken in adaptive walks. *J. Theor. Biol.* 220:241–247.
- Orr, H. A. 2006. The distribution of fitness effects among beneficial mutations in Fisher's geometric model of adaptation. *J. Theor. Biol.* 238:279–285.
- Orr, H. A. 2005. The genetic theory of adaptation: a brief history. *Nat. Rev. Genet.* 6:119–127.
- Orr, H. A. 1998. The population genetics of adaptation: the distribution of factores fixed during adaptive evolution. *Evolution (N. Y.)*. 52:935–949.
- Ostrowski, E. A., D. E. Rozen, and R. E. Lenski. 2005. Pleiotropic effects of beneficial mutations in *Escherichia coli*. *Evolution (N. Y.)*. 59:2343–2352.

- Parmesan, C. 2006. Ecological and Evolutionary Responses to Recent Climate Change. *Ann. Rev. Ecol. Syst.* 37:637–669.
- Perfeito, L., A. Sousa, T. Bataillon, and I. Gordo. 2014. Rates of fitness decline and rebound suggest pervasive epistasis. *Evolution (N. Y.)*. 68:150–162.
- Philippi, T., and J. Seger. 1989. Hedging one's evolutionary bets, revisited. *Trends Ecol. Evol.* 4:41–44.
- Phillips, P. C. 2008. Epistasis - the essential role of gene interactions in the structure and evolution of genetic systems. *Nat Rev Genet* 9:855–867.
- Plucain, J., T. Hindré, M. Le Gac, O. Tenaillon, S. Cruveiller, C. Médigue, N. Leiby, W. R. Harcombe, C. J. Marx, R. E. Lenski, and D. Schneider. 2014. Epistasis and allele specificity in the emergence of a stable polymorphism in *Escherichia coli*. *Science (80-.)*. 343:1366–1369.
- Polechová, J., and N. H. Barton. 2015. Limits to adaptation along environmental gradients. *Proc. Natl. Acad. Sci.* 112:6401–6406.
- Polechová, J., N. Barton, and G. Marion. 2009. Species' range: adaptation in space and time. *Am. Nat.* 174:E186-204.
- Qi, Q., M. Toll-Riera, K. Heilbron, G. M. Preston, and R. C. MacLean. 2016. The genomic basis of adaptation to the fitness cost of rifampicin resistance in *Pseudomonas aeruginosa*. *Proc. R. Soc. B Biol. Sci.* 283:20152452.
- Rainey, P. B., and M. Travisano. 1998. Adaptive radiation in a heterogeneous environment. *Nature* 394:69–72.
- Ramiro, R. S., H. Costa, and I. Gordo. 2016. Macrophage adaptation leads to parallel evolution of genetically diverse *Escherichia coli* small-colony variants with increased fitness in vivo and antibiotic collateral sensitivity. *Evol. Appl.* 9:994–1004.
- Rodríguez-Verdugo, A., B. S. Gaut, and O. Tenaillon. 2013. Evolution of *Escherichia coli* rifampicin resistance in an antibiotic-free environment during thermal stress. *BMC Evol. Biol.* 13:50.
- Rozen, D. E., and R. E. Lenski. 2000. Long-Term Experimental Evolution in *Escherichia coli*. VIII. Dynamics of a Balanced Polymorphism. *Am. Nat.* 155:24–35.
- Schick, A., S. F. Bailey, and R. Kassen. 2015. Evolution of Fitness Trade-Offs in Locally Adapted Populations of *Pseudomonas fluorescens*. *Am. Nat.* 186:S48–S59.
- Sella, G., and A. E. Hirsh. 2005. The application of statistical physics to evolutionary biology. *Proc. Natl. Acad. Sci. U. S. A.* 102:9541–6.
- Shull, F. A. 1935. Weismann and Haeckel: One hundred years. *Science (80-.)*. 81:443–452.
- Simpson, G. G. 1944. *Tempo and Mode in Evolution*. New York: Columbia Univ. Press.
- Sousa, A., S. Magalhaes, and I. Gordo. 2012a. Cost of antibiotic resistance and the geometry of

- adaptation. Mol. Biol. Evol. 29:1417–1428.
- Sousa, A., S. Magalhães, and I. Gordo. 2012b. Cost of antibiotic resistance and the geometry of adaptation. Mol. Biol. Evol. 29:1417–28.
- Stern, D. L. 2013. The genetic causes of convergent evolution. Nat. Rev. Genet. 14:751–64.
- Szamecz, B., G. Boross, D. Kalapis, K. Kovács, G. Fekete, Z. Farkas, V. Lázár, M. Hrtyan, P. Kemmeren, M. J. a. Groot Koerkamp, E. Rutkai, F. C. P. Holstege, B. Papp, and C. Pál. 2014. The Genomic Landscape of Compensatory Evolution. PLoS Biol. 12:e1001935.
- Takahashi, Y., and M. Kawata. 2013. A comprehensive test for negative frequency-dependent selection. Popul. Ecol. 55:499–509.
- Tenaillon, O. 2014. The Utility of Fisher's Geometric Model in Evolutionary Genetics. Annu. Rev. Ecol. Evol. Syst. 45:179–201.
- Trindade, S., A. Sousa, and I. Gordo. 2012. Antibiotic resistance and stress in the light of Fisher's model. Evolution (N. Y). 66:3815–3824.
- Turner, P. E., V. Souza, and R. E. Lenski. 1996. Tests of ecological mechanisms promoting the stable coexistence of two bacterial genotypes. Ecology 77:2119–2129.
- Via, S., and R. Lande. 1985. Genotype-environment interaction and the evolution of phenotypic plasticity. Evolution (N. Y). 39:505–522.
- Weeks, A. R., and A. a Hoffmann. 2008. Frequency-dependent selection maintains clonal diversity in an asexual organism. Proc. Natl. Acad. Sci. U. S. A. 105:17872–17877.
- Weinreich, D. M., Y. Lan, C. Scott Wylie, and R. B. Heckendorn. 2013. Should evolutionary geneticists worry about higher-order epistasis? Curr. Opin. Genet. Dev. 23:700–707.
- Weinreich, D. M., R. a Watson, and L. Chao. 2005. Perspective: Sign epistasis and genetic constraint on evolutionary trajectories. Evolution 59:1165–1174.
- Whitlock, M. C., and P. C. Phillips. 2000. The exquisite corpse: A shifting view of the shifting balance. Trends Ecol. Evol. 15:347–348.
- Whitlock, M. C., P. C. Phillips, F. B.-G. Moore, and S. J. Tonsor. 1995. Multiple fitness peaks and epistasis. Annu. Rev. Ecol. Syst. 26:601–629.
- Wilson, G. B., and J. N. B. Bell. 1990. Studies on the tolerance to sulphur dioxide of grass populations in polluted areas: VI. The genetic nature of tolerance in *Lolium perenne* L. New Phytol. 116:313–317.
- Wiser, M. J., N. Ribeck, and R. E. Lenski. 2013. Long-Term Dynamics of Adaptation in Asexual Populations. Science (80-.). 342:1364–1367.
- Wright, S. 1932. The roles of mutation, inbreeding, crossbreeding and selection in evolution.

Yeaman, S. 2013. Genomic rearrangements and the evolution of clusters of locally adaptive loci. Proc. Natl. Acad. Sci. U. S. A. 110:E1743-51.

Yeaman, S. 2015. Local adaptation by alleles of small effect. Am. Nat. 186:S000–S000.

Yeaman, S., and M. C. Whitlock. 2011. The genetic architecture of adaptation under migration-selection balance. Evolution (N. Y). 65:1897–1911.

Annexe 1: The genetic architecture of local adaptation in a continuous space (N. Harmand*, F. Laroche*, F. Debarre, T. Lenormand)

Model description

Phenotypes

We consider stabilizing selection on a trait z . Individuals are diploids and N_{loc} loci positioned on the same chromosome additively contribute to the trait. Loci can harbor three alleles: an allele with effect 0, an allele with effect a on the phenotype and an allele with an effect $b > a$. Possible values for z are discrete and belong to the set $\{ka + lb \mid k, l \in \mathbb{N} \text{ and } k + l < 2N_{loc}\}$.

Landscape

We consider a landscape, containing X consecutive sites on a line (Figure 1). All sites have the same carrying capacity K_{max} (the maximum number of adults that can simultaneously maintain in it). Sites are designated through their index x in the line (increasing from 1 to X when going from left to right in the landscape). The landscape contains two zones: a central zone, $x_{left} \leq x \leq x_{right}$ and a peripheral zone $x_{left} > x$ or $x_{right} < x$. Defining L as the breadth of the central zone, x_{left} and x_{right} are determined as follows: $x_{left} = \lfloor \frac{X-L}{2} \rfloor$ and $x_{right} = \lceil \frac{X+L}{2} \rceil$. In each site x , we define an optimal level of trait $z_{opt}(x)$. $z_{opt}(x)$ is chosen as follows: $z_{opt}(x) = 0$ in the peripheral zone and $z_{opt}(x) = 2\Omega$ in the central zone, where Ω is a selection intensity parameter (see below).

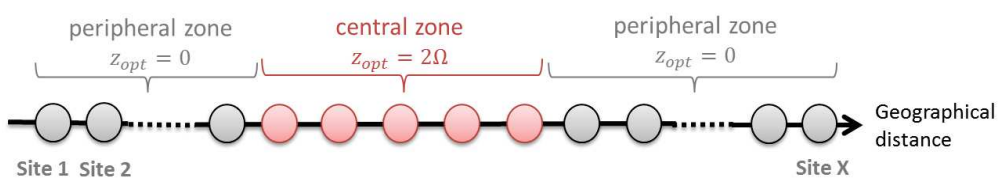


Figure 1: Schematic representation of the spatially explicit model in which simulations were performed. Parameters notations refer to those used in the text.

Life cycles

The life cycle (=one generation) occurs as follows (Figure 2). Within a site, adults produce a very large number of juveniles through sexual reproduction. The genotype of juveniles is determined by randomly sampling two adults at the former generation, generating one gamete per adult (including recombination) and associating the two gametes. The number of recombination events per meiosis follows a Poisson distribution with parameter I_{rec} . Those recombination events are randomly positioned between loci without allowing two events to occur with same loci. Note that same adult can be chosen two times (i.e. selfing is allowed). Mutations events occur on the gametes with a probability μ toward allele a , $\mu/100$ toward allele b and $(1-\mu - \mu/100)$ toward allele 0.

Juveniles then migrate from their natal site to a maturation site. Migration is modeled by n_{rep} displacement events. A displacement event is either moving to a neighbor site (with probability m) either staying in the current site (with probability $1 - m$). When moving, individuals have equal chance to move in both directions. If an individual end its migration sequence out of the landscape, it is eliminated. Juveniles that reach a maturation patch in the landscape undergo a trait-dependent mortality that depends on the difference between their phenotypes z , the local optimal phenotype $z_{opt}(x)$ and the selection intensity Ω . The probability for a juvenile to die is

$$e^{-\frac{(z-z_{opt}(x))^2}{\Omega^2}}.$$

Adult fecundity is high enough to ensure that K_{max} or more juveniles survive in every site. A regulation then occurs through the random sampling of K_{max} juveniles among the surviving ones. Those juveniles constitute the adults of the next generation. Other juveniles are discarded.

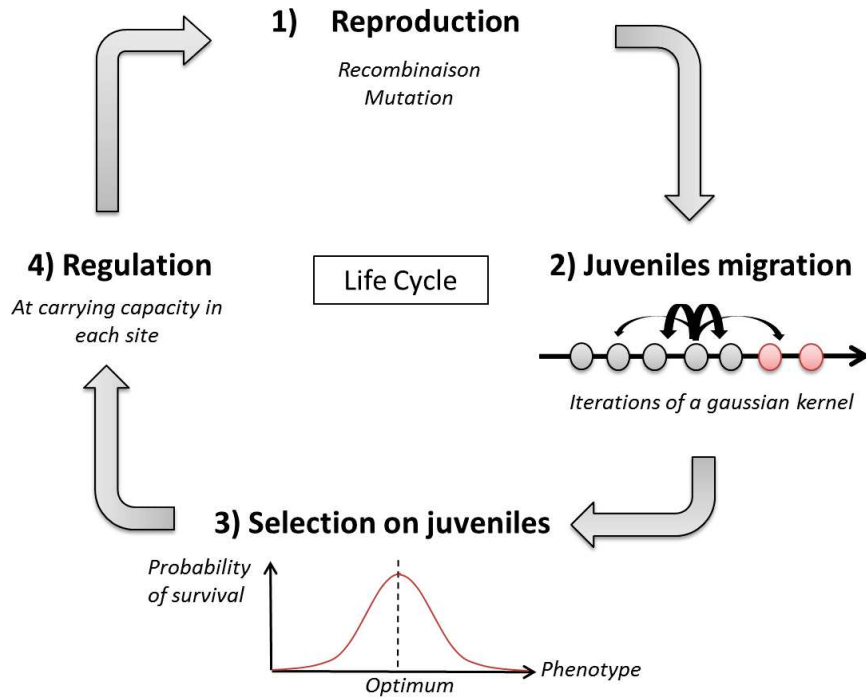


Figure 2: Schematic life cycle simulated in the spatially explicit model.

Simulations

Simulations were performed during T_{max} generations using baseline parameters reported in table 1. Each combination of parameters was replicated 100 times. The initial state was set with all the populations containing K_{max} individuals having only alleles 0 at all the loci.

Analysis of simulations outputs

In each simulation, we recorded the allelic frequencies observed at each locus in a central population ($x = 50$) of the landscape after T_{max} generations. We computed the sums of the frequencies of small (resp. large) effects across the $2N_{loc}$ loci. We also measured three aggregation parameters which quantifies whether (i) small effect alleles are closer one from another on the chromosome than expected when randomly shuffled, (ii) large effect alleles are closer one from another on the chromosome than expected when randomly shuffled and (iii) small effects are closer to large effects on the chromosome than expected when randomly shuffled.

N_{loc}	50
a	$0.05 \times \Omega = 0.05$
b	$0.25 \times \Omega = 0.25$
I_{rec}	$0.01 \times N_{loc} = 0.5$
μ	$10 / (N_{loc} \times K_{max} \times X \times 2)$
X	100
K_{max}	5, 20
L	0, 1, 5, 8, 10, 12, 13, 15, 17, 20, 25, 30, 40, 50, 60, 70, 80, 90, 98
Ω	1
n_{rep}	10
m	0.5
T_{max}	10000, 100000

Table 1. Baseline parameters used in simulations

Résumé : De nos jours plus que jamais, il est nécessaire d'anticiper et de comprendre les réponses évolutives des organismes vivants, face à des habitats instables et hétérogènes. Mais à quel point cela est-il possible ? Reproduire l'ensemble du déroulé d'une trajectoire évolutive nécessite de pouvoir décrire, d'une part, le « matériel » disponible pour s'adapter (c'est-à-dire les effets phénotypiques associés à la variabilité génétique produite), d'autre part, comment agissent les forces évolutives, associées à un contexte écologique, pour aboutir à un certain « assemblage » de ce matériel. Dans sa version la plus simple, ce processus évolutif peut-être décrit par plusieurs cycles d'événements de mutations-sélection conduisant à l'adaptation d'une population à son environnement. Cette dynamique correspond assez bien à celle qui est décrite par les populations bactériennes dans les expériences d'évolution contrôlées en laboratoire. Parallèlement, les modèles de paysages adaptatifs (phénotypiques), et en particulier le modèle géométrique de Fisher, sont des outils très puissants pour formuler des prédictions générales et quantitativement testables sur ces trajectoires évolutives. Cependant, ils restent très théoriques et ont été largement pensés dans un contexte écologique simplifié. Au cours de cette thèse, nous avons identifié les déterminants (mutationnels et sélectifs) des trajectoires évolutives à long terme de populations bactériennes s'adaptant dans différents contextes environnementaux. Une première partie des résultats est mise en lumière par la validation expérimentale et la reconstruction de la topographie du paysage adaptatif généré par différentes doses d'un antibiotique, le long d'un gradient. Une deuxième partie expérimentale vise à intégrer une composante biotique (une autre bactérie) à ce même contexte environnemental. Les processus évolutifs intervenant au cours d'une coévolution à long terme maintenue par sélection fréquence-dépendante, y sont étudiés.

Mots clés : Evolution expérimentale, Paysages adaptatifs, Sélection fréquence-dépendante, Compromis adaptatifs, Gradient environnemental, Trajectoire évolutive, *Escherichia coli*, *Citrobacter freundii*, Modèle géométrique de Fisher

Summary: Today more than ever, it is crucial to anticipate and understand the evolutionary responses of living organisms faced with heterogeneous and unstable habitats. But to what extent is this possible? To reproduce an entire evolutionary trajectory, we must first describe the “material” available for adaptation (e.g. the phenotypic effects associated with the existing and novel genetic variability), and second describe the way evolutionary forces, shaped by the ecological context, result in specific “assemblies” of this material. At its simplest, this evolutionary process can be described by several cycles of mutation-selection events, leading to the adaptation of a population to an environment. This process is reflected in the evolutionary trajectories of bacterial lineages undergoing controlled experimental evolution in the lab. Concurrently, adaptive (phenotypic) landscape models, and especially Fisher's geometrical model of adaptation, are powerful tools to formulate general predictions, which can then be tested on such evolutionary trajectories. However, they remain highly theoretical, and are widely conceived in a simple ecological context. In this thesis, we identified the (mutational and selective) determinants of the evolutionary trajectories of bacterial lines adapting to various environmental contexts. A first set of results regards evolution along a gradient of antibiotic doses, and their relevance is highlighted by experimental validation and by the reconstruction of the underlying adaptive landscape. A second experimental part integrates a biotic component (another bacteria) to the same environmental context. The evolutionary processes acting throughout the resulting long-term coevolution – maintained by frequency-dependent selection – are studied.

Key words: Experimental evolution, Adaptive landscapes, Frequency-dependent selection, Fitness trade-offs, Environmental gradient, Evolutionary trajectory, *Escherichia coli*, *Citrobacter freundii*, Fisher's Geometrical Model